ACCURATE DETECTION AND CORRECTION OF TECHNICAL AND NON-TECHNICAL LOSSES USING SMART METERING

BY

ABDULLAH LAIQ SHAH

A Thesis Presented to the

DEANSHIP OF GRADUATE STUDIES

KING FAHD UNIVERSITY OF PETROLEUM & MINERALS

DHAHRAN, SAUDI ARABIA

In Partial Fulfillment of the
Requirements for the Degree of

MASTER OF SCIENCE

In

ELECTRICAL ENGINEERING

May 2018

KING FAHD UNIVERSITY OF PETROLEUM & MINERALS

DHAHRAN- 31261, SAUDI ARABIA

DEANSHIP OF GRADUATE STUDIES

This thesis, written by **ABDULLAH LAIQ SHAH** under the direction of his thesis advisor and approved by his thesis committee, has been presented and accepted by the Dean of Graduate Studies, in partial fulfillment of the requirements for the degree of **MASTER OF SCIENCE IN ELECTRICAL ENGINEERING.**

Dr. Ali T. Al-Awami
(Advisor)

Dr. Ali A. Al-Shaikhi
Department Chairman

Dr. Wessam A. Mesbah
(Co-Advisor)

Dr. Salam A. Zummo
Dean of Graduate Studies

Dr. Ibrahim M. Elamin
(Member)

20/12/2018
Date

Dr. Muhammad Khalid
(Member)

Dr. Suhail I. Al-Dharrab
(Member)

To my beloved parents

ACKNOWLEDGMENTS

First, I would like to thank my thesis advisor Dr. Ali Al-Awami for his continues assistant and support of my thesis work. His door was always open for any help I needed, whether in this work or any other aspect of my career. He impressed me with his motivation and immense knowledge in the field of power engineering which provided me a chance for creativity and innovation. He always was patient and helpful and one could not wish friendlier advisor than him. Also, I would like to thank my co-advisor Dr. Wessam Mesbah for his great support of my thesis and career. He provided me a big opportunity for contribution, thanks to his previous state-of-art work that I was lucky to work on. His comments were always valuable and steering me in the right direction.

Beside my advisor and co-advisor, I would like to thank all the committee members for accepting to be involved in my thesis. Also, I want to thank Deanship of Scientific Research at KFUPM for funding this work. Moreover, I want to thank the chairman of EE Department Dr. Ali Al-Shaikhi and all the people supported me in any aspect during my graduate study. My sincere thanks also go to my great university (KFUPM) for providing me the scholarship, opportunity to teach labs, and wonderful social experience.

Last but not least, I would like to thank my family for their spiritual unfailing support throughout my entire life. Thank you for what you do for me.

TABLE OF CONTENTS

LIST OF TABLES

LIST OF FIGURES

LIST OF ABBREVIATIONS

ADC	:	Analog to Digital Converter
AMI	:	Advanced Metering Infrastructure
BAN	:	Building Area Network
CT	:	Current Transformer
DAC	:	Digital to Analog Converter
DS	:	Distribution System
DSE	:	Distribution Stat Estimation
DSP	:	Digital Signal Processor
ECRA	:	Electricity & Cogeneration Regulatory Authority
EMIC	:	Energy Metering Integrated Circuit
FAN	:	Field Area Network
HAN	:	Home Area Network
IAN	:	Industrial Area Network
IC	:	Integrated Circuit
IED	:	Intelligent Electronic Device
MISO	:	Master in Slave out
MOSI	:	Master out Slave in
NAN	:	Neighborhood Area Network
NPV	:	Net Present Value
NTL	:	Non-Technical Losses
PGA	:	Programmable Gain Amplifier
PMU	:	Phasor Measurement Unit

PPM	:	Parts Per Million
PWM	:	Pulse Wide Modulation
RTC	:	Real Time Clock
SCADA	:	Supervisory Control and Data Acquisition
SCLK	:	Serial Clock
SEC	:	Saudi Electricity Company
SPI	:	Serial Peripheral Interface
SS	:	Slave Select
SVM	:	Support Vector Machine
TL	:	Technical Losses
VT	:	Voltage Transformer
WAN	:	Wide Area Network

ABSTRACT

Full Name : [Abdullah Laiq Sanagul Shah]

Thesis Title : [Accurate Detection and Correction of Technical and Non-Technical Losses Using Smart Metering]

Major Field : [Electrical Engineering]

Date of Degree : [May 2018]

The power losses in the electric power grid are categorized into technical and non-technical losses. Global annual cost of non-technical losses (NTL) to electricity providers is around 96 billion US dollars, according to Northeast Group, LCC. NTL can be due to tampering with smart meters, attacking data transmitted from smart meters, tapping service cables, or malfunctioning of smart meters. To accurately detect and correct NTL in the distribution system, it is essential to first estimate the technical losses. Estimating the technical losses requires the knowledge of the network topology and cables impedances, which might not be readily available for the concerned utility company. This work proposes two main contributions. First, an algorithm that is created for high rate synchronized measurements that features two main functions: estimating the cables impedances and estimating the technical and non-technical power losses. Second, a novel method that offers a new unit of measurement for energy losses calculation to overcome two practical issues in smart metering, the time skew problem and the estimation of energy losses when the measurements of smart meters are reported at low frequency. In addition to that, this work proposes a full design of smart meter to be used in the future for hardware implementation of a meter capable of recording the new unit of measurement. Finally, simulations performed, and the results verified that the proposed algorithms outperformed previous algorithms and showed a more accurate estimation of TL and NTL.

ملخص الرسالة

الاسم الكامل: عبدالله لائق سناجل شاه

عنوان الرسالة: الكشف الدقيق عن الخسائر الفنية وغير الفنية وتصحيحُها باستخدام القياس الذكيّ

التخصص: الهندسة الكهربائية

تاريخ الدرجة العلمية: مايو ٢٠١٨

تُصنف خسائر الطاقة في شبكة الطاقة الكهربائية إلى خسائر فنية وغير فنية. تبلغ التكلفة السنوية العالمية من الخسائر غير الفنية لمزوّدي الكهرباء حوالي ٩٦ مليار دولارٍ أمريكيّ، وفقاً لشركة "نورث إيست جروب" المحدودة. يمكن أن تنشأ الخسائر غير الفنية بسبب العبث بالعدادات الذكية، أو مهاجمة البيانات المنقولة من العدادات الذكية، أو تفريع كابلات الخدمة، أو عُطلٍ في العدادات الذكية. للكشف بدقةٍ عن الخسائر غير الفنية في نظام التوزيع وتصحيحها؛ من الضروريّ تقدير الخسائر الفنية أولاً. تقدير الخسائر الفنية يتطلب معرفة البنية الطوبولوجية للشبكة والمعاوقات الكهربائية للكابلات، والتي قد لا تكون متاحةً بسهولةٍ لشركة المرافق المعنيّة. يقترح هذا العمل إسهامين رئيسيّين. الأول، خوارزميةٌ تم إنشاؤها للقياسات المتزامنة ذات المعدل المرتفع، والتي تتميز بعمليتين رئيسيّتين: تقدير معاوقات الكابلات، وتقدير خسائر الطاقة الفنية وغير الفنية. الثاني، طريقةٌ جديدةٌ توفّر وحدة قياسٍ جديدةً لحساب خسائر الطاقة؛ للتغلب على مسألتين عمليتين في القياس الذكيّ: مشكلة تخالف الوقت، وتقدير خسائر الطاقة عندما تُنقل قياسات العدادات الذكيّة بترددٍ منخفضٍ. بالإضافة إلى ذلك، يقترح هذا العمل تصميماً كاملاً لعدادٍ ذكيٍّ بمخططاتٍ تفصيليةٍ لاستخدامها في المستقبل لتنفيذ عداد قادر على تسجيل وحدة القياس الجديدة. وأخيراً، تمت محاكاة الخوارزميات والحلول المقترحة، حيث أن نتائج المحاكاة أثبتت أن الخوارزميات المقترحة قادرة على كشف وتصحيح أدق للخسائر الفنية وغير الفنية.

CHAPTER 1

INTRODUCTION

1.1 Background and Motivation

Smart metering is an essential requirement in developing smart grids, and advanced billing systems. Smart meters are digital meters that are capable to measure different electrical components such as voltage, current, active power, reactive power, time of use, and total harmonic distortion. In addition to that, smart meters provide two-way communication capability between the customer and the utility company.

Smart meters will benefit electric utilities in Kingdom of Saudi Arabia KSA as well as overall benefits to its national economy. Developing smart metering infrastructure will reduce operating costs as well as improving the network losses of the utility company. Figure 1.1 shows the net present worth of installing smart meters all over the country based on 15-year time frame [1]. The study has been done by The Electricity and Cogeneration Regulatory Authority ECRA. It shows a net present worth of 1.615 Billion SR by investing 7.548 Billion SR in implementing the smart metering system.

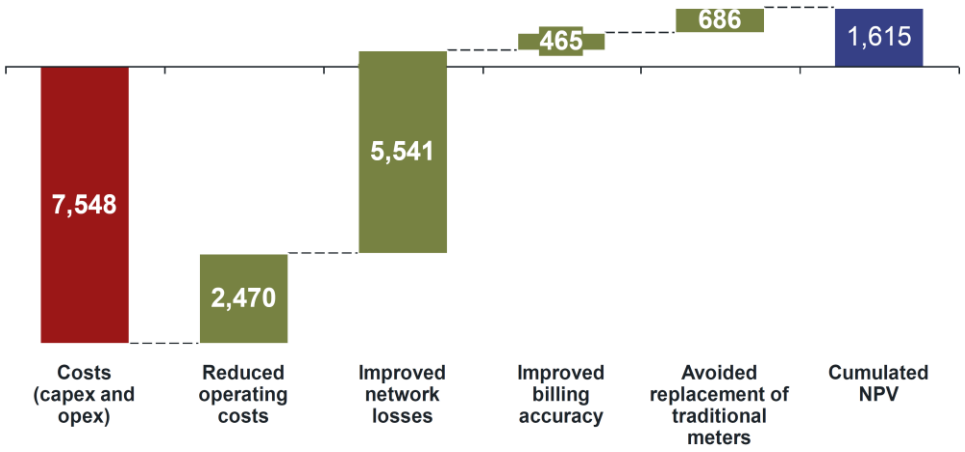

Figure 1.1: Business case results of smart meter benefits to electric utility companies in Million SR

Besides the total benefits to the utility company, the benefits to the national economy of Saudi Arabia is much more than that (over 100 Billion SR over a 15-year timeframe). Figure 1.2 shows the total benefits of the smart metering system to KSA [1].

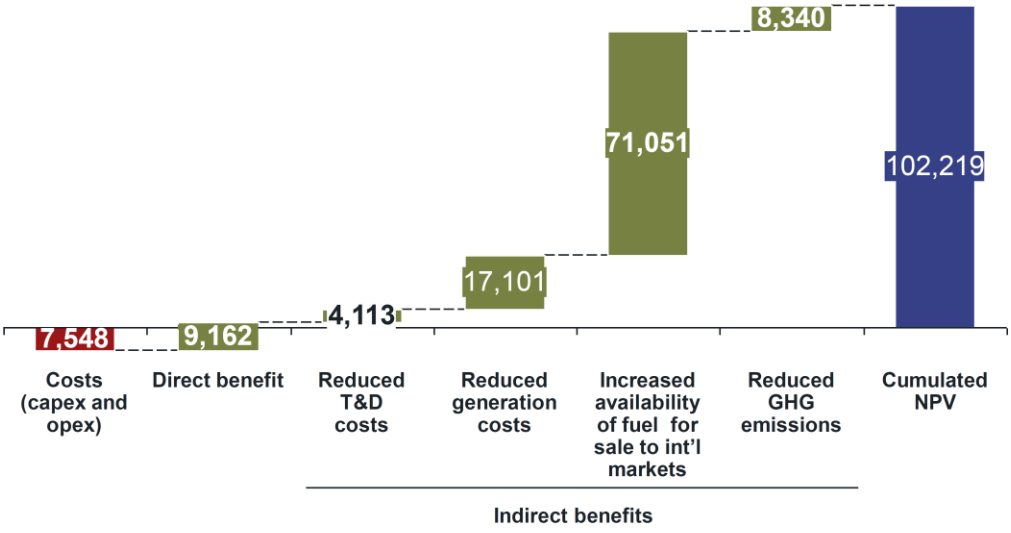

Figure 1.2: Business case results of smart meter benefits to Saudi Arabia in Million SR

Therefore, Saudi Arabia is going to install 12 Million smart meters by 2025 [2]. The proposed roadmap of smart meters and smart grid implementation is done by ECRA and shown in Figure 1.3 [1].

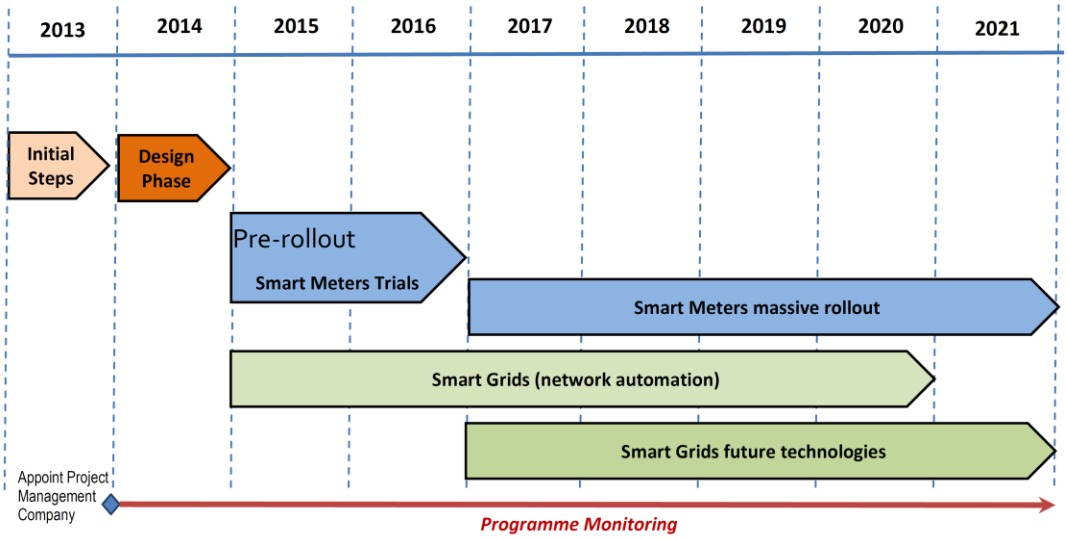

Figure 1.3: Smart meters & smart grid implementation roadmap

On the other hand, the smart metering will add software and communication layers to the metering infrastructure which allows tampering with the metering and billing data locally or remotely in addition to conventional physical tampering of meters. In 2009, a utility company in Puerto Rico (USA) asked FBI to investigate in widespread electricity theft which then found to be done by using optical converter connected to a laptop and with using a software that is available online, the attackers were able to tamper the readings of the meters by changing some settings. The tampering was offered to households and commercial users for $300 and $3000 respectively [3]. Nowadays, smart meter attackers can hack into the smart meter and reprogram it with low-cost tools and moderate knowledge in computers with the help of software that can be easily found on the Internet [4]. Although AMI will add more variability to the metering system, they will provide semi-real-time data for the utility company which could be used in detecting attacks on the metering and billing system.

The wrong reading of smart meters due to malfunction or attack can cause huge loss for power companies. Figure 1.4 shows the energy losses growth in Saudi Arabia, these losses are due to two factors, first is technical losses (TL) which come from the heat losses in transmission and distribution systems, substations, and other natural losses in equipment needed for implementing the power system. The second is the non-technical losses (NTL) which comes from electricity theft, unregistered users, inaccurate readings of meters, and inaccurate billing by the utility company. Compared to some developed countries, Saudi Arabia has higher overall network losses as shown in Figure 1.5 [1]. This difference in network losses can be due to the difference of KSA system's technical losses as well as non-technical losses compared to other systems.

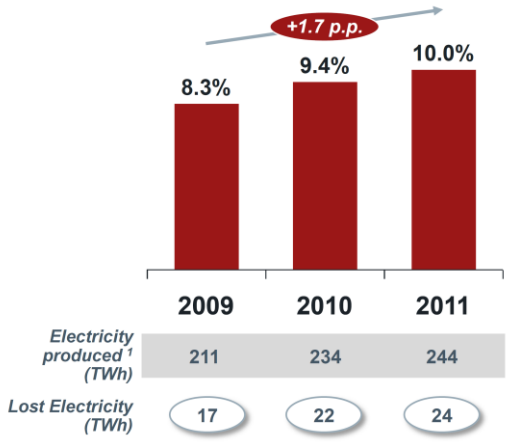

Figure 1.4: Electric energy losses in KSA

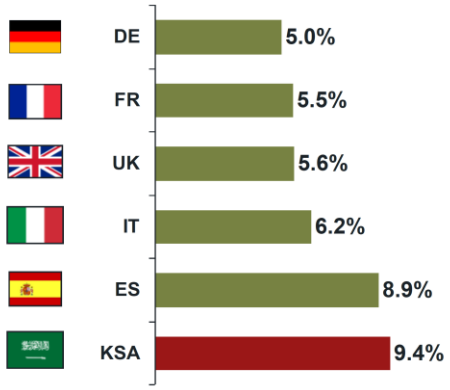

Figure 1.5: KSA's network losses compared to other countries in 2010

In the United States, the electricity losses due to theft estimated to be between 1.5% to 2% of the total electricity generated which costs utilities around $6 billion dollars on annual basis [5]. Electricity theft rate can differ from one country to another, and it can be as big as 50% of distributed electricity in some developing countries [4]. In India, the losses related to electricity theft approximated to be around $4.5 billion which is around 1.5% of India's GDP [6]. Figure 1.6 published by International Energy Agency (IEA) shows the total electricity losses (both TL and NTL) for some countries in the year 2014.

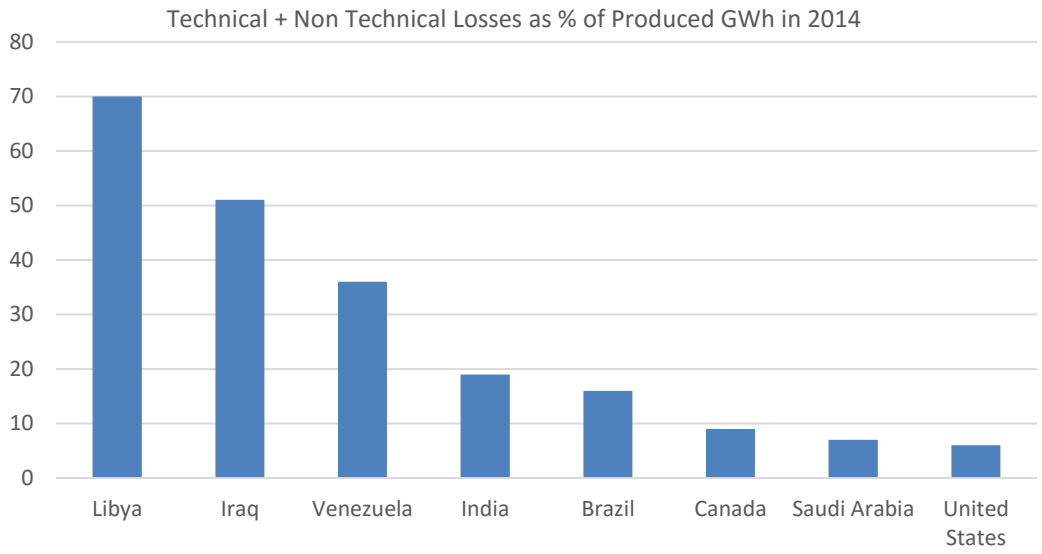

Figure 1.6: Electric energy losses in some countries, generated based on IEA data of 2014

Global energy theft was estimated to be around $25 billion every year, where the amount of electricity stolen exceeds the generation capacity installed in U.K., France, and Germany combined [7]; much recent report offered by Northeast Group LLC, estimates the global annual losses of $96 billion due to non-technical losses [8]. Besides the fact that electricity theft causes losses related to uncharged electricity, the utility company needs to increase the installed system capacity to mitigate the electricity consumption that is not paid for. Moreover, the non-technical losses are causing an increase in electricity bill for the legitimate end usurers in deregulated markets, which may lead to increase the theft rate due to increase in electricity prices. Moreover, high rates of distribution power losses weather TL or NTL may affect the quality of power supplied to the end users [7].

1.2 Problem Description

To reduce the non-technical losses in the distribution network, the development and implementation of robust NTL detector are essential. The sources of NTL presented in [4]

as customer theft, noncustomer theft, nonpayment by the customer, and actions of an employee of the utility company. Here we will divide the sources of NTL into three main types: NTL due to error, NTL due to attack, and unpaid bills. NTL due to error is any cause of losses due to human error or fault in the measurement or information system such as faulty metering equipment, inaccurate calibration of metering equipment, and an error in the information system. The second is the losses due to attack on the system such as physical attack or attack on the information system.

Physical attack can be any type of physical attack such as tapping distribution line, tampering with smart meter (bypassing the meter for big loads, connecting jumper parallel with cable entering the CT, reverse the current direction in bidirectional meters, replacing the CT with another with higher turns ratio, changing the software setting, and disconnecting the neutral). An attack on information system can be any attack that such as cyber-attack or agreement with an employee in a utility company. The sources of NTL are summarized in Figure 1.7.

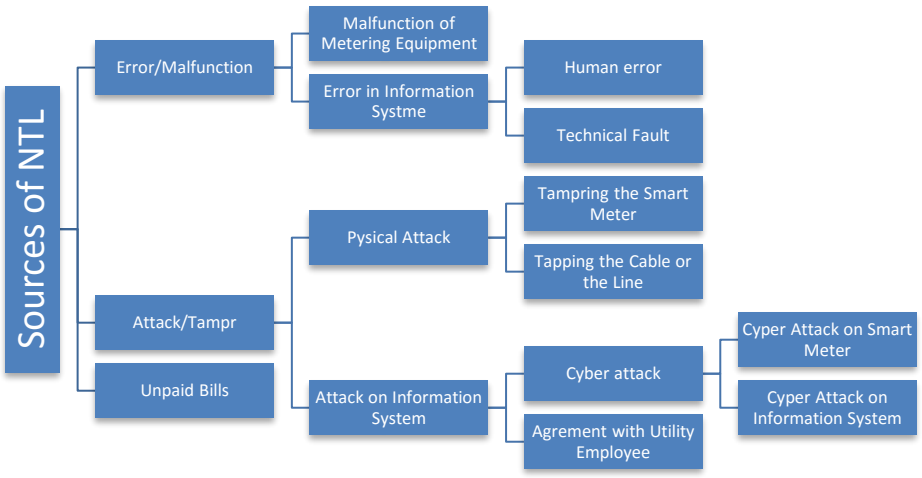

Figure 1.7: Sources of non-technical losses in the distribution system

To detect the NTL and estimate the amount of lost power, the power flows in the distribution secondary need to be examined. These are the challenges when examining the power flow in the distribution systems:

- The measurements are taken from metering equipment that is installed at different locations; hence, the power losses must be determined.

- To estimate the power losses, first, the cable impedances of the distribution secondaries must be determined which are usually not readily available to the concerned utility company.

- The estimation is based on measurements of smart meters and other meters that are installed in the distribution system. The challenge here is that these meters are not phasor measurement units (PMUs) which means some state estimation techniques cannot be applied (e.g. KCL at a specific node cannot be applied using RMS currents without phase angle information).

- The RMS measurements received from smart meters are not synchronized to an accurate common time reference, i.e. there is time skew between the measurements. This issue is coming from the drift of real time clock at different temperatures, e.g. one of the commercial smart meters in KSA can guarantee only a drift of RTC not greater than 0.5 second per day. Therefore, the statement "power in equals power out" is not applicable to measurements that are skewed in time.

- Smart meters usually report the energy data for a specific period, not the real-time power. This means that the real-time RMS current also will not be available, and the average RMS current availability is not sufficient to estimate the energy losses.

These challenges need to be solved for accurate detection and correction of technical and non-technical losses in distribution secondaries. This work will propose solutions to solve all problems explained above without requiring any additional hardware.

1.3 Thesis Contribution

This work aims to design a secure smart metering system that utilizes a method presented in [9] to detect and correct errors in smart meters. The structure and detailed design of smart energy meters will be explained as well as the required modification to currently used smart meters to implement the proposed solutions. In addition to that, the practical challenges explained in the previous section will be solved for more accurate detection and correction of NTL. The outcome of this work will be:

- Estimation of power losses in distribution secondaries using the already existing smart meters for two systems:
    - System reporting real-time power data at high rate.
    - System reporting energy data at a low rate.
- Estimation of cable impedances using the already existing smart meters for two systems:
    - System reporting real-time power data at high rate.

    - System reporting energy data at a low rate.

- Overcome the issue of unavailability of phase angle.
- Overcome the issue of time skew in smart meters data.
- Overcome the issue of energy losses estimation when the reported data are energy data, e.g. when the system reports the energy say each half an hour instead of real-time power.
- Modify an algorithm presented in [9] for more accurate detection and correction of technical and non-technical losses.
- Simulate the proposed algorithms and solutions for detecting NTL.
- Compare the modified algorithms to algorithms presented in [9].
- Provide a design of smart meter to be used in the future for implementation of proposed solutions, e.g. this work will propose a new unit of measurement to be measured by the smart meter for energy losses estimation.

The features that are provided by the proposed algorithms in this thesis are not available in any previous work. The simulations verified the ability of the algorithm for accurate estimation of technical and non-technical losses in distribution secondary.

CHAPTER 2

LITERATURE REVIEW

Wrong reading of electricity meter can be classified into two main categories; malfunction, and attack. Malfunction of a smart meter can occur due to inaccurate calibration or physical damage to the meter, which can result in higher or lower reading than the actual or disconnected from the utility. AMI attackers are classified in [10] into six types, first are curious eavesdroppers whose goal is to tamper to serve their curiosity. The second are the electricity thieves to reduce electricity bill or steal by tapping from distribution lines. Third are malicious eavesdroppers where they aim to collect metering data to use it in some activities such as housebreaking. Then swanky attackers who want to show their abilities in attacking others. Also, active attackers who may want to lunch large-scale subversive attack on a specific utility or country. Finally, intrusive data management agencies that aim to collect customer data for economic and marketing purposes. This work is focusing on detecting NTL whether it is related to attack/tamper or error/malfunction. The first section of this chapter shows the different techniques used in the literature for detecting NTL and the second section explains the different methods used in the previous work to implement smart meters for prototyping.

2.1 Detecting Non-Technical Losses

There are different classifications used to categorize NTL detection techniques, in [10] the NTL detection methods are classified into state-based, classification-based, and game

theory-based. In [11], the detection techniques pointed out are harmonic generator deployment, support vector machine, and using center observer meter. In this work, a more comprehensive classification will be used to classify the reviewed publications, it was proposed in [12] and classifies the NTL detection techniques into three categories: a theoretical study, non-hardware solution, and hardware solution.

2.1.1 Theoretical Study

A theoretical study is focused on defining and analyzing different factors that could be related to electricity theft such as region's economic condition, market characteristics, and sociodemographics. Most of the studies show the relationship between socioeconomic status and fraud behavior as cause and effect approach to locating rejoin of high theft rates. In [13], Turkey's socioeconomic data of 8 years (from 2002-2010) along with data of electricity theft and its price used to determine socioeconomic fraud motives. It concluded that the most dominant factors causing fraud behavior are education level, amount of income, social capital, the percentage of rural population, temperature, amount of agricultural production, and electricity price.

Positive association with electricity theft found in areas with higher electricity price, higher temperature distance form comfort temperature, a higher percentage of rural population, and a higher agricultural production rate. A negative correlation with electricity theft found in areas of people with higher education level, higher income, and higher social capital.

In [14], various socioeconomic factors that can affect electricity theft rate referred to; such as electricity price, income level, characteristics of the population, agricultural load,

unemployment rate, education level, corruption level, political instability, urbanization, the probability of detection, and temperature.

These theoretical studies can help in locating areas with high electricity theft rates as well as they will be useful in determining better energy policies and regulations to reduce the causes of fraud behavior. On the other hand, these studies cannot be used to quantify and locate specific tampering cases for utility companies.

2.1.2 Non-Hardware Solution

The non-hardware solution is mainly based on statistical analysis such as classification, estimation, and game theory. In some cases, the non-hardware solution requires additional hardware such as energy meter or PMU at distribution transformer.

A. Classification

Classification-based techniques mainly use the data received from individual meters such as active power, reactive power, voltage, current, time of use, customer information, and inspection notes. It is detecting NTL by performing statistical analysis on load profiles' data to detect unexpected behavior using artificial intelligence techniques such as machine learning or expert systems. Classification methods that are based on end user data can detect NTL in the receiving end only. It uses consumption patterns to predict future expected patterns and compare it with the actual profile. Classification of the load profiles into correct and wrong requires supervised training for the algorithm on historical data with known outcomes to track the performance parameters. In [15] three different methods applied on around 700 K consumer's data which is monthly consumption data four 4 constitutive years as well as around 400 K inspection data to detect NTL. The first method

used to detect NTL is a Boolean Logic expert system which consists of 14 rules created by CHOICE Technologies team where a satisfaction of at least one rule will indicate a non-technical loss. The same 14 rules were fuzzified to depend on membership function and a degree of relation rather than sold zero or one. Also, Support Vector Machine (SVM) classifier was used to create optimal decision function that is based on minimum classification error. It concluded that the SVM and optimized fuzzy logic outperformed the simple Boolean logic. The most common classification-based technique currently used by researchers is SVM with detection rate of approximately (60-70) % [10].

Classification based techniques cannot determine the actual power consumed during the period of attack (i.e. between the time of the attack and the time of detection). In addition to that, advanced attackers can provide demand profile that is difficult to be detected by the algorithm. Also, the supervised training requires a large number of predetermined load profiles which need to be confirmed by many inspections, and in addition to the data used for training could not represent the future attaches' characteristics. Finally, field testing and inspection will be required to confirm the suspected attacks.

B. State Estimation

Another non-hardware approach that is used to detect non-technical losses is state estimation of the distribution secondary which is done by comparing data received from smart meters with the estimated parameters [16], [17], [18], [19]. In [16], smart meter malfunction or tampering is being detected by utilizing distribution state estimation (DSE) algorithm and analysis of variance (ANOVA) to detect meters with non-technical losses. The method firstly will detect an abnormality on distribution transformer level, then it will locate the error on the low voltage side. The proposed method utilizes smart meters that

are connected to consumer house, intelligent electronic devices (IED) that are connected to the distribution transformer, the network topology, and the SCADA system. In [17], state estimation is used to detect non-technical losses in distribution network by assuming that data can be collected from smart meters connected to households and phasor measurement units (PMUs) and intelligent electronic devices (IED) connected to distribution transformer. The method is based on a comparison of two parameters, the voltage and the current; then the difference is calculated between the estimated values by state estimator and the values measured by smart meters. In [18] the technical losses are separated from non-technical losses to estimate the amount of electricity theft by using energy balance between the distribution transformer and energy readings of smart meters. The losses were estimated in [18] by assuming that the relation between the magnitude of the current and the time is piecewise linear. In addition to that, each house is modeled as single-phase load connected by separate cable to the distribution transformer. In [19] the work in [18] was extended to consider the effect of temperature on the technical losses assuming that a sensor near the network will send the temperature data every 30 minutes and will be the same for all users in the group. Besides the assumption of a linear relationship between the time and the current, none of [18] or [19] can detect which meter is in error.

All state-estimation techniques used in the literature assumes that the measurements done in distribution transformer is correct to detect wrong reading in consumer's meter. In addition to that, many of NTL detection techniques that are based on state estimation requires an accurate model of network topology, which can change due to change in cable temperature, system upgrade, and aging of cables. Moreover, the current smart meters

used by utilities do not provide synchro-phasor measurements due to the high cost of this technology at this time; hence, practical challenges such as time delay discrepancy between the readings of typical smart meters and low-frequency resolution of received data is not considered in-state estimation-based NTL detection techniques.

C. Game Theory

Third non-hardware approach found in the literature was based on game theory equilibrium point as optimal choices for distribution utility and consumers. In [4], a game of theory model used to detect NTL by observing the electricity usage behavior when customers are strategic. It considers both investment and electricity tariff structure decisions for the distribution utility for unregulated monopoly as well as perfect competition. The game model used in [4] is the leader-follower game, where the utility company is the leader that chooses first its tariff structure and amount of investment in theft detection and the consumers are the followers where they make their decisions of the amount of electricity used based on that. The utility company assumed to make their decisions based on predetermined number of electricity thieves and the consumers assumed to make their decisions based on tariff structure and the probability of being detected. The probability of being detected is based on the amount of electricity stolen and distribution utility investment in fraud detection; as any of them increases, the probability of detection increases. The distribution utility revenue assumed to come from billed electricity and the fines collected form detected customers. The framework proposed helps in detecting NTL using the expected energy usage by legitimate and fraud consumers with help of a realization of probability density function.

2.1.3 Hardware Solution

Hardware solution proposes redundant meters or other addition of hardware to the metering system to detect and estimate NTL. The additional hardware can be an addition to the monitoring infrastructure and/or improvement of the metering unit. The latest can be achieved by any additional specification to the currently used metering hardware such as sending a signal to utility company when the meter is disconnected from the mains. Improving the monitoring infrastructure can be achieved by adding redundant metering units or other types of sensors to the AMI to help in detecting NTL; a simple example of the addition to the monitoring infrastructure can be doubling the meters to detect wrong readings, this technique will double the cost of meters and it will double the required communication bandwidth; moreover, in some cases, there will be ambiguity about which of the two meters is in error [9]. Doubling meters are usually used for big commercial or industrial loads by some utility companies. Hardware solutions can detect NTL in specific regions only, e.g. adding sensors to the smart meter cannot detect NTL that comes from tapping the distribution line.

2.2 Design and Implementation of Smart Metering System

In the literature, different designs used to implement smart meters that have processing and communication capability which can provide real-time data for the utility and the consumer. A personal computer was used as a central processing unit and user interface in [20], [21]. Microcontrollers were used as main processing units in [22], [23], [24], [25]. Different types of Arduinos were used as processing unit of the smart meter such as Arduino UNO, Arduino PRO, Arduino MICRO, Arduino MEGA, Arduino Zero. These

microcontrollers were programmed using a C++ programming language and can receive voltage and current signals and send control commands to loads. Moreover, these microcontrollers were connected to different communication modules such as Wi-Fi, GSM, and ZigBee. Other types of microcontrollers have been used in prototyping such as STM32F407VG [26] and STM32F107VCT6 [27] from Waveshare, PIC18F4550 [28], [29] and PIC32MX460F512L [30] from Microchip, MSP430FE423A from Texas Instruments [31], and AT89S52 [32].

The communication unit is also required for the smart meter in to send metering data to the utility such as voltage, current, real power, reactive power, time of use, and outages. Also, the communication unit is required to receive the command signals from the utility company. The type of communication used in the smart meter will affect the physical range of the communication channel, bandwidth and data rate, the amount of power consumed by the communication module, and the cost. There are many wired and wireless communication technologies that can allow two-way communication between the smart meter and the utility company. Wired technologies provide high data rates and can be used for home area network, neighborhood area network, field area network and wide area networks. Different wired technologies that are available now are Fiber Optic, DSL, Coaxial Cable, PLC, and Ethernet.

On the other hand, wireless technologies are flexible and have low installation cost and they are recommended for most of neighborhood and field area networks in smart grid [33]. There are different types of wireless technologies that can be added to smart meters such as ZigBee, Wi-Fi, Bluetooth, Cellular, Wireless Mesh, Wi-MAX, and Satellite Internet. Each type has advantages and disadvantages and the most widely used wireless technology

in previous work is ZigBee due to its low power consumption. There are different ZigBee modules that are amiable for prototyping, these modules can be connected to microcontrollers via I/O ports for two-way communication between two microcontrollers. ZigBee based modules were used for prototyping in ([23-26],[30-23]), GSM communication modules were used in [24-27], and power line communication PLC was used in [26], [31]. Using different communication modules, we can perform two-way communication between different smart meters and to the utility. Moreover, using Wi-Fi modules we can connect the smart meters to the internet to provide real-time data and control for the user or the utility. Table 1 shows the comparison of different technologies that can be used in smart grid and smart metering system; it is a recreation of the exact same Table 1 in [33].

Table 1: Different Types of Communication Technologies for Smart Grid Applications in **[33]**

Medium	Technology	Standard/ Protocol	Max. theoretical data rate	Coverage Range	Network		
					HAN BAN IAN	NAN FAN	WAN
Wired Communication Technologies	Fiber optic	PON	155 Mbps–2.5 Gbps	Up to 60 km			x
		WDM	40 Gbps	Up to 100 km			x
		SONE/SDH	10 Gbps	Up to 100 km			x
	DSL	ADSL	1–8 Mbps	Up to 5 km		x	
		HDSL	2 Mbps	Up to 3.6 km		x	
		VDSL	15–100 Mbps	Up to 1.5 km		x	
	Coaxial Cable	DOCSIS	172 Mbps	Up to 28 km		x	
	PLC	HomePlug	14–200 Mbps	Up to 200 m	x		
		Narroband	10–500 kbps	Up to 3 km	x	x	
	Ethernet	802.3x	10 Mbps–10 Gbps	Up to 100 m	x	x	
Wireless Communication Technologies	Z-Wave	Z-Wave	40 kbps	Up to 30 m	x		
	Bluetooth	802.15.1	721 kbps	Up to 100 m	x		
	ZigBee	ZigBee	250 kbps	Up to 100 m	x	x	
		ZigBee Pro	250 kbps	Up to 1600 m	x	x	
	WiFi	802.11x	2–600 Mbps	Up to 100 m	x	x	
	WiMAX	802.16	75 Mbps	Up to 50 km		x	x
	Wireless Mesh	Various (e.g., RF mesh, 802.11, 802.15, 802.16)	Depending on selected protocols	Depending on deployment	x	x	
	Cellular	2G	14.4 kbps	Up to 50 km		x	x
		2.5G	144 kbps			x	x
		3G	2 Mbps			x	x
		3.5G	14 Mbps			x	x
		4G	100 Mbps			x	x
	Satellite	Satellite Internet	1 Mbps	100–6000 km			x

Voltage and current can be measured using different types of sensors. The most widely used sensors are current transformers, shunt resistors, hall effect current sensors, and Rogowski coil. Current transformers are widely used for current sensing due to low power dissipation, low cost, and its high immunity to external interferences. On the other hand, current transformers are not linear and saturate at higher current levels. Also, the secondary winding of current transformer should be kept close by burden impedance and if the secondary side of CT was opened the current transformer will be damaged. There are

different types of CTs available in the market such as ASM series which is used as basic current indicator, AC series that is the most commonly used and it is designed to measure specific rated current, AP series which provides the highest accuracy but low current rating, and C-CT series which can measure current ranges from 0.1 up to 300 A with accuracy of 1%. The current is being measured by measuring the voltage on the burden impedance and then the AC voltage must be conditioned, filtered, sampled, and quantized to be ready as input to the microcontroller. Shunt resistors (i.e. resistor connected series with the line) are very cost effective, but it dissipates big amount of power if the current is high, or if we used shunt resistor with very low resistance the voltage drop will be very small, and we will need very sensitive sensors to measure small voltage drop on the shunt resistor. Another type of current sensor that is widely used for prototyping is hall effect sensor module. It can measure currents up to 150 A and it can be connected to the microcontroller. Another module available is analog current input module from National Instruments (NI 9247 C Series), this module can measure current up to 50 A RMS and it has embedded data acquisition system which has a sampling rate of 50 kS/s. This module provides very accurate measurement, but it costs around 6000 S.R. Similar modules has been used with 5 A RMS current rating (NI 9225 C Series) to implement smart meter in [20]. Hall effect current sensor was used by [22], Digital energy meter [23], current transducer [26], [27].

To measure the voltage potential transformer or voltage divider can be used to scale down the actual voltage. The potential transformer will allow for electrical isolation of low and high voltage sides then the secondary of the transformer is connected to an analog to digital converter to convert the AC voltage to a digital output representing quantized voltage signal. On the other hand, if resistive voltage divider is used to scale down the voltage

optocoupler should be used between the high voltage side and the low voltage side for isolation.

For the processing, communication, and control units to perform tasks they require a DC power source. The power can be taken from the main line to an AC to DC converter and then to different units of the smart meter. Moreover, a backup rechargeable battery is needed to provide required energy during outages and emergencies. Moreover, LCD display is needed to present the real-time values of different electrical quantities such as active power and power factor.

CHAPTER 3

METHODOLOGY

This chapter will explain the methodology used to detect and correct the non-technical losses in the distribution network. Section 3.1 will provide the general description of the system; i.e. metering unit and detection algorithm. In Section 3.2, a novel method will be proposed to estimate the service cable impedance. Section 3.3 will then propose a modified algorithm that considers the power losses into account. Finally, Section 3.4 will propose a novel derived unit of measurement to be measured by smart meters that will help in estimating the network topology and energy losses when there is time skew between the measurements and/or the measurements are taken at low resolution.

3.1 General Description of the System

3.1.1 Design of Metering Unit

The most basic function of the metering unit is to measure the voltage, current, and power factor and then calculate the real power, and reactive power consumed in a specific period. Unlike conventional power meters, smart meters have processing and communication capability which can provide real-time data for the utility and the consumer. The general block diagram of the smart meter is shown in Figure 3.1 and the schematics of the final design in shown Appendix C. The details of each component in the final design is discussed.

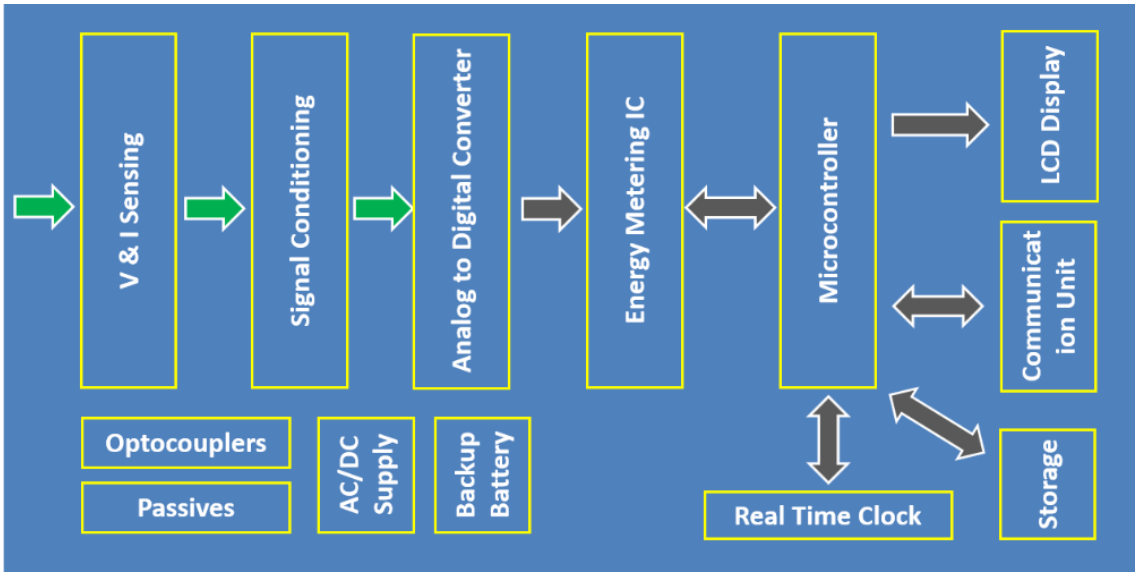

Figure 3.1: General block diagram of smart meter

A. Measuring the Voltage

There are different methods that can be used to measure the voltage such as potential transformer or voltage divider circuit. Voltage divider circuit uses simple two resistors to step down the line voltage to value that is suitable to be read by ADC. This method is low cost since it needs only two resistors to perform the task, but on the other hand, this method will not isolate the high voltage circuitry form the low voltage electronics. Therefore, surge protection can be used to protect the low voltage electronics form high voltage surges. In addition to that, optocouplers can be used also to isolate the two grounds. It is desired to choose high value resistors to divide the voltage to minimize the power losses in the resistors. Another method that can be used to measure the voltage is by using potential transformers which will step down the voltage to desired level that is suitable for the ADC. This method allows isolation of high voltage circuitry form the low voltage circuitry, but the cost will be higher than the voltage divider method. Potential transformers are similar to power transformers, but they are rated at much lower power that is consumed by the burden resistors on the secondary side of the potential transformers.

In our design, we are going to use small 1.1VA transformer to step down the voltage from 230V RMS to 10V RMS [34]. Voltage divider circuit will be used to further step down the voltage to the range of analog to digital converter in the microcontroller.

Figure 3.2: 230/10V transformer

B. Measuring the Current

Current can be measured using different sensors such as shunt resistors, hall effect current sensors, Rogowski coils, and current transformers. Shunt resistors cost is the lowest, but they dissipate big amount of power for reasonable voltage drop. E.g. for voltage drop of 1V at 100A line current, the shunt resistor must be 10 mΩ which will dissipate 100W when the line current is 100A. On the other hand, using very small shunt resistor will result in very small voltage drop which cannot be detected by common ADC used with energy measurement IC unless an amplifier is used, which means additional cost and power consumption. In addition to that, shut resistor terminals will be directly coming from the high voltage line and isolation circuitry will be required for protection of electronic components. Figure 3.3 shows commercially available shunt resistor used to measure current up to 100A, its resistance is 1 mΩ with tolerance of 0.25%.

Figure 3.3: Commercially available shunt resistor

Hall effect based current sensors is generating output voltage proportional to the magnetic field generated by the current that passes in the conductor. This type of sensor provides isolation between high voltage line and the electronic components. In addition to that, the power consumption of hall effect based current sensors is low. On the other hand, hall effect current sensors are not immune to magnetic interference and the measurements can be disturbed by external magnetic fields. Figure 3.4 shows commercially available 100A hall effect based current sensor which can be used for both AC and DC currents.

Figure 3.4: Commercially available hall effect based current sensor

Rogowski coil sensors are used to measure the AC current. It provides output proportional to the rate of change of current. The coil is wounded around non-magnetic core, which makes them operate linearly over wide range of currents due to the absence of iron core.

On the other hand, the output voltage is not directly proportional to the primary current, and integrator circuit is required to integrate the voltage waveform to represent the current. The integrator circuit requires DC supply and will introduce more cost and losses in the metering unit. Figure 3.5 shows 100A commercially available Rogowski coil.

Figure 3.5: Commercially available Rogowski coil

The most common type of current sensor that is currently used in smart meters is the current transformer (CT), current transformers convert the current in primary side into attenuated current in secondary side which passes through an ammeter (short circuit) or burden resistor for measurement. Current transformers are different from voltage transformers since the number of turns on the primary side is only one turn (the conductor in which the current passes) or very few turns. Current transformer secondary side should never be kept as open circuit since that will damage it because the current in the primary side is not affected by the secondary side impedance.

Current transformers provide isolation between the primary and secondary side and typical current transformers used for metering and protection converts full-scale primary current into 1A or 5A secondary current in most industrial scale metering and protection systems. On the other hand, the current transformers used by residential smart meters usually have much less secondary current. Current transformers consume a low amount of power and

provide high accuracy, but they saturate when the primary current exceeds the limit of the current that can be handled by the iron core. Figure 3.6 shows 100A commercially available current transformer.

Figure 3.6: Commercially available Current Transformer

Current transformer is used in this design to measure the line currents as can be seen in Figure 3.6 [35]. Since the experiment will be performed on programmable loads in the lab and the measurements will be much less than an actual residential load profile, the current transformers used are rated at 80A for check meters and 30A for regular meters to utilize the full range of CT which leads for better accuracy in measurement of current. Some of the current transformers' specification are shown in Table 2.

Table 2: CT Specification **[35]**

Attribute	30A CT	80A CT
Rated frequency (Hz)	50/60	50/60
Operating current range (A_{rms})	0.1 to 30	0.1 to 80
Turns ratio	3000:1	3000:1
Current magnitude accuracy	1%	1%
Full scale output current (mA_{rms})	10	26.6
Phase shift (degrees)	1.7±1.0	1.7±1.0
Withstanding voltage (V_{rms})	2200	2200

The output voltage characteristics at different values of burden resistors for the 30A CT is shown in Figure 3.7. We can see the effect of burden resistor on the output voltage and the saturation of the CT. High values of burden resistors cause CT saturation at values less than the rated. In addition to that, more power will be consumed in the burden resistor. On the other hand, very small values of burden resistor will lead very small output voltage signal which will be less immune to external noise (less SNR).

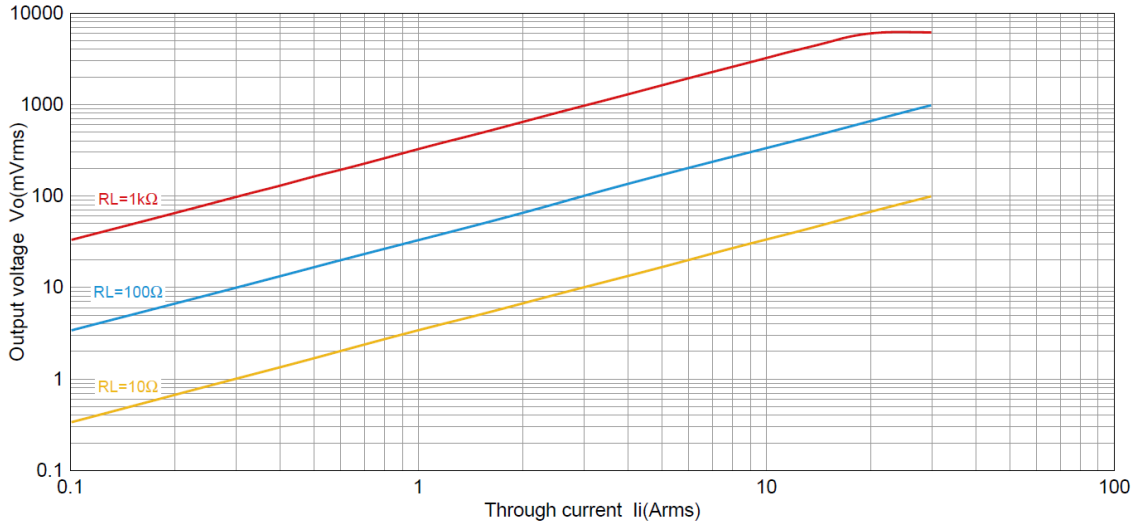

Figure 3.7: Output voltage characteristics of the 30A CT **[35]**

C. Signal Conditioning

Signal conditioning is necessary before applying the real-time signal to the analog to digital converter. The essential analog signals that are measured by the smart meters are the voltage and the current, where the voltage is sinusoidal waveform which may contain some harmonics and the current can take any shape depending on the type of load that draws the current and hence in most cases, the current waveform will contain more harmonics than the voltage waveform. To get the best accuracy and low signal to noise ratio, the analog signal must be manipulated to minimize external noise.

There are many processes performed for signal conditioning such as amplification, attenuation, conversion, isolation, filtering, and linearization. Here we will explain the most common signal conditioning types used in smart meters.

1) Amplification:

Amplification is used to increase the voltage level to better utilize the full range of the analog to digital converter ADC and consequently higher resolution and better sensitivity.

Amplification must be performed just after sensing the signal from the sensor to minimize external noise in the path of the analog signal, this will maximize the signal to noise ratio in the signal measured at the output of the signal. Since the voltage and current transformers that we will use in this design will not need any amplification because of their relatively high secondary side voltage.

2) Attenuation:

Attenuation is required to reduce the range of sensor output analog signal to the range of ADC. It is preferable to perform attenuation as close as possible to the ADC to increase SNR. In the smart meter that we designed, the voltage transformer output is 10V, but the ADC works in the range of ±1.65V. Therefore, the output voltage of voltage transformer is attenuated using voltage divider resistors to reduce the 14.14 peak voltage to value less than 1.65V. Therefore, a voltage divider of 1kΩ and 100Ω used to reduce the voltage by a factor of 11, which means at a rated voltage of 230V the secondary voltage will be 10V and the voltage after voltage divider circuit will be 0.909V (peak of 1.28V). Now, the ADC can measure voltages in the range of 0 up to 295V. The power losses in the transformer's burden resistors is around 91mW where the voltage transformer is rated at 1.1VA. Here we used relatively big values of secondary burden resistors to reduce the power losses and increase the accuracy since the transformer's voltage regulation will be low when used at much lower than its rated power.

Another factor that must be considered is the accuracy of the resistor over the operating range since the value of the resistor can change due to change in temperature. The temperature of the resistor can change due to change of environment temperature or heat generated by the power dissipation in the resistor. Therefore, it is necessary to choose a

resistor with low temperature coefficient and rated at higher power dissipation value than operating range required. Figure 3.8 shows the 1kΩ metal film resistor we used, the 100Ω resistor also metal film resistor that has the exact same characteristics. The burden resistors used here are 0.25W metal film resistors having temperature coefficient 25ppm/℃ (parts per million per degree centigrade), Table 3 shows the detailed attributes of the resistors used.

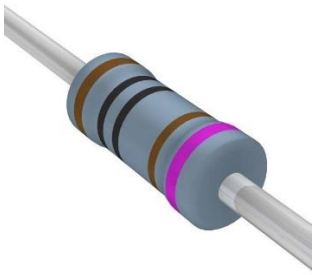

Figure 3.8: 1kΩ metal film resistor

Table 3: Resistors' Attributes

Tolerance	±0.1%
Composition	Metal film
Operating temperature	-55℃ to 155℃
Temperature coefficient	±25ppm/℃
Rated power	0.25W

3) Conversion:

The output of the current transformer is attenuated current, but the ADC input need to be voltage signal, therefore, the current signal need to be converted to a voltage signal using burden resistor. The burden resistor used should be selected so that full scale of ADC is

utilized and making sure that the CT will not be saturated at values in the range of interest. The burden resistor used are thin film resistors with values of 36 and 120 Ohms for 80A and 30A CTs respectively.

4) Isolation:

Isolation of low voltage circuitry from high voltage circuity is necessary to avoid damage to electronic components. Ground isolation can be achieved either by using optical isolation or electromagnetic isolation. Optical isolation can be achieved by using optoisolator which transfers an electrical signal from one side to another using light. Since many commercial smart meters have voltage divider circuit directly connected to the high voltage circuit, optoisolators are used to isolate the ground of ADC and the microcontroller form the high voltage ground. In our design, the potential transformer will provide electromagnetic isolation between the low voltage and the high voltage circuitry.

D. Analog to Digital Conversion

Analog to digital converter (ADC) converts analog signal to digital signal that can be processed in the energy measurement IC or the microcontroller. Three main characteristics must be considered in the selection of analog to digital converter; i.e. resolution, rate, and range. The resolution represents the number of discrete values that represent the analog signal, usually expressed in bits. E.g. 12-bit ADC can have 4096 different levels that can represent the analog input. The higher the resolution, the lowest the difference between the actual analog input and the digitalized output (lower quantization error). In the this design, we are going to use the 12-bit ADC intenerated in ATSAM3X8E microcontroller [36] that is utilized by Arduino DUE board [37].

The rate of the analog to digital converter is the number of samples per second since the voltage and current waveforms are not purely sinusoidal, oversampling is essential for accurate RMS calculations. The ATSAM3X8E microcontroller has a sampling rate of 1 MSPS [36], but the actual sampling will depend on the length of RMS calculations' instructions executed and the clock frequency (i.e. 84 MHz).

The range of analog to digital converter is the input voltage range that can be quantized by the analog to digital converter. To reduce the quantization error, the full range of ADC must be utilized and some margin for overvoltage or overcurrent incidents. In the microcontroller that we will use, the range is 0 to 3.3V. The voltage and the current transformers' neutrals will be connected to 1.65V with respect to the microcontroller ground for DC biasing as shown in Figure 3.9 and Figure 3.10 respectively.

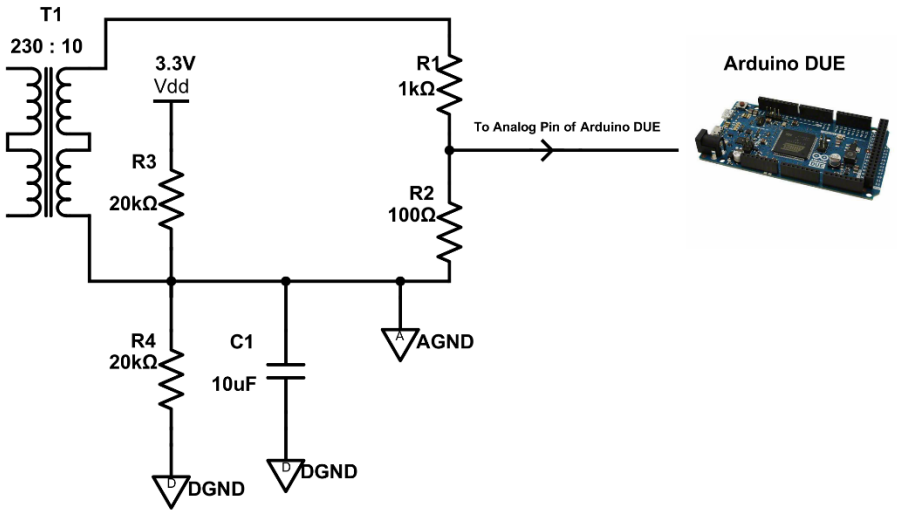

Figure 3.9: Voltage transformer connection

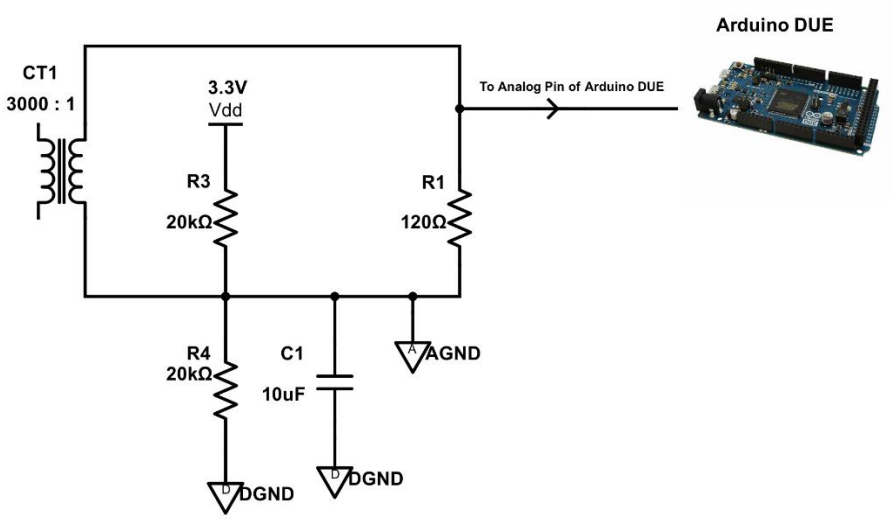

Figure 3.10: Current transformer connection

E. Energy Metering IC

Some of commercial smart meters have energy metering IC EMIC in addition to the microcontroller to do all the processing required for energy calculations. Others contain only the microcontroller, which will be used to perform all the metering calculations and communications. The energy metering IC is basically a fixed function digital signal processor DSP that performs signal processing required for metering applications. The digital signal processing that can be performed by the EMIC are scaling, filtering, integration, phase calibration, zero-crossing detection, RMS calculations, energy calculations, and THD calculations. Some EMICs have embedded programmable gain amplifiers PGA and analog to digital converters in addition to the digital signal processor. Figure 3.11 shows the functional block diagram of commercially available metering IC (i.e. ADE7880 from Analog Devices).

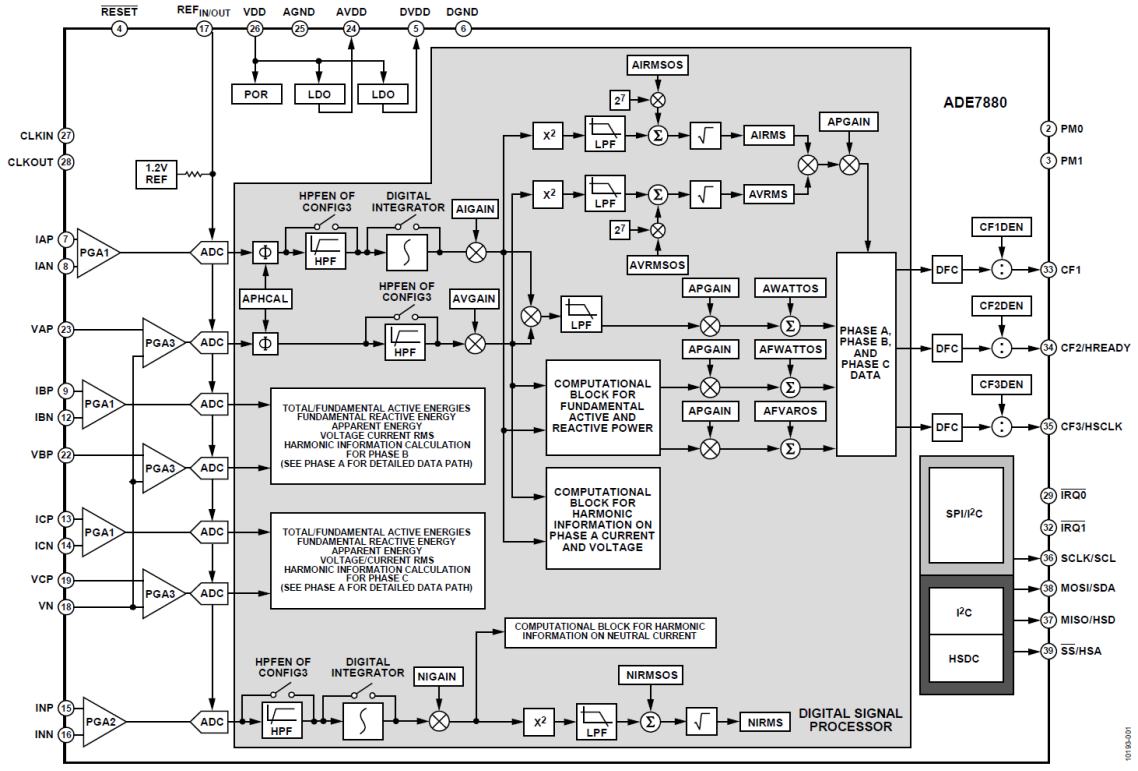

Figure 3.11: Commercially Available Energy Metering IC **[38]**

Before placing the energy metering IC for operation. It should be firstly configured by selecting operation mode, activating the embedded filters, and activating embedded integrators according to the requirement of each design. Then the calibration values such as phase compensation and scaling factors for both voltage and current should be configured. The energy metering ICs are usually slave devices, and they can be configured by sending write command via SPI/I^2C followed by the address of register to be configured flowed by the value in twos complement format. Based on the configuration of the energy metering IC, the DSP inside the IC will perform all the calculations in harmony. The calculated values are then stored in harmonic calculation registers that can be accessed by the microcontroller via SPI or I^2C communication protocols. The harmonic calculation registers can be accessed by the microcontroller by sending read command to the EMIC

followed by the register address. The EMIC will provide the value of harmonic calculation in the register specified by the microcontroller after receiving the address of register immediately. The microcontroller should be programmed according to the datasheet of EMIC; each EMIC has different interface timing parameters as well as different communication protocols.

E.g. if SPI is chosen to be the communication interface, the serial clock signal will be provided by the microcontroller and the MOSI, MISO, SS will be connected as shown in Figure 3.12. The speed of data transmission will depend on the frequency of the serial clock (SCLK), it can be in the range of few MHz's for common EMICs. There are four operation modes for SPI that defines the normal state of serial clock when there is no operation (normally high or normally low) and the time where the data is sampled (i.e. sampled on clock transition from high-to-low or sampled on lock transition from low-to-high). Each EMIC has its own SPI mode defined by the manufacturer that must be followed for communication.

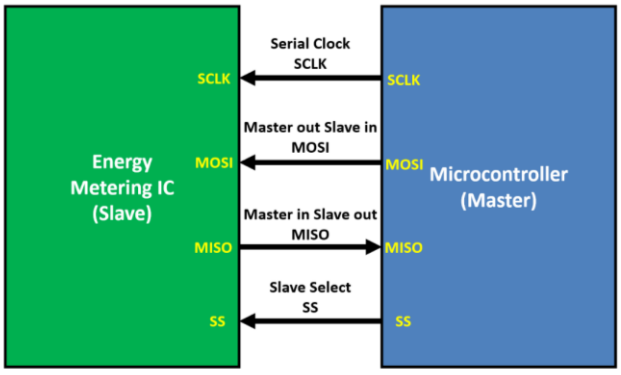

Figure 3.12: SPI interface between the EMIC and the microcontroller

The microcontroller can perform write operation by firstly enabling the slave by making SS pin low. Then the write command (sequence of bits defined by EMIC manufacturer)

will be placed on the MOSI data bus. Synchronously, the EMIC will sample the data from MOSI data bus and initialize the write operation. After that, the microcontroller will place the address of register on the MOSI data bus which will let the EMIC point to the target register. Finally, the value to be written will be placed on MOSI data bus and the EMIC will write that value to the register. It is common practice in industry to read back the value form the register to confirm successful write operation. The read operation has the same sequence as write operation except that the register value will be transmitted on the MISO data bus starting with the first clock transition after the last bit of register address received.

In our design, the microcontroller will be used to do all the digital signal processing required for metering.

F. Microcontroller

The brain of the smart meter is the microcontroller, it performs all the tasks such as information management, user interface, communication management, calculation of electricity bill, application of tariff structure, data storage, recording incidents, and tampering detection. In addition to that, it also can replace the energy metering IC and the analog to digital converter. In our design, we are going to use the microcontroller to perform all the tasks of the three blocks shown in Figure 3.1 (i.e. ADC, EMIC, and the microcontroller).

The microcontroller that will be used for the design is Arduino DUE [37], which utilizes the powerful 32-bit Atmel SAM3X8E microcontroller [36]. Figure 3.13 shows a top view of Arduino DUE board which clearly shows all the I/O pins. Arduino is open source hardware and software platform, which means all the hardware design files and schematics

as well as the software tools are available for free and can be used by anyone. Hence, all the Arduino boars can be duplicated from the schematics and used for any commercial or non-commercial products, but without using Arduino trademark. Arduino is the first open source hardware that is widely spread, which created a big global community that will accelerate the growth of the tool and its applications.

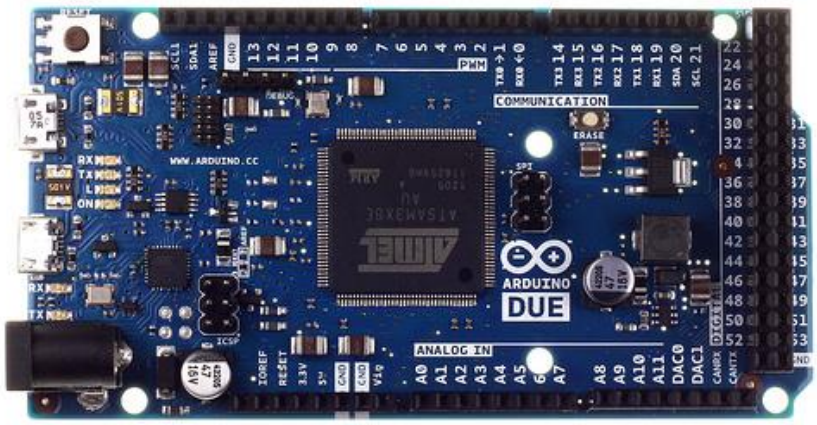

Figure 3.13: Top view of Arduino DUE board

The Arduino DUE has 12 analog input pins that can be configured as a maximum of 12-bit ADC. In addition to that, it has 2 digital to analog converters DAC having a resolution of 12-bits. Moreover, it has 54 digital I/O pins where 12 of them can be used for pulse width modulation MWM. It operates at 84 MHz clock frequency and can provide up to 800mA on the 3.3V pin.

The microcontroller will perform all the computations required to determine the true RMS voltage and current, active power, reactive power, and power factor. First digital low pass filter will be applied to the digital signals that represent the analog values. The Arduino DUE can sample at 12-bit resolution, which means the analog signals will be represented by 12-bit numbers (i.e. 0 to 4095). After application of the low pass filter and magnitude

and phase compensation, the voltage and current samples (i.e. $V[i]$ and $I[i]$) will be ready for calculations. Two types of computations will be performed on the samples (i.e. instantaneous calculations and the RMS calculations). The instantaneous calculations will determine the instantaneous power using the two samples available as shown below:

$$P[i] = V[i] \times I[i] \tag{1}$$

where $P[i]$ is the instantaneous power at instant i,

$V[i]$ is the instantaneous voltage at instant i, and

$I[i]$ is the instantaneous current at instant i.

The sequence of uniformly spaced (in time) values for a specific number of full voltage waveform cycles will be used for RMS calculations as the following:

$$V_{RMS}[n] = \sqrt{\frac{1}{k}\sum_{i=1}^{k} V[i]^2} \tag{2}$$

$$I_{RMS}[n] = \sqrt{\frac{1}{k}\sum_{i=1}^{k} I[i]^2} \tag{3}$$

where k is the number of instants used for RMS calculations,

$V_{RMS}[n]$ is the RMS voltage during time interval n, and

$I_{RMS}[n]$ is the RMS current during time interval n.

The active power is basically the average of instantaneous power and can be calculated by averaging the sequence of instantaneous values as shown below:

$$P[n] = \frac{1}{k}\sum_{i=1}^{k} P[i] \tag{4}$$

where $P[n]$ is the active power at time interval n.

The rest of quantities can be calculated using RMS voltage, RMS current, and active power as:

$$S[n] = V_{RMS}[n] \times I_{RMS}[n] \tag{5}$$

$$Q[n] = \sqrt{S[n]^2 - P[n]^2} \tag{6}$$

$$p.f.[n] = \frac{P[n]}{S[n]} \tag{7}$$

where $S[n]$ is the apparent power during time interval n,

$Q[n]$ is the reactive power during time interval n, and

$p.f.[n]$ is the power factor during time interval n.

The calculations used here can measure the true RMS values of the quantities, which will work for any type of AC signals (i.e. both sinusoidal and non-sinusoidal waveforms). The number of instants captured (i.e. k) during the period of interest depend on the speed of ADC as well as the speed of code execution in the microcontroller. Therefore, we used the powerful 32-bit Arduino DUE microcontroller which have ca lock speed of 84 MHz and ADC update rate of 1 MSPS.

The duration of time interval n can be configured by modifying the code that calculates the RMS values. In our design, we used ta ime interval of 1 second in the calculation, so all the values calculated will represent the average values during 1 second (i.e. 60 cycles for the 60Hz system).

G. LCD Display and Data Storage

LCD display is needed to display the measurements and billing information for the user. In addition to that, data recording is essential for the smart meters to accumulate the data of measurements and alarms for certain period. In our design, we used colored Arduino

1.77" LCD display which comes with embedded micro SD card module. Figure 3.14 shows front view of the display used for our design.

Figure 3.14: Arduino 1.77" LCD display **[39]**

The LCD display and the micro SD card module will be connected to the microcontroller via SPI interface as shown in Figure 3.15. The SPI master can be used to control multiple slaves by activating the slave that need to be communicated with (it can be done by making the slave select pin low). The serial clock SCLK, master in slave out MISO, and master out slave in MOSI are shared between all the slaves.

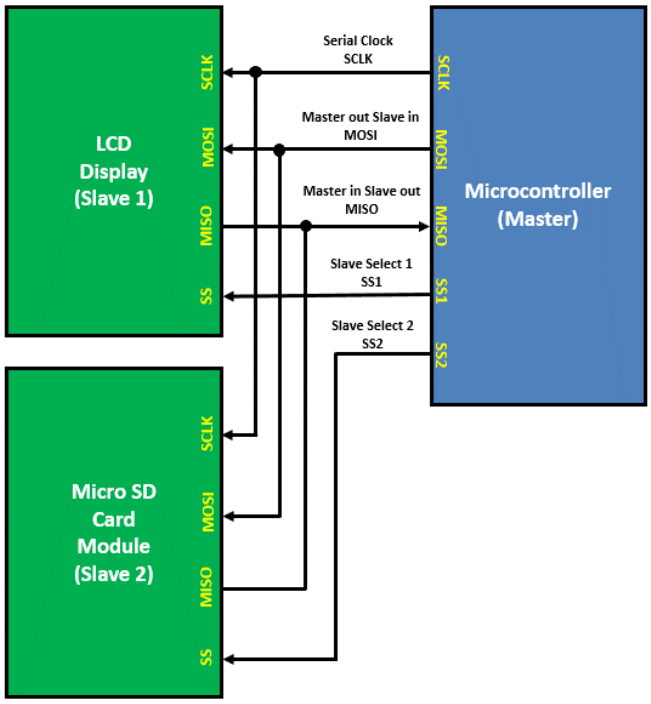

Figure 3.15: SPI Interface between the microcontroller and the LCD and SD card

H. Real Time Clock

To keep track of time accurately, real-time clock RTC with battery is required so that the system doesn't lose the track of time when the power goes down. In our design, we used RTC module that utilizes the DS3231 IC which has a crystal oscillator that is temperature compensated [40]. It keeps track of year, month, day, hour, minute, and second and can provide the time via I^2C communication protocol for data logging. It is accurate up to 3.5 ppm (parts per million) over temperature range of -40°C to 85°C.

Figure 3.16: DS3231 accurate integrated RTC

The DS3231 can communicate with the master device (i.e. the microcontroller) via I^2C communication protocol. Unlike SPI interface, the I2C uses only two connections for data transmission (i.e. clock line and data line) as shown in Figure 3.17. In addition to that, multiple devices can be connected to the same two buses (SCL and SDA) where each device will be activated when the master sends the device address on the serial data line.

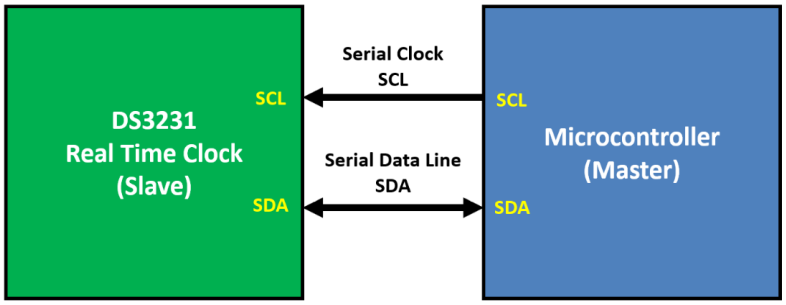

Figure 3.17: I^2C Interface between the microcontroller and the RTC

Both SCL and SDA are connected to pull up resistor (i.e. their state is normally high when there is no communication). The communication is initiated when the master place a start bit on the SDA line (i.e. pulling SDA line low), after that the master will start the clock for synchronous communication. After that, the microcontroller will send the device address on the SDA line so that RTC is initiated (for the DS3231 the device address is 1101000). Then the microcontroller will send write bit (i.e. 0) and the RTC will respond by sending

back acknowledge bit (i.e. 0) to confirm successful initiation. After that, the microcontroller will send word address to the RTC to set the register pointer to the required register. Now, the value of the register can be read by setting the microcontroller to send read bit (i.e. 1) to initiate read operation, next the RTC will send acknowledge bit (i.e. 0) to the microcontroller to indicate that the RTC read is enabled. Then the RTC will output the data and the microcontroller will place acknowledge bit each time one byte is received.

I. Communication Unit

The communication unit is required for the smart meter in to send metering data such as RMS voltage, RMS current, real power, reactive power, and time of use to the utility company. Also, the communication unit is required to receive the command signals from the utility for testing and clock calibration. There are many wired and wireless communication technologies that can allow two-way communication between the smart meter and the utility company. The type of communication used in the smart meter will affect the physical range of the communication channel, bandwidth and data rate, the amount of power consumed by the communication module, and the cost. Wired technologies provide high data rates and can be used for home area network, neighborhood area network, field area network and wide area networks. Different wired technologies that are available now are Fiber Optic, DSL, Coaxial Cable, PLC, and Ethernet.

On the other hand, wireless technologies are flexible and have low installation cost and they are recommended for most of the neighborhood and field area networks in smart grid [33]. There are different types of wireless technologies that can be added to smart meters such as ZigBee, Wi-Fi, Bluetooth, Cellular, Wireless Mesh, Wi-MAX, and Satellite

Internet. Each type has advantages and disadvantages and the most widely used wireless technology is ZigBee due to its low power consumption.

In the proposed design, we are going to use ZigBee module which is capable to communicate with the microcontroller using serial communication. It can be used as transmitter or receiver, which makes it good choice for mesh networks that features low power consumption. Figure 3.18 shows the ZigBee module that is used in this design.

Figure 3.18: ZigBee module, (Digi XBee S2C ZigBee)

Some features of this module is shown in Table 4.

Table 4: ZigBee module general specifications

Attribute	Value
Non-line of sight range (indoor)	60 m
Lin-of-sight range (outdoor)	1200 m
Current during transmission	33 mA (boost mode) 59 mA (normal mode)
Current during receiving	28 mA (boost mode) 45 mA (normal mode)
Operating voltage	2.1 V ~ 3.6 V

The ZigBee module can be interfaced with the microcontroller using SPI as shown in. The SPI master can be used to control multiple slaves by activating the slave that need to be communicated with (it can be done by making the slave select pin low). The serial clock SCLK, master in slave out MISO, and master out slave in MOSI are shared between all the slaves.

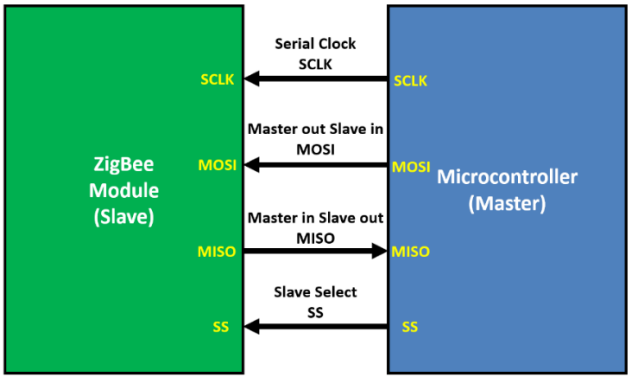

Figure 3.19: SPI Interface between the microcontroller and the ZigBee module

The schematics of the final design is shown in Appendix C. Next, the detection algorithm is explained in detail.

3.1.2 Detection Algorithm

For detection algorithm, a novel method proposed in [9] will be used to design a system that can detect and correct errors in smart meters. This method uses coding which is originally used to detect and correct binary data in communication systems. It is done by adding redundant data to the original message, this redundant data will be analyzed by the receiver to detect and correct errors. The redundant data is designed liner combination of original bits which carry some of their characteristics. In [9], Hamming code is used to detect and correct errors of meters, this method needs an accurate estimation of power losses in the cable. In this section, the Hamming code and its application to the smart

metering system will be explained in detail. Subsections 3.1.2.1 and 3.1.2.2 is explaining the hamming code and its application to smart meters; the model and equations derived are performed on example of 4 regular meters and 3 check meters for simplicity. The example can be generalized for N regular meters and M check meters where the condition $N \leq 2^M - M - 1$ must be satisfied.

A. Coding

Coding was originally used in binary data transmission where we need to transmit N bit via channel, M additional bits can be added that carries designed charlatanistic of original N bits. Which will result in total of $N + M$ bits need to be transmitted. Figure 3.20 shows simplified model of communication system that uses coding to detect and correct errors. Hamming code is one of the coding schemes which was developed in 1950 by Richard Hamming to detect and correct single error in binary data transmission. This code uses M check bits to detect and correct $2^M - M - 1$ data bits; e.g. if $M = 10 \rightarrow 2^{10} - 10 - 1 = 1013$, here only 10 bits required to detect and correct single error in 1013 data bits.

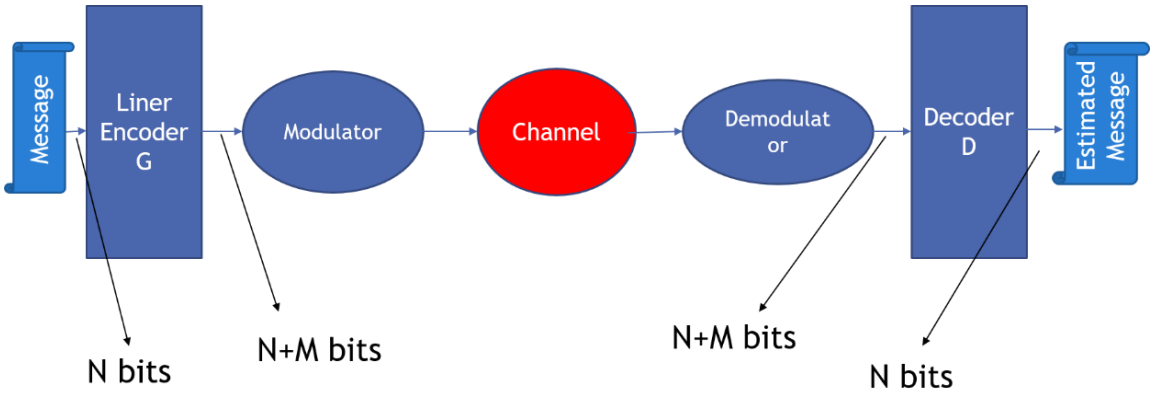

Figure 3.20: Coding in Communication System

Here, the coding of 4 data bits with 3 check bits are used (i.e. Hamming(7,4)) to show how the hamming code works; assume that we want to code the following block of data that consists of four bits:

$$\boldsymbol{b} = [b_1 \;\; b_2 \;\; b_3 \;\; b_4] \tag{8}$$

where $\boldsymbol{b}$ is the vector of data bits to be transmitted, and

b_i is bit number i to be transmitted.

The vector of data bits will be multiplied by the generator matrix G to generate code word $\boldsymbol{x}$ which consist of 7 bits as shown:

$$\begin{aligned} \boldsymbol{x} = \boldsymbol{b} \cdot G &= [b_1 \;\; b_2 \;\; b_3 \;\; b_4] \left(\begin{array}{cccc|ccc} 1 & 0 & 0 & 0 & 1 & 1 & 0 \\ 0 & 1 & 0 & 0 & 1 & 0 & 1 \\ 0 & 0 & 1 & 0 & 0 & 1 & 1 \\ 0 & 0 & 0 & 1 & 1 & 1 & 1 \end{array}\right) \\ &= [x_1 \;\; x_2 \;\; x_3 \;\; x_4 \;\; x_5 \;\; x_6 \;\; x_7] \end{aligned} \tag{9}$$

Here the first four values will represent the message bits that will be sent, and the last three numbers are check parity bits which carry the designed linear combination of original message bits (here it is a Modulo-2 addition, i.e. XORing bits). Also, we can see that the generator matrix G can be rewritten as:

$$G = [\, I_{4\times4} \;\; H_{4\times3} \,] \tag{10}$$

where $I_{4\times4}$ is identity matrix and $H_{4\times3}$ is designed based on hamming code algorithm is simplified by Table 5 and steps below:

1- Count the number of bits required to be sent (i.e. N)
   - Here it is 4 bits
2- Calculate the number of parity check bits required using ($N = 2^M - M - 1$)
   - Here it is 3 bits
3- Create table with the first row shows bit positions

- Here there are $4 + 3 = 7$ positions

4- All bit positions of power two are positions of parity check bits
   - Here they are P1, P2, and P3

5- All other bits are data bits
   - Here they are D1, D2, D3, and D4

6- Create row for parity bit coverage
   - Here they are named P1, P2, and P3

7- Find the data bits covered by each parity bit (Px) systematically as following
   - Starting at position of parity bit (Px)
     i. For first parity bit (P1): mark one position and leave one position
     ii. For second parity bit (P2): mark two positions and leave two positions
     iii. For third parity bit (P3): mark four positions and leave four positions
     iv. For parity bit number M (PM): mark 2^M positions and leave 2^M positions until reaching the end of table

8- Now $H_{4\times3}$ can be filled as shown below
   - First column related to first parity bit (i.e. P1)
   - So, P1 covers D1, D2, and D4 which leads to first column to be $[1\ 1\ 0\ 1]^T$
   - Similarly, P2 covers D1, D3, and D4 which leads to second column to be $[1\ 0\ 1\ 1]^T$
   - Similarly, P3 covers D2, D3, and D4 which leads to third column to be $[0\ 1\ 1\ 1]^T$

Table 5: General Rule for Hamming Code

Bit Position	1	2	3	4	5	6	7
Data Bits	P1	P2	D1	P3	D2	D3	D4
P1	x		x		x		x
P2		x	x			x	x
P3				x	x	x	x

The code word $\boldsymbol{x} = [x_1\ x_2\ x_3\ x_4\ x_5\ x_6\ x_7]$ is transmitted and the received string will be $\hat{\boldsymbol{x}} = x + e = [\hat{x}_1\ \hat{x}_2\ \hat{x}_3\ \hat{x}_4\ \hat{x}_5\ \hat{x}_6\ \hat{x}_7]$ where $\boldsymbol{e}$ is an error vector with elements $\{0,\ 1\}$ and the addition is Modulo-2 addition; for case of error in x_5, the error vector e will be as $\boldsymbol{e} = [0\ 0\ 0\ 0\ 1\ 0\ 0]$ and $\hat{x}_5 \neq x_5$.

The received string $\hat{\boldsymbol{x}}$ will be multiplied by the decoding matrix D to detect if there is an error and the location of the error. The decoding matrix D must be orthogonal to generator matrix G so that their multiplication results a matrix of size $N \times N$ of all elements equal to zero as shown below:

$$G \cdot D = \left(\begin{array}{cccc|ccc} 1 & 0 & 0 & 0 & 1 & 1 & 0 \\ 0 & 1 & 0 & 0 & 1 & 0 & 1 \\ 0 & 0 & 1 & 0 & 0 & 1 & 1 \\ 0 & 0 & 0 & 1 & 1 & 1 & 1 \end{array}\right) \begin{pmatrix} 1 & 1 & 0 \\ 1 & 0 & 1 \\ 0 & 1 & 1 \\ 1 & 1 & 1 \\ 1 & 0 & 0 \\ 0 & 1 & 0 \\ 0 & 0 & 1 \end{pmatrix} = \begin{pmatrix} 0 & 0 & 0 \\ 0 & 0 & 0 \\ 0 & 0 & 0 \\ 0 & 0 & 0 \end{pmatrix} \qquad (11)$$

We can see that the decoding matrix is taking the form $D = [H_{4\times3}^T\ \ I_{3\times3}]^T$ where, $I_{3\times3}$ is identity matrix of size 3 and $H_{4\times3}^T$ is matrix of size 3×4 which is transpose of $H_{4\times3}$. Now we will define syndrome vector as following:

$$\boldsymbol{s} = \hat{\boldsymbol{x}} \cdot D = [s_1\ \ s_2\ \ s_3\ ] \qquad (12)$$

Which is of size 1×3 and it indicates whether there is an error or not and the location of the error. E.g. when $\boldsymbol{s} = [0\ 0\ 0]$ it is indication of no error, and when $s = [1\ 1\ 0]$ it indicates an error in $\hat{x}_1$. The location of error can be determined by comparing the form of syndrome vector to the rows of the decoding matrix D, where each row of D represents the form of syndrome vector for an error in the bit position equal to the row number in decoding

matrix D. Next, the error detection calculation is shown for two cases, i.e. no error and single error in data bits.

1) No Error:

When there is no error in any of the transmitted bits then, $\hat{\boldsymbol{x}} = \boldsymbol{x}$, as shown:

$$s = x \cdot D = [x_1 \ x_2 \ x_3 \ x_4 \ x_5 \ x_6 \ x_7] \begin{pmatrix} 1 & 1 & 0 \\ 1 & 0 & 1 \\ 0 & 1 & 1 \\ 1 & 1 & 1 \\ 1 & 0 & 0 \\ 0 & 1 & 0 \\ 0 & 0 & 1 \end{pmatrix} = b \cdot G \cdot D$$

$$= [b_1 \ b_2 \ b_3 \ b_4] \left(\begin{array}{cccc|ccc} 1 & 0 & 0 & 0 & 1 & 1 & 0 \\ 0 & 1 & 0 & 0 & 1 & 0 & 1 \\ 0 & 0 & 1 & 0 & 0 & 1 & 1 \\ 0 & 0 & 0 & 1 & 1 & 1 & 1 \end{array}\right) \begin{pmatrix} 1 & 1 & 0 \\ 1 & 0 & 1 \\ 0 & 1 & 1 \\ 1 & 1 & 1 \\ 1 & 0 & 0 \\ 0 & 1 & 0 \\ 0 & 0 & 1 \end{pmatrix} \tag{13}$$

$$= [b_1 \ b_2 \ b_3 \ b_4] \begin{pmatrix} 0 & 0 & 0 \\ 0 & 0 & 0 \\ 0 & 0 & 0 \\ 0 & 0 & 0 \end{pmatrix} = [0 \ 0 \ 0]$$

2) One Error:

When there is an error in any of the transmitted bits then $\hat{\boldsymbol{x}} = \boldsymbol{x} + \boldsymbol{e}$, as shown:

$$\boldsymbol{s} = \hat{x} \cdot D = [\hat{x}_1\ \hat{x}_2\ \hat{x}_3\ \hat{x}_4\ \hat{x}_5\ \hat{x}_6\ \hat{x}_7] \begin{pmatrix} 1 & 1 & 0 \\ 1 & 0 & 1 \\ 0 & 1 & 1 \\ 1 & 1 & 1 \\ 1 & 0 & 0 \\ 0 & 1 & 0 \\ 0 & 0 & 1 \end{pmatrix} = (b \cdot G + e) \cdot D$$

$$= \left([b_1\ b_2\ b_3\ b_4] \left(\begin{array}{cccc|ccc} 1 & 0 & 0 & 0 & 1 & 1 & 0 \\ 0 & 1 & 0 & 0 & 1 & 0 & 1 \\ 0 & 0 & 1 & 0 & 0 & 1 & 1 \\ 0 & 0 & 0 & 1 & 1 & 1 & 1 \end{array} \right) \right. \tag{14}$$

$$\left. + [e_1\ \ e_2\ \ e_3\ \ e_4\ \ e_5\ \ e_6\ \ e_7] \right) \cdot \begin{pmatrix} 1 & 1 & 0 \\ 1 & 0 & 1 \\ 0 & 1 & 1 \\ 1 & 1 & 1 \\ 1 & 0 & 0 \\ 0 & 1 & 0 \\ 0 & 0 & 1 \end{pmatrix}$$

$$= [0\ \ 0\ \ 0] + e \cdot D = e \cdot D = [s_1\ \ s_2\ \ s_3\ ]$$

B. Application to Smart Meters

In [9], the hamming code is applied to a smart metering system where the data bits will be replaced by smart meter readings (i.e. real numbers). The system configuration shown in Figure 3.21 consists of four loads connected to single distribution bus by individual cables; each load has a smart meter that reads the amount of power consumed. Additional three check meters are connected across the cables that take designed combination of cables' power measurements. In [9], two cases of the system are addressed; i.e. no presence of power losses in cables and with the presence of power losses in the cables.

1) No power losses in the cables:

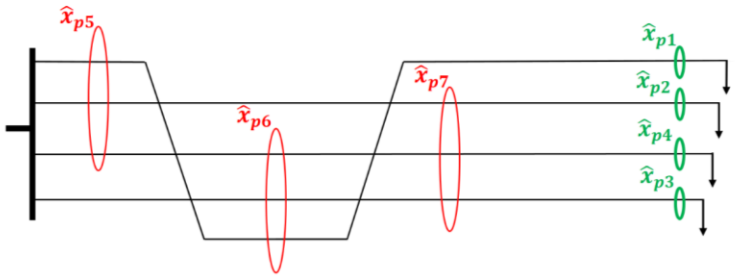

Figure 3.21: System Configuration

From Figure 3.21, The vector $\hat{\boldsymbol{x}}_{\boldsymbol{p}}$ can be defined as:

$$\hat{\boldsymbol{x}}_{\boldsymbol{p}} = [\hat{x}_{p1}\ \hat{x}_{p2}\ \hat{x}_{p3}\ \hat{x}_{p4}\ \hat{x}_{p5}\ \hat{x}_{p6}\ \hat{x}_{p7}] \tag{15}$$

where $\hat{\boldsymbol{x}}_{\boldsymbol{p}}$ is a vector of measured power by all meters, and

$\hat{x}_{pi}$ is the power reading of meter i.

Now, the vector $\boldsymbol{x}_{\boldsymbol{p}}$ can be defines as:

$$\boldsymbol{x}_{\boldsymbol{p}} = [x_{p1}\ x_{p2}\ x_{p3}\ x_{p4}\ x_{p5}\ x_{p6}\ x_{p7}] \tag{16}$$

where $\boldsymbol{x}_{\boldsymbol{p}}$ is a vector of actual power flow supposed to be measured by all meters, and

x_{pi} is the actual power consumption supposed to be measured by meter i.

If all meters' readings are correct then, $\hat{\boldsymbol{x}}_{\boldsymbol{p}} = \boldsymbol{x}_{\boldsymbol{p}}$, and if one meter is in error then, $\hat{\boldsymbol{x}}_{\boldsymbol{p}} = \boldsymbol{x}_{\boldsymbol{p}} + \boldsymbol{e}$ where $\boldsymbol{e} = [e_1\ e_2\ e_3\ e_4\ e_5\ e_6\ e_7]$. The check meters are connected so that they measure the designed combination of power flow that is based on generator matrix G as shown below:

$$\begin{aligned}\hat{x}_p &= [\hat{x}_{p1}\ \hat{x}_{p2}\ \hat{x}_{p3}\ \hat{x}_{p4}] \cdot \left(\begin{array}{cccc|ccc} 1 & 0 & 0 & 0 & 1 & 1 & 0 \\ 0 & 1 & 0 & 0 & 1 & 0 & 1 \\ 0 & 0 & 1 & 0 & 0 & 1 & 1 \\ 0 & 0 & 0 & 1 & 1 & 1 & 1 \end{array}\right) \\ &= [\,\hat{x}_{p1}\,,\ \hat{x}_{p2}\,,\ \hat{x}_{p3}\,,\ \hat{x}_{p4}\,,\hat{x}_{p1}+\hat{x}_{p2}+\hat{x}_{p4}\,,\hat{x}_{p1}+\hat{x}_{p3} \\ &+\hat{x}_{p4}\,,\hat{x}_{p2}+\hat{x}_{p3}+\hat{x}_{p4}\,] \\ &= [\hat{x}_{p1}\ \hat{x}_{p2}\ \hat{x}_{p3}\ \hat{x}_{p4}\ \hat{x}_{p5}\ \hat{x}_{p6}\ \hat{x}_{p7}]\end{aligned} \tag{17}$$

The decoding matrix D must be modified since Modulo-2 addition will not detect and correct the error when the values are real numbers. The modification is done to the identity matrix as shown below:

$$D^* = [H_{4\times3}^T \quad -I_{3\times3}]^T = \begin{pmatrix} 1 & 1 & 0 \\ 1 & 0 & 1 \\ 0 & 1 & 1 \\ 1 & 1 & 1 \\ -1 & 0 & 0 \\ 0 & -1 & 0 \\ 0 & 0 & -1 \end{pmatrix} \tag{18}$$

Application of the modified decoding matrix is shown for two cases, i.e., no mete in error and one meter in error.

Case 1: No meter in error:

$$\begin{aligned}\boldsymbol{s_p} = \hat{\boldsymbol{x}}_{\boldsymbol{p}}.D^* &= [\hat{x}_{p1}\ \hat{x}_{p2}\ \hat{x}_{p3}\ \hat{x}_{p4}\ \hat{x}_{p5}\ \hat{x}_{p6}\ \hat{x}_{p7}] \cdot \begin{pmatrix} 1 & 1 & 0 \\ 1 & 0 & 1 \\ 0 & 1 & 1 \\ 1 & 1 & 1 \\ -1 & 0 & 0 \\ 0 & -1 & 0 \\ 0 & 0 & -1 \end{pmatrix} \\ &= [x_{p1}\ x_{p2}\ x_{p3}\ x_{p4}\ x_{p5}\ x_{p6}\ x_{p7}] \cdot \begin{pmatrix} 1 & 1 & 0 \\ 1 & 0 & 1 \\ 0 & 1 & 1 \\ 1 & 1 & 1 \\ -1 & 0 & 0 \\ 0 & -1 & 0 \\ 0 & 0 & -1 \end{pmatrix} \\ &= [0\ 0\ 0]\end{aligned} \tag{19}$$

Case 2: One meter in error:

$$\begin{aligned} \boldsymbol{s_p} = \hat{\boldsymbol{x}}_{\boldsymbol{p}}.D^* &= \begin{bmatrix} \hat{x}_{p1} & \hat{x}_{p2} & \hat{x}_{p3} & \hat{x}_{p4} & \hat{x}_{p5} & \hat{x}_{p6} & \hat{x}_{p7} \end{bmatrix} \begin{pmatrix} 1 & 1 & 0 \\ 1 & 0 & 1 \\ 0 & 1 & 1 \\ 1 & 1 & 1 \\ -1 & 0 & 0 \\ 0 & -1 & 0 \\ 0 & 0 & -1 \end{pmatrix} \\ &= \left(\begin{bmatrix} x_{p1} & x_{p2} & x_{p3} & x_{p4} & x_{p5} & x_{p6} & x_{p7} \end{bmatrix} \right. \\ &\quad \left. + \begin{bmatrix} e_1 & e_2 & e_3 & e_4 & e_5 & e_6 & e_7 \end{bmatrix} \right) \begin{pmatrix} 1 & 1 & 0 \\ 1 & 0 & 1 \\ 0 & 1 & 1 \\ 1 & 1 & 1 \\ -1 & 0 & 0 \\ 0 & -1 & 0 \\ 0 & 0 & -1 \end{pmatrix} \\ &= \begin{bmatrix} s_{p1} & s_{p2} & s_{p3} \end{bmatrix} \end{aligned} \tag{20}$$

Here $\boldsymbol{s_p}$ will be one row of decoding matrix D multiplied by a scaler which represents the magnitude of error. The location of error can be determined by comparing the form of syndrome vector to the rows of the decoding matrix D, where each row of D represents the form of syndrome vector for an error in the meter number equal to the row number in decoding matrix D. The error vector $\boldsymbol{e}$ can be created based on syndrome vector, where all the entries of $\boldsymbol{e}$ will be zero except one entry which corresponds to the meter in error. The correct values can be determined by subtracting the error vector to the meter readings as shown below:

$$\begin{aligned} \hat{x}_{p_{corrected}} &= \begin{bmatrix} \hat{x}_{p1} & \hat{x}_{p2} & \hat{x}_{p3} & \hat{x}_{p4} & \hat{x}_{p5} & \hat{x}_{p6} & \hat{x}_{p7} \end{bmatrix} \\ &\quad - \begin{bmatrix} e_1 & e_2 & e_3 & e_4 & e_5 & e_6 & e_7 \end{bmatrix} \\ &= \begin{bmatrix} x_{p1} & x_{p2} & x_{p3} & x_{p4} & x_{p5} & x_{p6} & x_{p7} \end{bmatrix} \end{aligned} \tag{21}$$

2) Presence of power losses in the cables

Since the regular meters are installed at load centers and the check meters are installed at distribution bus, there will be power losses in the cables which may lead the coding scheme

to fail. When there is power losses in the cables, the readings of regular meters must be multiplied by a factor in the coding scheme to account for power losses in the cables. To see the effect of power losses in the cables on detection scheme, we will define δ_i where it represents the actual amount of power losses in cable i as percentage of regular meter reading. The factor δ_i will be added in generator matrix G_{loss} for the case of no error and calculate the syndrome vector as shown below:

$$
\begin{aligned}
\boldsymbol{s_p} &= [x_{p1}\ \ x_{p2}\ \ x_{p3}\ \ x_{p4}\ ].G_{loss}.D^* \\
&= [x_{p1}\ \ x_{p2}\ \ x_{p3}\ \ x_{p4}\ ] \\
&\cdot \left(\begin{array}{cccc|ccc} 1-\delta_1 & 0 & 0 & 0 & 1 & 1 & 0 \\ 0 & 1-\delta_2 & 0 & 0 & 1 & 0 & 1 \\ 0 & 0 & 1-\delta_3 & 0 & 0 & 1 & 1 \\ 0 & 0 & 0 & 1-\delta_4 & 1 & 1 & 1 \end{array}\right) \\
&\cdot \begin{pmatrix} 1 & 1 & 0 \\ 1 & 0 & 1 \\ 0 & 1 & 1 \\ 1 & 1 & 1 \\ -1 & 0 & 0 \\ 0 & -1 & 0 \\ 0 & 0 & -1 \end{pmatrix} \\
&= \begin{pmatrix} (1-\delta_1)x_{p1} \\ (1-\delta_2)x_{p2} \\ (1-\delta_3)x_{p3} \\ (1-\delta_4)x_{p4} \\ x_{p1}+x_{p2}+x_{p4} \\ x_{p1}+x_{p3}+x_{p4} \\ x_{p2}+x_{p3}+x_{p4} \end{pmatrix}^{\mathrm{T}} \cdot \begin{pmatrix} 1 & 1 & 0 \\ 1 & 0 & 1 \\ 0 & 1 & 1 \\ 1 & 1 & 1 \\ -1 & 0 & 0 \\ 0 & -1 & 0 \\ 0 & 0 & -1 \end{pmatrix} \\
&= \begin{pmatrix} -\delta_1 x_{p1} - \delta_2 x_{p2} - \delta_4 x_{p4} \\ -\delta_1 x_{p1} - \delta_3 x_{p3} - \delta_4 x_{p4} \\ -\delta_2 x_{p2} - \delta_3 x_{p3} - \delta_4 x_{p4} \end{pmatrix}^{T} \neq [0\ 0\ 0\ ]
\end{aligned}
\tag{22}
$$

It can be seen that the syndrome vector $\boldsymbol{s_p}$ resulted in non-zero values for case of no error, therefore the decoding matrix D^* need to be modified to account for power losses by adding the term $\hat{\delta}_i$ to the decoding matrix which represent the estimated ratio of power losses in cable i. The modified decoding matrix $\widetilde{D}$ is shown below:

$$\widetilde{D} = \begin{pmatrix} \frac{1}{1-\hat{\delta}_1} & \frac{1}{1-\hat{\delta}_1} & 0 \\ \frac{1}{1-\hat{\delta}_2} & 0 & \frac{1}{1-\hat{\delta}_2} \\ 0 & \frac{1}{1-\hat{\delta}_3} & \frac{1}{1-\hat{\delta}_3} \\ \frac{1}{1-\hat{\delta}_4} & \frac{1}{1-\hat{\delta}_4} & \frac{1}{1-\hat{\delta}_4} \\ -1 & 0 & 0 \\ 0 & -1 & 0 \\ 0 & 0 & -1 \end{pmatrix} \tag{23}$$

Now, the syndrome vector is calculated as:

$$\begin{aligned} \boldsymbol{s_p} &= \begin{bmatrix} x_{p1} & x_{p2} & x_{p3} & x_{p4} \end{bmatrix} \cdot G_{loss} \cdot \widetilde{D} \\ &= \begin{pmatrix} (1-\delta_1)x_{p1} \\ (1-\delta_2)x_{p2} \\ (1-\delta_3)x_{p3} \\ (1-\delta_4)x_{p4} \\ x_{p1}+x_{p2}+x_{p4} \\ x_{p1}+x_{p3}+x_{p4} \\ x_{p2}+x_{p3}+x_{p4} \end{pmatrix}^{\mathrm{T}} \cdot \begin{pmatrix} \frac{1}{1-\hat{\delta}_1} & \frac{1}{1-\hat{\delta}_1} & 0 \\ \frac{1}{1-\hat{\delta}_2} & 0 & \frac{1}{1-\hat{\delta}_2} \\ 0 & \frac{1}{1-\hat{\delta}_3} & \frac{1}{1-\hat{\delta}_3} \\ \frac{1}{1-\hat{\delta}_4} & \frac{1}{1-\hat{\delta}_4} & \frac{1}{1-\hat{\delta}_4} \\ -1 & 0 & 0 \\ 0 & -1 & 0 \\ 0 & 0 & -1 \end{pmatrix} \\ &= \begin{pmatrix} \frac{\hat{\delta}_1-\delta_1}{1-\hat{\delta}_1}x_{p1} + \frac{\hat{\delta}_2-\delta_2}{1-\hat{\delta}_2}x_{p2} + \frac{\hat{\delta}_4-\delta_4}{1-\hat{\delta}_4}x_{p4} \\ \frac{\hat{\delta}_1-\delta_1}{1-\hat{\delta}_1}x_{p1} + \frac{\hat{\delta}_3-\delta_3}{1-\hat{\delta}_3}x_{p3} + \frac{\hat{\delta}_4-\delta_4}{1-\hat{\delta}_4}x_{p4} \\ \frac{\hat{\delta}_2-\delta_2}{1-\hat{\delta}_2}x_{p2} + \frac{\hat{\delta}_3-\delta_3}{1-\hat{\delta}_3}x_{p3} + \frac{\hat{\delta}_4-\delta_4}{1-\hat{\delta}_4}x_{p4} \end{pmatrix}^{T} \end{aligned} \tag{24}$$

When the estimated power losses equal to the actual power losses (i.e. $\hat{\delta}_i = \delta_i$), the syndrome vector for the case of no error will be zero (i.e. $\boldsymbol{s_p} = [0\ 0\ 0]$). If the value of δ_i is not estimated accurately, it may lead the coding scheme to fail. Therefore, it is essential

to develop a method to accurately estimate the power losses in each cable, and this is one of the contributions of this thesis.

3.2 Estimation of Power Losses

Installation of the regular meters and the check meters at different locations will cause differences in readings between the regular meters and the check meters due to power losses in the cables. This might cause the coding scheme to fail and syndrome vector $\boldsymbol{s_p}$ will give wrong results. To estimate the power losses, the network topology is needed. In this section we will propose a method to estimate the power losses using the smart meters' measurements. First, the formulation power losses proposed in [9] will be modified for more accurate estimation because the power losses cannot be modeled as constant ratio of active power as will be explained next.

The active power losses in cable i equals to $\delta_i(t)p_i(t)$, where $\delta_i(t)$ is the ratio of active power losses in cable i at time t referred to active power injection into cable i, and $p_i(t)$ is the active power injected at cable i at time t. Now, the following equation can be derived:

$$\hat{\delta}_i(t)p_i(t) = p_i(t) - x_{pi}(t) \tag{25}$$

where $x_{pi}(t)$ is the active power consumed by load i at time t.

Now, assuming that we have the value R_i that is the resistance of cable i then,

$$\delta_i(t)p_i(t) = I_i^2(t)R_i \tag{26}$$

consequently,

$$\delta_i(t) = \frac{I_i^2(t)R_i}{x_{pi}(t) + I_i^2(t)R_i} \tag{27}$$

We can see that $\delta_i(t)$ is function of time and it depends on the active power consumption as well as the current. The current depends on the active power, reactive power, and voltage at receiving end. This means that the value of δ_i in (24) is function of time and cannot be presented by a constant ratio of active power consumption. In addition to that, using time varying δ_i, i.e. $\delta_i(t)$ in (27), requires the RMS current flowing in cable i and the active power consumption of load i. These values can be obtained from regular meter i for case of no error or an error in one of the check meters. But for an error in one of the regular meters (which can be the case for most errors), the values obtained to calculate $\delta_i(t)$ will be wrong, and consequently failure of the algorithm.

Next, the issues addressed will be solved using novel methods. *Subsection 3.3.1* will propose new method to estimate the cable impedance form the already existing system when there is no error, and *Subsection 3.1.2* will propose modified algorithm that is capable to include the power losses in the detection algorithm for all three cases (i.e. no meter in error, check meter in error, and regular meter in error). In addition to that, *Subsection 3.1.2* will address and solve the issue of non-technical losses that is related to other types of attacks such as cable taping. All the solutions proposed doesn't require any additional hardware to the system (i.e. no cost will be added to the original system).

3.2.1 Estimation of Cable Impedance

To see the effect of power losses we can assume that there are power losses in all cables, then,

$$\begin{aligned} x_{p5} &= x_{p1} + x_{p2} + x_{p4} + P_{1_{losses}} + P_{2_{losses}} + P_{4_{losses}} \\ x_{p6} &= x_{p1} + x_{p3} + x_{p4} + P_{1_{losses}} + L_{3_{losses}} + P_{4_{losses}} \\ x_{p7} &= x_{p2} + x_{p3} + x_{p4} + P_{2_{losses}} + P_{3_{losses}} + P_{4_{losses}} \end{aligned} \quad (28)$$

where $P_{i_{losses}}$ is the power losses in cable i.

We have three equations and four unknowns need to be determined for this case, where for case when there are M check meters there will be M equations and $2^M - M - 1$ unknowns need to be determined which cannot be solved using these equations derived from check meters. To solve this issue, we can define new equation as the addition of all three equations as:

$$\begin{aligned} &\hat{x}_{p5} + \hat{x}_{p6} + \hat{x}_{p7} - 2\hat{x}_{p1} - 2\hat{x}_{p2} - 2\hat{x}_{p3} - 3\hat{x}_{p4} \\ &= 2P_{1_{losses}} + 2P_{2_{losses}} + 2P_{3_{losses}} + 3P_{4_{losses}} \end{aligned} \quad (29)$$

Since all the unknowns in (29) (i.e. $P_{1_{losses}}$, $P_{2_{losses}}$, $P_{3_{losses}}$, and $P_{4_{losses}}$) are changing with time, the equation will be presented as:

$$\begin{aligned} &x_{p5}(\mathrm{t}) + x_{p6}(\mathrm{t}) + x_{p7}(\mathrm{t}) - 2x_{p1}(\mathrm{t}) - 2x_{p2}(\mathrm{t}) - 2x_{p3}(\mathrm{t}) - 3x_{p4}(\mathrm{t}) \\ &= 2P_{1_{losses}}(\mathrm{t}) + 2P_{2_{losses}}(\mathrm{t}) + 2P_{3_{losses}}(\mathrm{t}) + 3P_{4_{losses}}(\mathrm{t}) \end{aligned} \quad (30)$$

where $x_{pi}(t)$ is the correct active power consumption measured by meter i at time t, and

$P_{i_{losses}}(\mathrm{t})$ is the power losses in cable i at time t.

Since the power losses is changing at each time instant, the unknowns in (30) (i.e. $P_{1_{losses}}(\mathrm{t})$, $P_{2_{losses}}(\mathrm{t})$, $P_{3_{losses}}(\mathrm{t})$, and $P_{4_{losses}}(\mathrm{t})$) will be changed to fixed values along with changing values that can be measured by smart meters (i.e. the RMS current). Because the distribution secondary cables are relatively short and operate at low voltages, the shunt capacitance and conductance can be ignored [41]. Consequently, the RMS current at

sending and receiving end will be the same and the active power losses can be calculated as:

$$P_{i_{losses}}(\mathrm{t}) = R_i I_i^2(t) \tag{31}$$

where R_i is the series resistance of cable i, and

$I_i(t)$ is the correct RMS current that is measured by meter i.

Now, equation (30) can be changed to:

$$\begin{aligned} x_{p5}(t) + x_{p6}(t) + x_{p7}(t) - 2x_{p1}(t) - 2x_{p2}(t) - 2x_{p3}(t) - 3x_{p4}(t) \\ = 2R_1 I_1^2(t) + 2R_2 I_2^2(t) + 2R_3 I_3^2(t) + 3R_4 I_4^2(t) \end{aligned} \tag{32}$$

Now, we can generate four different independent equations from four different time instants (i.e. t_1, t_2, t_3, and t_4) to solve for the four unknowns R_1, R_2, R_3, and R_4.

The same can be applied to reactive power as shown:

$$\begin{aligned} x_{q5}(\mathrm{t}) + x_{q6}(\mathrm{t}) + x_{q7}(\mathrm{t}) - 2x_{q1}(\mathrm{t}) - 2x_{q2}(\mathrm{t}) - 2x_{q3}(\mathrm{t}) - 3x_{q4}(\mathrm{t}) \\ = 2Q_{1_{losses}}(\mathrm{t}) + 2Q_{2_{losses}}(\mathrm{t}) + 2Q_{3_{losses}}(\mathrm{t}) + 3Q_{4_{losses}}(\mathrm{t}) \end{aligned} \tag{33}$$

where,

$$Q_{i_{losses}}(\mathrm{t}) = X_i I_i^2(t) \tag{34}$$

and,

$$\begin{aligned} x_{q5}(t) + x_{q6}(t) + x_{q7}(t) - 2x_{q1}(t) - 2x_{q2}(t) - 2x_{q3}(t) - 3x_{q4}(t) \\ = 2X_1 I_1^2(t) + 2X_2 I_2^2(t) + 2X_3 I_3^2(t) + 3X_4 I_4^2(t) \end{aligned} \tag{35}$$

where $x_{qi}(\mathrm{t})$ it the actual reactive power measured by meter i at time t,

$Q_{i_{losses}}(\mathrm{t})$, is the reactive power losses in cable i at time t,

X_i is the series reactance of cable i.

Using (32) and (35), four independent equations can be derived from four different time instants (i.e. t_1, t_2, t_3, and t_4) to solve for the unknowns (R_1, R_2, R_3, R_4) and (X_1, X_2, X_3, X_4). The same can be generalized for case of M check meters where we need $2^M - M - 1$ different operating points (i.e. t_1, t_2, ... , t_{2^M-2-1}) to solve for (R_1, R_2, … R_{2^M-M-1}) and (X_1, X_2, … X_{2^M-M-1}). The cable impedance can be calculated once when no meter is in error on a regular basis (to account for potential system reconfiguration and cable aging), then it can be used in detection algorithm as will be explained next.

3.2.2 Modified Detection Algorithm

To include the active and reactive power losses in the calculation, the syndrome vector will be calculated for both active and reactive power and also the power losses will be included in the calculation as:

$$\tilde{\boldsymbol{s}}_{\boldsymbol{p}} = \hat{\boldsymbol{x}}_{\boldsymbol{p}} \cdot D + \widehat{\boldsymbol{P}}_L \cdot D, \tag{36}$$

where,

$$\widehat{\boldsymbol{P}}_L = \begin{pmatrix} R_1\hat{I}_1^2 \\ R_2\hat{I}_2^2 \\ R_3\hat{I}_3^2 \\ R_4\hat{I}_4^2 \\ 0 \\ 0 \\ 0 \end{pmatrix}^{\mathrm{T}}, \tag{37}$$

$\tilde{\boldsymbol{s}}_{\boldsymbol{p}}$ is the modified active power syndrome vector,

$\hat{\boldsymbol{x}}_{\boldsymbol{p}}$ is the vector of active power consumption measured by all meters,

$\widehat{\boldsymbol{P}}_L$ is vector of active power losses calculations based on measurements received form regular meters,

$\hat{I}_i$ is the RMS current measured be meter i, and

D is the decoding matrix.

The same can be applied to reactive power losses as:

$$\tilde{s}_{\boldsymbol{q}} = \widehat{\boldsymbol{x}}_{\boldsymbol{q}} \cdot D + \widehat{\boldsymbol{Q}}_{\boldsymbol{L}} \cdot D, \tag{38}$$

where,

$$\widehat{\boldsymbol{Q}}_{\boldsymbol{L}} = \begin{pmatrix} X_1\hat{I}_1^2 \\ X_2\hat{I}_2^2 \\ X_3\hat{I}_3^2 \\ X_4\hat{I}_4^2 \\ 0 \\ 0 \\ 0 \end{pmatrix}^{\mathrm{T}}, \tag{39}$$

$\tilde{\boldsymbol{s}}_{\boldsymbol{q}}$ is the modified reactive power syndrome vector,

$\widehat{\boldsymbol{x}}_{\boldsymbol{q}}$ is the vector of active power consumption measured by all meters,

$\widehat{\boldsymbol{Q}}_L$ is vector of reactive power losses calculations based on measurements received form regular meters, and

D is the decoding matrix.

For errors in smart meters, there are three possible scenarios which are: no meter in error, check meter in error, and regular meter in error. In addition to that, the estimation of other sources of non-technical losses will be addressed as well. The modified algorithm for each type is explained next.

A. No Meter in Error

When there is no meter in error, then the following equations will be satisfied:

$$\hat{\boldsymbol{x}}_{\boldsymbol{p}} = \boldsymbol{x}_{\boldsymbol{p}} \tag{40}$$

$$\hat{\boldsymbol{x}}_{\boldsymbol{q}} = \boldsymbol{x}_{\boldsymbol{q}} \tag{41}$$

$$\hat{\boldsymbol{P}}_{\boldsymbol{L}} = \boldsymbol{P}_{\boldsymbol{L}} \tag{42}$$

$$\hat{\boldsymbol{Q}}_{\boldsymbol{L}} = \boldsymbol{Q}_{\boldsymbol{L}} \tag{43}$$

where,

$\boldsymbol{x}_{\boldsymbol{p}}$ is the vector of actual active power supposed to be measured by all meters,

$\boldsymbol{x}_{\boldsymbol{q}}$ is the vector of actual reactive power supposed to be measured by all meters,

$\boldsymbol{P}_{\boldsymbol{L}}$ is the vector of actual active power losses, and

$\boldsymbol{Q}_{\boldsymbol{L}}$ is the vector of actual reactive power losses.

Therefore, the active and reactive power's syndrome vectors must return zeros as:

$$\begin{aligned}
\tilde{\boldsymbol{s}}_{\boldsymbol{p}} &= \hat{\boldsymbol{x}}_{\boldsymbol{p}} \cdot D + \hat{\boldsymbol{P}}_{L} \cdot D = \boldsymbol{x}_{\boldsymbol{p}} \cdot D + \boldsymbol{P}_{L} \cdot D \\
&= \begin{pmatrix} x_{p1} \\ x_{p2} \\ x_{p3} \\ x_{p4} \\ x_{p5} \\ x_{p6} \\ x_{p7} \end{pmatrix}^{\mathrm{T}} \begin{pmatrix} 1 & 1 & 0 \\ 1 & 0 & 1 \\ 0 & 1 & 1 \\ 1 & 1 & 1 \\ -1 & 0 & 0 \\ 0 & -1 & 0 \\ 0 & 0 & -1 \end{pmatrix} + \begin{pmatrix} R_1 I_1^2 \\ R_2 I_2^2 \\ R_3 I_3^2 \\ R_4 I_4^2 \\ 0 \\ 0 \\ 0 \end{pmatrix}^{\mathrm{T}} \begin{pmatrix} 1 & 1 & 0 \\ 1 & 0 & 1 \\ 0 & 1 & 1 \\ 1 & 1 & 1 \\ -1 & 0 & 0 \\ 0 & -1 & 0 \\ 0 & 0 & -1 \end{pmatrix} \\
&= \begin{pmatrix} x_{p1} + x_{p2} + x_{p4} - x_{p5} + R_1 I_1^2 + R_2 I_2^2 + R_4 I_4^2 \\ x_{p1} + x_{p3} + x_{p4} - x_{p6} + R_1 I_1^2 - R_3 I_3^2 + R_4 I_4^2 \\ x_{p2} + x_{p3} + x_{p4} - x_{p7} + R_2 I_2^2 + R_3 I_3^2 + R_4 I_4^2 \end{pmatrix}^{T} \\
&= [\,0 \quad 0 \quad 0\,]
\end{aligned} \tag{44}$$

The same can be applied to reactive power as:

$$\tilde{s}_q = \hat{x}_q \cdot D + \hat{Q}_L \cdot D = x_q \cdot D + Q_L \cdot D$$

$$= \begin{pmatrix} x_{q1} \\ x_{q2} \\ x_{q3} \\ x_{q4} \\ x_{q5} \\ x_{q6} \\ x_{q7} \end{pmatrix}^{\mathrm{T}} \begin{pmatrix} 1 & 1 & 0 \\ 1 & 0 & 1 \\ 0 & 1 & 1 \\ 1 & 1 & 1 \\ -1 & 0 & 0 \\ 0 & -1 & 0 \\ 0 & 0 & -1 \end{pmatrix} + \begin{pmatrix} X_1 I_1^2 \\ X_2 I_2^2 \\ X_3 I_3^2 \\ X_4 I_4^2 \\ 0 \\ 0 \\ 0 \end{pmatrix}^{\mathrm{T}} \begin{pmatrix} 1 & 1 & 0 \\ 1 & 0 & 1 \\ 0 & 1 & 1 \\ 1 & 1 & 1 \\ -1 & 0 & 0 \\ 0 & -1 & 0 \\ 0 & 0 & -1 \end{pmatrix} \tag{45}$$

$$= \begin{pmatrix} x_{q1} + x_{q2} + x_{q4} - x_{q5} + X_1 I_1^2 + X_2 I_2^2 + X_4 I_4^2 \\ x_{q1} + x_{q3} + x_{q4} - x_{q6} + X_1 I_1^2 + X_3 I_3^2 + X_4 I_4^2 \\ x_{q2} + x_{q3} + x_{q4} - x_{q7} + X_2 I_2^2 + X_3 I_3^2 + X_4 I_4^2 \end{pmatrix}^T$$

$$= [\,0 \quad 0 \quad 0\,]$$

B. Check Meter in Error

When a check meter is in error, the vector of active and reactive power measurement will not equal to the actual values supposed to be measured by check meters, but the vectors of active and reactive power losses, i.e., (42) and (43), will be correct since they are calculated based on measurements received form regular meters only, therefore:

$$\hat{x}_p \neq x_p \tag{46}$$

$$\hat{x}_q \neq x_q \tag{47}$$

The syndrome vector will result in a vector that has a form similar to one of the rows of decoding matrix multiplied by a scaler equal to the magnitude of error, e.g. assuming an error in the measurement of check meter 6, the syndrome vector will result in:

$$
\begin{aligned}
\tilde{s}_{\boldsymbol{p}} &= \hat{\boldsymbol{x}}_{\boldsymbol{p}} \cdot D + \hat{\boldsymbol{P}}_L \cdot D = \hat{\boldsymbol{x}}_{\boldsymbol{p}} \cdot D + \boldsymbol{P}_L \cdot D \\
&= \begin{pmatrix} x_{p1} \\ x_{p2} \\ x_{p3} \\ x_{p4} \\ x_{p5} \\ x_{p6} + e_{x_{p6}} \\ x_{p7} \end{pmatrix}^{\mathrm{T}} \begin{pmatrix} 1 & 1 & 0 \\ 1 & 0 & 1 \\ 0 & 1 & 1 \\ 1 & 1 & 1 \\ -1 & 0 & 0 \\ 0 & -1 & 0 \\ 0 & 0 & -1 \end{pmatrix} + \begin{pmatrix} R_1 I_1^2 \\ R_2 I_2^2 \\ R_3 I_3^2 \\ R_4 I_4^2 \\ 0 \\ 0 \\ 0 \end{pmatrix}^{\mathrm{T}} \begin{pmatrix} 1 & 1 & 0 \\ 1 & 0 & 1 \\ 0 & 1 & 1 \\ 1 & 1 & 1 \\ -1 & 0 & 0 \\ 0 & -1 & 0 \\ 0 & 0 & -1 \end{pmatrix} \\
&= \begin{pmatrix} x_{p1} + x_{p2} + x_{p4} - x_{p5} + R_1 I_1^2 + R_2 I_2^2 + R_4 I_4^2 \\ x_{p1} + x_{p3} + x_{p4} - (x_{p6} + e_{x_{p6}}) + R_1 I_1^2 - R_3 I_3^2 + R_4 I_4^2 \\ x_{p2} + x_{p3} + x_{p4} - x_{p7} + R_2 I_2^2 + R_3 I_3^2 + R_4 I_4^2 \end{pmatrix}^T \\
&= [\, 0 \quad -e_{x_{p6}} \quad 0 \,]
\end{aligned}
\tag{48}
$$

where $e_{x_{p6}}$ is the error in active power measurement of check meter number 6.

We can see that the form of the syndrome vector is similar to row 6 of decoding matrix D multiplied by a scaler equal to the magnitude of error. Now, the measurement vector (i.e. $\hat{\boldsymbol{x}}_{\boldsymbol{p}}$**)** can be corrected by subtracting the error vector as:

$$
\hat{\boldsymbol{x}}_{\boldsymbol{p}_{corrected}} = \hat{\boldsymbol{x}}_{\boldsymbol{p}} - \boldsymbol{e}_{\boldsymbol{x}_{\boldsymbol{p}}}, \tag{49}
$$

where,

$$
\boldsymbol{e}_{\boldsymbol{x}_{\boldsymbol{p}}} = [0 \quad 0 \quad 0 \quad 0 \quad 0 \quad e_{x_{p6}} \quad 0] \tag{50}
$$

$\hat{\boldsymbol{x}}_{\boldsymbol{p}_{corrected}}$ is the vector of actual active power supposed to be measured by all meters, and $\boldsymbol{e}_{\boldsymbol{x}_{\boldsymbol{p}}}$ is error vector of active power.

The same can be applied to reactive power as:

$$\tilde{s}_q = \hat{x}_q \cdot D + \hat{Q}_L \cdot D = \hat{x}_q \cdot D + Q_L \cdot D$$

$$= \begin{pmatrix} x_{q1} \\ x_{q2} \\ x_{q3} \\ x_{q4} \\ x_{q5} \\ x_{q6} + e_{x_{q6}} \\ x_{q7} \end{pmatrix}^{\mathrm{T}} \begin{pmatrix} 1 & 1 & 0 \\ 1 & 0 & 1 \\ 0 & 1 & 1 \\ 1 & 1 & 1 \\ -1 & 0 & 0 \\ 0 & -1 & 0 \\ 0 & 0 & -1 \end{pmatrix} + \begin{pmatrix} X_1 I_1^2 \\ X_2 I_2^2 \\ X_3 I_3^2 \\ X_4 I_4^2 \\ 0 \\ 0 \\ 0 \end{pmatrix}^{\mathrm{T}} \begin{pmatrix} 1 & 1 & 0 \\ 1 & 0 & 1 \\ 0 & 1 & 1 \\ 1 & 1 & 1 \\ -1 & 0 & 0 \\ 0 & -1 & 0 \\ 0 & 0 & -1 \end{pmatrix} \quad (51)$$

$$= \begin{pmatrix} x_{q1} + x_{q2} + x_{q4} - x_{q5} + X_1 I_1^2 + X_2 I_2^2 + X_4 I_4^2 \\ x_{q1} + x_{q3} + x_{q4} - (\hat{x}_{q6} + e_{x_{q6}}) + X_1 I_1^2 + X_3 I_3^2 + X_4 I_4^2 \\ x_{q2} + x_{q3} + x_{q4} - x_{q7} + X_2 I_2^2 + X_3 I_3^2 + X_4 I_4^2 \end{pmatrix}^T$$

$$= [0 \quad -e_{x_{q6}} \quad 0\,]$$

and,

$$\hat{x}_{q_{corrected}} = \hat{x}_p - e_{x_q}, \quad (52)$$

where,

$$e_{x_q} = [0 \quad 0 \quad 0 \quad 0 \quad 0 \quad e_{x_{q6}} \quad 0] \quad (53)$$

$e_{x_{q6}}$ is the error in reactive power measurement of check meter number 6,

$\hat{x}_{q_{corrected}}$ is the vector of actual reactive power supposed to be measured by all meters, and

e_{x_q} is error vector of reactive power.

This method can be used for any combination of errors in one of the check meter measurements (i.e. error in active power measurement, error in reactive power measurement, error in RMS current measurement, error in RMS voltage measurement, or any combination of these errors).

C. Regular Meter in Error

When a regular meter is in error, the active and reactive power measurement will be wrong (i.e. (46) and (47)) as well as the active and reactive power losses vectors as shown:

$$\widehat{\boldsymbol{P}}_{\boldsymbol{L}} \neq \boldsymbol{P}_{\boldsymbol{L}} \tag{54}$$

$$\widehat{\boldsymbol{Q}}_{\boldsymbol{L}} \neq \boldsymbol{Q}_{\boldsymbol{L}} \tag{55}$$

The syndrome vector will result in a vector that has a form similar to one of rows of decoding matrix multiplied by a scaler equal to the magnitude of error in addition to other nonlinear terms, to demonstrate that, we will assume an error in measurement of regular meter number 3, the active power's syndrome vector will result in:

$$\begin{aligned}
\tilde{\boldsymbol{s}}_{\boldsymbol{p}} &= \widehat{\boldsymbol{x}}_{\boldsymbol{p}} \cdot D + \widehat{\boldsymbol{P}}_{\boldsymbol{L}} \cdot D \\
&= \begin{pmatrix} x_{p1} \\ x_{p2} \\ x_{p3} + e_{x_{p3}} \\ x_{p4} \\ x_{p5} \\ x_{p6} \\ x_{p7} \end{pmatrix}^{\mathrm{T}} \begin{pmatrix} 1 & 1 & 0 \\ 1 & 0 & 1 \\ 0 & 1 & 1 \\ 1 & 1 & 1 \\ -1 & 0 & 0 \\ 0 & -1 & 0 \\ 0 & 0 & -1 \end{pmatrix} \\
&\quad + \begin{pmatrix} R_1\hat{I}_1^2 \\ R_2\hat{I}_2^2 \\ R_3\left(\hat{I}_3 + e_{I_3}\right)^2 \\ R_4\hat{I}_4^2 \\ 0 \\ 0 \\ 0 \end{pmatrix}^{\mathrm{T}} \begin{pmatrix} 1 & 1 & 0 \\ 1 & 0 & 1 \\ 0 & 1 & 1 \\ 1 & 1 & 1 \\ -1 & 0 & 0 \\ 0 & -1 & 0 \\ 0 & 0 & -1 \end{pmatrix} \\
&= \begin{pmatrix} 0 \\ e_{x_{p3}} + 2R_3\hat{I}_3 e_{I_3} + R_3 e_{I_3}^2 \\ e_{x_{p3}} + 2R_3\hat{I}_3 e_{I_3} + R_3 e_{I_3}^2 \end{pmatrix}^{T}
\end{aligned} \tag{56}$$

where $e_{x_{p3}}$ is the error in active power measurement of regular meter 3, and e_{I_3} is the error in current measurement of regular meter 3.

The reactive power's syndrome vector will result in:

$$
\begin{aligned}
\tilde{s}_q &= \hat{x}_q \cdot D + \hat{Q}_L \cdot D \\
&= \begin{pmatrix} x_{q1} \\ x_{q2} \\ x_{q3} + e_{x_{q3}} \\ x_{q4} \\ x_{q5} \\ x_{q6} \\ x_{q7} \end{pmatrix}^{\mathrm{T}} \begin{pmatrix} 1 & 1 & 0 \\ 1 & 0 & 1 \\ 0 & 1 & 1 \\ 1 & 1 & 1 \\ -1 & 0 & 0 \\ 0 & -1 & 0 \\ 0 & 0 & -1 \end{pmatrix} \\
&\quad + \begin{pmatrix} X_1 I_1^2 \\ X_2 I_2^2 \\ X_3 (I_3 + e_{I_3})^2 \\ X_4 I_4^2 \\ 0 \\ 0 \\ 0 \end{pmatrix}^{\mathrm{T}} \begin{pmatrix} 1 & 1 & 0 \\ 1 & 0 & 1 \\ 0 & 1 & 1 \\ 1 & 1 & 1 \\ -1 & 0 & 0 \\ 0 & -1 & 0 \\ 0 & 0 & -1 \end{pmatrix} \\
&= \begin{pmatrix} 0 \\ e_{x_{q3}} + 2X_3 I_3^2 e_{I_3} + X_3 e_{I_3}^2 \\ e_{x_{q3}} + 2X_3 I_3^2 e_{I_3} + X_3 e_{I_3}^2 \end{pmatrix}^{T}
\end{aligned}
\tag{57}
$$

where $e_{x_{q3}}$ is the error in reactive power measurement of regular meter 3.

We can see that the syndrome vector includes the error in active and reactive power measurements (i.e. $e_{x_{p3}}$, and $e_{x_{q3}}$), but it also includes additional terms that will affect the corrected values; therefore, the syndrome vector cannot be used directly to correct the measurement of regular meter. To determine the actual value, we can use the measurement of one of the check meters measuring the current of the meter in error and subtract the measurements of other regular meters. As can we see the configuration in Figure 3.21, to determine I_3 we can say:

$$
\begin{aligned}
I_7 &= I_2 + I_3 + I_4 \\
\rightarrow\ I_3 &= I_7 - I_2 - I_4
\end{aligned}
\tag{58}
$$

Now, I_3 calculated using (58) can be used to calculate the correct vector of active and reactive power losses, i.e. $\boldsymbol{P_L}$ and $\boldsymbol{Q_L}$, to be used then in (56) and (57). On the other hand, (58) can only be applied when the phase difference between the sending end bus voltage and all the currents is the same, i.e. $\theta_v - \theta_{I_2} = \theta_v - \theta_{I_3} = \theta_v - \theta_{I_4}$ because the smart meters can provide the RMS currents not the phaser currents. Since it is not uncommon that the power factor of each load is different, equation (58) cannot be used for estimation of I_3.

This issue can be solved by determining I_3 from addition of the wrong active and reactive power measured to the wrong active and reactive power losses calculated in (56) and (57), then subtract the mismatch detected form the syndrome vector which will add up and will equal to the actual active and reactive power at sending end as:

$$\begin{aligned} x_{p_{sd3}} &= \left(x_{p3} + e_{x_{p3}}\right) + R_3\left(I_3 + e_{I_3}\right)^2 - \left(e_{x_{p3}} + 2R_3 I_3^2 e_{I_3} + R_3 e_{I_3}^2\right) \\ &= x_{p3} + R_3 I_3^2 \end{aligned} \tag{59}$$

and,

$$\begin{aligned} x_{q_{sd3}} &= \left(x_{q3} + e_{x_{q3}}\right) + X_3\left(I_3 + e_{I_3}\right)^2 - \left(e_{x_{q3}} + 2X_3 I_3^2 e_{I_3} + X_3 e_{I_3}^2\right) \\ &= x_{q3} + X_3 I_3^2 \end{aligned} \tag{60}$$

where $x_{p_{sd3}}$ is the actual active power at sending end, and

$x_{q_{sd3}}$ is the actual reactive power at sending end.

Now, the RMS current at the sending end can be calculated as:

$$I_{3_{corrected}} = \frac{\sqrt{x_{p_{sd3}}^2 + x_{q_{sd3}}^2}}{V_{sd_{rms}}} \tag{61}$$

and the actual active and reactive power can be calculated as:

$$x_{p3} = x_{p_{sd3}} - I_{3_{corrected}}^2 R_3 \tag{62}$$

and,

$$x_{q3} = x_{q_{sd3}} - I_{3_{corrected}}^2 X_3 \tag{63}$$

where $I_{3_{corrected}}$ is the actual (corrected) RMS current at sending end, and

$V_{sd_{rms}}$ is the RMS voltage at sending end measured by any check meter (i.e. 5, 6, or 7).

Now, the magnitude of error can be calculated as:

$$e_{x_{p3}} = \hat{x}_{p3} - x_{p3} \tag{64}$$

and,

$$\boldsymbol{e_{x_p}} = [0 \quad 0 \quad e_{x_{p3}} \quad 0 \quad 0 \quad 0 \quad 0] \tag{65}$$

$e_{x_{p3}}$ is the error in active power measurement of regular meter number 3, and the same can be applied to reactive power as:

$$e_{x_{q3}} = \hat{x}_{q3} - x_{q3} \tag{66}$$

and,

$$\boldsymbol{e_{x_q}} = [0 \quad 0 \quad e_{x_{q3}} \quad 0 \quad 0 \quad 0 \quad 0] \tag{67}$$

where $e_{x_{q3}}$ is the error in reactive power measurement of regular meter number 3.

Equations (59) and (60) can be used for any error in regular meters (i.e. error in active power, error in reactive power, error in RMS current, error in RMS voltage, or any combination these errors).

This method can detect any type of attack on smart meters and/or any type of malfunction in the metering unit that affects the measurements of power consumption. The attack can be physical such as connecting a jumper between the same phase terminals of a smart meter

to enforce some current to bypass the CT, connecting some loads directly to the incoming cable before going to the meter, changing the CT of the meter with one having higher turns ratio, … etc. Also, it can detect any type of cyber-attack on the meter and/or its data that is aiming to tamper with power measurements of smart meters such as: changing the firmware of smart meter locally or remotely, attacking the communication system, attacking the information system of the utility company, … etc.

D. Other Sources of NTL

After inspection, if the service provider found that the mismatch in syndrome vector was due to other source of NTL such as cable tapping, then the regular meter is not in error and by using the data stored in the database the power consumed due to the new source of NTL can be calculated as:

$$\begin{aligned}\tilde{\boldsymbol{s}}_{\boldsymbol{p}} &= \hat{\boldsymbol{x}}_{\boldsymbol{p}} \cdot D + \hat{\boldsymbol{P}}_{\boldsymbol{L}} \cdot D = \boldsymbol{x}_{\boldsymbol{p}} \cdot D + \boldsymbol{P}_{\boldsymbol{L}} \cdot D \\ &= \begin{pmatrix} x_{p1} \\ x_{p2} \\ x_{p3} \\ x_{p4} \\ x_{p5} \\ x_{p6} \\ x_{p7} \end{pmatrix}^{\mathrm{T}} \begin{pmatrix} 1 & 1 & 0 \\ 1 & 0 & 1 \\ 0 & 1 & 1 \\ 1 & 1 & 1 \\ -1 & 0 & 0 \\ 0 & -1 & 0 \\ 0 & 0 & -1 \end{pmatrix} \\ &+ \begin{pmatrix} R_1 I_1^2 \\ R_2 I_2^2 \\ R_3 I_3^2 \\ R_4 I_4^2 \\ 0 \\ 0 \\ 0 \end{pmatrix}^{\mathrm{T}} \begin{pmatrix} 1 & 1 & 0 \\ 1 & 0 & 1 \\ 0 & 1 & 1 \\ 1 & 1 & 1 \\ -1 & 0 & 0 \\ 0 & -1 & 0 \\ 0 & 0 & -1 \end{pmatrix} \neq [0 \quad 0 \quad 0] \end{aligned} \tag{68}$$

Here all the smart meters readings are correct, but the syndrome vector will return non-zero numbers due to another source of NTL. The check meter readings x_{p5}, x_{p6}, and x_{p7} will include an additional term e_{NTL_p} that represents the power consumed due to the new

source of NTL. For example, if $e_{NTL_{p3}}$ is the active power related to cable 3, then (68) will result in:

$$\tilde{\boldsymbol{s}}_{\boldsymbol{p}} = \hat{\boldsymbol{x}}_{\boldsymbol{p}} \cdot D + \hat{\boldsymbol{P}}_{\boldsymbol{L}} \cdot D = \boldsymbol{x}_{\boldsymbol{p}} \cdot D + \boldsymbol{P}_{\boldsymbol{L}} \cdot D = [0 \quad -e_{NTL_{p3}} \quad -e_{NTL_{p3}}] \qquad (69)$$

Similarly, the reactive power syndrome vector can be written as:

$$\tilde{\boldsymbol{s}}_{\boldsymbol{q}} = \hat{\boldsymbol{x}}_{\boldsymbol{q}} \cdot D + \hat{\boldsymbol{Q}}_{\boldsymbol{L}} \cdot D = \boldsymbol{x}_{\boldsymbol{p}} \cdot D + \boldsymbol{P}_{\boldsymbol{L}} \cdot D = [0 \quad -e_{NTL_{q3}} \quad -e_{NTL_{q3}}] \qquad (70)$$

where $e_{NTL_{q3}}$ is the reactive power NTL related to cable 3.

Here $e_{NTL_{p3}}$ and $e_{NTL_{q3}}$ will appear in all check meters taking measurement of cable corresponding to the cable being tapped. Furthermore, $e_{NTL_{p3}}$ and $e_{NTL_{q3}}$ include the direct and indirect NTL related to the attack, e.g., if the source of NTL was tapping the service cable, the values $e_{NTL_{p3}}$ and $e_{NTL_{q3}}$ represents the sum of power consumed and the power losses added to the service cable because of the tapping. Here we can consider the power losses in the cable as NTL instead of being TL; because this amount of losses would not exist if the source of NTL had not been present.

3.3 Practical Challenges

Commercially available metering systems usually have metering data reported at a rate equal to or lower than once every 15-minutes to minimize the bandwidth requirements and the power consumption in the communication layer. For instance, the default rate of real-time data measurement of a metering system offered by PG&E is one set of data each hour [42]. Using high data rates will require a big investment in the communication infrastructure (e.g. using fiber optics instead of wireless mesh networks). Applying the detection algorithm to the data received have two main issues, i.e. time skew between the

data stream received from different meters, and measurement of energy losses form energy information.

3.3.1 Time Skew

To accurately detect and correct the errors in smart meters, it is necessary to have the data synchronized accurately to a common reference time frame during data logging; otherwise, the detection algorithm may fail due to nature of the residential loads where there is always rapid change in the demand curve when an appliance turns on and off. Figure 3.22 shows the time skew between two quantities, $x_1(t)$ and $x_2(t)$, where $x_1(t_1 - \epsilon)$ will be compared to $x_2(t_1)$ instead of $x_1(t_1)$.

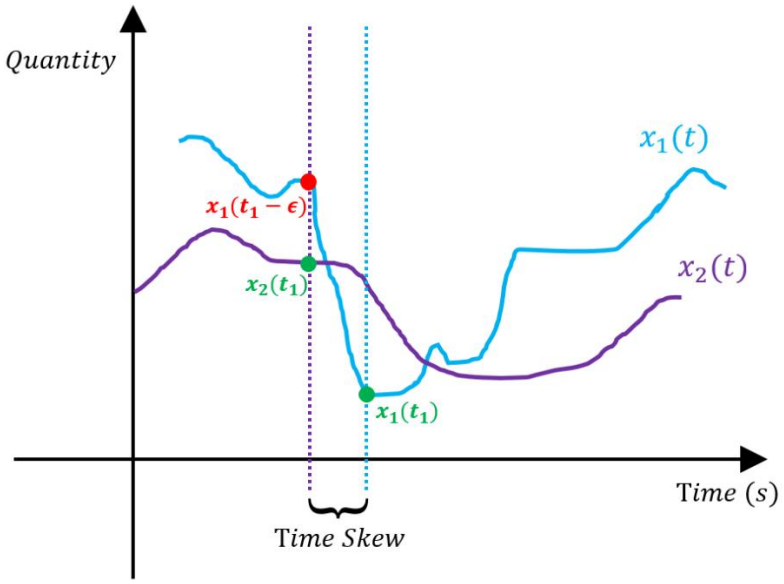

Figure 3.22: Demonstration of time skew problem

The received data need to be accurately synchronized where a small-time skew (e.g. 1 second) may cause the detection algorithm to fail. Synchronized data logging to a common time reference can be achieved using phasor measurement units (PMUs) where all devices

are synchronized using timing signal received from GPS, but installation of PMUs has two main issues; first, they are too expensive to be installed as smart meters for residential customers (at least at the current PMU prices). Second, reporting real time data of all residential customers by PMUs requires bigger communication bandwidth which will require more investment in communication infrastructure.

This issue can be solved by using the active and reactive energy consumption instead of real-time power. The energy is basically the area under the power curve, using the area under the active and reactive power will reduce the error that is caused by time skew as can be seen in Figure 3.23. The load profiles shown in the Figure 3.23 does not represent actual load profile data ant it is used only for demonstration of concept.

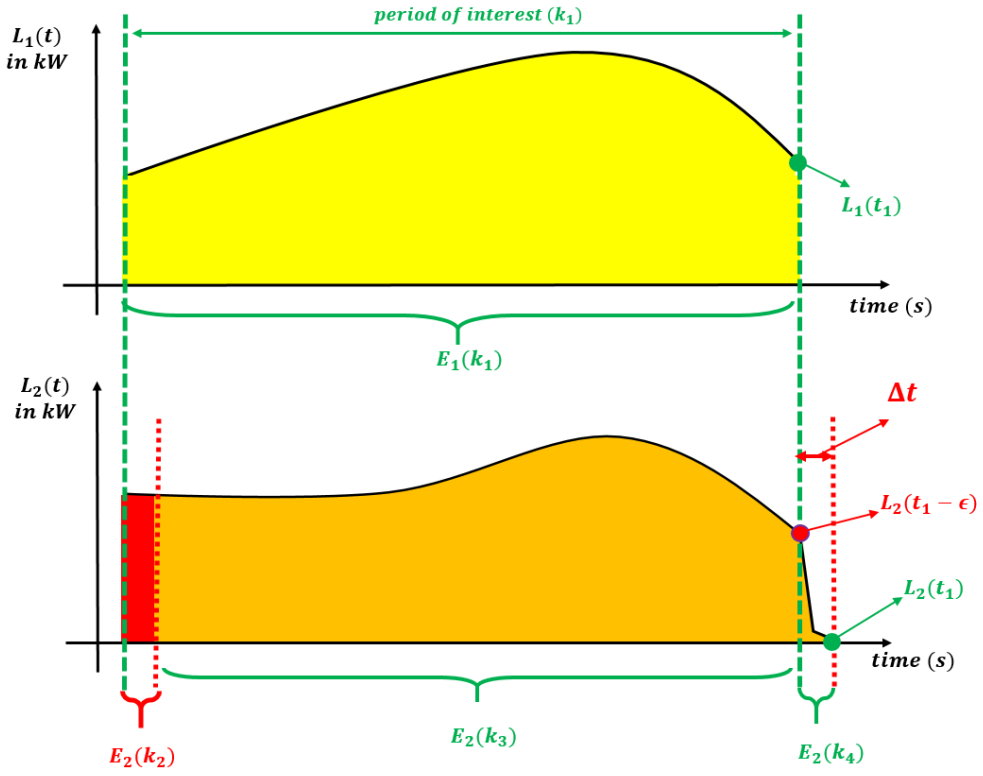

Figure 3.23: Demonstration of the effect of using the area in reducing the error cause by time skew

It can be seen that the reference time window (green dotted vertical lines) represents the period of interest to compare two different load profiles, $L_1(t)$ and $L_2(t)$. As can be seen, there is time skew between the two data streams where the data related to load profile $L_2(t)$ is leading the data related to $L_1(t)$ by time Δt. If we used the active power in the detection algorithm, $L_2(t_1 - \epsilon)$ will be compared to $L_1(t_1)$ instead of $L_2(t_1)$. Which will lead to percentage error as shown:

$$\% \, error_L = \left| \frac{L_2(t_1) - L_2(t_1 - \epsilon)}{L_2(t_1)} \right| \times 100 \tag{71}$$

On the other hand, if we used the energies (areas) to compare the measurements of the two load profiles, $E_2(k_2) + E_2(k_3)$ will be compared to $E_1(k_1)$ instead of $E_2(k_3) + E_2(k_4)$. Which will lead to percentage error as shown:

$$\begin{aligned} \% \, error_E &= \left| \frac{E_2(k_3) + E_2(k_4) - E_2(k_2) - E_2(k_3)}{E_2(k_3) + E_2(k_4)} \right| \times 100 \\ &= \left| \frac{E_2(k_4) - E_2(k_2)}{E_2(k_3) + E_2(k_4)} \right| \times 100 \end{aligned} \tag{72}$$

It can be seen that $E_2(k_3)$ is removed from the percentage error calculation, which will reduce the error as percentage of actual value greatly. As the value of $E_2(k_3)$ becomes bigger, the percentage error will reduce. The value of $E_2(k_3)$ can be increased if we used bigger period of interest, i.e. energy accumulation for longer time. Now with the use of energy instead of power, the percentage error due to time skew will be reduced, the computation power required will reduce, and the communication bandwidth requirement will reduce as well. Looking at Figure 3.23, the following inequality is valid:

$$\left| \frac{E_2(k_4) - E_2(k_2)}{E_2(k_3) + E_2(k_4)} \right| \ll \left| \frac{L_2(t_1) - L_2(t_1 - \epsilon)}{L_2(t_1)} \right| \tag{73}$$

On the other hand, the usage of energy will create other challenges such as estimation of energy losses in the period of interest as will be addressed next.

3.3.2 Estimation of Energy Losses

Using energies instead of real-time power in detection algorithm will reduce the error due to time skew and will reduce the bandwidth required since the smart meter will report the active and reactive energy consumed in a specific period without reporting the real-time power consumption. On the other hand, this will create a challenge in the estimation of energy losses because the energy losses cannot be estimated from the load energy data only. For illustration, the energy losses in two identical cables will be calculated for a period of one hour as shown in Figure 3.24. Because the distribution secondary cables are relatively short and operate at low voltage levels, the shunt capacitance and conductance can be ignored [41].

The two loads simulated that consume the same amount of energy during a period of one hour. The load profiles are based on actual load profiles of a house at different times during the day, L_1 the load profile of the house from 08:30 to 09:30, and L_2 is the load profile from 14:40 to 15:40. Since it was not possible to find two time slots in the real load profile that consumes the exact same energy during one hour, we added constant base power consumption to the load profile L_1 to make it consume the same amount of energy as L_2 during one hour for demonstration.

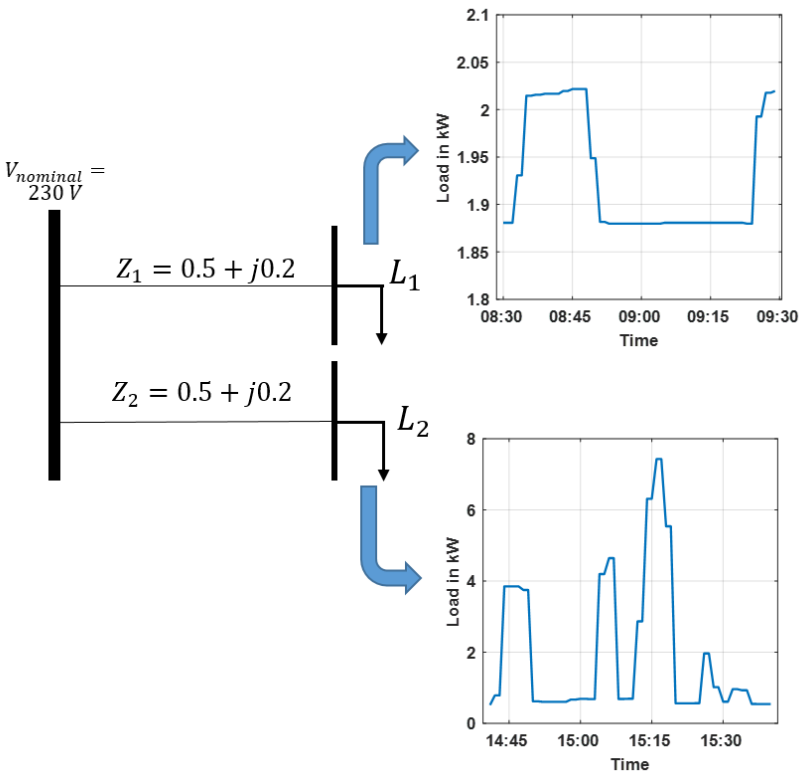

Figure 3.24: Case study of two loads consuming the same amount of energy in an hour

The simulation results are summarized in Table 6, and show that for the same amount of consumed energy in an hour, the energy losses in each cable is different. From the demonstration example, we can see that it is not possible to determine the energy losses in the cable using the energy consumption data even if we have the network topology because the energy losses will mainly depend on the real-time RMS current passing in the cable. The real-time RMS current depends on real-time active power, reactive power, and voltage of the load.

Table 6: Energy losses in identical cables

Attribute	L_1	L_2
Duration ($minutes$)	60	60
Energy consumed (kWh)	1.92711	1.92711
Energy losses (Wh)	35.13	72.47
% of energy losses	1.82 %	3.76 %

To solve this issue, we can use phasor measurement units (PMUs) which report real-time current that can be used to estimate the real-time active power losses (using I^2R) and accumulate the calculated power losses to determine the active energy losses in the cable during period of interest. But as mentioned earlier, we will assume that the PMUs are not used as smart meters due to their high cost at this time. Therefore, we proposed a novel derived unit of measurement to be measured by the smart meter in the same manner of energy to calculate the energy losses in the cables. The smart meters can be reprogrammed to measure the area under the squared current as:

$$AR_{I^2} = \int_{-\frac{T}{2}}^{\frac{T}{2}} I_{rms}^2(t)\, dt \tag{74}$$

where AR_{I^2} is the area under the squared current curve in $(A^2 \cdot s)$, and

$I_{rms}(t)$ is the RMS current at time t.

For discrete values, it can be calculated as:

$$AR_{I^2} = \frac{1}{f_s}\sum_{i=1}^{N} I_{rms}^2(i) \tag{75}$$

where f_s is the number of samples per second, and

$I_{rms}(i)$ is the rms current at instant i.

The active energy losses in the cables are directly proportional to the squared current as:

$$E_{P_L}(k) = \frac{AR_{I^2}(k) \times R}{\alpha} \tag{76}$$

where $E_{P_L}(k)$ is the active energy consumed during period k in (kWh),

$AR_{I^2}(k)$ is the area under the squared current during period k in $(A^2 \cdot s)$

R is the cable resistance in (Ω), and

α is constant ($\alpha = 1000 \times 60 \times 60$).

Now, we can use (76) to calculate the energy losses in each cable even if AR_{I^2} is being send by the smart meter at low frequency (e.g. hourly). Equation (76) is used in the previous example with two cables to calculate the energy losses using only one measurement in the specified hour for both loads. The same can be applied to reactive energy losses as:

$$E_{Q_L}(k) = \frac{AR_{I^2}(k) \times X}{\alpha} \tag{77}$$

where $E_{q_L}(k)$ is the reactive energy consumed during period k in $(kVarh)$, and

X is the series reactance of the cable in (Ω).

Next, the solutions proposed to overcome the issue of time skew and low rate measurements will be applied to the tampering detection system. The new measurer can be applied to detection algorithm; first for estimating the cable resistance and reactance as

explained in subsection *3.3.3*, and then to the detection algorithm as explained in subsection *3.3.4*.

3.3.3 Application to Cable Impedance Estimator

In this section, the instantaneous real-time measurements will be replaced by low rate measurements to estimate the cable impedance, therefore, (32) and (35) will become:

$$\hat{E}_{p5}(k) + \hat{E}_{p6}(k) + \hat{E}_{p7}(k) - 2\hat{E}_{p1}(k) - 2\hat{E}_{p2}(k) - 2\hat{E}_{p3}(k) - 3\hat{E}_{p4}(k) = \frac{2R_1 AR_{I_1^2}(k)}{\alpha} + \frac{2R_2 AR_{I_2^2}(k)}{\alpha} + \frac{2R_3 AR_{I_3^2}(k)}{\alpha} + \frac{3R_4 AR_{I_4^2}(k)}{\alpha} \quad (78)$$

and,

$$\hat{E}_{q5}(k) + \hat{E}_{q6}(k) + \hat{E}_{q7}(k) - 2\hat{E}_{q1}(k) - 2\hat{E}_{q2}(k) - 2\hat{E}_{q3}(k) - 3\hat{E}_{q4}(k) = \frac{2X_1 AR_{I_1^2}(k)}{\alpha} + \frac{2X_2 AR_{I_2^2}(k)}{\alpha} + \frac{2X_3 AR_{I_3^2}(k)}{\alpha} + \frac{3X_4 AR_{I_4^2}(k)}{\alpha} \quad (79)$$

where,

$E_{pi}(k)$ is the active energy consumption measured at meter i during period k in kWh,

$E_{qi}(k)$ is the reactive energy consumption measured at meter i during period k in $kVarh$,

$AR_{I_i^2}(k)$ is the area under the squared RMS current measured by meter i during period k,

R_i is the series resistance of cable i, and

X_i is is the series reactance of cable i.

The value of resistance and series reactance can be estimated by using (78) and (79) at four different periods (i.e. k, $k+1$, $k+2$, and $k+3$). The same can be generalized for case of M check meters where $2^M - M - 1$ different periods needed to solve for R_1, R_2, … R_{2^M-M-1} and X_1, X_2, … X_{2^M-M-1}. The cable impedance can be calculated once when no

meter is in error on a regular basis (to account for potential system reconfiguration and cable aging), then it can be used in detection algorithm as explained in subsection *3.3.4*.

3.3.4 Application to Modified Detection Algorithm

To include the active energy losses in the syndrome vector calculation, () and () will be modified and calculated as:

$$\tilde{\boldsymbol{s}}_{\boldsymbol{E_p}}(k) = \widehat{\boldsymbol{E}}_{\boldsymbol{p}}(k) \cdot D + \widehat{\boldsymbol{E}}_{\boldsymbol{P_L}}(k) \cdot D \tag{80}$$

where,

$$\widehat{\boldsymbol{E}}_{\boldsymbol{P_L}}(k) = \begin{pmatrix} \frac{\widetilde{AR}_{\hat{I}_1^2}(k)\, R_1}{\alpha} \\ \frac{\widetilde{AR}_{\hat{I}_2^2}(k)\, R_2}{\alpha} \\ \frac{\widetilde{AR}_{\hat{I}_3^2}(k)\, R_3}{\alpha} \\ \frac{\widetilde{AR}_{\hat{I}_4^2}(k)\, R_4}{\alpha} \\ 0 \\ 0 \\ 0 \end{pmatrix}^{\mathrm{T}} \tag{81}$$

$\tilde{\boldsymbol{s}}_{\boldsymbol{E_p}}(k)$ is the active energy syndrome vector for the period k,

$\widehat{\boldsymbol{E}}_{\boldsymbol{p}}(k)$ is vector of active energy measurements of all meters for the period k,

$\widetilde{AR}_{\hat{I}_i^2}(k)$ the area under the squared current measured by meter i for the period k,

$\widehat{\boldsymbol{E}}_{\boldsymbol{P_L}}(k)$ is vector of active energy losses calculated for the period k, and

D is the decoding matrix shown in (18).

The same can be applied to reactive power losses as:

$$\tilde{\boldsymbol{s}}_{\boldsymbol{E_q}}(k) = \widehat{\boldsymbol{E}}_{\boldsymbol{q}}(k) \cdot D + \widehat{\boldsymbol{E}}_{\boldsymbol{Q_L}}(k) \cdot D \tag{82}$$

where,

$$\widehat{\boldsymbol{E}}_{\boldsymbol{Q_L}}(k) = \begin{pmatrix} \frac{\widetilde{AR}_{\hat{I}_1^2}(k)\ X_1}{\alpha} \\ \frac{\widetilde{AR}_{\hat{I}_2^2}(k)\ X_2}{\alpha} \\ \frac{\widetilde{AR}_{\hat{I}_3^2}(k)\ \mathrm{X}_3}{\alpha} \\ \frac{\widetilde{AR}_{\hat{I}_4^2}(k)\ \mathrm{X}_4}{\alpha} \\ 0 \\ 0 \\ 0 \end{pmatrix}^{\mathrm{T}} \tag{83}$$

$\tilde{\boldsymbol{s}}_{\boldsymbol{E_q}}(k)$ is the reactive energy syndrome vector for the period k,

$\widehat{\boldsymbol{E}}_{\boldsymbol{q}}(k)$ is vector of reactive energy measurements of all meters for the period k, and

$\widehat{\boldsymbol{E}}_{\boldsymbol{Q_L}}(k)$ is vector of active energy losses calculated for the period k.

For errors in smart meters, there are three possible scenarios which are: no meter in error, check meter in error, and regular meter in error. In addition to that, the estimation of other sources of non-technical losses will be addressed as well. Next, the modified algorithm for each type is explained.

A. No Meter in Error

When there is no meter in error at duration k, the following equations will be satisfied:

$$\widehat{\boldsymbol{E}}_{\boldsymbol{p}}(k) = \boldsymbol{E}_{\boldsymbol{p}}(k) \tag{84}$$

$$\widehat{\boldsymbol{E}}_{\boldsymbol{q}}(k) = \boldsymbol{E}_{\boldsymbol{q}}(k) \tag{85}$$

$$\widehat{\boldsymbol{E}}_{\boldsymbol{P_L}}(k) = \boldsymbol{E}_{\boldsymbol{P_L}}(k) \tag{86}$$

$$\widehat{\boldsymbol{E}}_{\boldsymbol{Q_L}}(k) = \boldsymbol{E}_{\boldsymbol{Q_L}}(k) \tag{87}$$

where,

$\boldsymbol{E_p}(k)$ is the vector actual (correct) active energies supposed to be measured by the smart meters for duration k,

$\boldsymbol{E_q}(k)$ is the vector actual (correct) reactive energies supposed to be measured by the smart meters for duration k,

$\boldsymbol{E_{P_L}}(k)$ is the vector actual (correct) active energy losses supposed to be calculated for duration k, and

$\boldsymbol{E_{Q_L}}(k)$ is the vector actual (correct) reactive energy losses supposed to be calculated for duration k.

Therefore, the active and reactive energies' syndrome vectors will return zeros as:

$$\tilde{\boldsymbol{s}}_{\boldsymbol{E_p}}(k) = \widehat{\boldsymbol{E}}_{\boldsymbol{p}}(k) \cdot D + \widehat{\boldsymbol{E}}_{\boldsymbol{P_L}}(k) \cdot D = \boldsymbol{E_p}(k) \cdot D + \boldsymbol{E_{P_L}}(k) \cdot D$$

$$= \begin{pmatrix} E_{p1}(k) \\ E_{p2}(k) \\ E_{p3}(k) \\ E_{p4}(k) \\ E_{p5}(k) \\ E_{p6}(k) \\ E_{p7}(k) \end{pmatrix}^{\mathrm{T}} \begin{pmatrix} 1 & 1 & 0 \\ 1 & 0 & 1 \\ 0 & 1 & 1 \\ 1 & 1 & 1 \\ -1 & 0 & 0 \\ 0 & -1 & 0 \\ 0 & 0 & -1 \end{pmatrix} + \begin{pmatrix} \frac{AR_{I_1^2}(k)\, R_1}{\alpha} \\ \frac{AR_{I_2^2}(k)\, R_2}{\alpha} \\ \frac{AR_{I_3^2}(k)\, R_3}{\alpha} \\ \frac{AR_{I_4^2}(k)\, R_4}{\alpha} \\ 0 \\ 0 \\ 0 \end{pmatrix}^{\mathrm{T}} \begin{pmatrix} 1 & 1 & 0 \\ 1 & 0 & 1 \\ 0 & 1 & 1 \\ 1 & 1 & 1 \\ -1 & 0 & 0 \\ 0 & -1 & 0 \\ 0 & 0 & -1 \end{pmatrix} \quad (88)$$

$$= \begin{pmatrix} E_{p1}(k) + E_{p2}(k) + E_{p4}(\mathrm{k}) - E_{p5}(\mathrm{k}) + \frac{AR_{I_1^2}(k)\, R_1}{\alpha} + \frac{AR_{I_2^2}(k)\, R_2}{\alpha} + \frac{AR_{I_4^2}(k)\, R_4}{\alpha} \\ E_{p1}(k) + E_{p3}(k) + E_{p4}(\mathrm{k}) - E_{p6}(\mathrm{k}) + \frac{AR_{I_1^2}(k)\, R_1}{\alpha} + \frac{AR_{I_3^2}(k)\, R_3}{\alpha} + \frac{AR_{I_4^2}(k)\, R_4}{\alpha} \\ E_{p2}(k) + E_{p3}(k) + E_{p4}(\mathrm{k}) - E_{p7}(\mathrm{k}) + \frac{AR_{I_2^2}(k)\, R_2}{\alpha} + \frac{AR_{I_3^2}(k)\, R_3}{\alpha} + \frac{AR_{I_4^2}(k)\, R_4}{\alpha} \end{pmatrix}^{T}$$

$$= [0 \quad 0 \quad 0]$$

where,

$AR_{I_1^2}(k)$ is the actual (correct) area under the squared current supposed to be measured by meter i for the period k, and

$E_{pi}(k)$ is the actual (correct) active energy supposed to be measured by meter i for duration k.

The same can be applied to reactive power as:

$$\tilde{\boldsymbol{s}}_{\boldsymbol{E_q}}(k) = \widehat{\boldsymbol{E}}_{\boldsymbol{q}}(k) \cdot D + \widehat{\boldsymbol{E}}_{\boldsymbol{Q_L}}(k) \cdot D = \boldsymbol{E_q}(k) \cdot D + \boldsymbol{E_{Q_L}}(k) \cdot D$$

$$= \begin{pmatrix} E_{q1}(k) \\ E_{q2}(k) \\ E_{q3}(k) \\ E_{q4}(k) \\ E_{q5}(k) \\ E_{q6}(k) \\ E_{q7}(k) \end{pmatrix}^{\mathrm{T}} \begin{pmatrix} 1 & 1 & 0 \\ 1 & 0 & 1 \\ 0 & 1 & 1 \\ 1 & 1 & 1 \\ -1 & 0 & 0 \\ 0 & -1 & 0 \\ 0 & 0 & -1 \end{pmatrix} + \begin{pmatrix} \frac{AR_{I_1^2}(k)\, X_1}{\alpha} \\ \frac{AR_{I_2^2}(k)\, X_2}{\alpha} \\ \frac{AR_{I_3^2}(k)\, X_3}{\alpha} \\ \frac{AR_{I_4^2}(k)\, X_4}{\alpha} \\ 0 \\ 0 \\ 0 \end{pmatrix}^{\mathrm{T}} \begin{pmatrix} 1 & 1 & 0 \\ 1 & 0 & 1 \\ 0 & 1 & 1 \\ 1 & 1 & 1 \\ -1 & 0 & 0 \\ 0 & -1 & 0 \\ 0 & 0 & -1 \end{pmatrix} \tag{89}$$

$$= \begin{pmatrix} E_{q1}(k) + E_{q2}(k) + E_{q4}(\mathrm{k}) - E_{q5}(\mathrm{k}) + \frac{AR_{I_1^2}(k)\, X_1}{\alpha} + \frac{AR_{I_2^2}(k)\, R_2}{\alpha} + \frac{AR_{I_4^2}(k)\, R_4}{\alpha} \\ E_{q1}(k) + E_{q3}(k) + E_{q4}(\mathrm{k}) - E_{q6}(\mathrm{k}) + \frac{AR_{I_1^2}(k)\, X_1}{\alpha} + \frac{AR_{I_3^2}(k)\, X_3}{\alpha} + \frac{AR_{I_4^2}(k)\, X_4}{\alpha} \\ E_{q2}(k) + E_{q3}(k) + E_{q4}(\mathrm{k}) - E_{q7}(\mathrm{k}) + \frac{AR_{I_2^2}(k)\, X_2}{\alpha} + \frac{AR_{I_3^2}(k)\, X_3}{\alpha} + \frac{AR_{I_4^2}(k)\, X_4}{\alpha} \end{pmatrix}^{T}$$

$$= [0 \quad 0 \quad 0]$$

$E_{pi}(k)$ is the actual (correct) reactive energy supposed to be measured by meter i for duration k.

B. Check Meter in Error

When check meter is in error during period k, the syndrome vector will result in a vector that has a form similar to one of the rows of decoding matrix multiplied by a scaler equal to the magnitude of error. The active and reactive energy losses calculations will be correct since it will depend only on the measurements received form regular meters; therefore, (86) and (87) will be applicable but (84) and (85) will not be applicable, therefore:

$$\widehat{\boldsymbol{E}}_{\boldsymbol{p}}(k) \neq \boldsymbol{E_p}(k) \tag{90}$$

$$\widehat{\boldsymbol{E}}_{\boldsymbol{q}}(k) \neq \boldsymbol{E}_{\boldsymbol{q}}(k) \tag{91}$$

To see the calculations for an error in check meters, we are going to assume an error in the measurement of check meter number 6 during period k, then the syndrome vector will result in:

$$\tilde{\boldsymbol{s}}_{\boldsymbol{E_p}}(k) = \widehat{\boldsymbol{E}}_{\boldsymbol{p}}(k) \cdot D + \widehat{\boldsymbol{E}}_{\boldsymbol{P_L}}(k) \cdot D = \widehat{\boldsymbol{E}}_{\boldsymbol{p}}(k) \cdot D + \boldsymbol{E}_{\boldsymbol{P_L}}(k) \cdot D$$

$$= \begin{pmatrix} E_{p1}(k) \\ E_{p2}(k) \\ E_{p3}(k) \\ E_{p4}(k) \\ E_{p5}(k) \\ E_{p6}(k) + e_{E_{p6}}(k) \\ E_{p7}(k) \end{pmatrix}^{\mathrm{T}} \begin{pmatrix} 1 & 1 & 0 \\ 1 & 0 & 1 \\ 0 & 1 & 1 \\ 1 & 1 & 1 \\ -1 & 0 & 0 \\ 0 & -1 & 0 \\ 0 & 0 & -1 \end{pmatrix} + \begin{pmatrix} \frac{AR_{I_1^2}(k)\, R_1}{\alpha} \\ \frac{AR_{I_2^2}(k)\, R_2}{\alpha} \\ \frac{AR_{I_3^2}(k)\, R_3}{\alpha} \\ \frac{AR_{I_4^2}(k)\, R_4}{\alpha} \\ 0 \\ 0 \\ 0 \end{pmatrix}^{\mathrm{T}} \begin{pmatrix} 1 & 1 & 0 \\ 1 & 0 & 1 \\ 0 & 1 & 1 \\ 1 & 1 & 1 \\ -1 & 0 & 0 \\ 0 & -1 & 0 \\ 0 & 0 & -1 \end{pmatrix} \tag{92}$$

$$= \begin{pmatrix} E_{p1}(k) + E_{p2}(k) + E_{p4}(\mathrm{k}) - E_{p5}(\mathrm{k}) + \frac{AR_{I_1^2}(k)\, R_1}{\alpha} + \frac{AR_{I_2^2}(k)\, R_2}{\alpha} + \frac{AR_{I_4^2}(k)\, R_4}{\alpha} \\ E_{p1}(k) + E_{p3}(k) + E_{p4}(\mathrm{k}) - E_{p6}(\mathrm{k}) - e_{E_{p6}}(k) + \frac{AR_{I_1^2}(k) R_1}{\alpha} + \frac{AR_{I_3^2}(k) R_3}{\alpha} + \frac{AR_{I_4^2}(k) R_4}{\alpha} \\ E_{p2}(k) + E_{p3}(k) + E_{p4}(\mathrm{k}) - E_{p7}(\mathrm{k}) + \frac{AR_{I_2^2}(k)\, R_2}{\alpha} + \frac{AR_{I_3^2}(k)\, R_3}{\alpha} + \frac{AR_{I_4^2}(k)\, R_4}{\alpha} \end{pmatrix}^{T}$$

$$= [0 \quad -e_{E_{p6}}(k) \quad 0]$$

where $e_{E_{pi}}(k)$ is the error in active energy measurement of meter i for period k.

We can see that the form of the syndrome vector is similar to row number 6 of decoding matrix D multiplied by a scaler equal to the magnitude of error. Now, the measurement vector, i.e. $\boldsymbol{E_p}(k)$, can be corrected by adding the error vector as:

$$\widehat{\boldsymbol{E}}_{\boldsymbol{p_{corrected}}}(k) = \widehat{\boldsymbol{E}}_{\boldsymbol{p}}(k) - \boldsymbol{e}_{\boldsymbol{E_p}}(k) = \boldsymbol{E}_{\boldsymbol{p}}(k) \tag{93}$$

where,

$$\boldsymbol{e}_{\boldsymbol{E_p}}(k) = [0 \quad 0 \quad 0 \quad 0 \quad 0 \quad e_{E_{p6}}(k) \quad 0] \tag{94}$$

$e_{E_{p6}}(k)$ is the error in active energy measurement of check meter number 6 for period k,

$\widehat{\boldsymbol{E}}_{\boldsymbol{p}_{corrected}}(k)$ is the vector of corrected active energy consumption supposed to be measured by all meters for period k, and

$\boldsymbol{e}_{\boldsymbol{E}_p}(k)$ is error vector of active energy for period k.

The same can be applied to reactive power as:

$$\tilde{\boldsymbol{s}}_{\boldsymbol{E}_q}(k) = \widehat{\boldsymbol{E}}_{\boldsymbol{q}}(k)\cdot D + \widehat{\boldsymbol{E}}_{\boldsymbol{Q}_L}(k)\cdot D = \widehat{\boldsymbol{E}}_{\boldsymbol{q}}(k)\cdot D + \boldsymbol{E}_{\boldsymbol{Q}_L}(k)\cdot D$$

$$= \begin{pmatrix} E_{q1}(k) \\ E_{q2}(k) \\ E_{q3}(k) \\ E_{q4}(k) \\ E_{q5}(k) \\ E_{q6}(k) + e_{E_{q6}}(k) \\ E_{q7}(k) \end{pmatrix}^{\mathrm{T}} \begin{pmatrix} 1 & 1 & 0 \\ 1 & 0 & 1 \\ 0 & 1 & 1 \\ 1 & 1 & 1 \\ -1 & 0 & 0 \\ 0 & -1 & 0 \\ 0 & 0 & -1 \end{pmatrix} + \begin{pmatrix} \frac{AR_{I_1^2}(k)\,X_1}{\alpha} \\ \frac{AR_{I_2^2}(k)\,X_2}{\alpha} \\ \frac{AR_{I_3^2}(k)\,X_3}{\alpha} \\ \frac{AR_{I_4^2}(k)\,X_4}{\alpha} \\ 0 \\ 0 \\ 0 \end{pmatrix}^{\mathrm{T}} \begin{pmatrix} 1 & 1 & 0 \\ 1 & 0 & 1 \\ 0 & 1 & 1 \\ 1 & 1 & 1 \\ -1 & 0 & 0 \\ 0 & -1 & 0 \\ 0 & 0 & -1 \end{pmatrix} \tag{95}$$

$$= \begin{pmatrix} E_{q1}(k) + E_{q2}(k) + E_{q4}(\mathrm{k}) - E_{q5}(\mathrm{k}) + \frac{AR_{I_1^2}(k)\,X_1}{\alpha} + \frac{AR_{I_2^2}(k)\,X_2}{\alpha} + \frac{AR_{I_4^2}(k)\,X_4}{\alpha} \\ E_{q1}(k) + E_{q3}(k) + E_{q4}(\mathrm{k}) - E_{q6}(\mathrm{k}) - e_{E_{q6}}(k) + \frac{AR_{I_1^2}(k)X_1}{\alpha} + \frac{AR_{I_3^2}(k)X_3}{\alpha} + \frac{AR_{I_4^2}(k)X_4}{\alpha} \\ E_{q2}(k) + E_{q3}(k) + E_{q4}(\mathrm{k}) - E_{q7}(\mathrm{k}) + \frac{AR_{I_2^2}(k)\,X_2}{\alpha} + \frac{AR_{I_3^2}(k)\,X_3}{\alpha} + \frac{AR_{I_4^2}(k)\,X_4}{\alpha} \end{pmatrix}^{T}$$

$$= [0 \quad -e_{E_{q6}}(k) \quad 0]$$

We can see that the form of the syndrome vector is similar to row number 6 of decoding matrix D multiplied by a scaler equal to the magnitude of error. Now, the measurement vector, i.e. $\boldsymbol{E}_{\boldsymbol{q}}(k)$, can be corrected by adding the error vector as:

$$\widehat{\boldsymbol{E}}_{\boldsymbol{q}_{corrected}}(k) = \widehat{\boldsymbol{E}}_{\boldsymbol{q}}(k) - \boldsymbol{e}_{\boldsymbol{E}_q}(k) = \boldsymbol{E}_{\boldsymbol{q}}(k) \tag{96}$$

where,

$$\boldsymbol{e}_{\boldsymbol{E}_q}(k) = [0 \quad 0 \quad 0 \quad 0 \quad 0 \quad e_{E_{q6}}(k) \quad 0] \tag{97}$$

$e_{E_{q6}}(k)$ is the error in reactive energy measurement of check meter number 6 for period k,

$\widehat{\boldsymbol{E}}_{\boldsymbol{q}_{corrected}}(k)$ is the vector of corrected reactive energy consumption supposed to be measured by all meters for period k, and

$\boldsymbol{e}_{\boldsymbol{E}_p}(k)$ is error vector of active energy for period k.

C. Regular Meter in Error

Unlike the case of a check meter in error, when regular meter is in error during period k, the active and reactive energy losses calculations related to the meter in error will be wrong, i.e. all of (84), (85), (86), and (87) are not applicable. Therefore, in addition to (90) and (91), the following also is true:

$$\widehat{\boldsymbol{E}}_{\boldsymbol{P}_L}(k) \neq \boldsymbol{E}_{\boldsymbol{P}_L}(k) \tag{98}$$

$$\widehat{\boldsymbol{E}}_{\boldsymbol{Q}_L}(k) \neq \boldsymbol{E}_{\boldsymbol{Q}_L}(k) \tag{99}$$

The syndrome vector will result in a vector that has a form similar to one of the rows of decoding matrix multiplied by a scaler equal to the magnitude of error plus the energy losses related to the meter in error. To demonstrate that, we will assume an error in measurement of regular meter number 3; hence, the active power's syndrome vector will result in:

$$\tilde{\boldsymbol{s}}_{\boldsymbol{E}_p}(k) = \widehat{\boldsymbol{E}}_{\boldsymbol{p}}(k) \cdot D + \widehat{\boldsymbol{E}}_{\boldsymbol{P}_L}(k) \cdot D$$

$$= \begin{pmatrix} E_{p1}(k) \\ E_{p2}(k) \\ E_{p3}(k) + e_{E_{p3}}(k) \\ E_{p4}(k) \\ E_{p5}(k) \\ E_{p6}(k) \\ E_{p7}(k) \end{pmatrix}^{\mathrm{T}} \begin{pmatrix} 1 & 1 & 0 \\ 1 & 0 & 1 \\ 0 & 1 & 1 \\ 1 & 1 & 1 \\ -1 & 0 & 0 \\ 0 & -1 & 0 \\ 0 & 0 & -1 \end{pmatrix} + \begin{pmatrix} \frac{AR_{I_1^2}(k)\, R_1}{\alpha} \\ \frac{AR_{I_2^2}(k)\, R_2}{\alpha} \\ \frac{\left(AR_{I_3^2}(k) + e_{AI_3}(k)\right) R_3}{\alpha} \\ \frac{AR_{I_4^2}(k)\, R_4}{\alpha} \\ 0 \\ 0 \\ 0 \end{pmatrix}^{\mathrm{T}} \begin{pmatrix} 1 & 1 & 0 \\ 1 & 0 & 1 \\ 0 & 1 & 1 \\ 1 & 1 & 1 \\ -1 & 0 & 0 \\ 0 & -1 & 0 \\ 0 & 0 & -1 \end{pmatrix} \tag{100}$$

$$=$$

$$\begin{pmatrix} E_{p1}(k) + E_{p2}(k) + E_{p4}(\mathrm{k}) - E_{p5}(\mathrm{k}) + \frac{AR_{I_1^2}(k)R_1}{\alpha} + \frac{AR_{I_2^2}(k)R_2}{\alpha} + \frac{AR_{I_4^2}(k)R_4}{\alpha} \\ E_{p1}(k) + E_{p3}(k) + e_{E_{p3}}(k) + E_{p4}(\mathrm{k}) - E_{p6}(\mathrm{k}) + \frac{AR_{I_1^2}(k)R_1}{\alpha} + \frac{(AR_{I_3^2}(k) + e_{AI_3}(k))R_3}{\alpha} + \frac{AR_{I_4^2}(k)R_4}{\alpha} \\ E_{p2}(k) + E_{p3}(k) + e_{E_{p3}}(k) + E_{p4}(\mathrm{k}) - E_{p7}(\mathrm{k}) + \frac{AR_{I_2^2}(k)\,R_2}{\alpha} + \frac{(AR_{I_3^2}(k) + e_{AI_3}(k))R_3}{\alpha} + \frac{AR_{I_4^2}(k)\,R_4}{\alpha} \end{pmatrix}^T$$

$$= \begin{pmatrix} 0 \\ e_{E_{p3}}(k) + \frac{e_{AI_3}(k)\,R_3}{\alpha} \\ e_{E_{p3}}(k) + \frac{e_{AI_3}(k)\,R_3}{\alpha} \end{pmatrix}^T$$

$e_{E_{p3}}(k)$ is the error in reactive energy measurement of check meter number 3 for period k,

$e_{AI_3}(k)$ is the error in the area under the squared current of meter number 3 for period k.

The same can be applied to reactive energy as:

$$\tilde{\boldsymbol{s}}_{\boldsymbol{E_p}}(k) = \widehat{\boldsymbol{E}}_{\boldsymbol{p}}(k) \cdot D + \widehat{\boldsymbol{E}}_{\boldsymbol{P_L}}(k) \cdot D$$

$$= \begin{pmatrix} E_{q1}(k) \\ E_{q2}(k) \\ E_{q3}(k) + e_{E_{q3}}(k) \\ E_{q4}(k) \\ E_{q5}(k) \\ E_{q6}(k) \\ E_{q7}(k) \end{pmatrix}^{\mathrm{T}} \begin{pmatrix} 1 & 1 & 0 \\ 1 & 0 & 1 \\ 0 & 1 & 1 \\ 1 & 1 & 1 \\ -1 & 0 & 0 \\ 0 & -1 & 0 \\ 0 & 0 & -1 \end{pmatrix} + \begin{pmatrix} \frac{AR_{I_1^2}(k)\,X_1}{\alpha} \\ \frac{AR_{I_2^2}(k)\,X_2}{\alpha} \\ \frac{\left(AR_{I_3^2}(k) + e_{AI_3}(k)\right)X_3}{\alpha} \\ \frac{AR_{I_4^2}(k)\,X_4}{\alpha} \\ 0 \\ 0 \\ 0 \end{pmatrix}^{\mathrm{T}} \begin{pmatrix} 1 & 1 & 0 \\ 1 & 0 & 1 \\ 0 & 1 & 1 \\ 1 & 1 & 1 \\ -1 & 0 & 0 \\ 0 & -1 & 0 \\ 0 & 0 & -1 \end{pmatrix} \quad (101)$$

$$=$$

$$\begin{pmatrix} E_{q1}(k) + E_{q2}(k) + E_{q4}(\mathrm{k}) - E_{q5}(\mathrm{k}) + \frac{AR_{I_1^2}(k)X_1}{\alpha} + \frac{AR_{I_2^2}(k)X_2}{\alpha} + \frac{AR_{I_4^2}(k)X_4}{\alpha} \\ E_{q1}(k) + E_{q3}(k) + e_{E_{q3}}(k) + E_{q4}(\mathrm{k}) - E_{q6}(\mathrm{k}) + \frac{AR_{I_1^2}(k)X_1}{\alpha} + \frac{(AR_{I_3^2}(k) + e_{AI_3}(k))X_3}{\alpha} + \frac{AR_{I_4^2}(k)X_4}{\alpha} \\ E_{q2}(k) + E_{q3}(k) + e_{E_{q3}}(k) + E_{q4}(\mathrm{k}) - E_{q7}(\mathrm{k}) + \frac{AR_{I_2^2}(k)\,X_2}{\alpha} + \frac{(AR_{I_3^2}(k) + e_{AI_3}(k))X_3}{\alpha} + \frac{AR_{I_4^2}(k)\,X_4}{\alpha} \end{pmatrix}^T$$

$$= \begin{pmatrix} 0 \\ e_{E_{q3}}(k) + \frac{e_{AI_3}(k)\,X_3}{\alpha} \\ e_{E_{q3}}(k) + \frac{e_{AI_3}(k)\,X_3}{\alpha} \end{pmatrix}^T$$

We can see that the syndrome vectors include the error in active and reactive energy measurements, i.e. $e_{E_{p3}}(k)$ and $e_{E_{q3}}(k)$, but it also includes additional terms that will affect the corrected values, i.e. $\frac{e_{AI_3}(k)\,R_3}{\alpha}$ and $\frac{e_{AI_3}(k)\,X_3}{\alpha}$. Therefore, the syndrome vector cannot be used directly to correct the measurement of regular meter. This can be solved by adding the wrong active and reactive energy measured to the wrong active and reactive energy losses calculated and subtract the mismatch detected form the syndrome vector which will add up and will equal to the actual (corrected) active and reactive energies at sending end as:

$$E_{p_{sd3}}(k) = \left(E_{p3}(k) + e_{E_{p3}}(k)\right) + \frac{(AR_{I_3^2}(k) + e_{AI_3}(k))\,R_3}{\alpha} - \left(e_{E_{p3}}(k) + \frac{e_{AI_3}(k)\,R_3}{\alpha}\right) = E_{p3}(k) + \frac{AR_{I_3^2}(k)\,R_3}{\alpha} \tag{102}$$

and,

$$E_{q_{sd3}}(k) = \left(E_{q3}(k) + e_{E_{q3}}(k)\right) + \frac{(AR_{I_3^2}(k) + e_{AI_3}(k))\,X_3}{\alpha} - \left(e_{E_{q3}}(k) + \frac{e_{AI_3}(k)\,X_3}{\alpha}\right) = E_{q3}(k) + \frac{AR_{I_3^2}(k)\,X_3}{\alpha} \tag{103}$$

where $E_{p_{sd3}}(k)$ is the actual (corrected) active energy at sending end of cable number 3, $E_{q_{sd3}}(k)$ is the actual (corrected) reactive energy at sending end of cable number 3.

Since the corrected values are the active and reactive energies at sending end, (61), (62), and (63) cannot be applied. Therefore, this algorithm can estimate the actual energy at sending end which equals to the actual energy consumed in addition to the actual energy losses in that cable, hence:

$$\hat{E}_{p_{corrected_3}}(k) = E_{p_{sd3}}(k) = E_{p3}(k) + \frac{AR_{I_3^2}(k)\,R_3}{\alpha} \tag{104}$$

and,

$$\hat{E}_{q_{corrected_3}}(k) = E_{q_{sd3}}(k) = E_{q3}(k) + \frac{AR_{I_3^2}(k)\, X_3}{\alpha} \tag{105}$$

D. Other Sources of NTL

After inspection, if the service provider found that the mismatch in syndrome vector was due to other source of NTL such as cable tapping, then the regular meter is not in error and all of (84), (85), (86), and (87) is applicable but the syndrome vector will not return zeros as shown:

$$\begin{aligned}
&\tilde{\boldsymbol{s}}_{\boldsymbol{E_p}}(k) = \hat{\boldsymbol{E}}_{\boldsymbol{p}}(k)\cdot D + \hat{\boldsymbol{E}}_{\boldsymbol{P_L}}(k)\cdot D = \boldsymbol{E_p}(k)\cdot D + \boldsymbol{E_{P_L}}(k)\cdot D \\
&= \begin{pmatrix} E_{p1}(k) \\ E_{p2}(k) \\ E_{p3}(k) \\ E_{p4}(k) \\ E_{p5}(k) \\ E_{p6}(k) \\ E_{p7}(k) \end{pmatrix}^{\mathrm{T}} \begin{pmatrix} 1 & 1 & 0 \\ 1 & 0 & 1 \\ 0 & 1 & 1 \\ 1 & 1 & 1 \\ -1 & 0 & 0 \\ 0 & -1 & 0 \\ 0 & 0 & -1 \end{pmatrix} + \begin{pmatrix} \frac{AR_{I_1^2}(k)\, R_1}{\alpha} \\ \frac{AR_{I_2^2}(k)\, R_2}{\alpha} \\ \frac{AR_{I_3^2}(k)\, R_3}{\alpha} \\ \frac{AR_{I_4^2}(k)\, R_4}{\alpha} \\ 0 \\ 0 \\ 0 \end{pmatrix}^{\mathrm{T}} \begin{pmatrix} 1 & 1 & 0 \\ 1 & 0 & 1 \\ 0 & 1 & 1 \\ 1 & 1 & 1 \\ -1 & 0 & 0 \\ 0 & -1 & 0 \\ 0 & 0 & -1 \end{pmatrix} \\
&= \begin{pmatrix} E_{p1}(k) + E_{p2}(k) + E_{p4}(\mathrm{k}) - E_{p5}(\mathrm{k}) + \frac{AR_{I_1^2}(k)\, R_1}{\alpha} + \frac{AR_{I_2^2}(k)\, R_2}{\alpha} + \frac{AR_{I_4^2}(k)\, R_4}{\alpha} \\ E_{p1}(k) + E_{p3}(k) + E_{p4}(\mathrm{k}) - E_{p6}(\mathrm{k}) + \frac{AR_{I_1^2}(k)\, R_1}{\alpha} + \frac{AR_{I_3^2}(k)\, R_3}{\alpha} + \frac{AR_{I_4^2}(k)\, R_4}{\alpha} \\ E_{p2}(k) + E_{p3}(k) + E_{p4}(\mathrm{k}) - E_{p7}(\mathrm{k}) + \frac{AR_{I_2^2}(k)\, R_2}{\alpha} + \frac{AR_{I_3^2}(k)\, R_3}{\alpha} + \frac{AR_{I_4^2}(k)\, R_4}{\alpha} \end{pmatrix}^{T} \\
&\neq [0 \quad 0 \quad 0]
\end{aligned} \tag{106}$$

Here all the smart meters readings are correct, but the syndrome vector will return non-zero numbers due to another source of NTL. The check meter readings $E_{p5}(k)$, $E_{p6}(k)$and $E_{p7}(k)$ will include an additional term $e_{NTL_{E_p}}(k)$ that represents the energy consumed due to the new source of NTL during period k. For example, if $e_{NTL_{E_{p3}}}(k)$ is the active energy losses due to tapping of cable number 3 during period k, then (106) will result in:

$$\tilde{\boldsymbol{s}}_{\boldsymbol{E_p}}(k) = \widehat{\boldsymbol{E}}_{\boldsymbol{p}}(k) \cdot D + \widehat{\boldsymbol{E}}_{\boldsymbol{P_L}}(k) \cdot D = \boldsymbol{E_p}(k) \cdot D + \boldsymbol{E_{P_L}}(k) \cdot D$$
$$= [0 \quad -e_{NTL_{E_{p3}}}(k) \quad -e_{NTL_{E_{p3}}}(k)] \tag{107}$$

Similarly, the reactive power syndrome vector can be written as:

$$\tilde{\boldsymbol{s}}_{\boldsymbol{E_q}}(k) = \widehat{\boldsymbol{E}}_{\boldsymbol{q}}(k) \cdot D + \widehat{\boldsymbol{E}}_{\boldsymbol{Q_L}}(k) \cdot D = \boldsymbol{E_q}(k) \cdot D + \boldsymbol{E_{Q_L}}(k) \cdot D$$
$$= [0 \quad -e_{NTL_{E_{q3}}}(k) \quad -e_{NTL_{E_{q3}}}(k)\,] \tag{108}$$

where $e_{NTL_{E_{q3}}}(k)$ is the reactive energy losses due to tapping of cable number 3 during period k.

Here $e_{NTL_{E_{p3}}}(k)$ and $e_{NTL_{E_{q3}}}(k)$ will appear in all check meters taking measurement of cable corresponding to the cable being tapped. Also, $e_{NTL_{E_{p3}}}(k)$ and $e_{NTL_{E_{q3}}}(k)$ include the direct and indirect NTL related to the attack during period k, e.g., if the source of NTL was tapping the service cable, the values $e_{NTL_{E_{p3}}}(k)$ and $e_{NTL_{E_{q3}}}(k)$ represents the sum of energy consumed and the energy losses added to the service cable because of the tapping. Here we can consider the energy losses in the cable as non-technical losses NTL instead of being technical losses TL; because this amount of losses would not exist if the source of NTL had not been present.

CHAPTER 4

RESULTS AND CONCLUSION

4.1 Simulation Results and Discussion

In this section, the method proposed is simulated on a system having four regular meters and three check meters as shown in Figure 3.21. The cables simulated are the commercially available $1/0$ AWG cables, each having a different length (i.e. 80, 100, 150, and 200 meters). The properties of cables are shown in Table 7. The shunt capacitance can be ignored for low voltage distribution secondary cables because of their relatively small length and low operating voltage [41]. The cables used here are relatively smaller than the cables used in distribution secondary since each cable here is feeding a single house as shown in Figure 3.21.

Table 7: Properties of Cables Used in Simulation

Attribute	Value
AWG	$1/0$
Stranding	19
Insulation Type	$XLPE$
Ampacity in Duct (A)	140
Operating Voltage (V)	230
Operating Temperature ($°C$)	50
AC Resistance ($m\Omega/m$), at 60 Hz	0.3821
Series Reactance ($m\Omega/m$), at 60 Hz	0.1605

The simulation is divided into two subsections to simulate two different system capabilities, i.e. system report metering data at high frequency, and a system that report metering data at low frequency. The high frequency measurement-based detection algorithm utilizes real time active power, reactive power, RMS voltage, and RMS current in detection and correction. On the other hand, the low frequency measurement-based detection algorithm is utilizing the active energy, reactive energy, and the area under the squared RMS current. Subsection 4.1.1 is discussing the simulation of a system that reports metering data at high frequency and Subsection 4.1.2 is discussing the simulation of a system that report metering data at low frequency.

4.1.1 Detection Algorithm for Systems Reporting Measurement Data at High Frequency

The simulation is based on actual house active power load profile that record the data at a rate of 1 measurement per minute representing the average power consumed during that minute. On the other hand, the reactive power, RMS current, and RMS voltage information were randomly generated to change at the same rate of active power, i.e. once each minute. Each minute data is then divided into 60 identical samples (i.e. one measurement each second) to simulate a system reporting the data at a frequency of 1 measurement per second. The case studies are performed on errors during one hour of the day, i.e. form 11:00 AM to 12:00 PM. The plots of all meters are shown in Appendix A, the plots are representing the actual load profiles when no meter is in error.

The cable resistances are estimated using (32) at four different time instants to generate four different independent equations. The generated equations are:

$$
\begin{aligned}
&0.247691917R_1 + 0.472187313R_2 + 0.260104410R_3 \\
&\quad + 0.705302415R_4 = 0.094420819 \\
&0.249784297R_1 + 0.463453535R_2 + 0.256968950R_3 \\
&\quad + 0.485609853R_4 = 0.077182446 \\
&0.259048629R_1 + 0.628052851R_2 + 1.056315575R_3 \\
&\quad + 0.517071482R_4 = 0.131973828 \\
&0.280608489R_1 + 0.575278840R_2 + 1.308054186R_3 \\
&\quad + 0.572785766R_4 = 0.149302459
\end{aligned}
\tag{109}
$$

These equations are solved to determine the cable resistances, the estimated resistances and their comparison to the actual values is summarized in Table 8. Similarly, the cable series reactances are estimated using (35) the same time instants used to estimate the cable resistances to generate four different independent equations. The generated equations are:

$$
\begin{aligned}
&0.247691917X_1 + 0.472187313X_2 + 0.260104410X_3 \\
&\quad + 0.705302415X_4 = 0.039661192 \\
&0.249784297X_1 + 0.463453535X_2 + 0.256968950X_3 \\
&\quad + 0.485609853X_4 = 0.032420263 \\
&0.259048629X_1 + 0.628052851X_2 + 1.056315575X_3 \\
&\quad + 0.517071482X_4 = 0.055435225 \\
&0.280608489X_1 + 0.575278840X_2 + 1.308054186X_3 \\
&\quad + 0.572785766X_4 = 0.062714066
\end{aligned}
\tag{110}
$$

These equations are solved to determine the cable series reactances, the estimated reactances and their comparison to the actual values is summarized in Table 8.

Table 8: Estimated Values of Cable Impedance

Attribute	Actual	Estimated	% Difference
$R_1(\Omega)$	0.030568	0.030568	0.00
$R_2(\Omega)$	0.038210	0.038210	0.00
$R_3(\Omega)$	0.057315	0.057315	0.00
$R_4(\Omega)$	0.076420	0.076420	0.00
$X_1(\Omega)$	0.012840	0.012840	0.00
$X_2(\Omega)$	0.016050	0.016050	0.00
$X_3(\Omega)$	0.024075	0.024075	0.00
$X_4(\Omega)$	0.032100	0.032100	0.00

The estimated values of resistances and reactances will be used in detection algorithms of all cause studies, i.e. check meter in error, regular meter in error, and other source of NTL.

A. Check Meter in Error

Random errors are created in both active and reactive power measurements of check meter number 7, as shown in Figure 4.1 and Figure 4.2 respectively. The active power measurement is corrected based on (49) which is taking the vector of active power measurements and the error vector (50) as input. The error vector, i.e. (50), can be determined from the syndrome vector (48). The input to the syndrome vector calculator are the cable resistances, active power measurements of all meters (regular and check), and the RMS current measurements of regular meters. The syndrome vector returns the difference between the actual value and measured value at each time instant. The corrected

active power profile is labeled in Figure 4.1 as *Corrected*. The corrected active power profile is the same as the actual active power profile with no error in estimation (i.e. 0%).

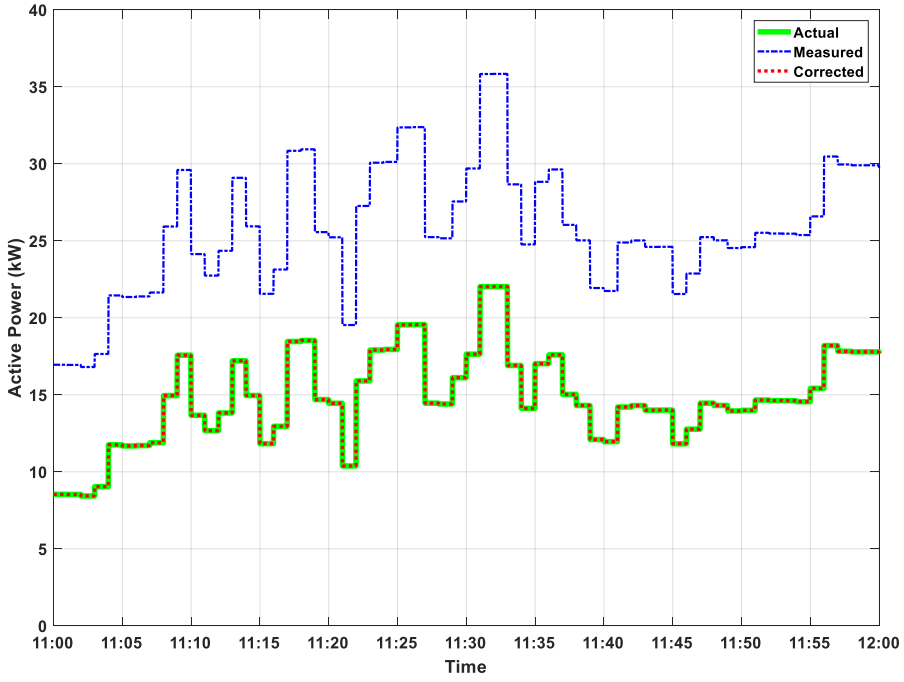

Figure 4.1: Active power of check meter no. 7 for one hour

Similarly, the reactive power measurement is corrected based on (52) which is taking the vector of reactive power measurements and the error vector (53) as input. The error vector, i.e. (52), can be determined from the syndrome vector (51). The input to the syndrome vector calculator is the cable reactances, reactive power measurements of all meters (regular and check), and the RMS current measurements of regular meters. The syndrome vector returns the difference between the actual value and measured value at each time instant. The corrected reactive power profile is labeled in Figure 4.2 as *Corrected*. The

corrected reactive power profile is the same as the actual reactive power profile with no error in estimation (i.e. 0%).

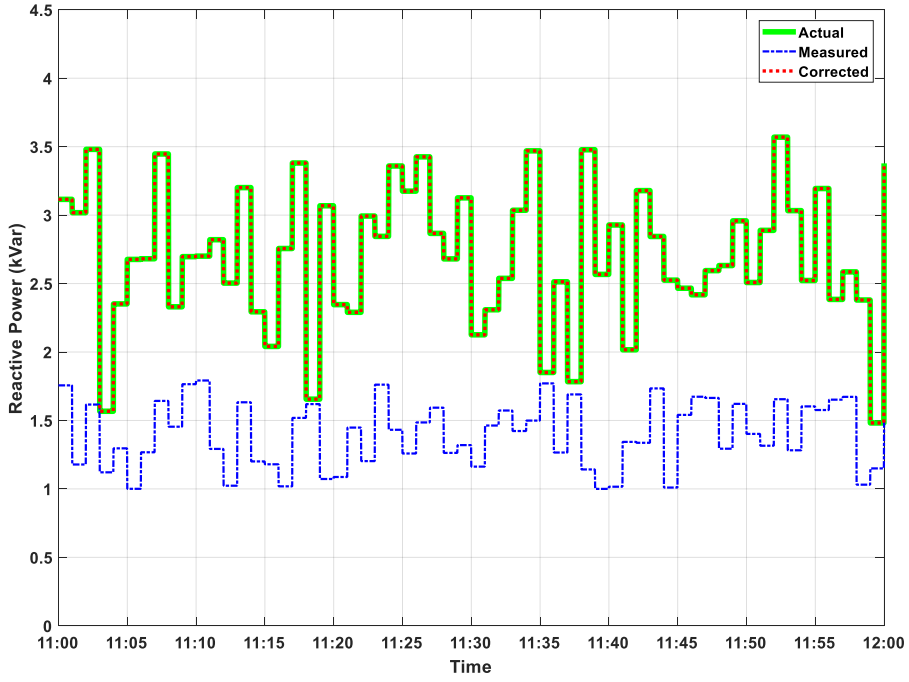

Figure 4.2: Reactive power of check meter no. 7 for one hour

The modified detection algorithm proposed in this work is compared to the original detection algorithm of [9]. The comparison is performed on two cases, first without power losses compensation by using (20), and second with power losses compensation by using (24).

The comparison of the algorithm proposed in [9] without power losses compensation in the calculation of syndrome vector, i.e. using (20), is shown in Figure 4.3 and Figure 4.4 respectively. Figure 4.3 shows the deviation of corrected active power from actual value and Figure 4.4 shows the deviation of corrected reactive power from actual value. Notice that the y-axis on the right are values multiplied by 10^{-5}.

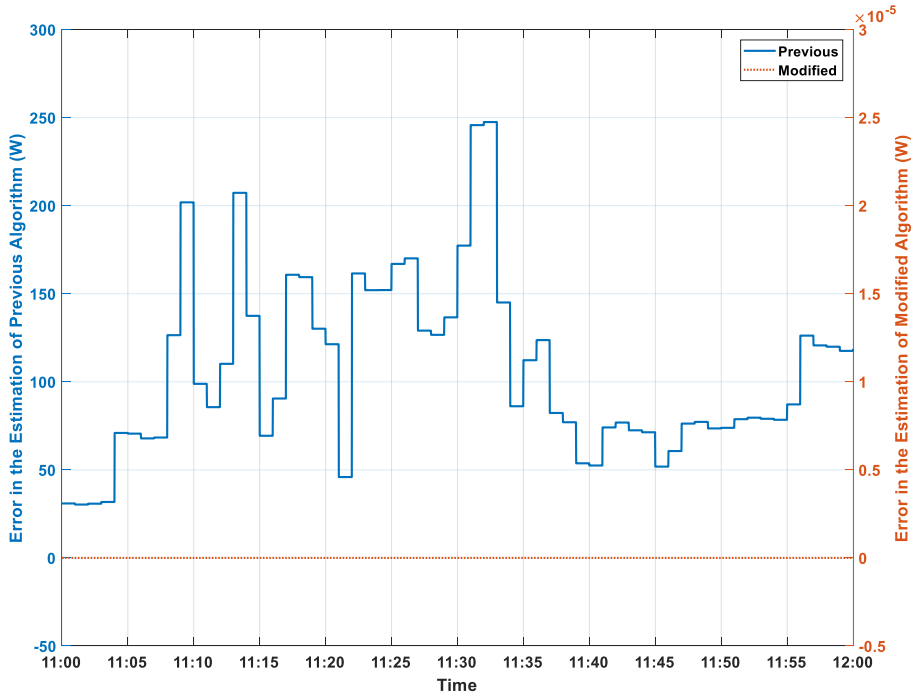

Figure 4.3: Comparison between the active power estimation of the previous algorithm with no power losses compensation and the modified algorithm for the case of check meter no. 7 in error

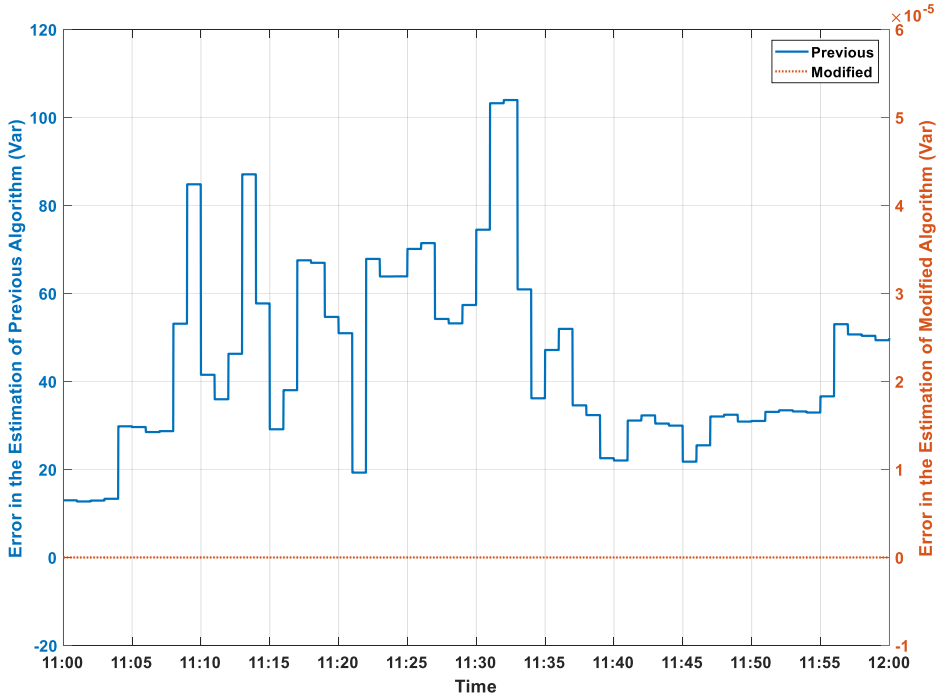

Figure 4.4: Comparison between the reactive power estimation of the previous algorithm with no power losses compensation and the modified algorithm for the case of check meter no. 7 in error

The comparison of the algorithm proposed in [9] with power losses compensation in the calculation of syndrome vector, i.e. using (24), is shown in Figure 4.5 and Figure 4.6 respectively. Using (24), there is no constant value δ_i that can be used as the correct ratio of power losses all the time, and consequently it is not possible to use $\hat{\delta}_i$ as estimated ratio of power losses. Therefore, we used the average ratio of power losses of 24 hours to represent the constant ratio of power losses in the detection algorithm. The average ratios of active and reactive power losses for the 24 hours are calculated and shown in Table 9.

Table 9: Ratios of Power Losses as Percentage to Delivered Power

Cable Number	Ratio of Active Power Losses	Ratio of Reactive Power Losses
Cable 1	0.28859%	0.98038 %
Cable 2	0.40082%	0.69828 %
Cable 3	0.60646%	2.23361 %
Cable 4	0.84177%	1.25407 %

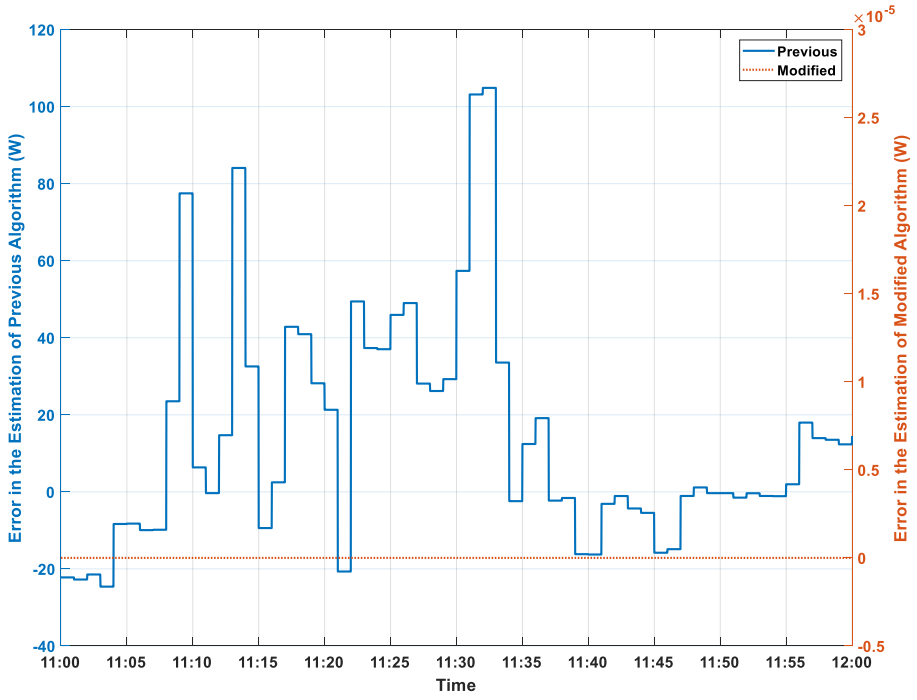

Figure 4.5: Comparison between the active power estimation of the previous algorithm with power losses compensation and the modified algorithm for the case of check meter no. 7 in error

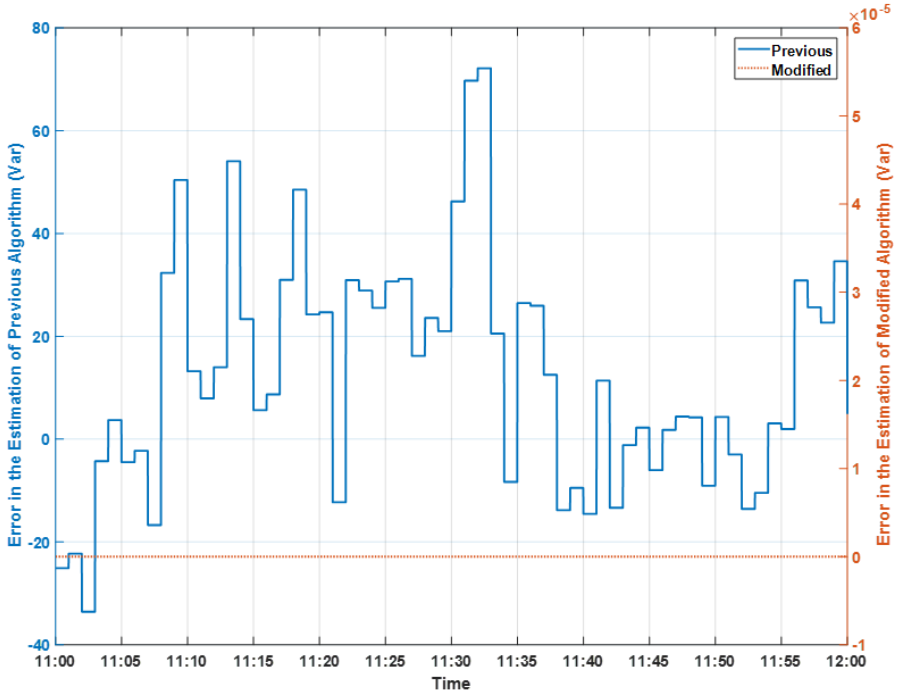

Figure 4.6: Comparison between the reactive power estimation of the previous algorithm with power losses compensation and the modified algorithm for the case of check meter no. 7 in error

As we can see from Figure 4.5 and Figure 4.6 , the modified detection algorithm outperformed the original detection algorithm that was proposed in [9] even with the use of power losses compensation. Notice that the y-axis on the right in Figure 4.5 and Figure 4.6 are values multiplied by 10^{-5}.

B. Regular Meter in Error

Random errors are created in all of: active power, reactive power, and RMS current measurements of regular meter number 4, as shown in Figure 4.7, Figure 4.8, and Figure 4.9 respectively. The active power measurement is corrected based on (62) which is taking the actual active power at sending end (59) and the the corrected RMS current at the sending end (61) as inputs. The actual active power at sending end, i.e. (59), is determined by addition of the wrong active power measured to the wrong active power losses calculated in (56), then subtract the mismatch detected form the syndrome vector (56) which will add up and will equal to the actual active and reactive power at sending end. The corrected active power profile is labeled in Figure 4.7 as *Corrected*. The corrected active power profile is the same as the actual active power profile with no error in estimation (i.e. 0%).

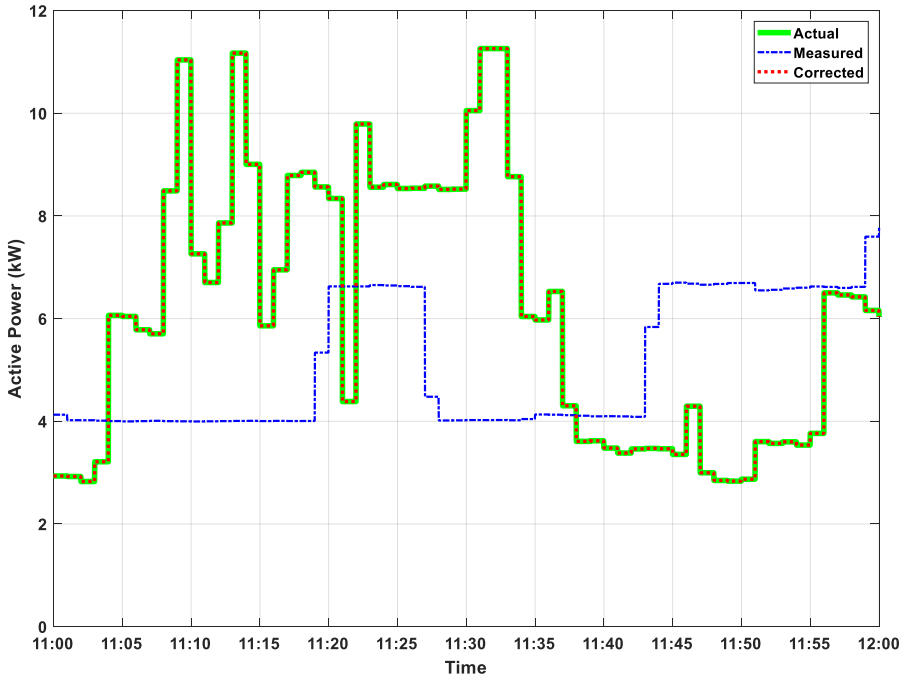

Figure 4.7: Active power of regular meter no. 4 for one hour

Similarly, the reactive power measurement is corrected and the corrected reactive power profile is labeled in Figure 4.8 as *Corrected*. The corrected reactive power profile is the same as the actual reactive power profile with no error in estimation (i.e. 0%).

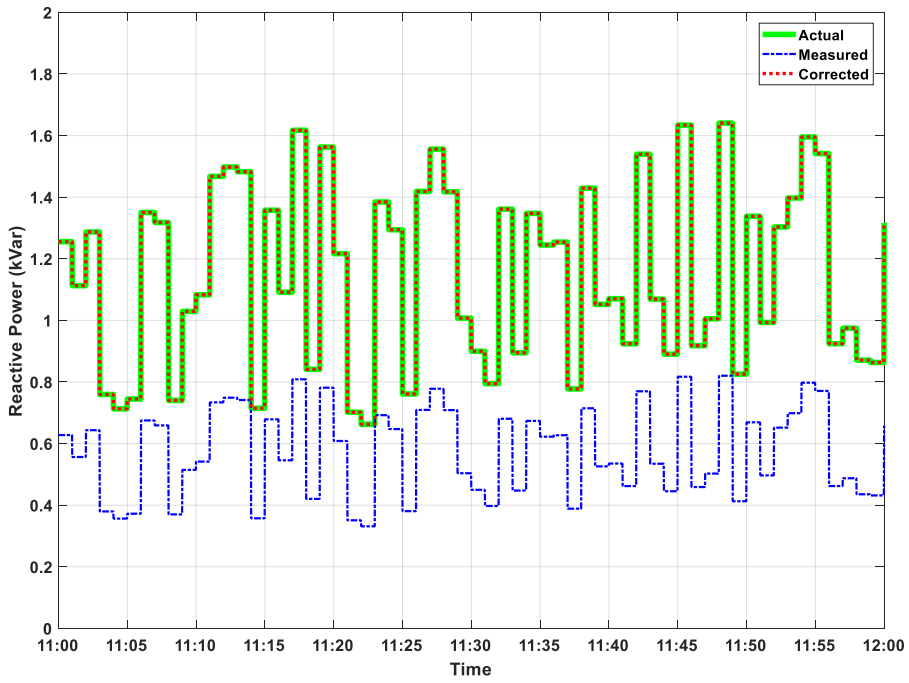

Figure 4.8: Reactive power of regular meter no. 4 for one hour

The RMS current is corrected based on (61), the input to (61) is the RMS voltage of check meter, active power at sending end (59), and reactive power at sending end (60). The RMS current profile is labeled in Figure 4.9 as *Corrected*. Which is the same as the actual active RMS current with no error in estimation (i.e. 0%).

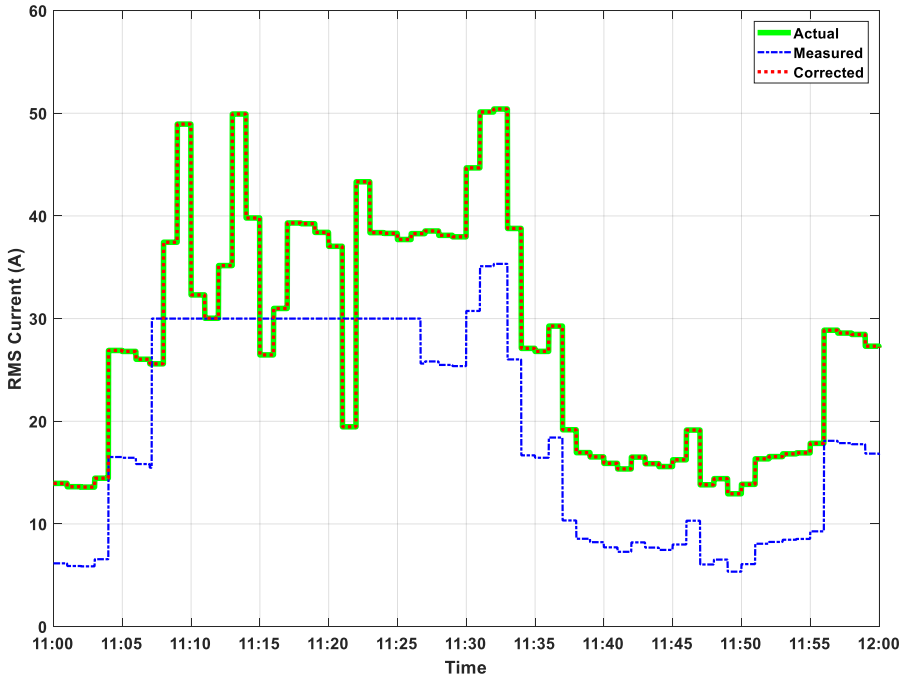

Figure 4.9: RMS current of regular meter no. 4 for one hour

The modified detection algorithm proposed in this work is compared to the original detection algorithm of [9]. The comparison is performed on two cases, first without power losses compensation, i.e. by using (20), and second with power losses compensation, i.e. by using (24).

The comparison of the algorithm proposed in [9] without power losses compensation in the calculation of syndrome vector, i.e. using (20), is shown in Figure 4.10 and Figure 4.11 respectively. Figure 4.10 shows the deviation of corrected active power from actual value and Figure 4.11 shows the deviation of corrected reactive power from actual value. Notice that the y-axis on the right are values multiplied by 10^{-5}.

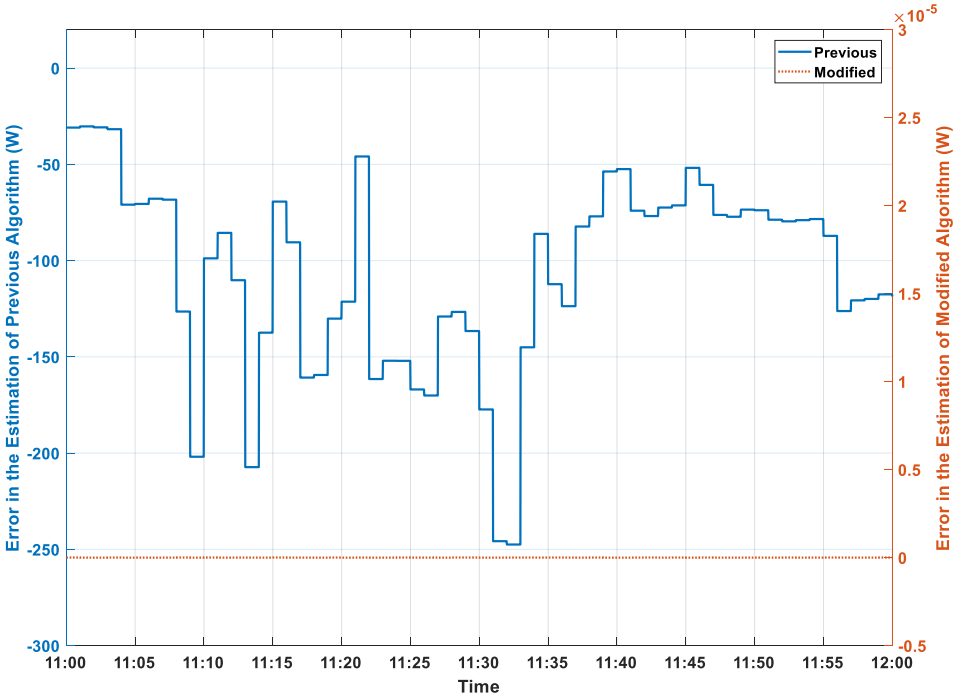

Figure 4.10: Comparison between the active power estimation of the previous algorithm with no power losses compensation and the modified algorithm for the case of regular meter no. 4 in error

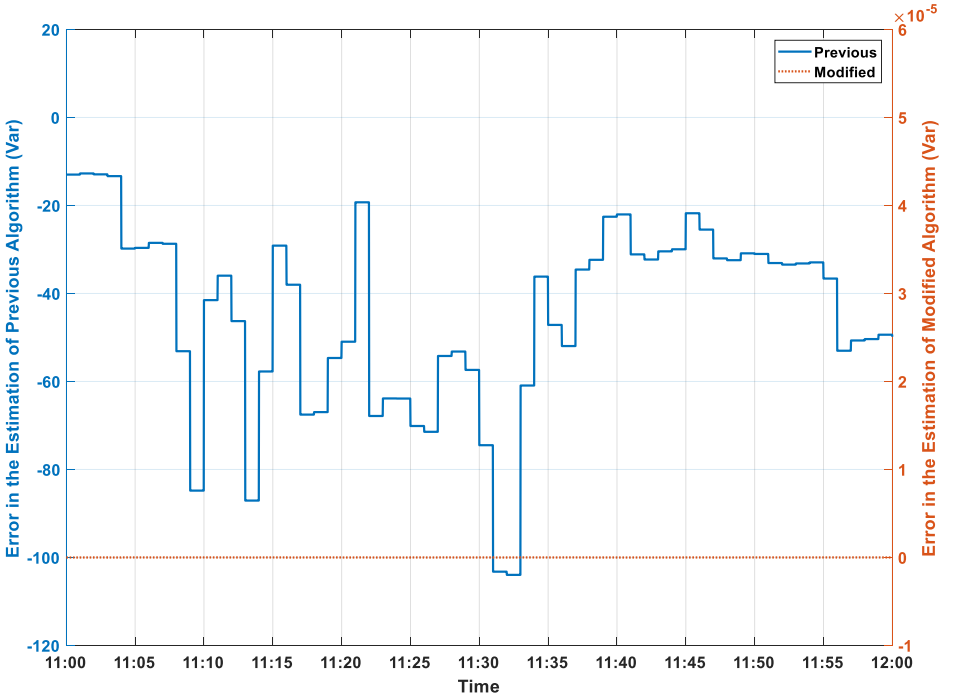

Figure 4.11: Comparison between the reactive power estimation of the previous algorithm with no power losses compensation and the modified algorithm for the case of regular meter no. 4 in error

The comparison of the algorithm proposed in [9] with power losses compensation in the calculation of syndrome vector, i.e. using (24), is shown in Figure 4.12 and Figure 4.13 respectively. The average ratios of active and reactive power losses for the 24 hours are calculated and shown in Table 9.

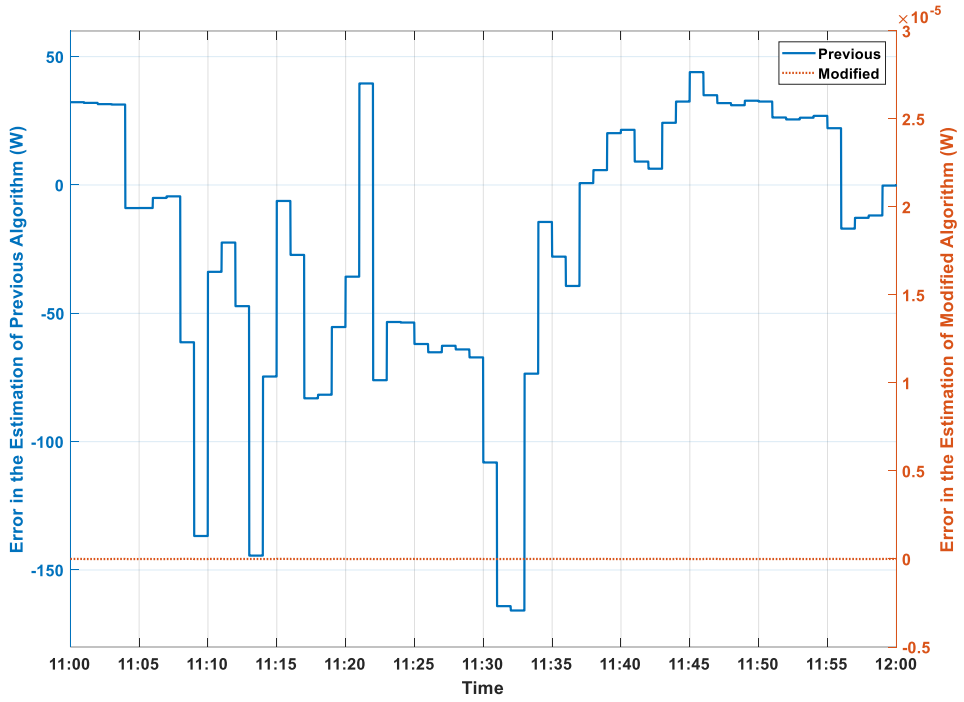

Figure 4.12: Comparison between the active power estimation of the previous algorithm with power losses compensation and the modified algorithm for the case of regular meter no. 4 in error

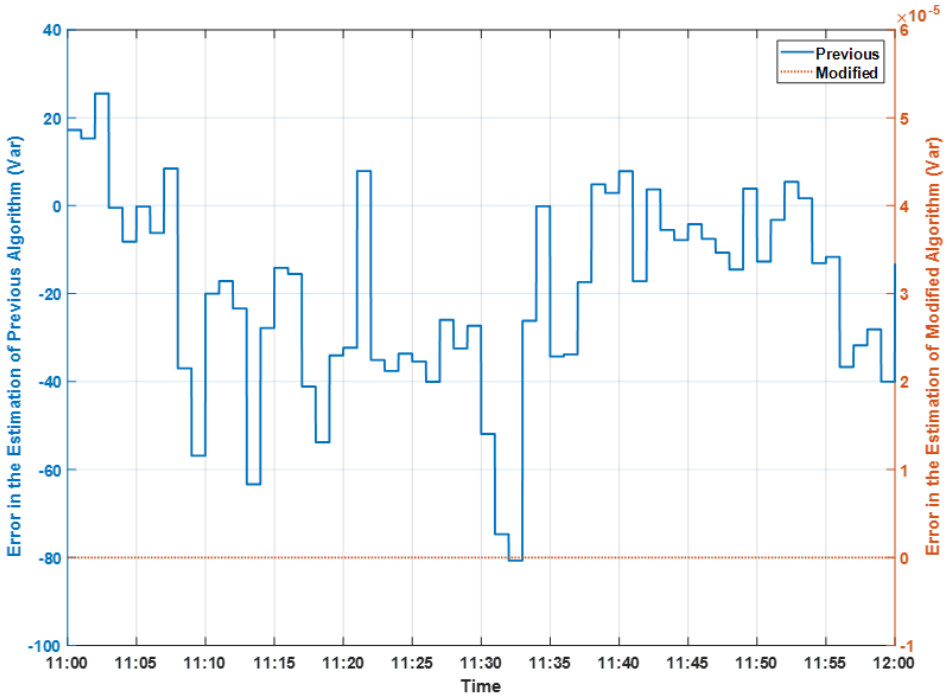

Figure 4.13: Comparison between the reactive power estimation of the previous algorithm with power losses compensation and the modified algorithm for the case of regular meter no. 4 in error

As we can see from Figure 4.12 and Figure 4.13, the modified detection algorithm outperformed the original detection algorithm that was proposed in [9] even with the use of power losses compensation. Notice that the y-axis on the right in Figure 4.12 and Figure 4.13 are values multiplied by 10^{-5}.

C. Another Source of NTL

Random active and reactive power consumption is created along cable number 4 to represent unauthorized tapping in the cable. The estimated power consumption (labeled as *Estimated NTL*) is the result of applying (69) and (70) on the measurements received form all meters. The estimated NTL is the summation of the power consumed and the power losses added to the distribution secondary due to cable tapping. As can be seen in Figure

4.14 and Figure 4.15, the active and reactive corrected power consumption are the same as the actual consumption with no error in estimation (i.e. 0%).

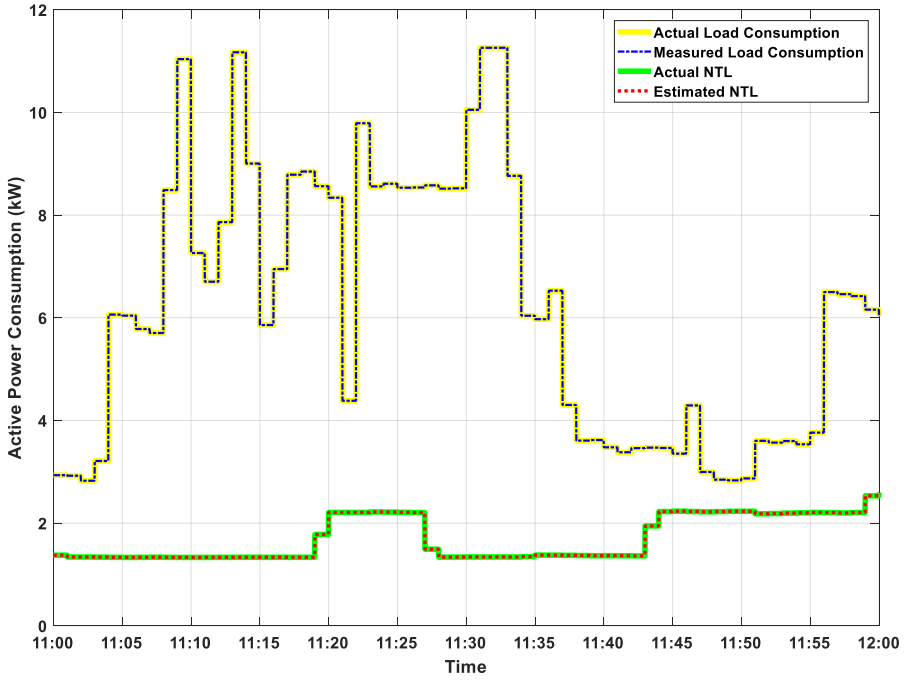

Figure 4.14: Active power tapped from cable no. 4

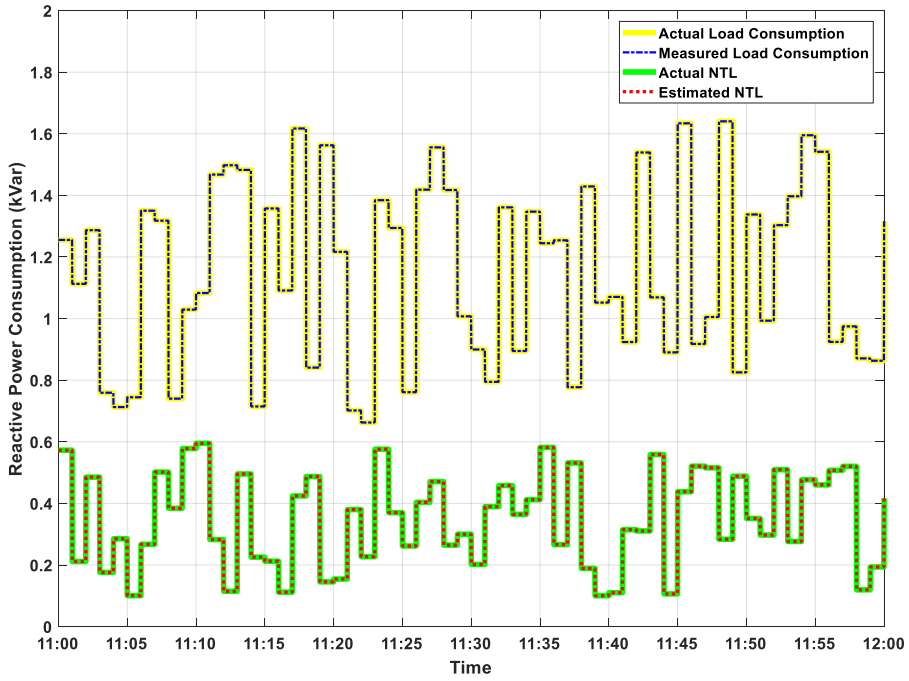

Figure 4.15: Reactive power tapped from cable no. 4

The modified detection algorithm proposed in this work is compared to the original detection algorithm of [9]. The comparison is performed on two cases, first without power losses compensation, i.e. by using (20), and second with power losses compensation, i.e. by using (24).

The comparison of the algorithm proposed in [9] without power losses compensation in the calculation of syndrome vector, i.e. using (20), is shown in Figure 4.16 and Figure 4.17 respectively. Figure 4.16 shows the deviation of corrected active power from actual value and Figure 4.17 shows the deviation of corrected reactive power from actual value. Notice that the y-axis on the right are values multiplied by 10^{-5}.

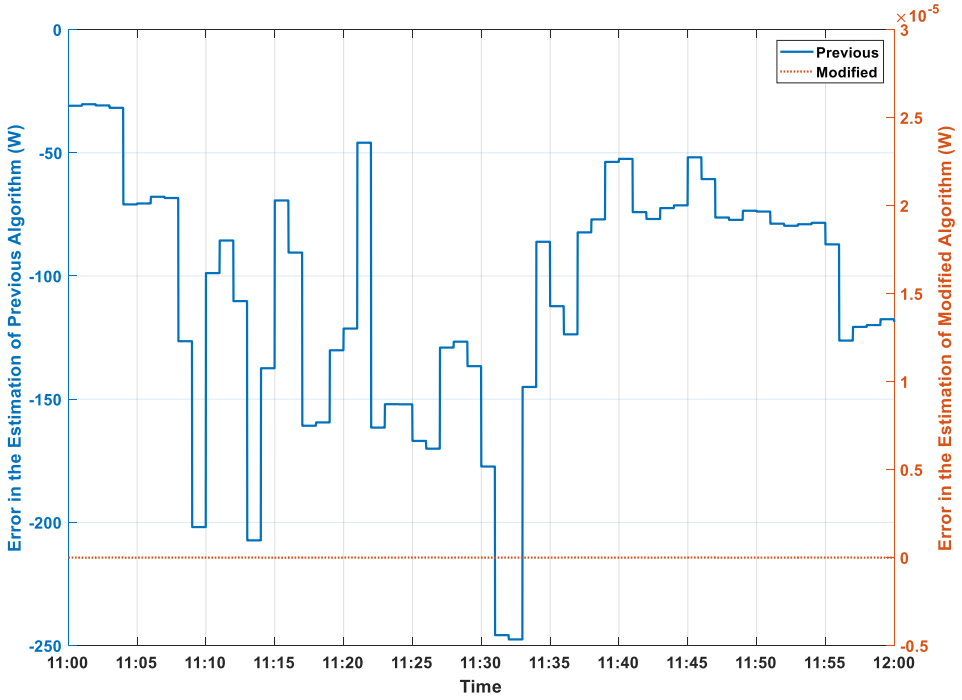

Figure 4.16: Comparison between the active power estimation of the previous algorithm with no power losses compensation and the modified algorithm for the case of tapping cable no. 4

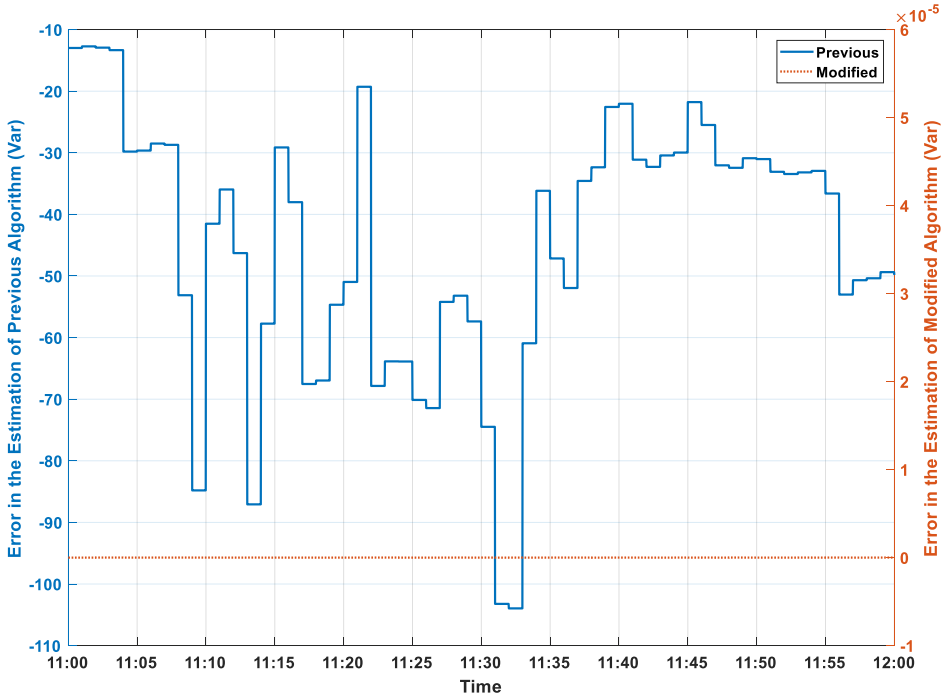

Figure 4.17: Comparison between the reactive power estimation of the previous algorithm with no power losses compensation and the modified algorithm for the case of tapping cable no. 4

The comparison of the algorithm proposed in [9] with power losses compensation in the calculation of syndrome vector, i.e. using (24), is shown in Figure 4.18 and Figure 4.19 respectively. The average ratios of active and reactive power losses for the 24 hours are calculated and shown in Table 9.

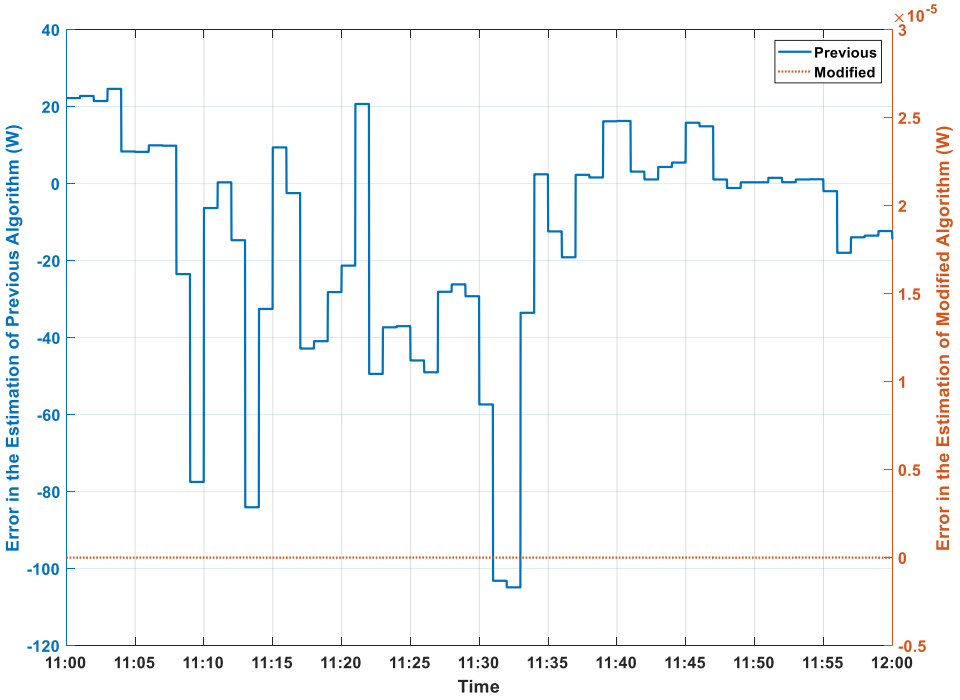

Figure 4.18: Comparison between the active power estimation of the previous algorithm with power losses compensation and the modified algorithm for the case of tapping cable no. 4

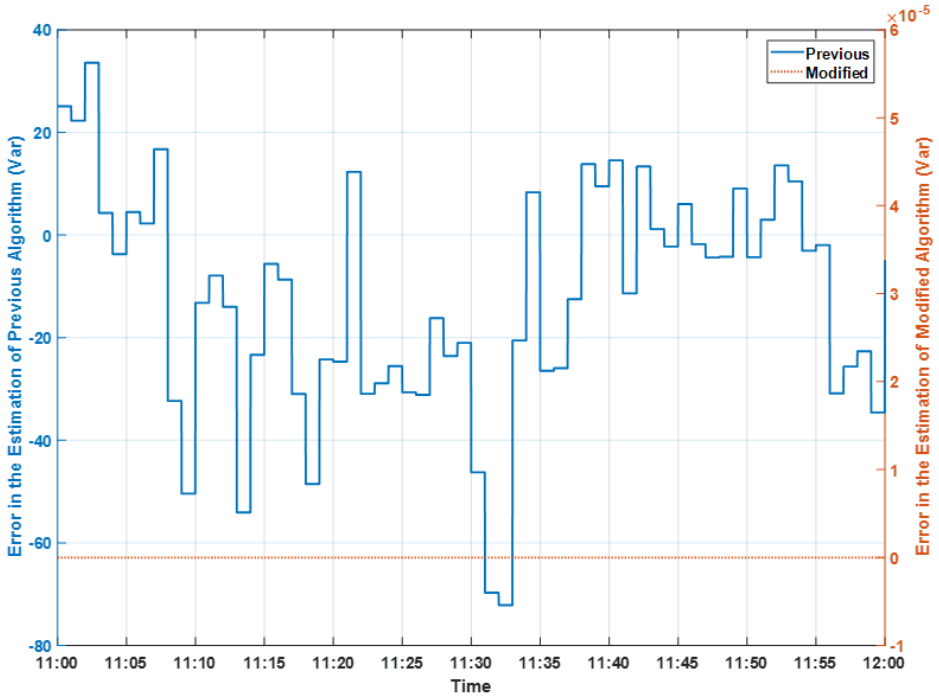

Figure 4.19: Comparison between the reactive power estimation of the previous algorithm with power losses compensation and the modified algorithm for the case of tapping cable no. 4

As we can see from Figure 4.18 and Figure 4.19, the modified detection algorithm outperformed the original detection algorithm that was proposed in [9] even with the use of power losses compensation. Notice that the y-axis on the right in Figure 4.18 and Figure 4.19 are values multiplied by 10^{-5}.

4.1.2 Detection Algorithm for Systems Reporting Measurement Data at Low Frequency

The measurements are assumed to be received once each hour; i.e., the default resolution of PG&E smart metering system [42]. The load profiles used are based on real house load profile data (same profile used in subsection 4.1.1) having a resolution of one measurement each minute, the measurements resolution reduced to one measurement each hour to show

the robustness of the proposed method in estimating the energy losses at low-rate measurements. The reactive power, RMS current, and RMS voltage information was randomly generated. The simulations are based on the active energy, reactive energy, and the area under the squared current measurements received on hourly basis. The case studies are performed on errors for one day, i.e. 24 hours. The plots of all meters are shown in Appendix B, the plots are representing the actual load profiles when no meter is in error.

Firstly, the cable resistances are estimated using (78) at four different time instants to generate four different independent equations. The generated equations are:

$$\begin{aligned}
&0.372628787R_1 + 1.175087757R_2 + 0.808581126R_3 \\
&\quad + 0.969002857R_4 = 0.176685646 \\
&0.385930272R_1 + 0.635761654R_2 + 0.777956112R_3 \\
&\quad + 1.298538639R_4 = 0.179912447 \\
&0.744203206R_1 + 0.593347770R_2 + 2.167513946R_3 \\
&\quad + 1.101911749R_4 = 0.253859780 \\
&1.642114276R_1 + 0.797488309R_2 + 0.681384437R_3 \\
&\quad + 0.769336342R_4 = 0.178514410
\end{aligned} \tag{111}$$

These equations are solved to determine the cable resistances, the estimated resistances and their comparison to the actual values is summarized in Table 10. Similarly, the cable series reactances are estimated using (79) the same time instants used to estimate the cable resistances to generate four different independent equations. The generated equations are:

$$\begin{aligned}
&0.372628787X_1 + 1.175087757X_2 + 0.808581126X_3 \\
&\quad + 0.969002857X_4 = 0.074216294 \\
&0.385930272X_1 + 0.635761654X_2 + 0.777956112X_3 \\
&\quad + 1.298538639X_4 = 0.075571703
\end{aligned} \tag{112}$$

$$0.744203206X_1 + 0.59334777X_2 + 2.167513946X_3 + 1.101911749X_4 = 0.106633066$$

$$1.642114276X_1 + 0.797488309X_2 + 0.681384437X_3 + 0.769336342X_4 = 0.074984462$$

These equations are solved to determine the cable series reactances, the estimated reactances and their comparison to the actual values is summarized in Table 10.

Table 10: Estimated Values of Cable Impedance Using Area Under the Squared Current

Attribute	Actual	Estimated	% Difference
$R_1(\Omega)$	0.030568	0.030568	0.00
$R_2(\Omega)$	0.038210	0.038210	0.00
$R_3(\Omega)$	0.057315	0.057315	0.00
$R_4(\Omega)$	0.076420	0.076420	0.00
$X_1(\Omega)$	0.012840	0.012840	0.00
$X_2(\Omega)$	0.016050	0.016050	0.00
$X_3(\Omega)$	0.024075	0.024075	0.00
$X_4(\Omega)$	0.032100	0.032100	0.00

Now, the estimated values of resistances and reactances will be used in detection algorithms of all cause studies, i.e. check meter in error, regular meter in error, and other source of NTL.

D. Check Meter in Error

Random errors are created in both active and reactive energy measurements of check meter number 5, as shown in Figure 3.22 and Figure 3.23 respectively. The active energy measurement is corrected based on (93) which is taking the vector of active energy measurements and the error vector (94) as input. The error vector, i.e. (94), can be determined from the syndrome vector (92). The input to the syndrome vector calculator is the cable resistances, active energy measurements of all meters (regular and check), and the area under the squared RMS current measurements of regular meters. The syndrome vector returns the difference between the actual value and measured value for each period. The corrected active power profile is labeled in Figure 3.22 as *Corrected*. The corrected active energy profile is the same as the actual active energy profile with no error in estimation (i.e. 0%).

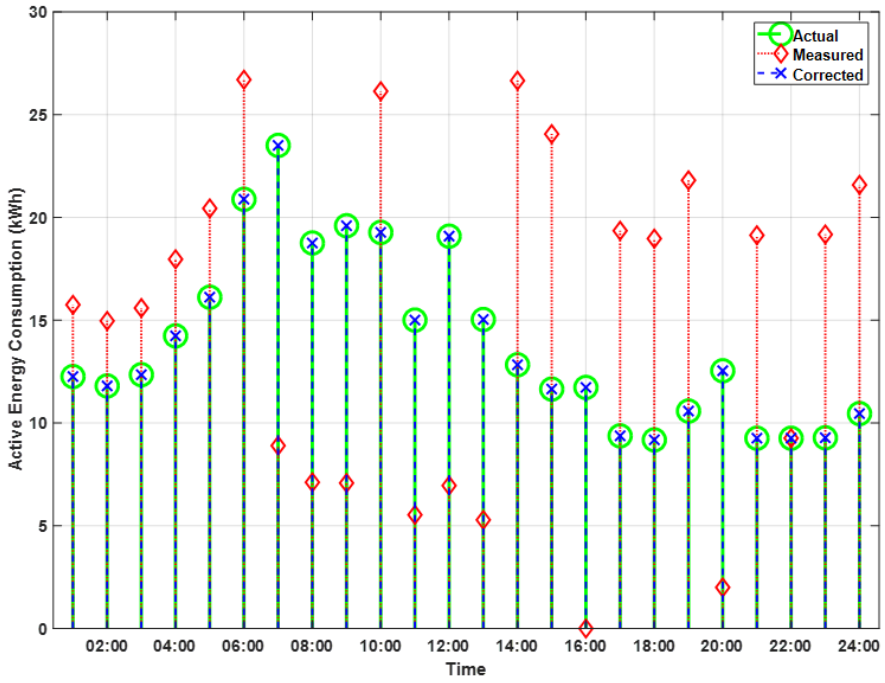

Figure 4.20: Active energy of check meter no. 5 for 24 hours

Similarly, the reactive energy measurement is corrected based on (96) which is taking the vector of reactive energy measurements (91) and the error vector (97) as inputs. The error vector, i.e. (97), can be determined from the syndrome vector (95). The input to the syndrome vector calculator is the cable reactances, reactive energy measurements of all meters (regular and check), and the area under the squared RMS current measurements of regular meters. The syndrome vector returns the difference between the actual value and measured value for each period. The corrected reactive energy profile is labeled in Figure **3.23** as *Corrected*. The corrected reactive energy profile is the same as the actual reactive energy profile with no error in estimation (i.e. 0%).

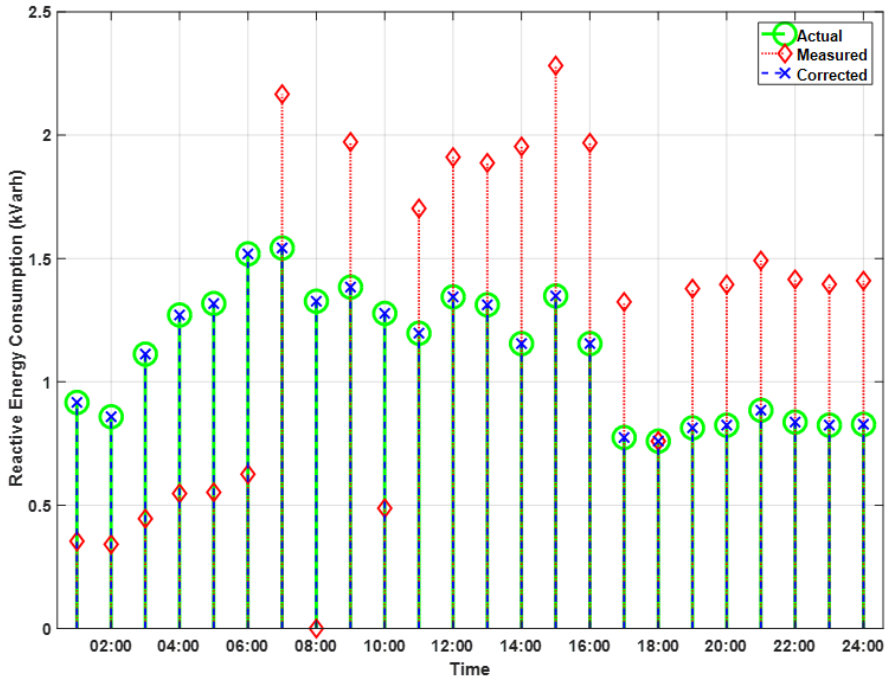

Figure 4.21: Reactive energy of check meter no. 5 for 24 hours

The modified detection algorithm proposed in this work is compared to the original detection algorithm of [9]. The comparison is performed on two cases, first without energy losses compensation, i.e. by using (20), and second with energy losses compensation, i.e. by using (24).

The comparison of the algorithm proposed in [9] without energy losses compensation in the calculation of syndrome vector, i.e. using (20), is shown in Figure 4.22 and Figure 4.23 respectively. Figure 4.22 shows the deviation of corrected active energy from actual value and Figure 4.23 shows the deviation of corrected reactive energy from actual value. Notice that the y-axis on the right are values multiplied by 10^{-6}.

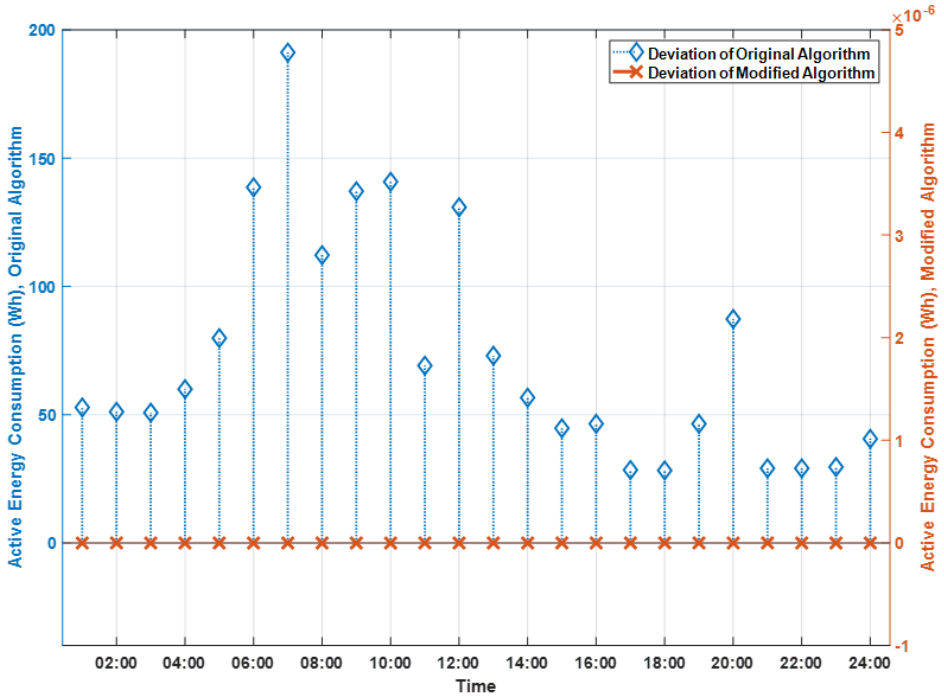

Figure 4.22: Comparison between the active energy estimation of the previous algorithm with no energy losses compensation and the modified algorithm for the case of check meter no. 5 in error

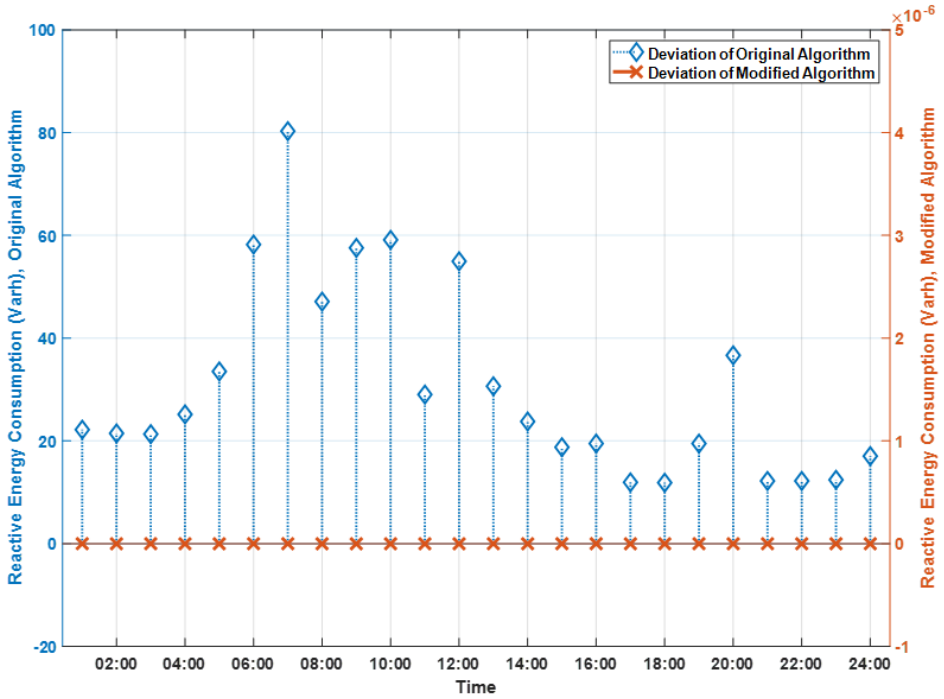

Figure 4.23: Comparison between the reactive energy estimation of the previous algorithm with no energy losses compensation and the modified algorithm for the case of check meter no. 5 in error

The comparison of the algorithm proposed in [9] with energy losses compensation in the calculation of syndrome vector, i.e. using (24), is shown in Figure 4.24 and Figure 4.25 respectively. Using (24), there is no constant value δ_i that can be used as the correct ratio of energy losses all the time, and consequently it is not possible to use $\hat{\delta}_i$ as estimated ratio of energy losses. Therefore, we used the average ratio of energy losses of 24 hours to represent the constant ratio of energy losses in the detection algorithm. The average ratios of active and reactive energy losses for the 24 hours are calculated and shown in Table 11.

Table 11: Ratios of Energy Losses as Percentage to Delivered Energy

Cable Number	Ratio of Active Energy Losses	Ratio of Reactive Energy Losses
Cable 1	0.28859%	0.98038 %
Cable 2	0.40082%	0.69828 %
Cable 3	0.60646%	2.23361 %
Cable 4	0.84177%	1.25407 %

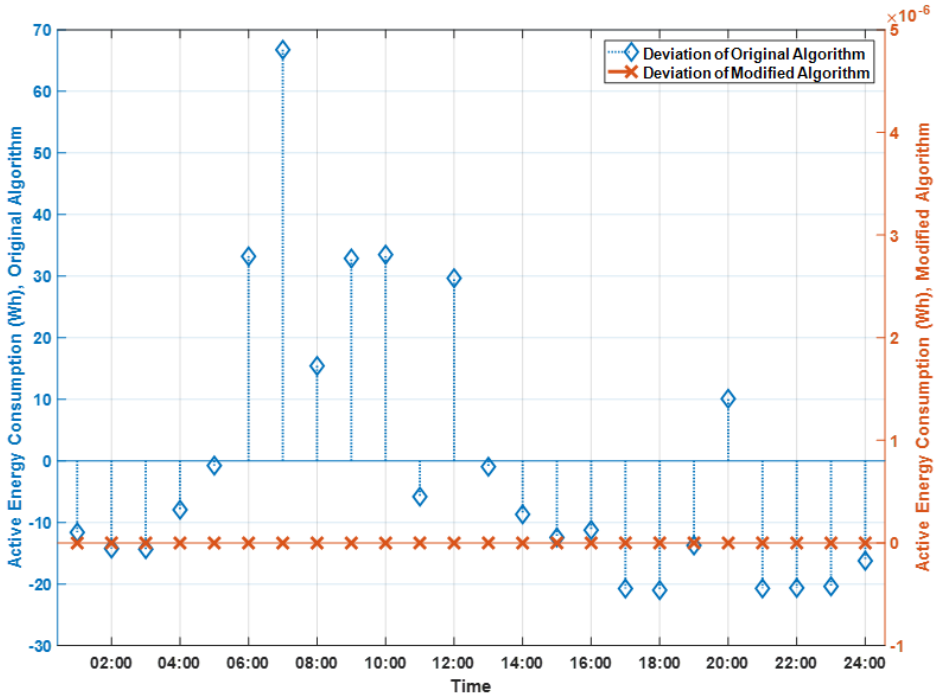

Figure 4.24: Comparison between the active energy estimation of the previous algorithm with energy losses compensation and the modified algorithm for the case of check meter no. 5 in error

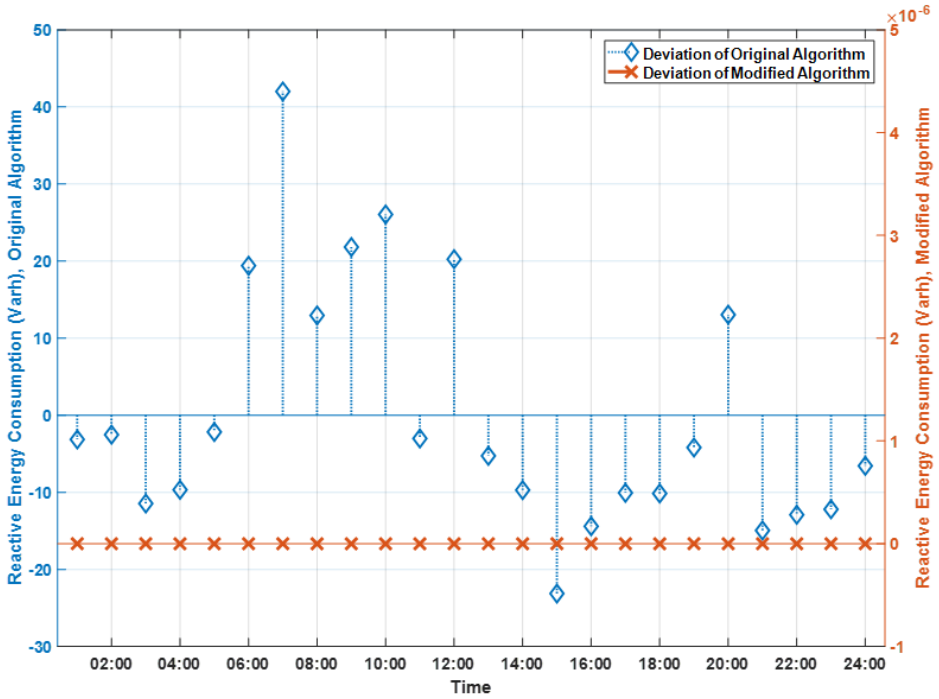

Figure 4.25: Comparison between the reactive energy estimation of the previous algorithm with energy losses compensation and the modified algorithm for the case of check meter no. 5 in error

As we can see from Figure 4.24 and Figure 4.25, the modified detection algorithm outperformed the original detection algorithm that was proposed in [9] even with the use of energy losses compensation. Notice that the y-axis on the right in Figure 4.24 and Figure 4.25 are values multiplied by 10^{-6}.

E. Regular Meter in Error

Random errors are created in all of: active energy, reactive energy, and the area under the squared RMS current measurements of regular meter number 2, as shown in Figure 4.26 and Figure 4.27 respectively. The active energy measurement is corrected based on (104) which is taking the actual active energy at sending end (102) as input. The actual active energy at sending end, i.e. (102), is determined by addition of the wrong active energy measured to the wrong active energy losses calculated inside syndrome vector (101), then subtract the mismatch detected form the syndrome vector (101) which will add up and will equal to the actual active energy at sending end. The corrected active energy profile is labeled in Figure 4.26 as *Corrected*. The corrected active energy profile is the same as the actual active energy added to it the actual active energy losses in cable number 2.

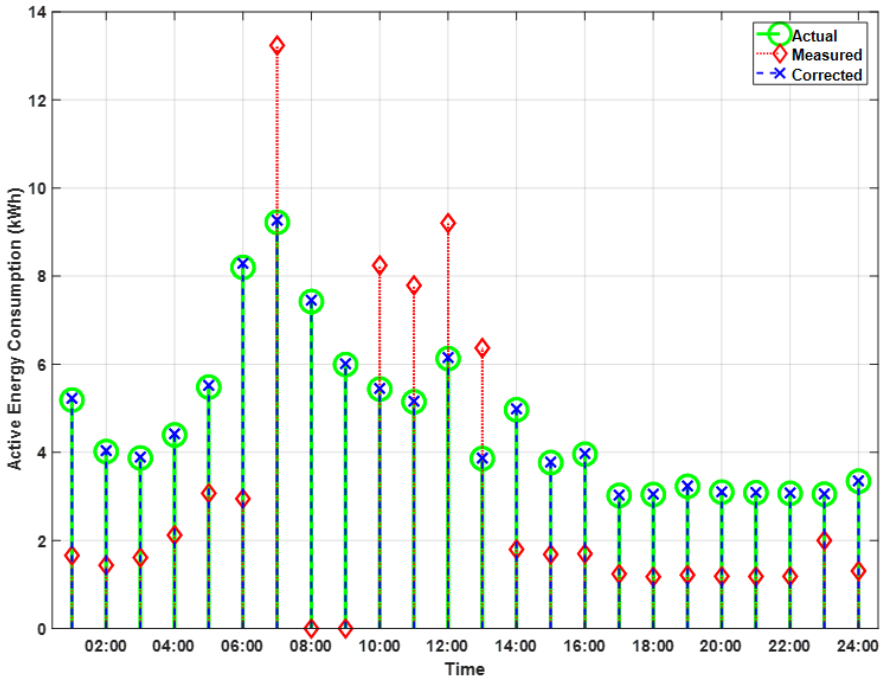

Figure 4.26: Active energy of regular meter no. 2 for 24 hours

Similarly, the reactive energy measurement is corrected and the corrected reactive energy profile is labeled in Figure 4.27 as *Corrected*. The corrected reactive energy profile is the same as the actual reactive energy added to it the actual reactive energy losses in cable number 2.

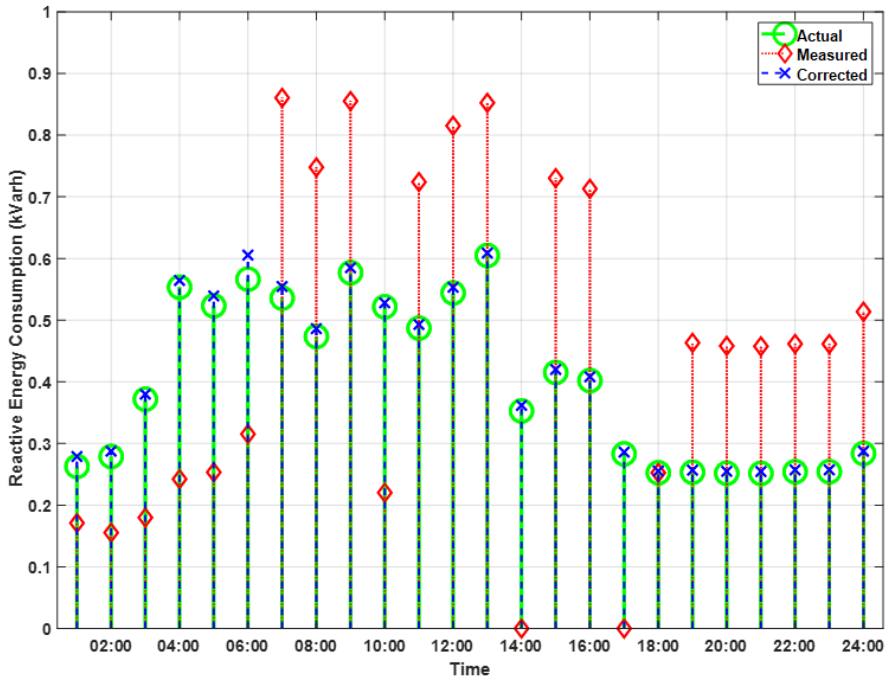

Figure 4.27: Reactive energy of regular meter no. 2 for 24 hours

The modified detection algorithm proposed in this work is compared to the original detection algorithm of [9]. The comparison is performed on two cases, first without power losses compensation, i.e. by using (20), and second with power losses compensation, i.e. by using (24).

The comparison of the algorithm proposed in [9] without power losses compensation in the calculation of syndrome vector, i.e. using (20), is shown in Figure 4.28 and Figure 4.29 respectively. Figure 4.28 shows the deviation of corrected active energy from actual value and Figure 4.29 shows the deviation of corrected reactive energy from actual value. Notice that the y-axis on the right are values multiplied by 10^{-6}.

We can see that both the modified and the original algorithms deviates from actual values and the deviation of modified algorithm is less than the deviation of original algorithm. In

addition to that, the deviation of modified algorithm is the magnitude of actual energy losses in cable number 2, where the deviation of original algorithm is due to error in estimation of energy losses of all cables related. Therefore, when the number of cables increase (e.g. system having 10 check meters and 1013 regular meters) the error in the estimation of original algorithm will be much higher than the error in estimation of the modified algorithm.

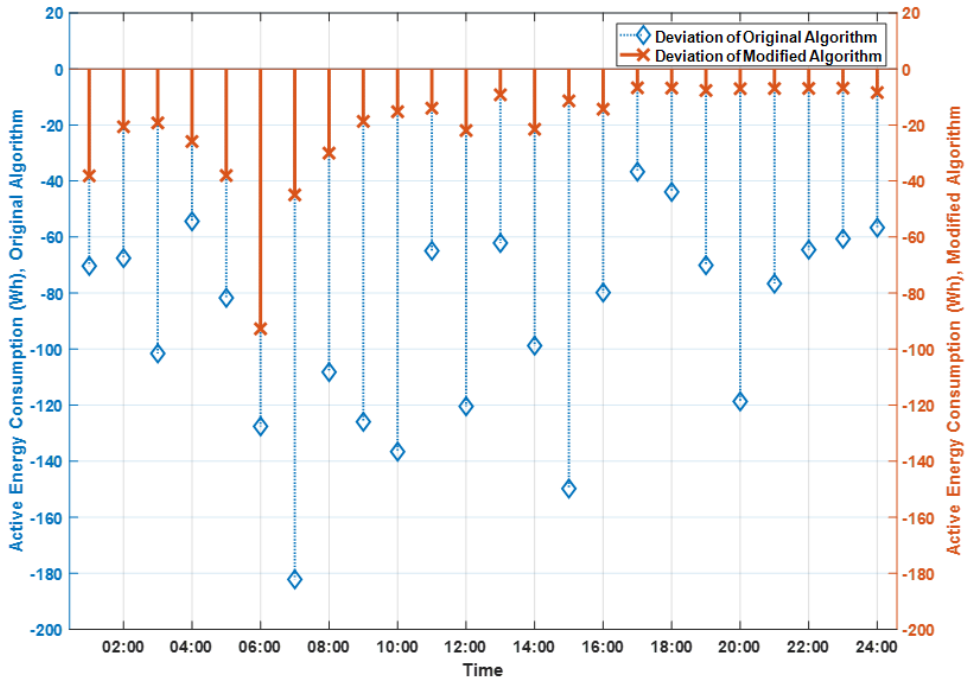

Figure 4.28: Comparison between the active energy estimation of the previous algorithm with no energy losses compensation and the modified algorithm for the case of regular meter no. 2 in error

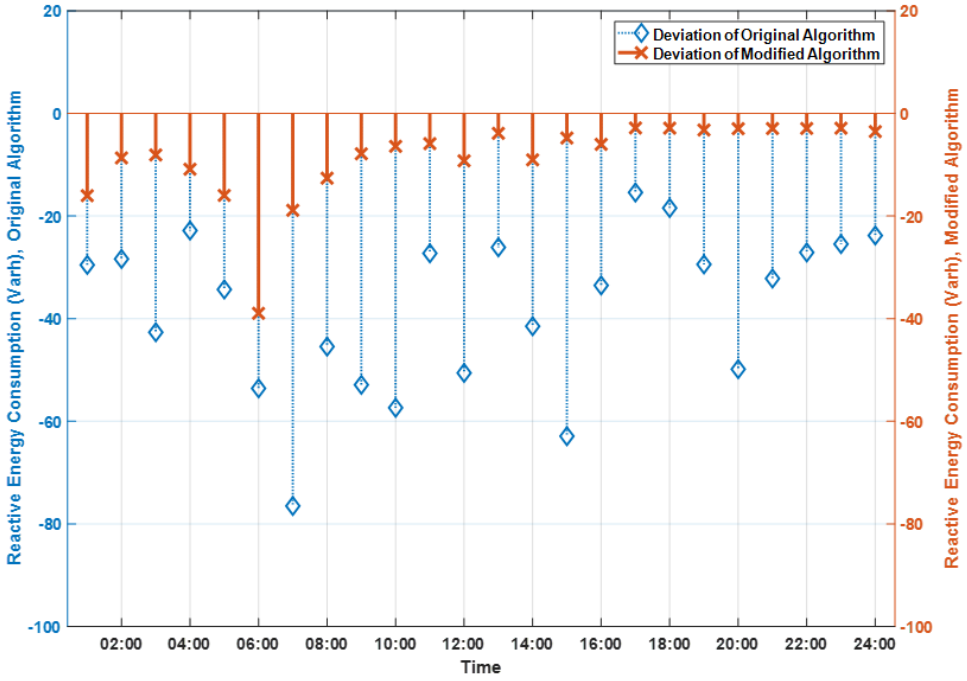

Figure 4.29: Comparison between the reactive energy estimation of the previous algorithm with no energy losses compensation and the modified algorithm for the case of regular meter no. 2 in error

The comparison of the algorithm proposed in [9] with power losses compensation in the calculation of syndrome vector, i.e. using (24), is shown in Figure 4.30 and Figure 4.31 respectively. The average ratios of active and reactive power losses for the 24 hours are calculated and shown in Table 11.

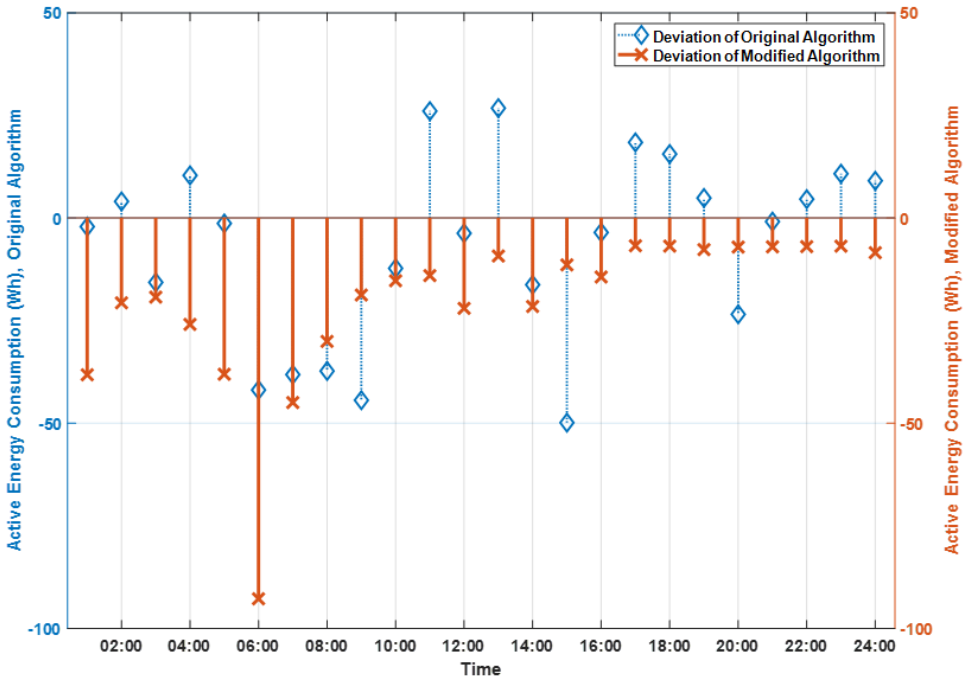

Figure 4.30: Comparison between the active energy estimation of the previous algorithm with energy losses compensation and the modified algorithm for the case of regular meter no. 2 in error

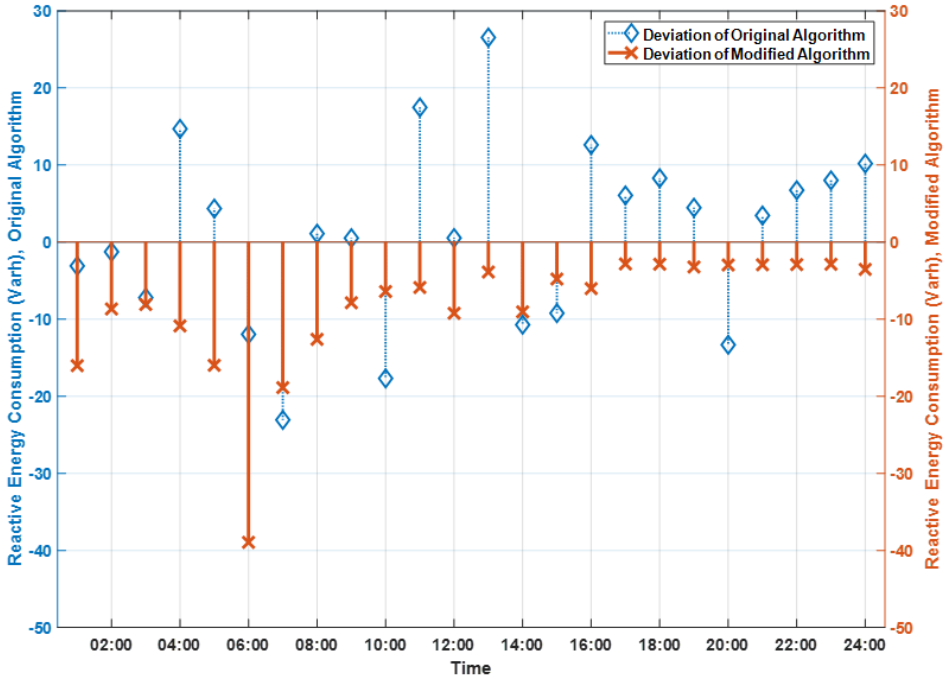

Figure 4.31: Comparison between the reactive energy estimation of the previous algorithm with energy losses compensation and the modified algorithm for the case of regular meter no. 2 in error

As we can see from Figure 4.30 and Figure 4.31, both the modified and the original algorithms deviates from actual values. In addition to that, the deviation of modified algorithm is the magnitude of actual energy losses in cable number 2, where the deviation of original algorithm is due to error in estimation of energy losses of all cables related. Therefore, when the number of cables increase (e.g. system having 10 check meters and 1013 regular meters) the error in the estimation of original algorithm will be much higher than the error in estimation of the modified algorithm.

F. Another Source of NTL

Random active and reactive energy consumption is created along cable number 2 to represent unauthorized tapping in the cable. The estimated energy consumption (labeled as *Estimated NTL*) is the result of applying (107) and (108) on the measurements received form all meters. The estimated NTL is the summation of the energy consumed and the energy losses added to the distribution secondary due to cable tapping. As can be seen in Figure 4.32 and Figure 4.33, the active and reactive corrected energy consumption are the same as the actual consumption with related losses with no error in estimation (i.e. 0%).

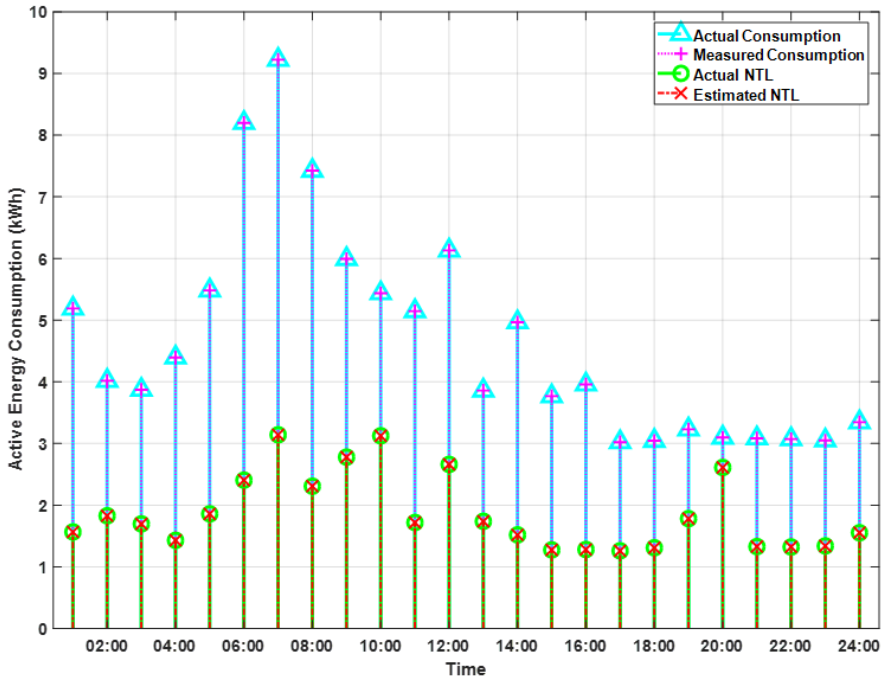

Figure 4.32: Active energy tapped from cable no. 2

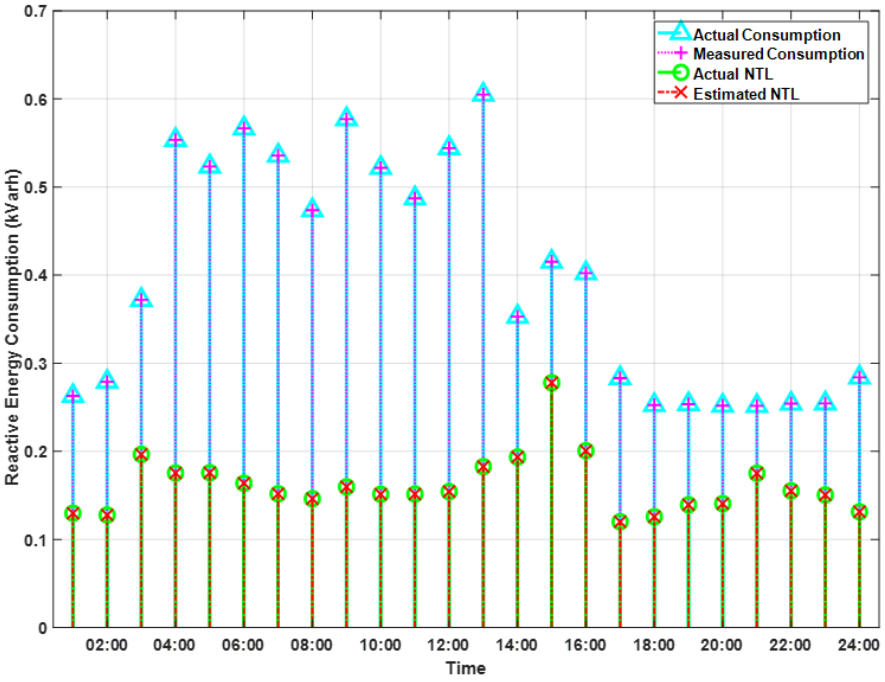

Figure 4.33: Reactive energy tapped from cable no. 2

The modified detection algorithm proposed in this work is compared to the original detection algorithm of [9]. The comparison is performed on two cases, first without energy losses compensation, i.e. by using (20), and second with energy losses compensation, i.e. by using (24).

The comparison of the algorithm proposed in [9] without energy losses compensation in the calculation of syndrome vector, i.e. using (20), is shown in Figure 4.34 and Figure 4.35 respectively. Figure 4.34 shows the deviation of corrected active energy from actual value and Figure 4.35 shows the deviation of corrected reactive energy from actual value. Notice that the y-axis on the right are values multiplied by 10^{-6} and 10^{-7}.

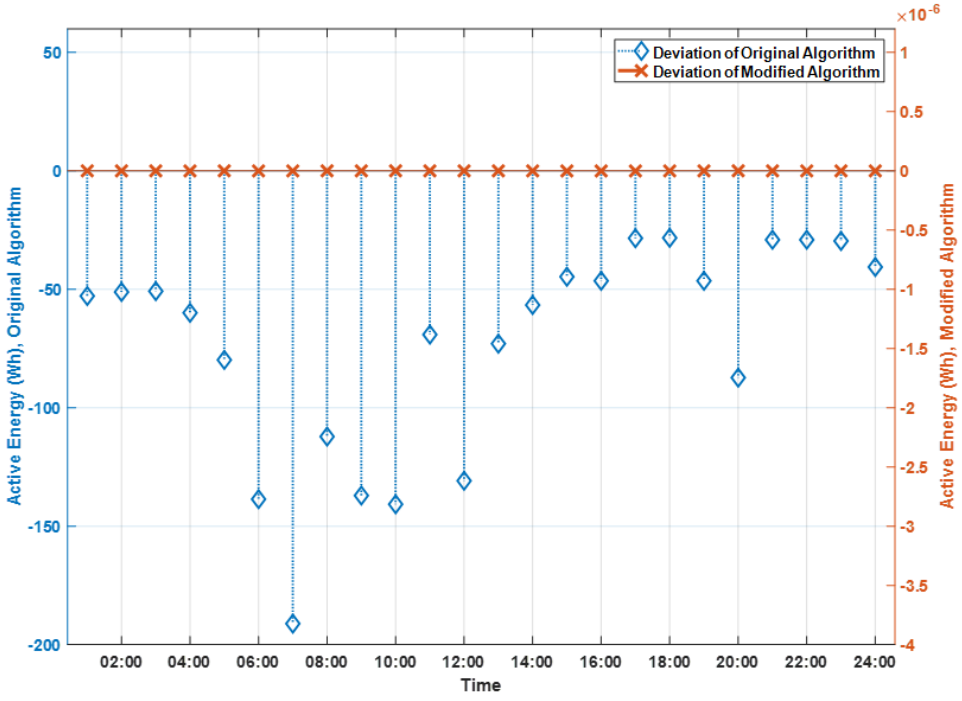

Figure 4.34: Comparison between the active energy estimation of the previous algorithm with no energy losses compensation and the modified algorithm for the case of tapping cable no. 2

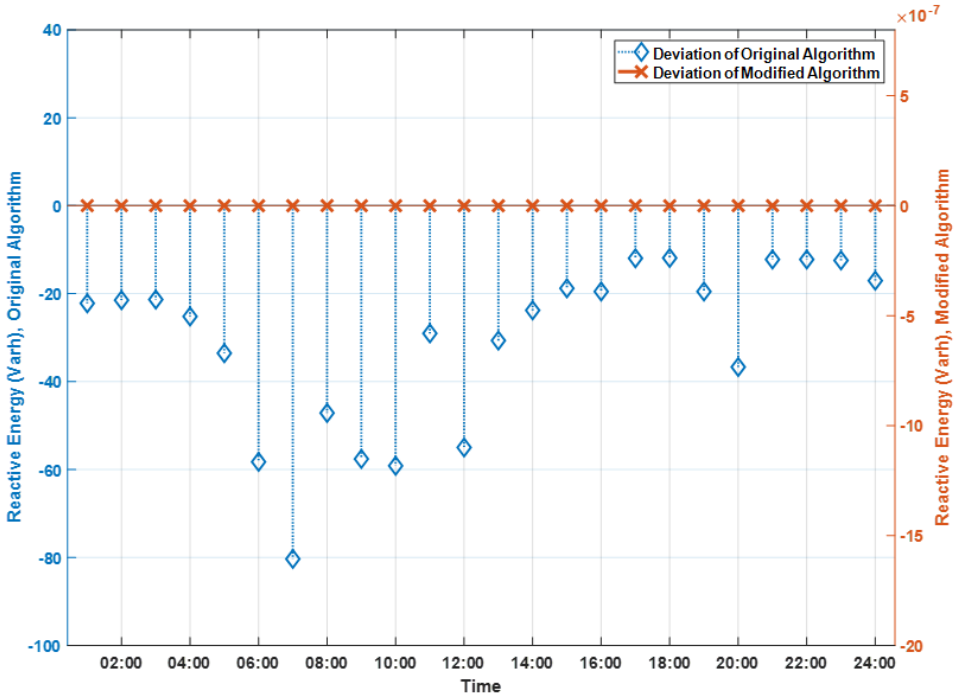

Figure 4.35: Comparison between the reactive energy estimation of the previous algorithm with no energy losses compensation and the modified algorithm for the case of tapping cable no. 2

The comparison of the algorithm proposed in [9] with power losses compensation in the calculation of syndrome vector, i.e. using (24), is shown in Figure 4.36 and Figure 4.37 respectively. The average ratios of active and reactive power losses for the 24 hours are calculated and shown in Table 11.

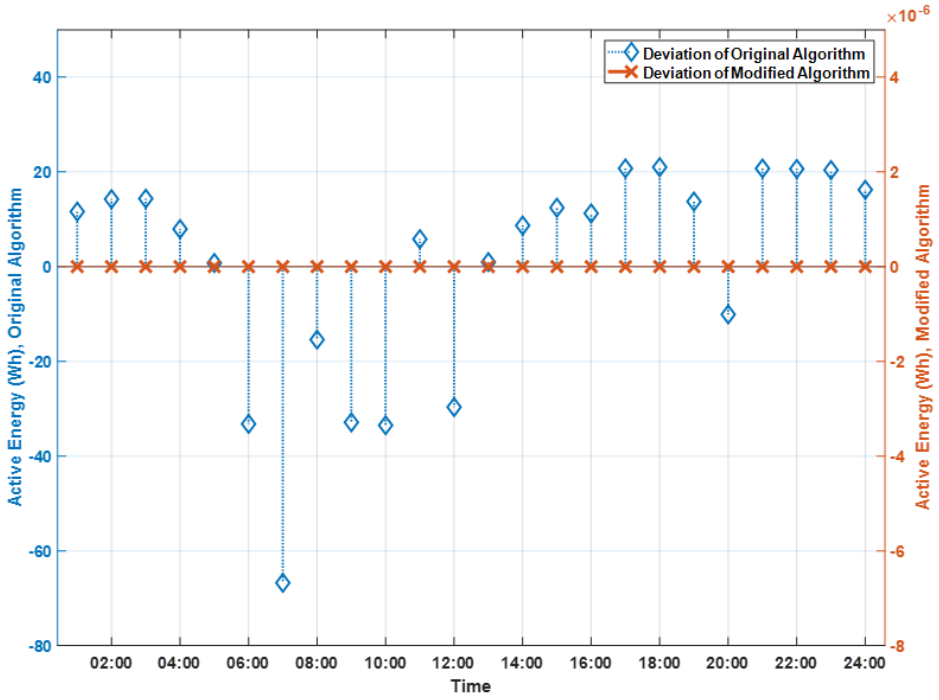

Figure 4.36: Comparison between the active energy estimation of the previous algorithm with energy losses compensation and the modified algorithm for the case of tapping cable no. 2

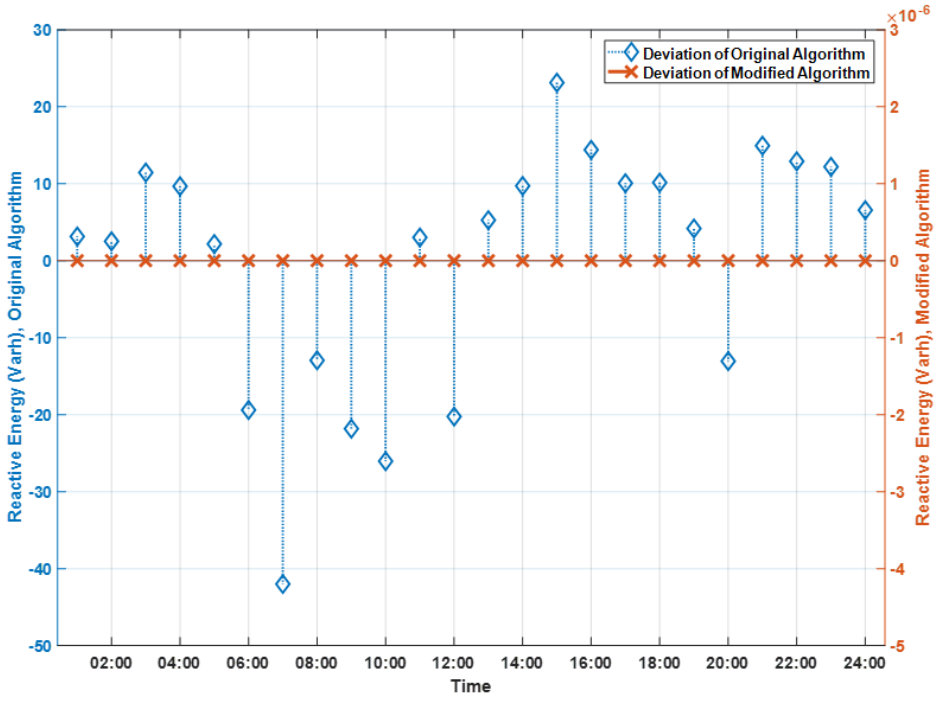

Figure 4.37: Comparison between the reactive energy estimation of the previous algorithm with energy losses compensation and the modified algorithm for the case of tapping cable no. 2

As we can see from Figure 4.36 and Figure 4.37, the modified detection algorithm outperformed the original detection algorithm that was proposed in [9] even with the use of power losses compensation. Notice that the y-axis on the right in Figure 4.36 and Figure 4.37 are values multiplied by 10^{-6}.

4.2 Conclusions and Recommendations

In conclusion, both proposed algorithms, i.e. the first algorithm for a system reporting data at high rate and the second algorithm for a system reporting data at low rate, showed accurate estimation of technical and non-technical losses. For the first algorithm, it included the calculation of power losses in service cables which lead to accurate values of syndrome vector and consequently accurate corrected consumption profiles that are identical to the actual consumption profiles with no error (0% error) for all error causes.

Moreover, the first algorithm was able to estimate cable impedances accurately using the already existing setup. In addition to that, first algorithm formulated detection of other sources of NTL such as tapping the service cable (i.e., all meters are measuring correct values but there is other source of losses related to unregistered consumer). The proposed algorithm for estimating the power consumed from other sources of NTL showed accurate estimation and it included the direct losses (i.e., actual power tapped) and the indirect losses (i.e., additional power losses in service cable due to power tapped).

The second algorithm also showed accurate estimation of TL and NTL when the system reports the data at low rate, e.g. hourly. Under the constraint of low data rate, the second algorithm showed ability to estimate cable impedance, energy losses, and detection and correction of non-technical losses. For the causes of no error, check meter in error, and cable tapping, the second algorithm resulted in exact values that are supposed to be measured (i.e. 0% error). In addition to that, the new unit of measurement proposed in this work made the second algorithm to be capable of accurate energy losses estimation when the meters report data at low rate. Also, by using the new unit of measurement, the error due to time skew cause by deviation of real time clock is reduced by big magnitude.

On the other hand, the second algorithm was not able to eliminate the power losses from the corrected values when the error is in a regular meter. This resulted in deviation was not far from the deviation of original algorithm (i.e. [9]) for the cause of 3 check meters and 4 regular meters. Notice that the second algorithm will outperform the original algorithm when used for a system having bigger number of meters; because the corrected value using the second algorithm will only include the energy losses related to the cable

feeding the meter in error, where the corrected values using the original algorithm will include the energy losses of all related cables.

For future work, we recommend that the second algorithm to be further improved for more accurate correction of errors in the third case (i.e. an error in a regular meters). In addition to that, we recommend that the proposed algorithms to be tested on hardware to verify the simulation results and evaluate other practical challenges. Also, the smart meter designed in this work to be implemented and the new unit of measurement to be added to the measuring capabilities. Finally, the new unit of measurement may be utilized in other applications in power system estimation and operation, such as proposing more accurate tariff structure that include the energy losses of the consumer based on the amount of kA^2h measured.

References

[1] "Smart Metering and Smart Grids Strategy for the Kingdom of Saudi Arabia," ECRA – Electricity & Co-generation Regulatory Authority, 2013.

[2] " SEC will install about 12 million smart meters by 2025 across the kingdom," Saudi Electricity Company, 2015. [Online]. Available: https://www.se.com.sa/en-us/pages/newsdetails.aspx?NId=265. [Accessed 23 September 2019].

[3] B. Krebs, "FBI: Smart Meter Hacks Likely to Spread," *Krebs on Security, In-depth Security News and Investigation,* 12 April 2012.

[4] S. Amin, G. A. Schwartz, A. A. Cardenas and S. S. Sastry, "Game-Theoretic Models of Electricity Theft Detection in Smart Utility Networks: Providing New Capabilities with Advanced Metering Infrastructure," *IEEE Control Systems,* vol. 35, no. 1, pp. 66-81, 2015.

[5] L. Wei, A. Sundararajan, A. I. Sarwat, S. Biswas and E. Ibrahim, "A distributed intelligent framework for electricity theft detection using benford's law and stackelberg game," in *2017 Resilience Week (RWS),* Wilmington, DE, USA, 2017.

[6] A. Chauhan and S. Rajvanshi, "Non-Technical Losses in Power System: A Review," in *2013 International Conference on Power, Energy and Control (ICPEC),* Sri Rangalatchum Dindigul, India, 2013.

[7] S. Yorukoglu, F. Nasibov, M. Mungan and M. Bagriyanik, "The Effect of the Types of Network Topologies on Nontechnical Losses in Secondary Electricity Distribution Systems," *IEEE Transactions on Industry Applications,* vol. 52, no. 5, pp. 3631-3643, 2016.

[8] "Electricity Theft and Non-Technical Losses: Global Markets, Solutions and Vendors," Northeast Group, LLC, Global, 2017.

[9] W. Mesbah, "Securing Smart Electricity Meters Against Customer Attacks," *IEEE Transactions on Smart Grid,* vol. PP, no. 99, 2017.

[10] R. Jiang, R. Lu, Y. Wang, J. Luo, C. Shen and X. S. Shen, "Energy-Theft Detection Issues for Advanced Metering Infrastructure in Smart Grid," *Tsinghua Science and Technology,* vol. 19, no. 2, pp. 105-120, 2014.

[11] T. Ahmad, "Non-technical loss analysis and prevention using smart meters," *Renewable and Sustainable Energy Reviews,* vol. 72, pp. 573-589, 2017.

[12] J. L. Viegas, P. R. Esteves, R. Melício, V. Mendes and S. M. Vieira, "Solutions for detection of non-technical losses in the electricity grid: A review," *Renewable and Sustainable Energy Reviews,* vol. 80, pp. 1256-1268, 2017.

[13] Ç. Yurtseven, "The causes of electricity theft: An econometric analysis of the case of Turkey," *Utilities Policy,* vol. 37, pp. 70-78, 2015.

[14] S. Saini, "Social and behavioral aspects of electricity theft: An explorative review," *International Journal of Research in Economics and Social Sciences (IJRESS),* vol. 7, no. 6, pp. 26-37, 2017.

[15] P. Glauner, A. Boechat, L. Dolberg, R. State, F. Bettinger, Y. Rangoni and D. Duarte, "Large-Scale Detection of Non-Technical Losses in Imbalanced Data Sets," in *2016 IEEE Power & Energy Society Innovative Smart Grid Technologies Conference (ISGT),* Minneapolis, MN, USA, 2016.

[16] S.-C. Huang, Y.-L. Lo and C.-N. Lu, "Non-Technical Loss Detection Using State Estimation and Analysis of Variance," *IEEE Transactions on Power Systems,* vol. 28, no. 3, pp. 2959-2966, 2013.

[17] J. B. Leite and J. R. S. Mantovani, "Detecting and Locating Non-technical Losses in Modern Distribution Networks," *IEEE Transactions on Smart Grid,* vol. PP, no. 99, pp. 1-1, 2017.

[18] D. Nikovski, Z. Wang, A. Esenther, H. Sun, K. Sugiura, T. Muso and K. Tsuru, "Smart Meter Data Analysis for Power Theft Detection," in *International Conference on Machine Learning and Data Mining in Pattern Recognion (MLDM),* New York, 2013.

[19] S. Sahoo, D. Nikovski, T. Muso and K. Tsuru, "Electricity theft detection using smart meter data," in *2015 IEEE Power & Energy Society Innovative Smart Grid Technologies Conference (ISGT),* Washington, DC, USA, 2015.

[20] A. Bhimte, R. K. Mathew and K. S, "Development of smart energy meter in LabVIEW for power distribution systems," in *2015 Annual IEEE India Conference (INDICON),* New Delhi, 2015.

[21] M. Kuzlu, M. Pipattanasomporn and S. Rahman, "Hardware Demonstration of a Home Energy Management System for Demand Response Applications," *IEEE Transactions on Smart Grid*, vol. 3, no. 4, pp. 1704-1711, 2012.

[22] H. Das and L. C. Saikia, "GSM enabled smart energy meter and automation of home appliances," in *2015 International Conference on Energy, Power and Environment: Towards Sustainable Growth (ICEPE)*, Shillong, 2015.

[23] A. Arif, M. Al-Hussain, N. Al-Mutairi, E. Al-Ammar, Y. Khan and N. Malik, "Experimental study and design of smart energy meter for the smart grid," in *2013 International Renewable and Sustainable Energy Conference (IRSEC)*, 2013.

[24] A. Charly, J. Reddy and S. Ashok, "Development of inbuilt Energy Management Controller for Smart meter," in *2014 IEEE International Conference on Advanced Communications, Control and Computing Technologies*, Ramanathapuram, 2014.

[25] M. M. Rahman, Noor-E-Jannat, M. O. Islam and M. S. Salakin, "Arduino and GSM based smart energy meter for advanced metering and billing system," in *2015 International Conference on Electrical Engineering and Information Communication Technology (ICEEICT)*, Dhaka, 2015.

[26] G. Aurilio, D. Gallo, C. Landi, M. Luiso and G. Graditi, "A low cost smart meter network for a smart utility," in *2014 IEEE International Instrumentation and Measurement Technology Conference (I2MTC) Proceedings*, Montevideo, 2014.

[27] G. D. Prete and C. Landi, "Real-time smart meter with embedded web server capability," in *2012 IEEE International Instrumentation and Measurement Technology Conference Proceedings*, Graz, 2012.

[28] D. M. L. B. Dissanayaka, C. T. J. Fernando and S. G. Abeyratne, "Smart meter based inverter controlling network for demand response applications in smart grids," in *2011 6th International Conference on Industrial and Information Systems*, Kandy, 2011.

[29] N. A. Kulatunga, S. Navaratne, J. Dole, C. Liyanagedera and T. Martin, "Hardware development for Smart Meter based innovations," in *IEEE PES Innovative Smart Grid Technologies*, Tianjin, 2012.

[30] S. Yaemprayoon, V. Boonplian and J. Srinonchat, "Developing an innovation smart meter based on CS5490," in *2016 13th International Conference on Electrical*

Engineering/Electronics, Computer, Telecommunications and Information Technology (ECTI-CON), Chiang, 2016.

[31] A. Garrab, A. Bouallegue and F. B. Abdallah, "A new AMR approach for energy saving in Smart Grids using Smart Meter and partial Power Line Communication," in *2012 First International Conference on Renewable Energies and Vehicular Technology*, Hammamet, 2012.

[32] G. K., "Design of Smart Meter Using Atmel 89S52 Microcontroller," *Procedia Technology*, vol. 21, pp. 376-380, 2015.

[33] M. Kuzlu, M. Pipattanasomporn and R. Saifur, "Communication network requirements for major smart grid applications in HAN, NAN and WAN," *Computer Networks*, vol. 67, pp. 74-88, 2014.

[34] TAMURA, "Three Flange Dual Primary 1.1VA PC Board Power Transformer," [Online]. Available: http://www.tamuracorp.com/clientuploads/pdfs/engineeringdocs/3FD-2XX.pdf. [Accessed 18 March 2018].

[35] TDK, "Clamp Type AC Current Sensors For Energy Management Systems," [Online]. Available: https://product.tdk.com/info/en/catalog/datasheets/sensor_current_cct_en.pdf. [Accessed 18 March 2018].

[36] MICROCHIP, "Atmel SMART ARM-based MCU," 3 January 2015. [Online]. Available: http://ww1.microchip.com/downloads/en/DeviceDoc/Atmel-11057-32-bit-Cortex-M3-Microcontroller-SAM3X-SAM3A_Datasheet.pdf. [Accessed 18 March 2018].

[37] Arduino, "ARDUINO DUE A000062," [Online]. Available: https://store.arduino.cc/usa/arduino-due. [Accessed 18 March 2018].

[38] ANALOG DEVICES, "Polyphase Multifunction Energy Metering IC with Harmonic Monitoring," [Online]. Available: http://www.analog.com/media/en/technical-documentation/data-sheets/ADE7880.pdf. [Accessed 18 March 2018].

[39] Huanan Electronic Technology, "Specification for LCD Module No. HTF0177SN-01," 24 June 2012. [Online]. Available: https://www.arduino.cc/en/uploads/Main/HTF0177SN-01-SPEC.pdf. [Accessed 21 March 2018].

[40] MAXIM INTEGRATED, "Extremely Accurate I2C-Integrated RTC/TCXO/Crystal," [Online]. Available: https://datasheets.maximintegrated.com/en/ds/DS3231-DS3231S.pdf. [Accessed 21 March 2018].

[41] J. Peppanen, C. Rocha, J. A. Taylor and R. C. Dugan, "Secondary Low-Voltage Circuit Models - How Good is Good Enough?," *IEEE Transactions on Industry Applications*, vol. PP, no. 99, pp. 1-1, 2017.

[42] Q. Sun, H. Li, Z. Ma, C. Wang, J. Campillo, Q. Zhang, F. Wallin and J. Guo, "A Comprehensive Review of Smart Energy Meters in Intelligent Energy Networks," *IEEE Internet of Things Journal*, vol. 3, no. 4, pp. 464-479, 2016.

[43] S. Al-Esa, "Electriciy Hunter Discover Electricy Tampring," Alwatan, 4 April 2012. [Online]. Available: http://alwatan.com.sa/Local/News_Detail.aspx?ArticleID=94014&CategoryID=5. [Accessed 23 Septemper 2017].

[44] "Saudi Electriciy Company Detects Millions of Electricity Tampring," Alarabiya, 26 February 2012. [Online]. Available: http://www.alarabiya.net/articles/2012/02/26/197127.html. [Accessed 23 September 2017].

Appendix A

Plots Related to Smart Meter Number 1

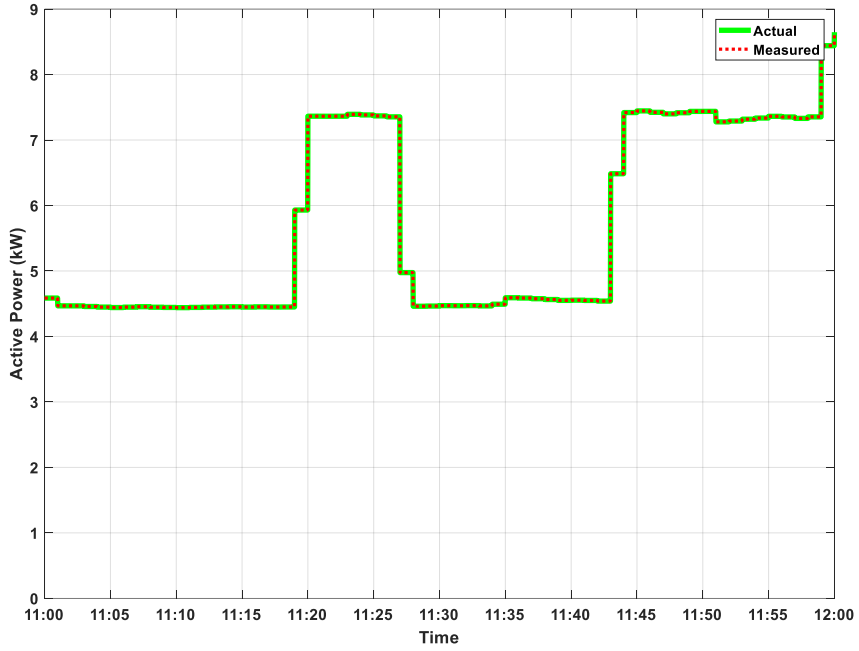

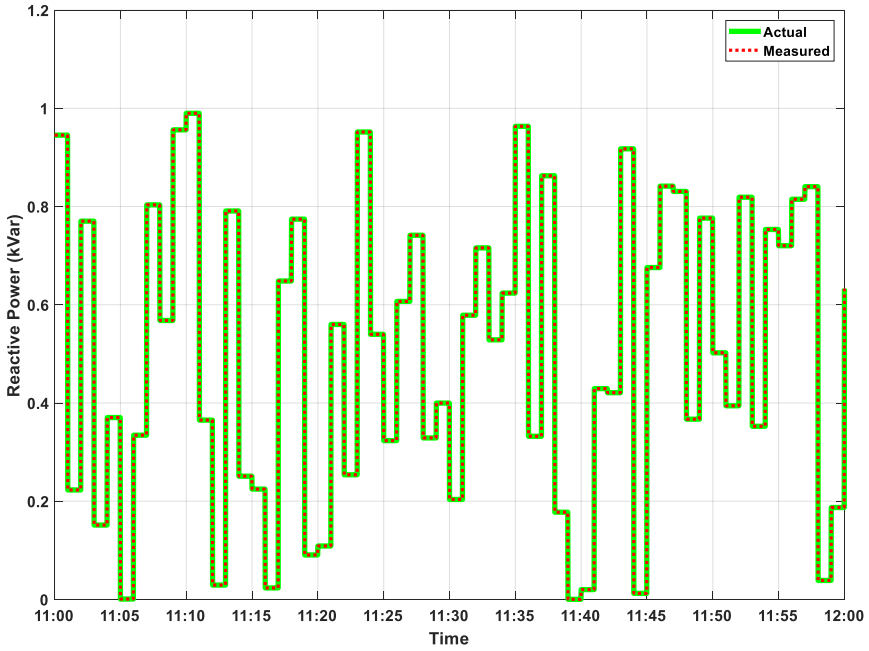

Plots Related to Smart Meter Number 1

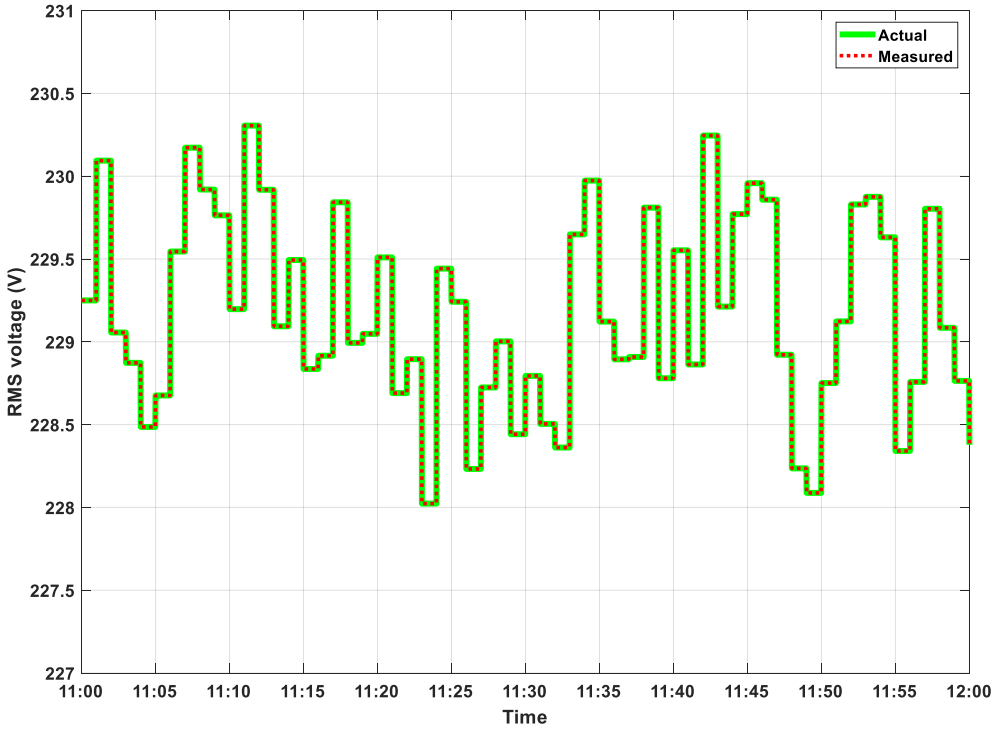

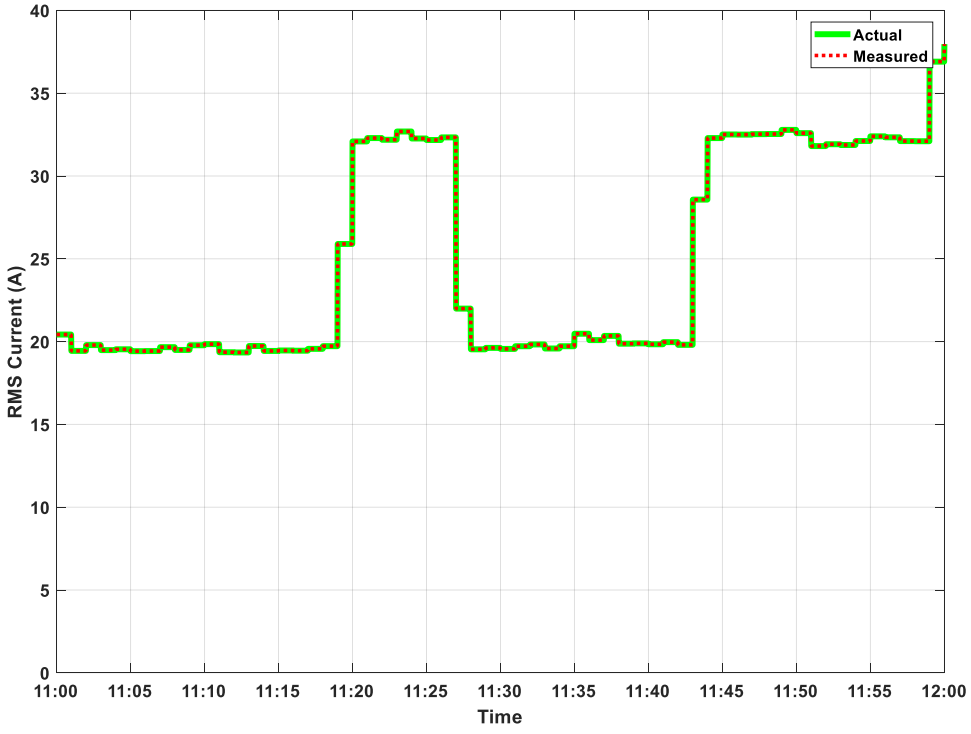

Plots Related to Smart Meter Number 2

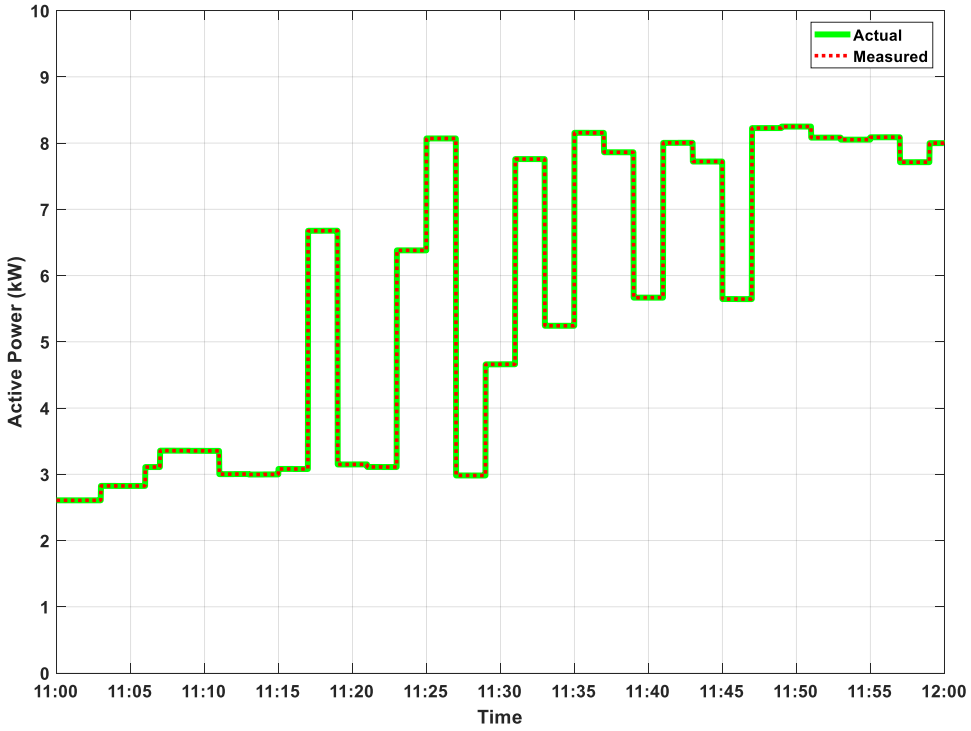

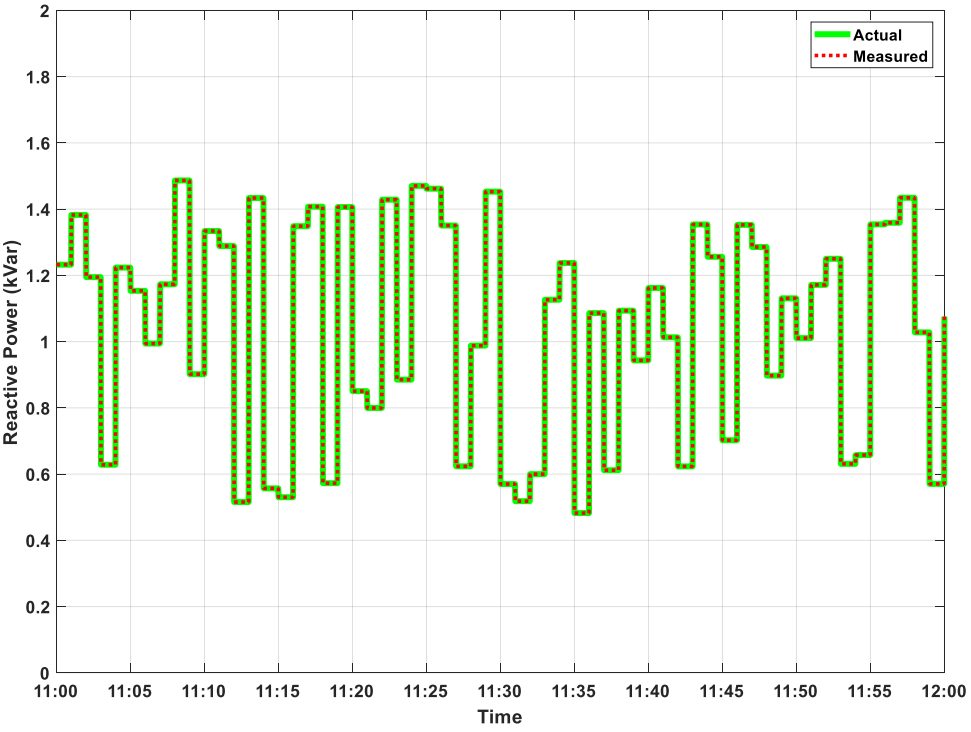

Plots Related to Smart Meter Number 2

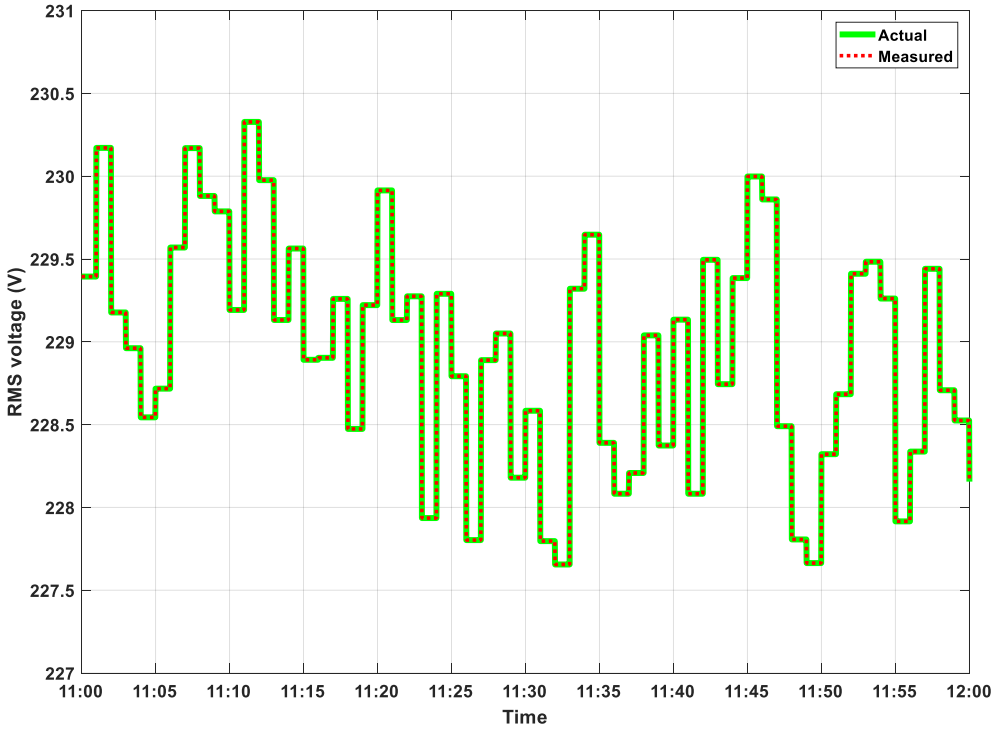

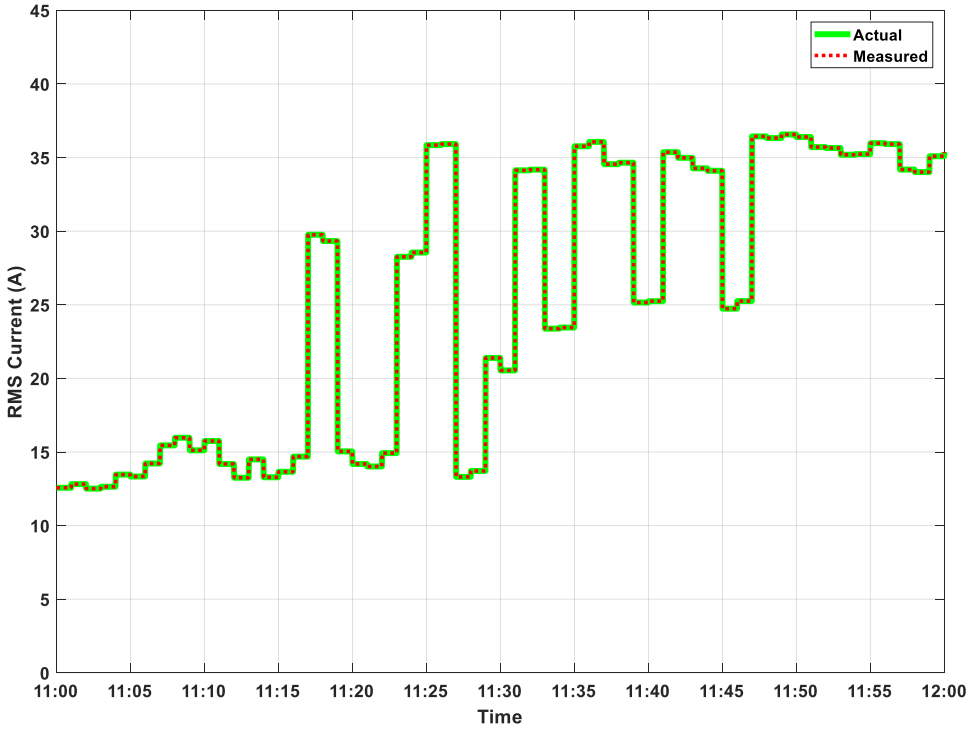

Plots Related to Smart Meter Number 3

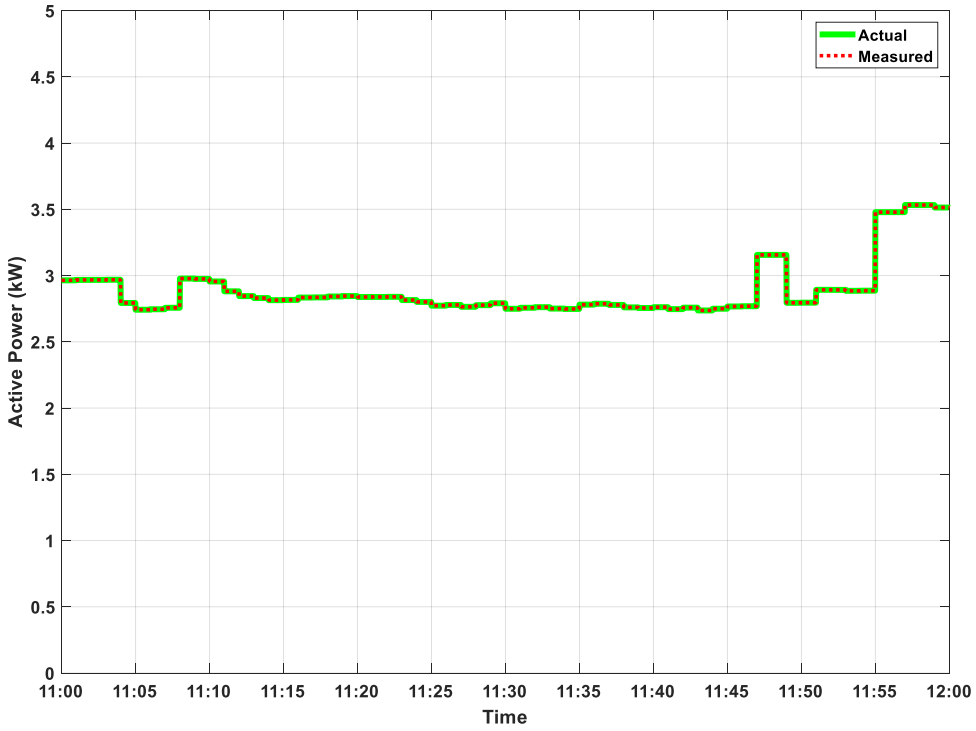

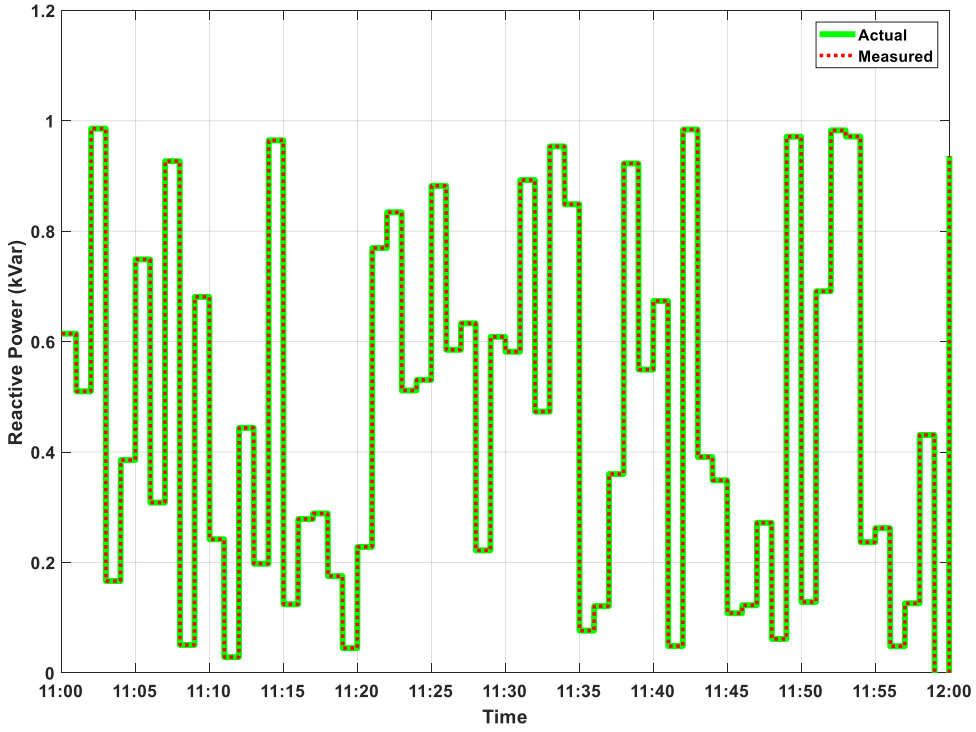

Plots Related to Smart Meter Number 3

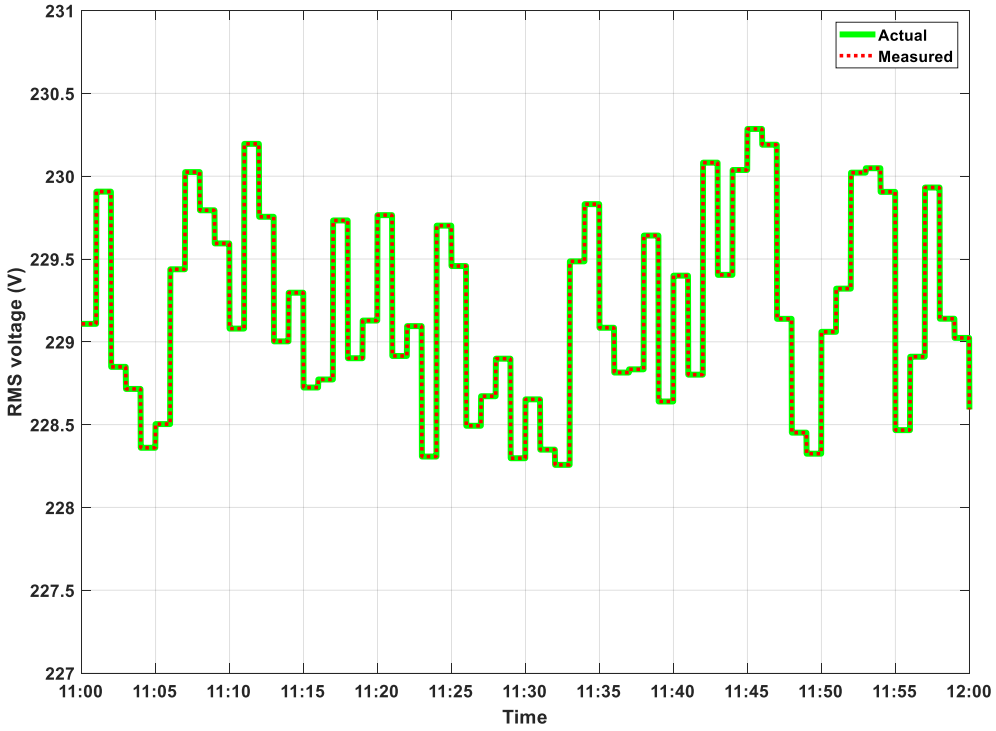

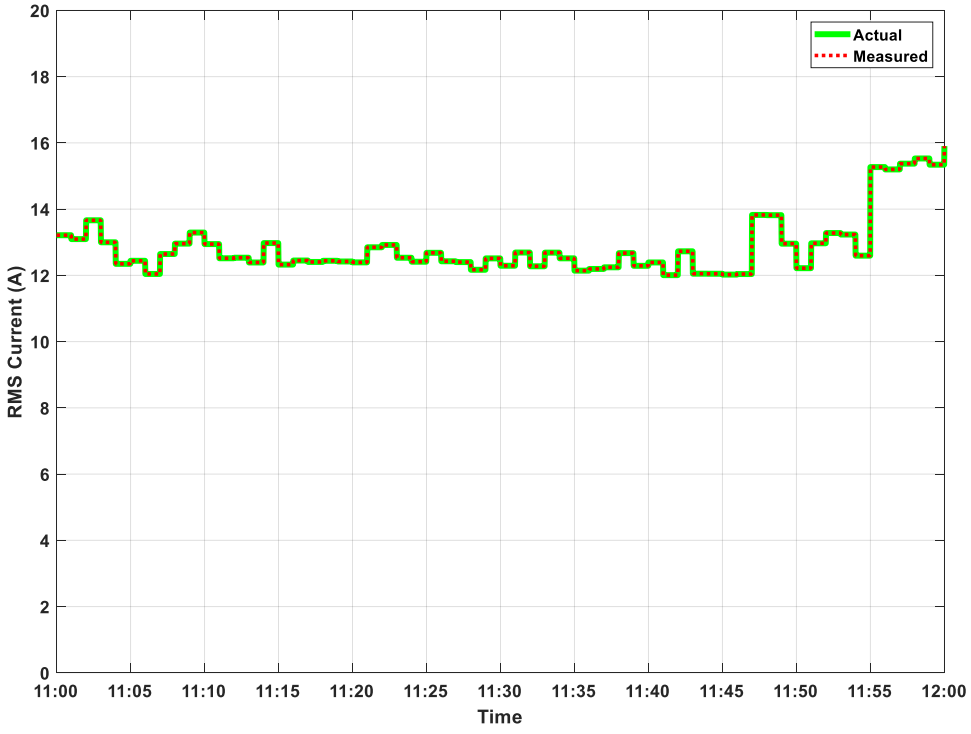

Plots Related to Smart Meter Number 4

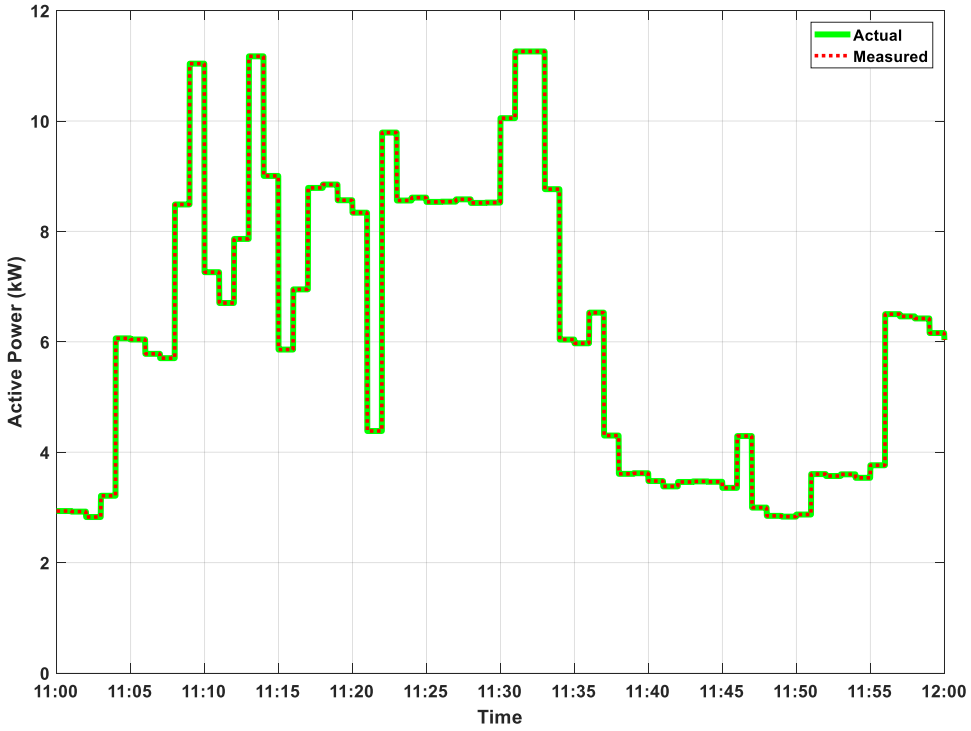

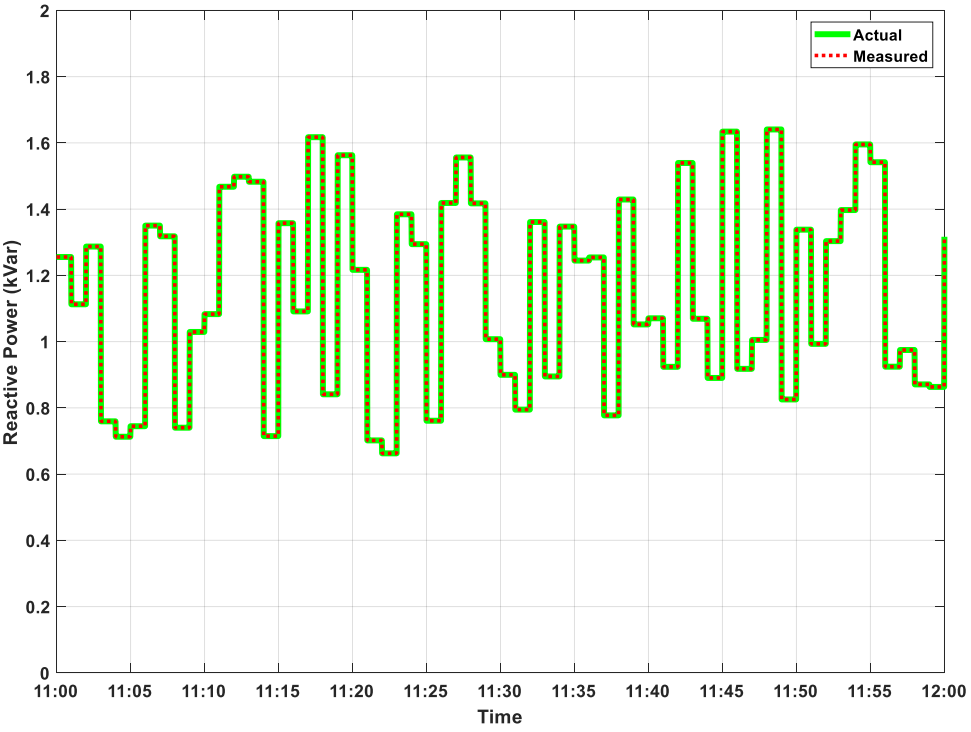

Plots Related to Smart Meter Number 4

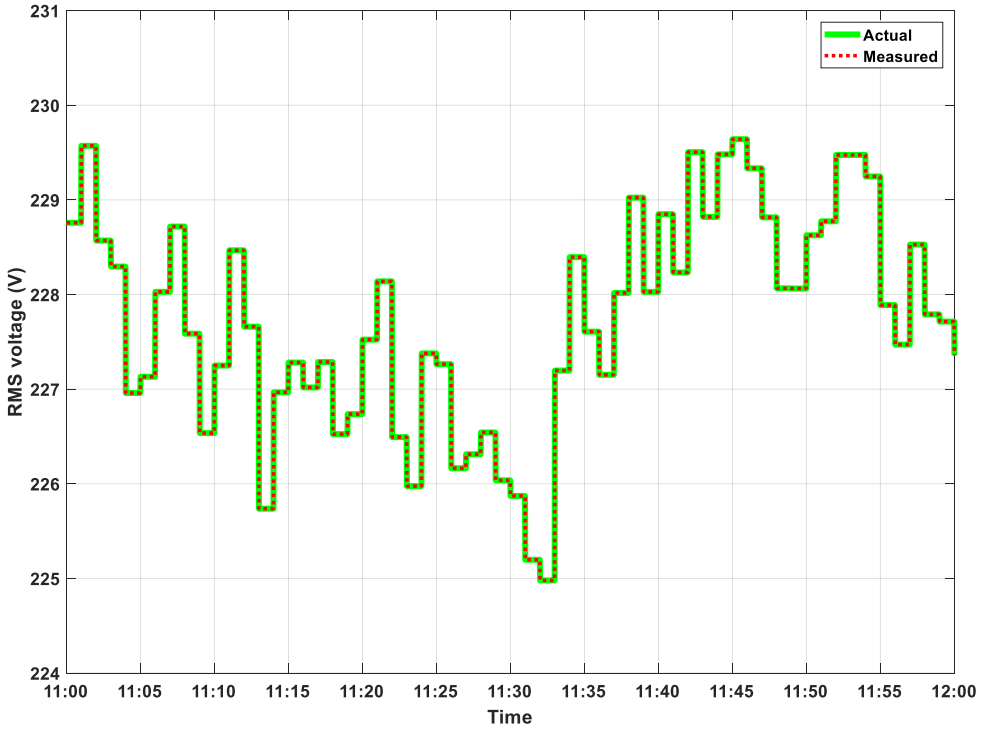

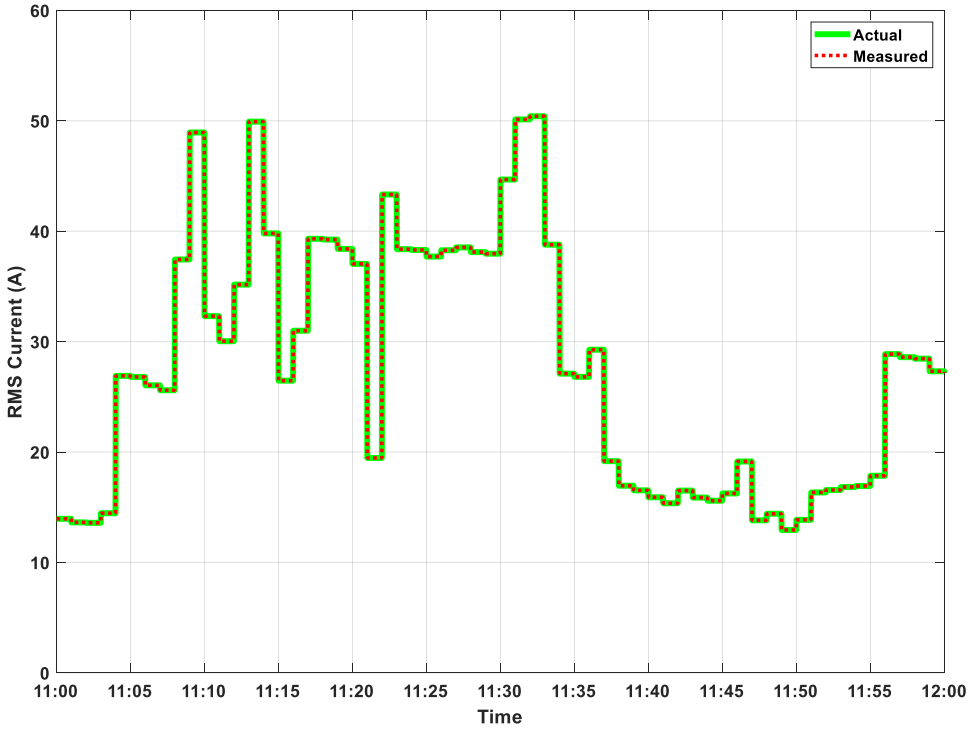

Plots Related to Smart Meter Number 5

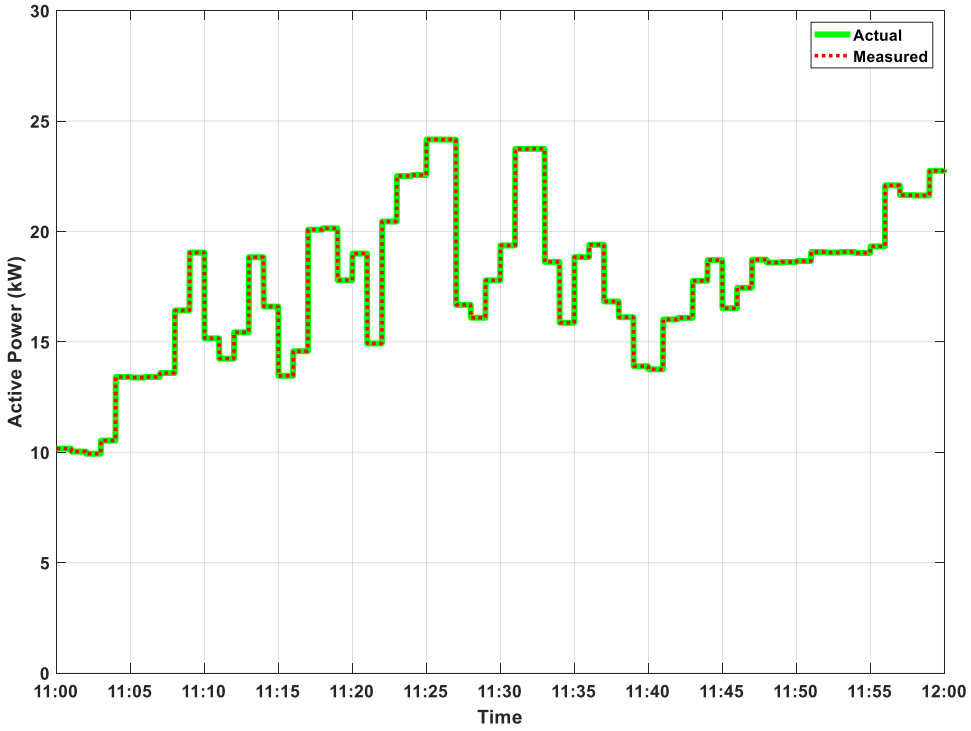

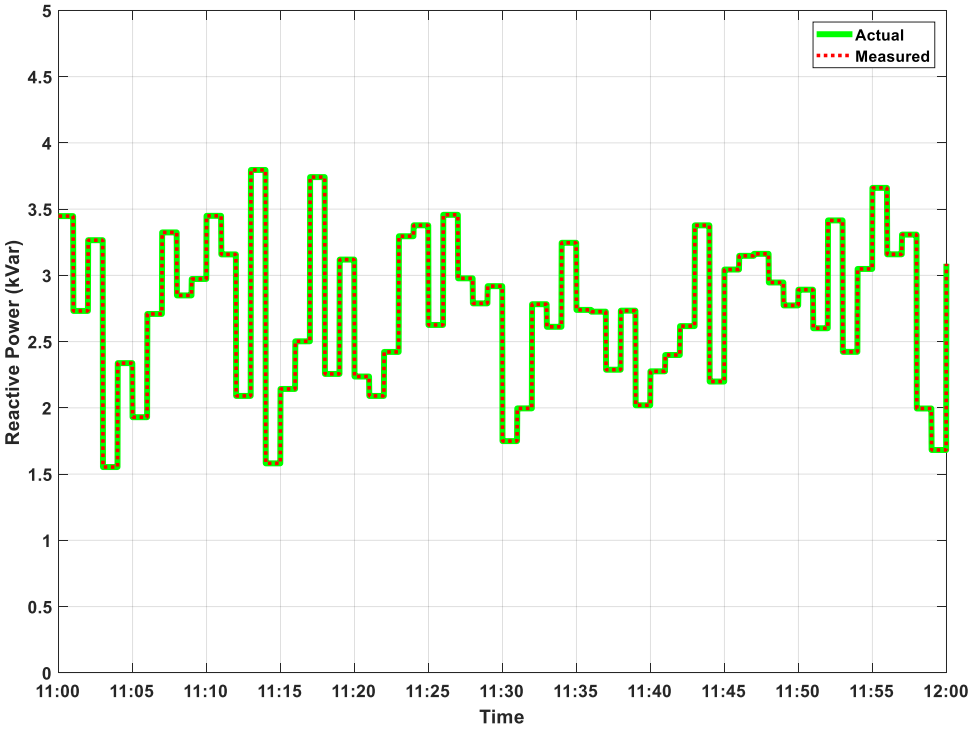

Plots Related to Smart Meter Number 5

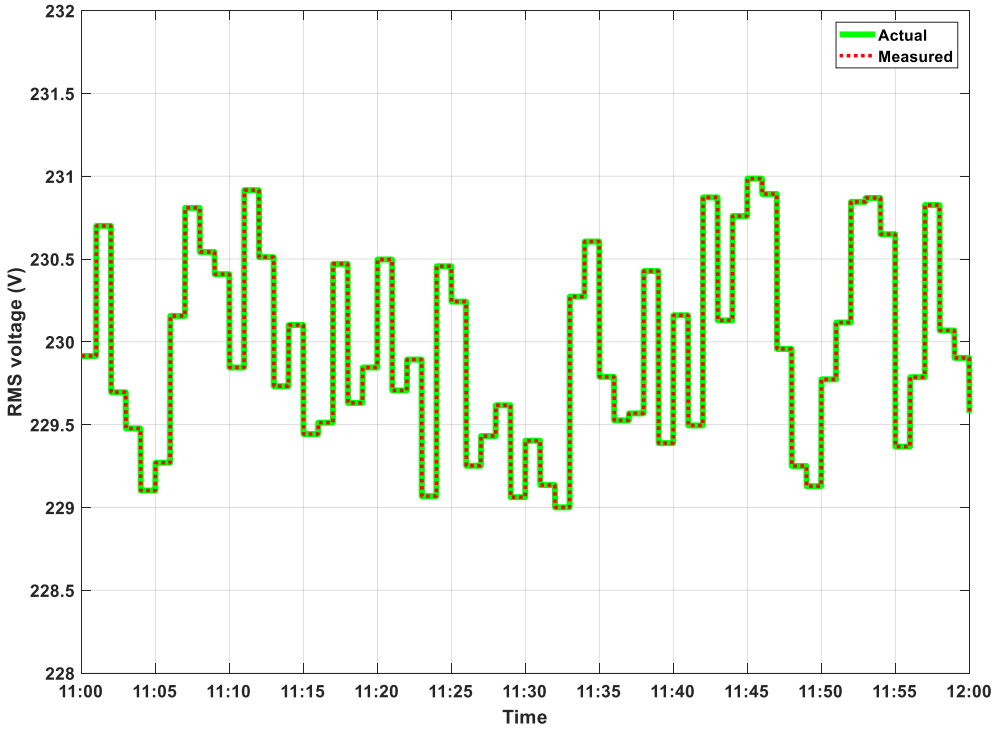

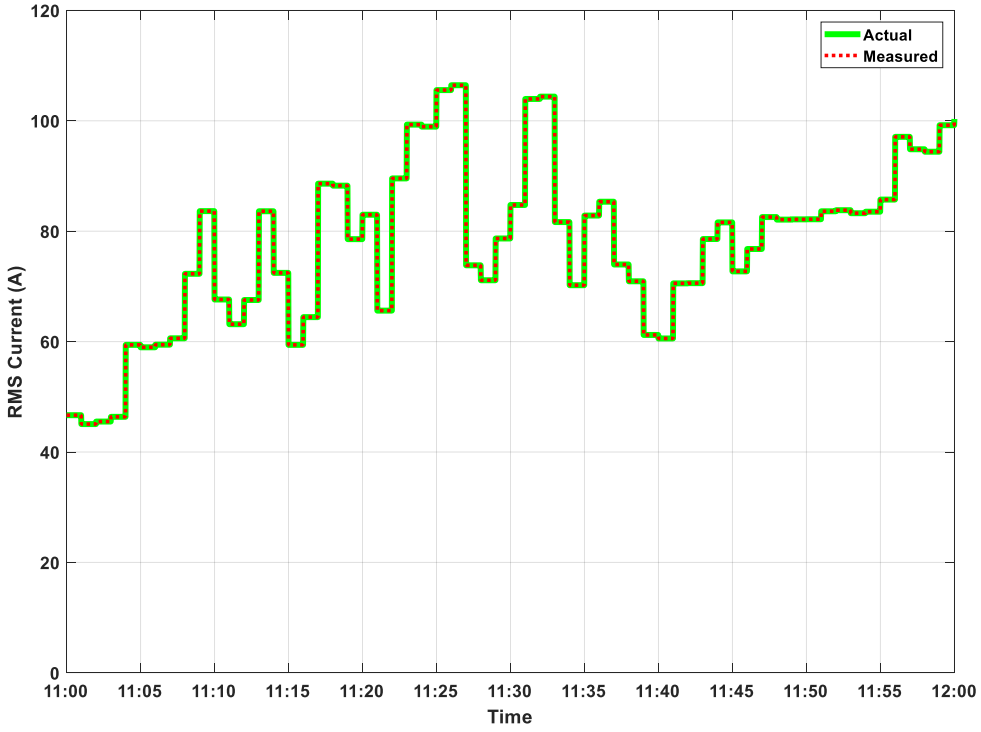

Plots Related to Smart Meter Number 6

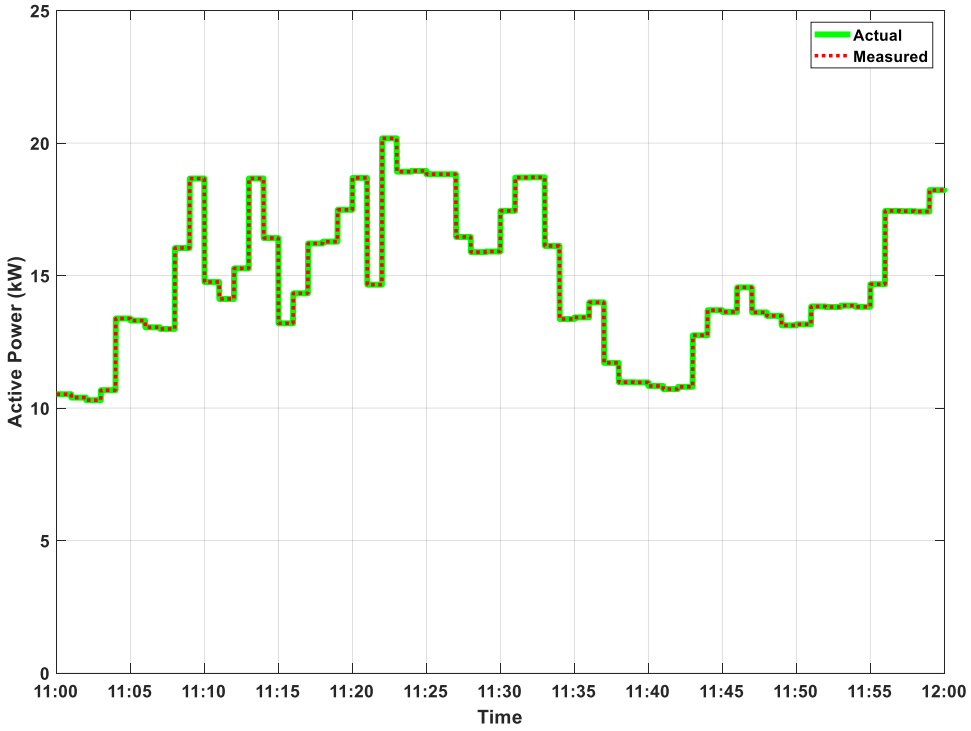

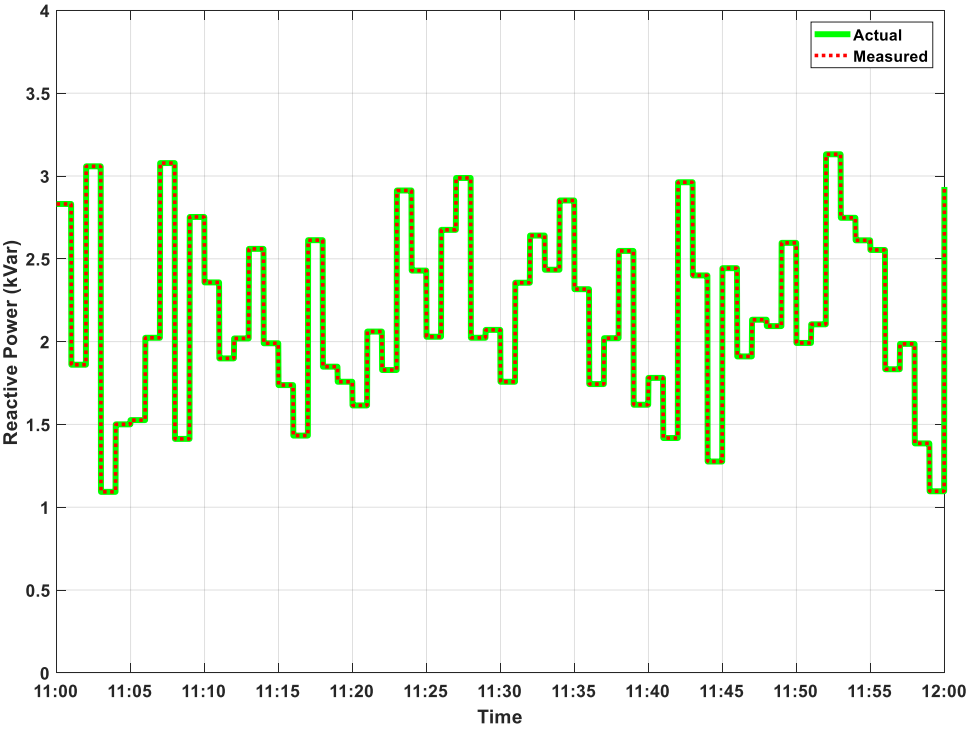

Plots Related to Smart Meter Number 6

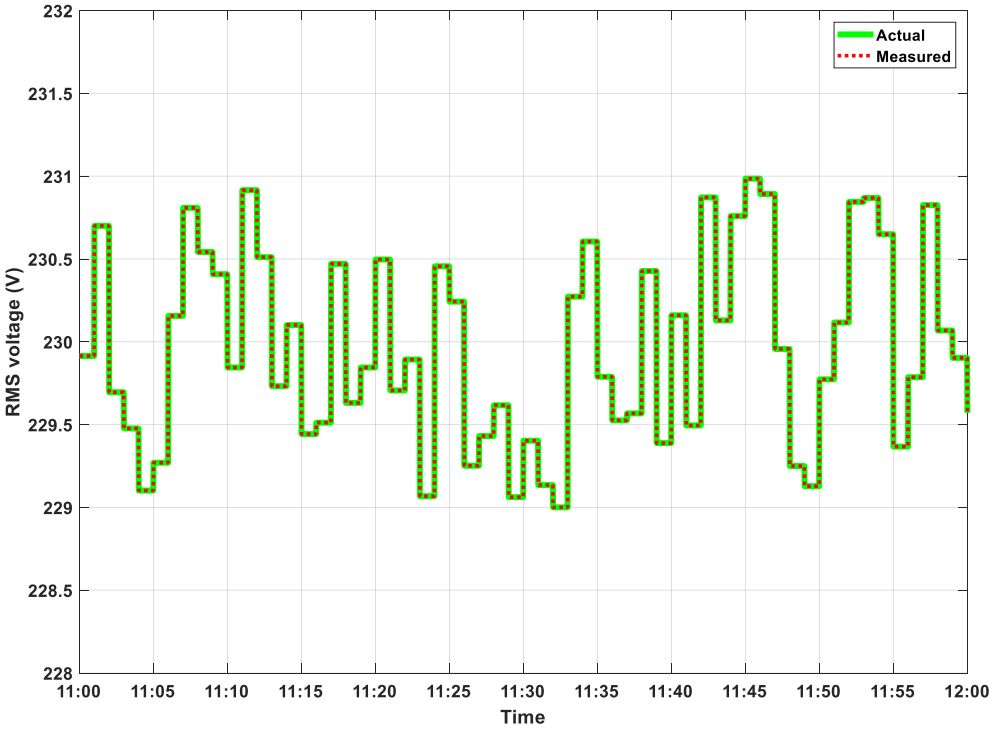

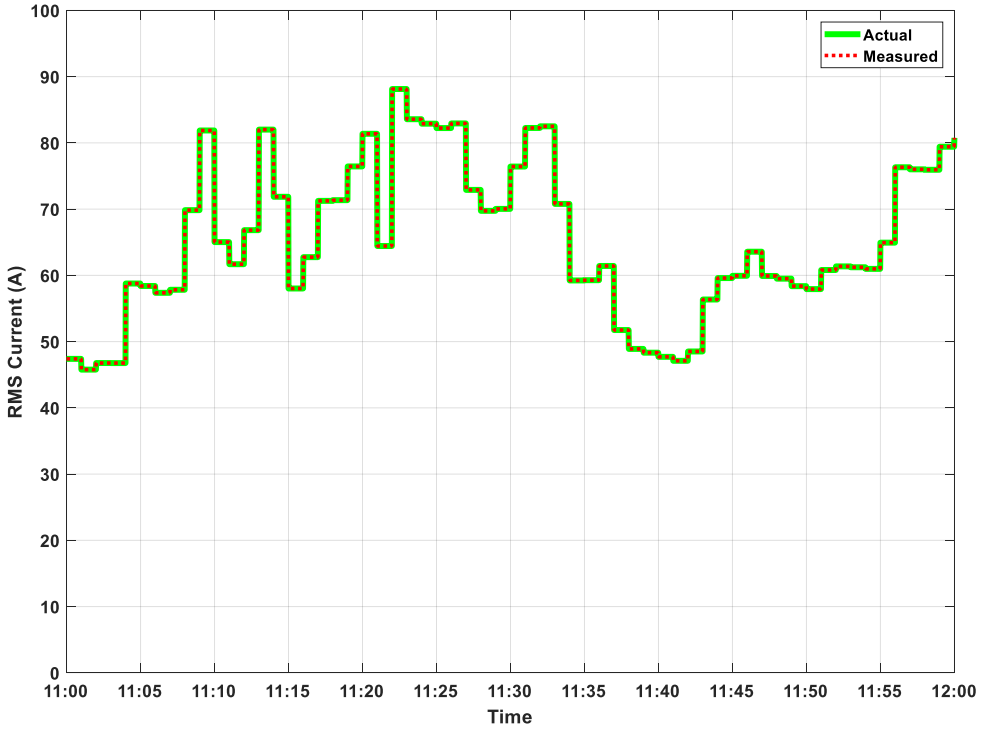

Plots Related to Smart Meter Number 7

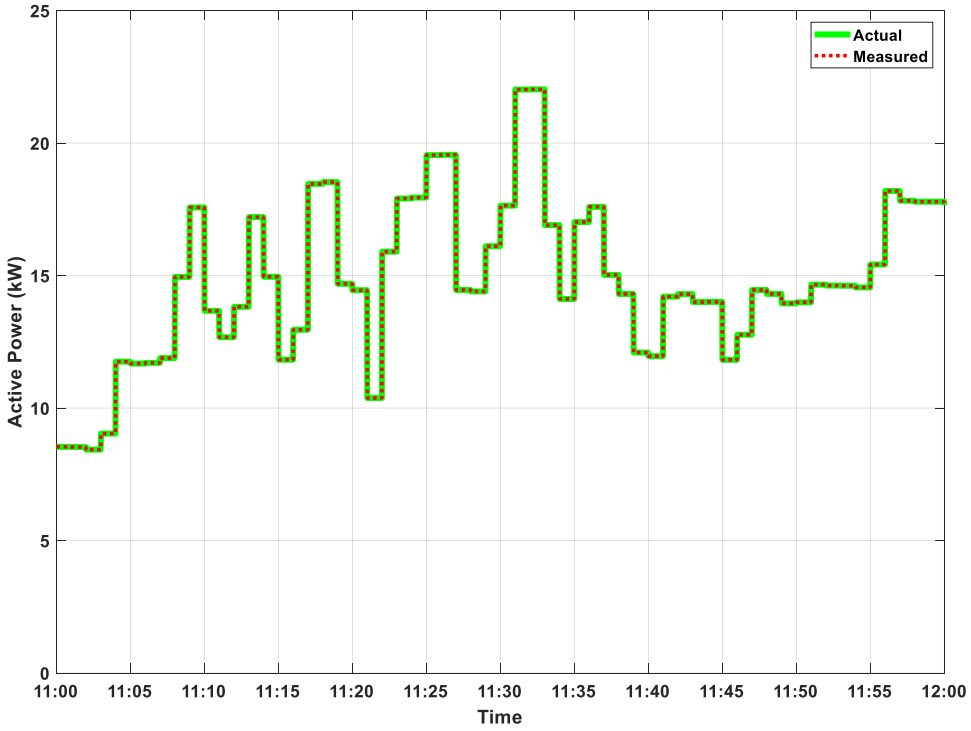

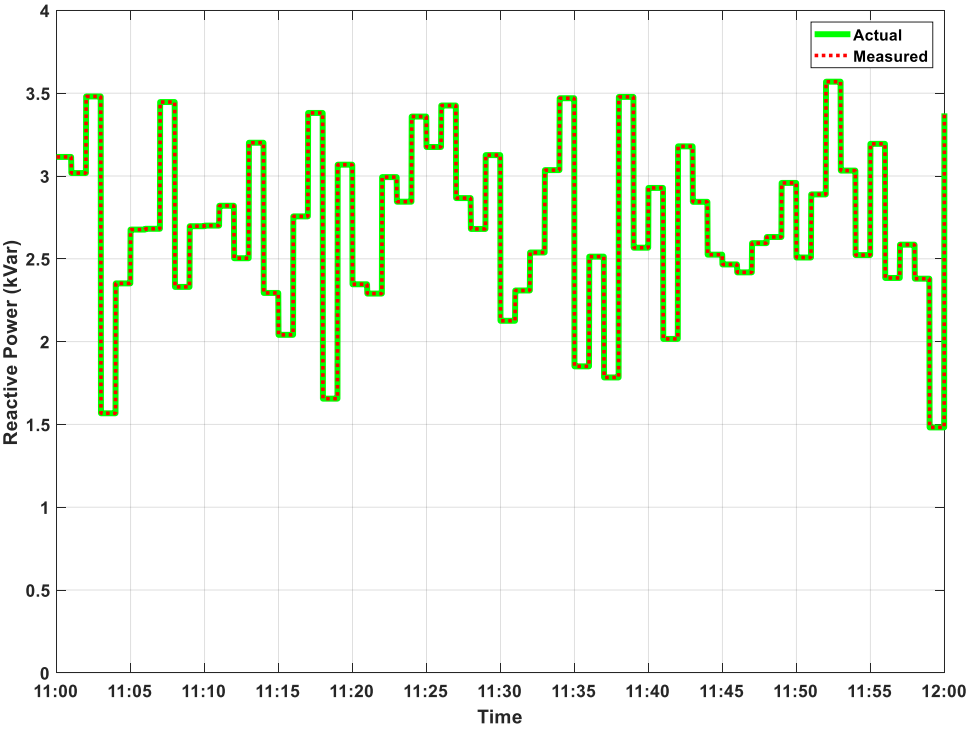

Plots Related to Smart Meter Number 7

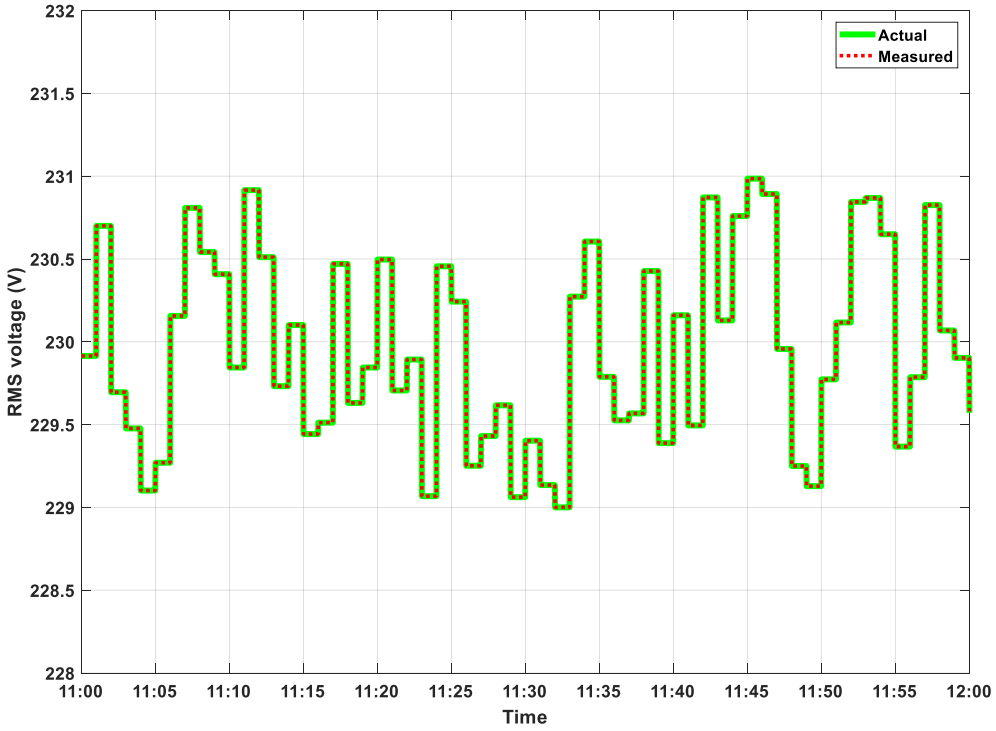

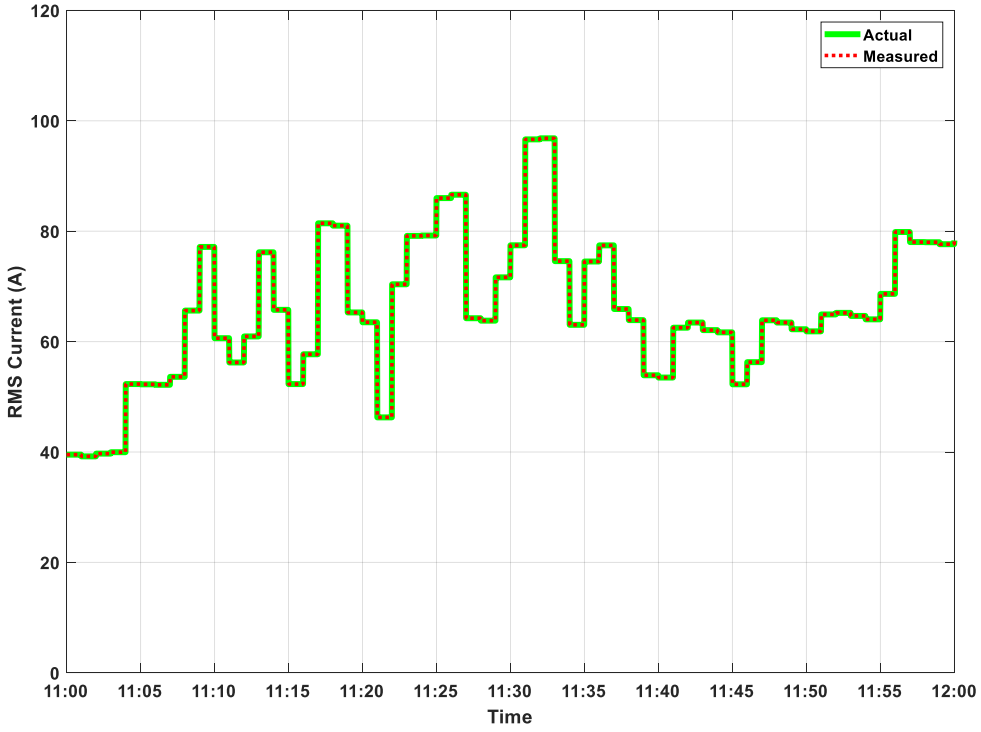

Power Losses of Cable Number 1

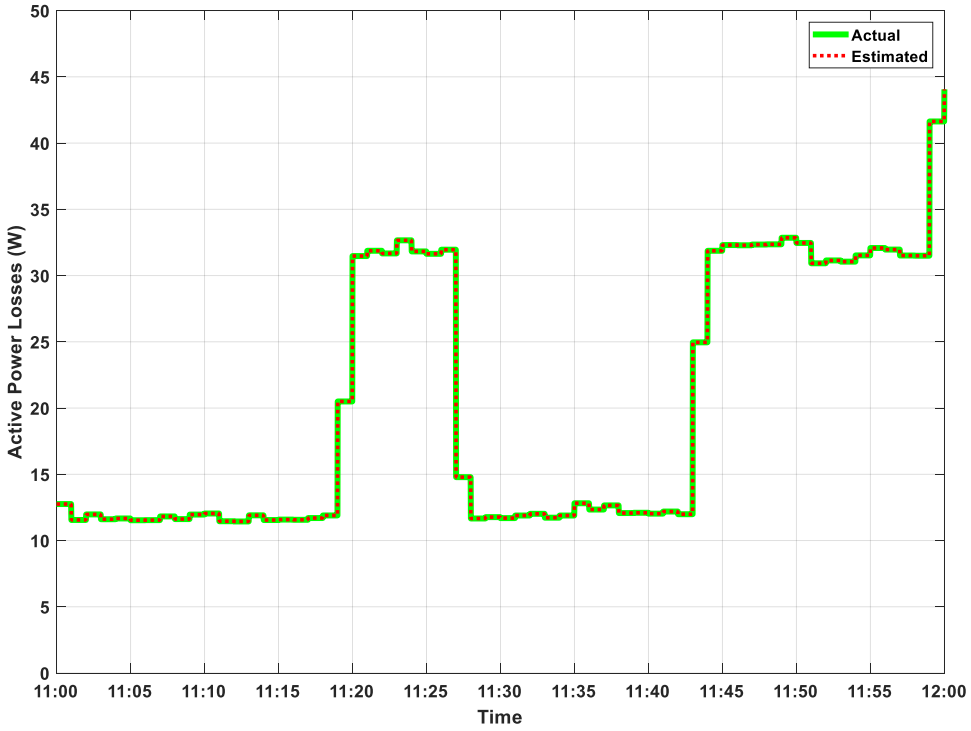

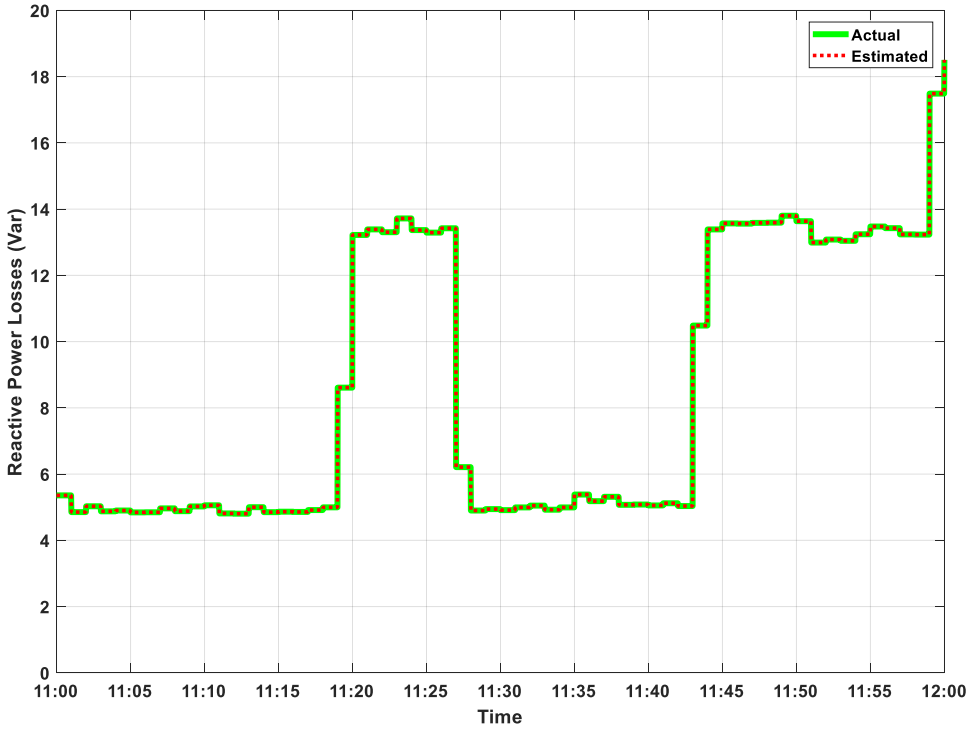

Power Losses of Cable Number 2

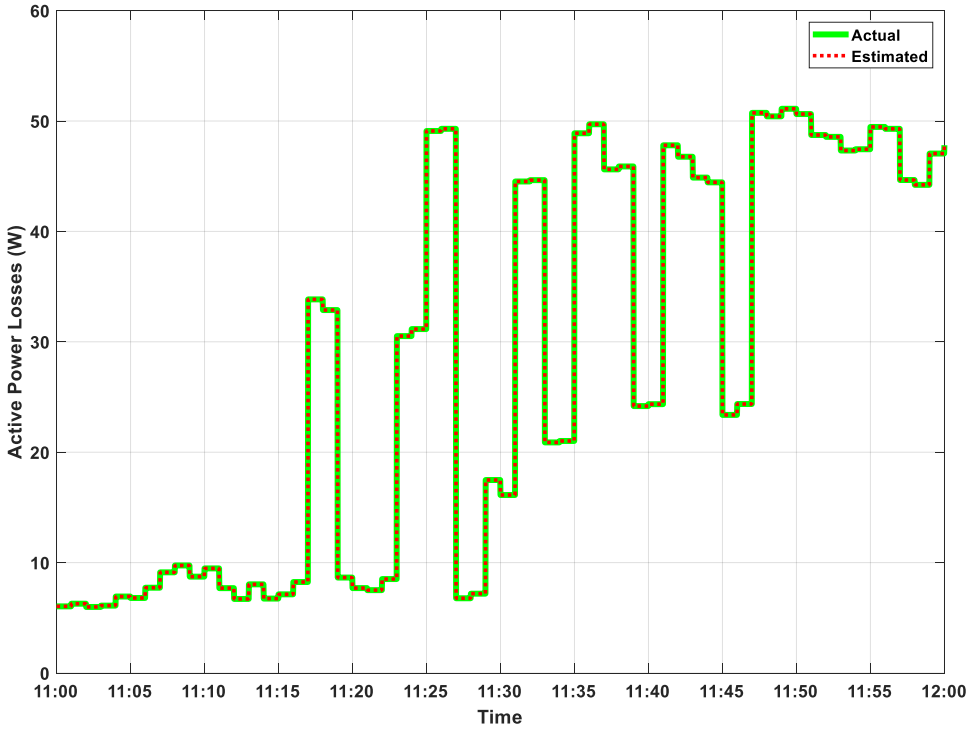

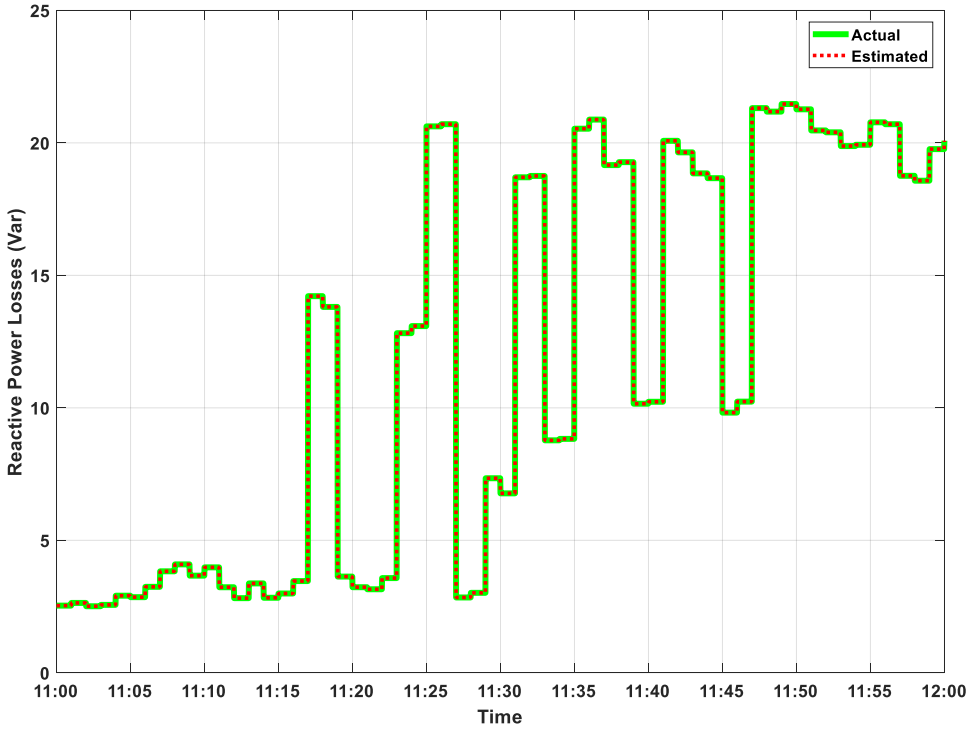

Power Losses of Cable Number 3

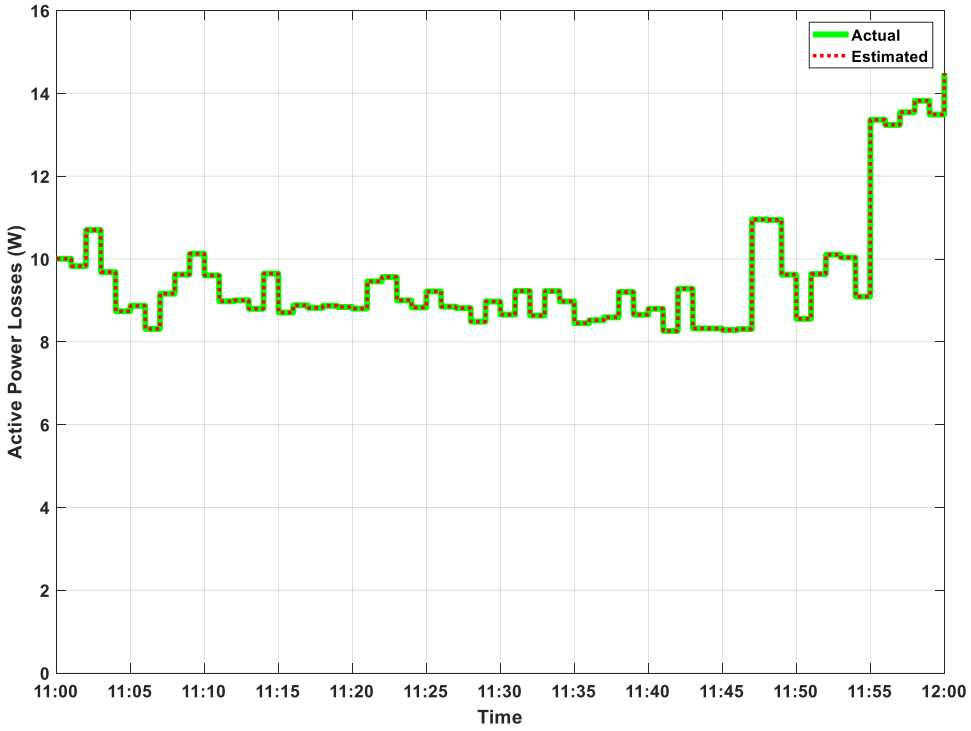

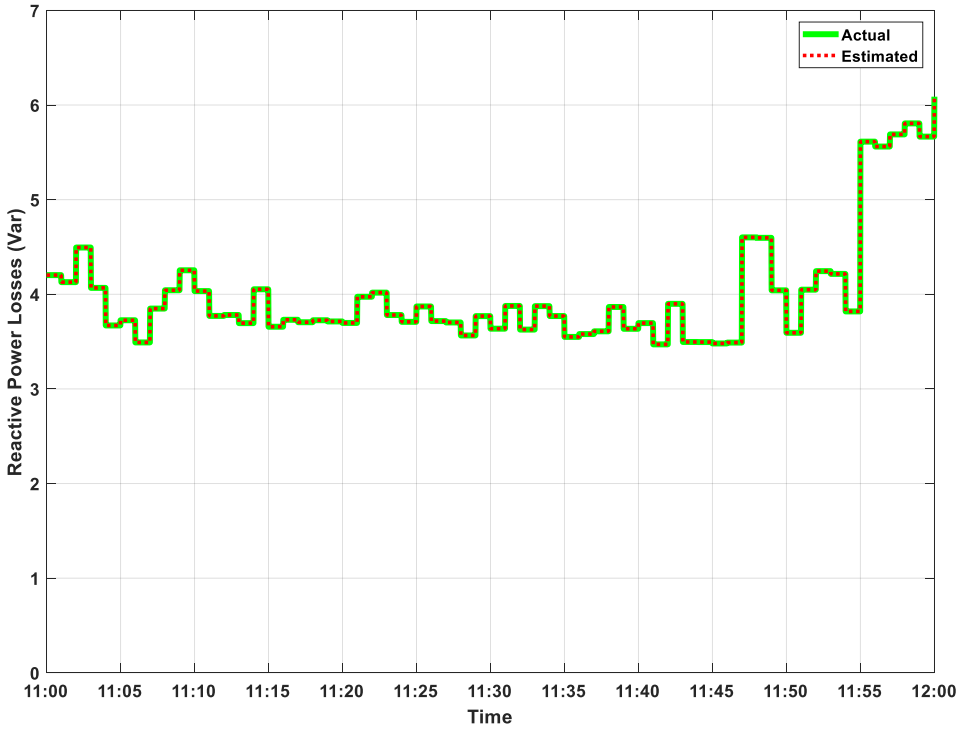

Power Losses of Cable Number 4

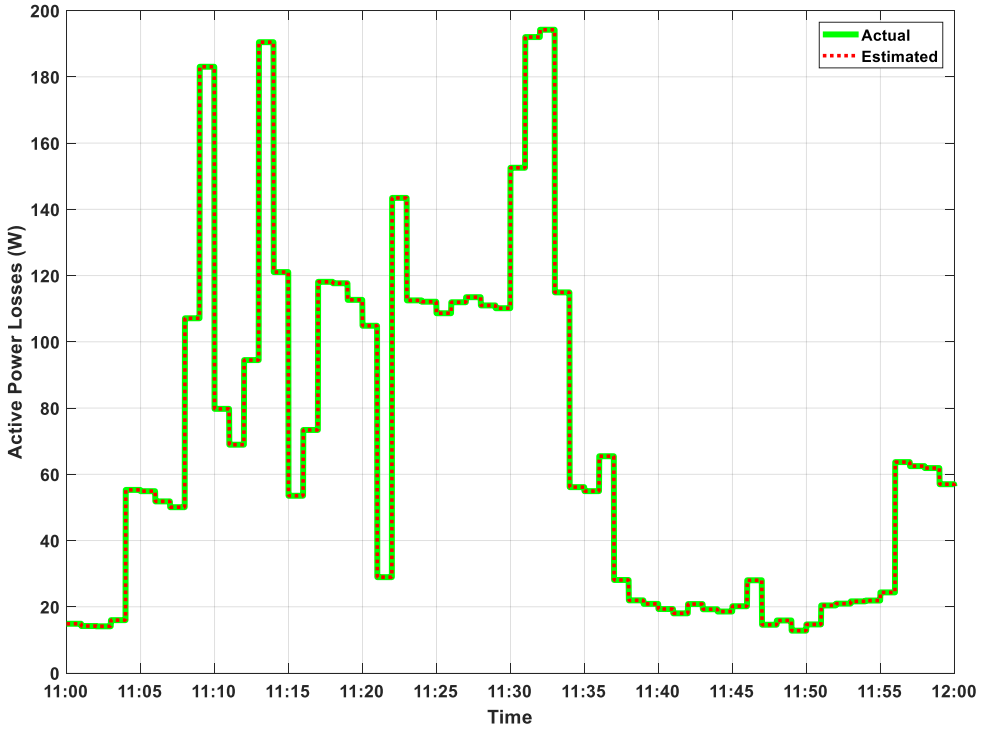

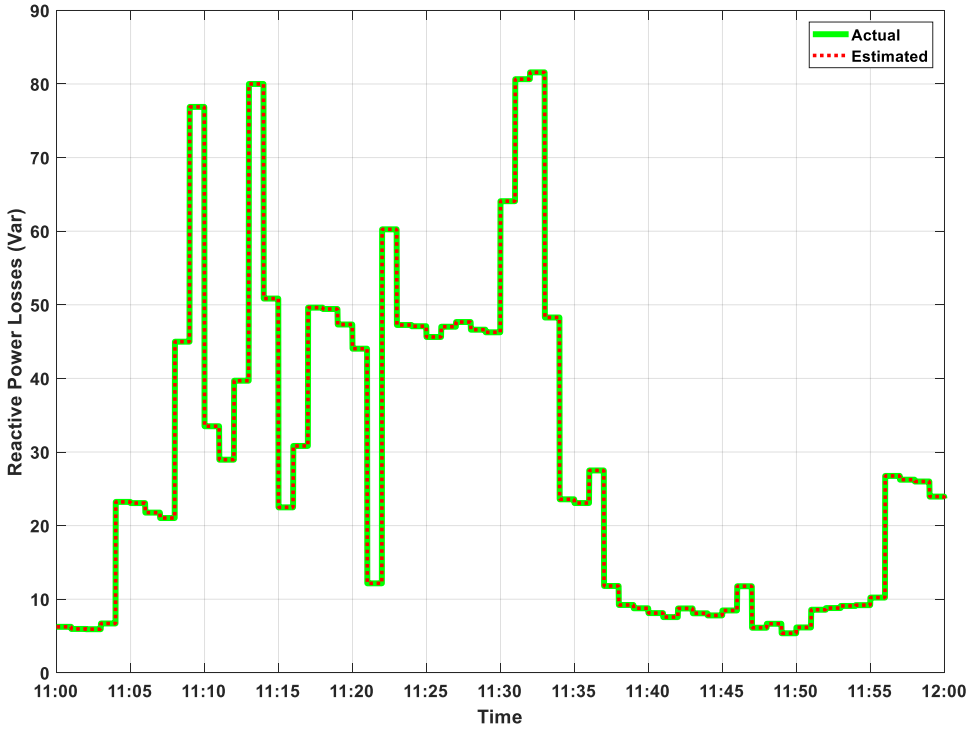

Appendix B

Plots Related to Smart Meter Number 1

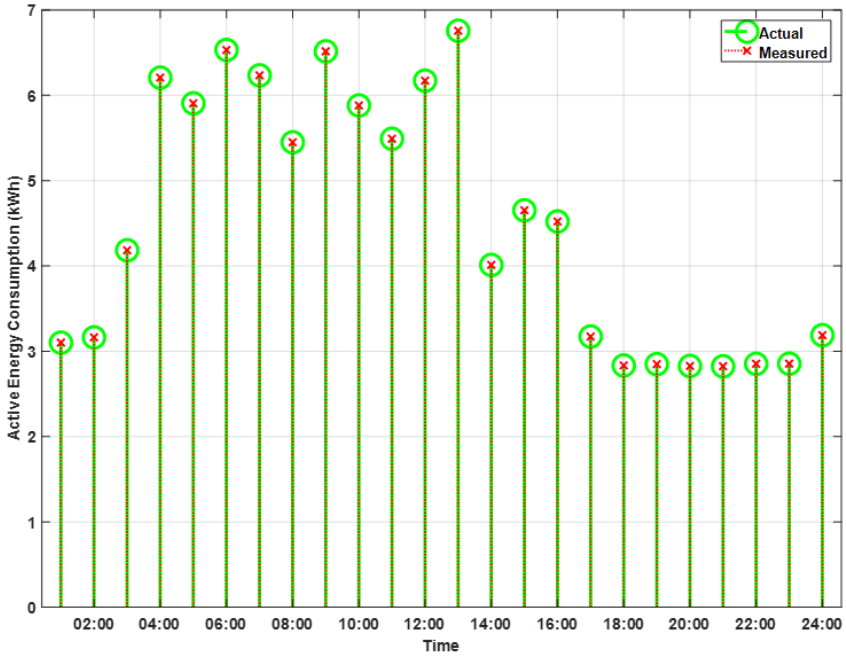

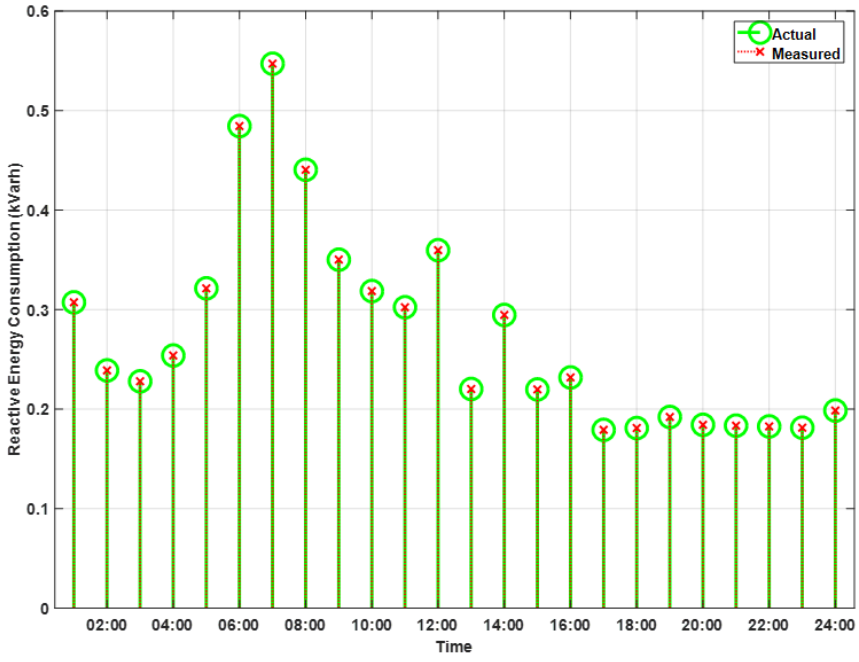

Plots Related to Smart Meter Number 1

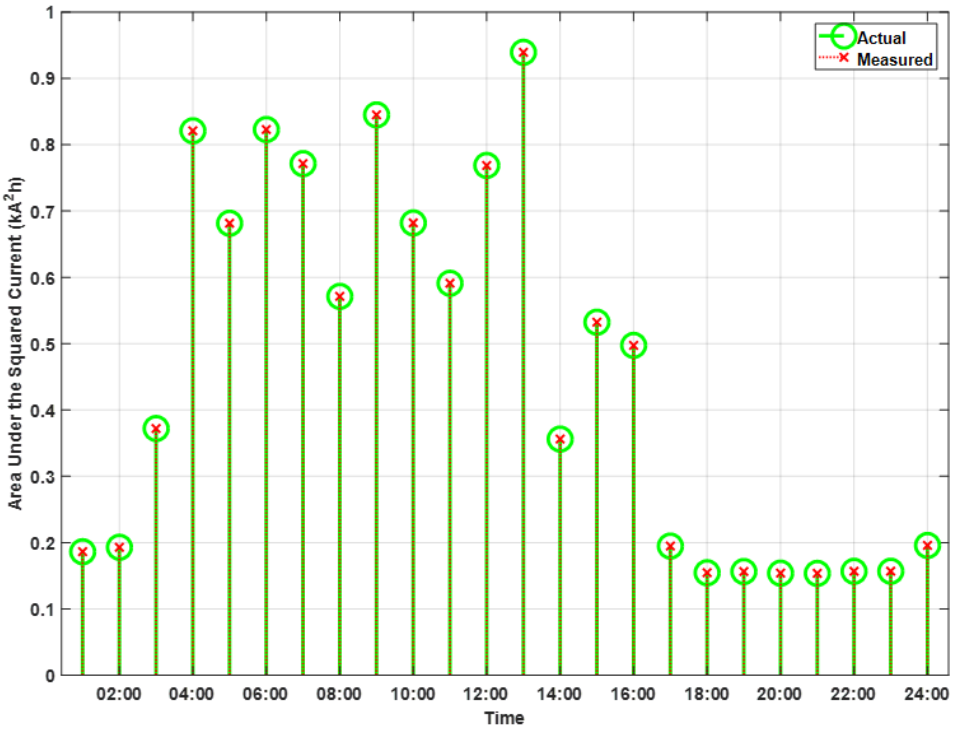

Plots Related to Smart Meter Number 2

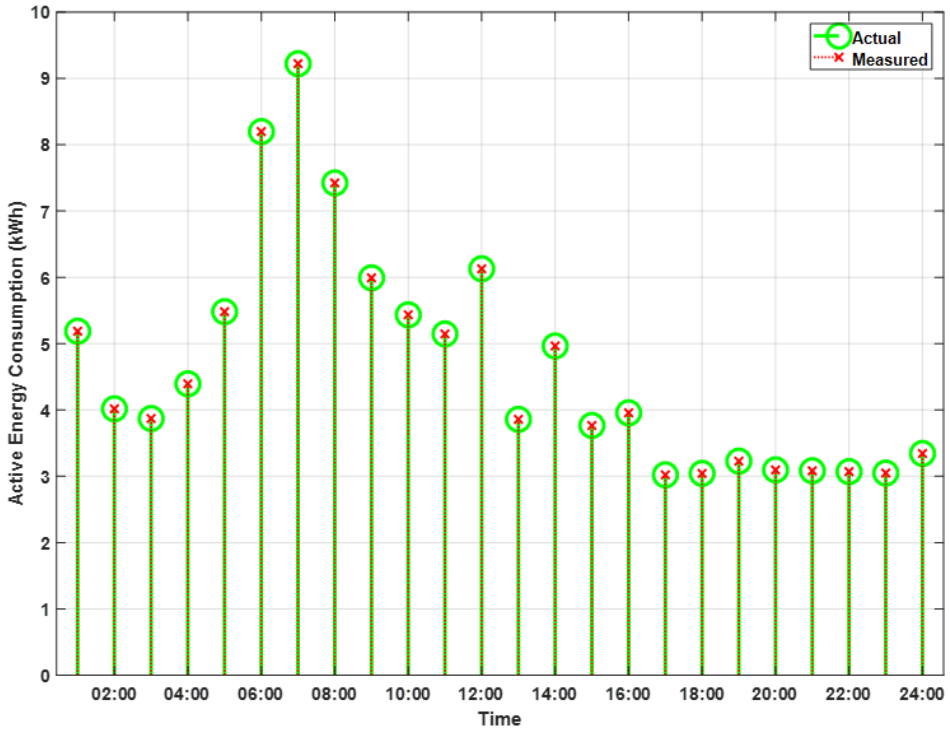

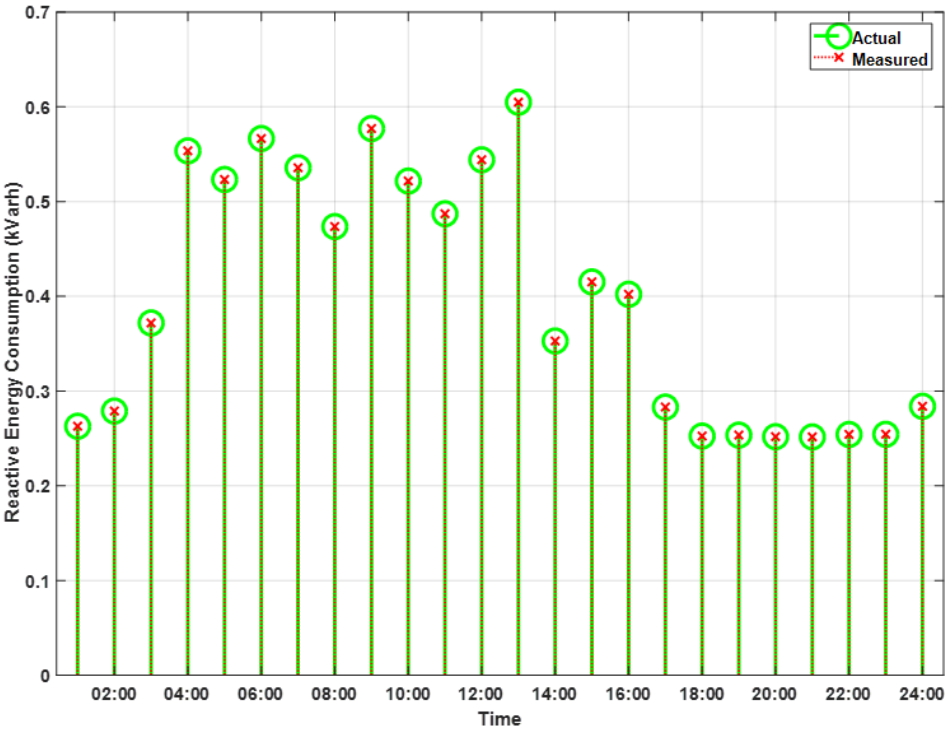

Plots Related to Smart Meter Number 2

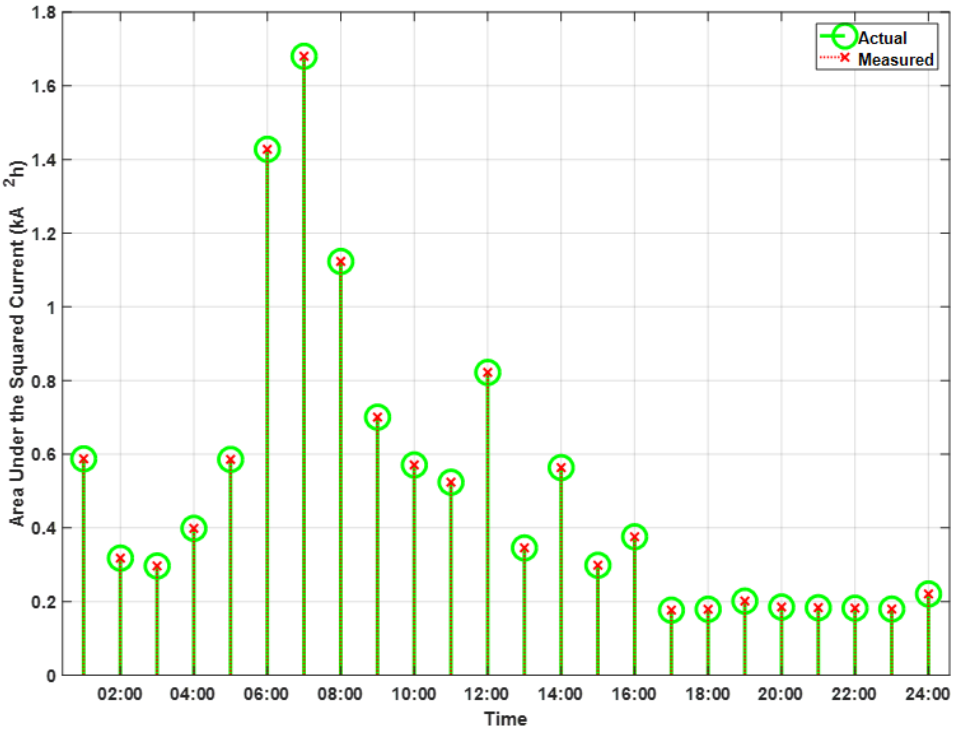

Plots Related to Smart Meter Number 3

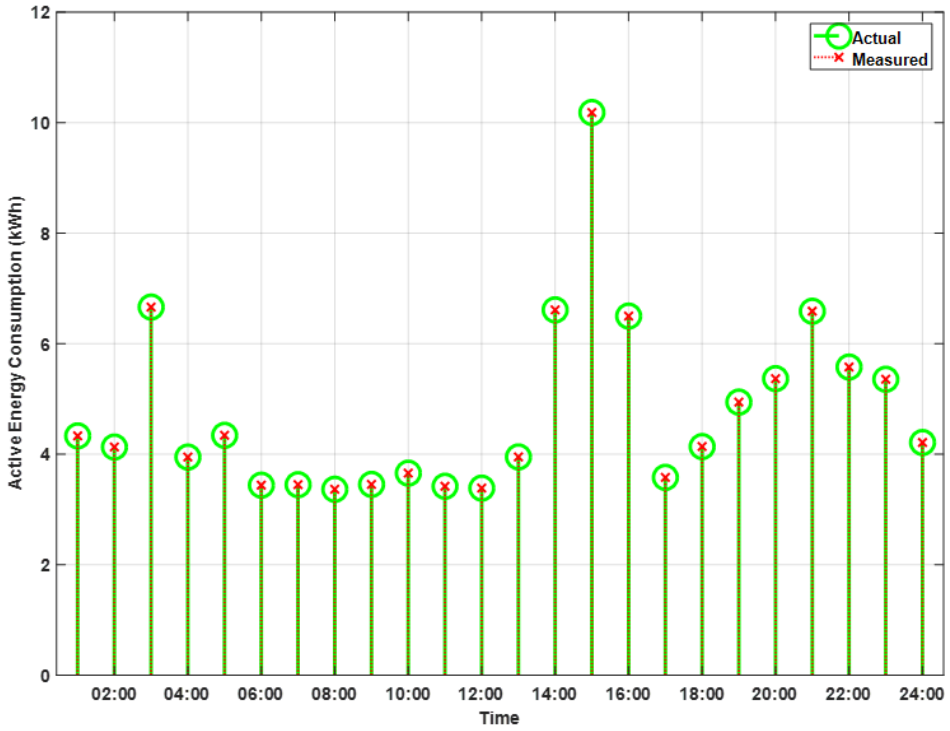

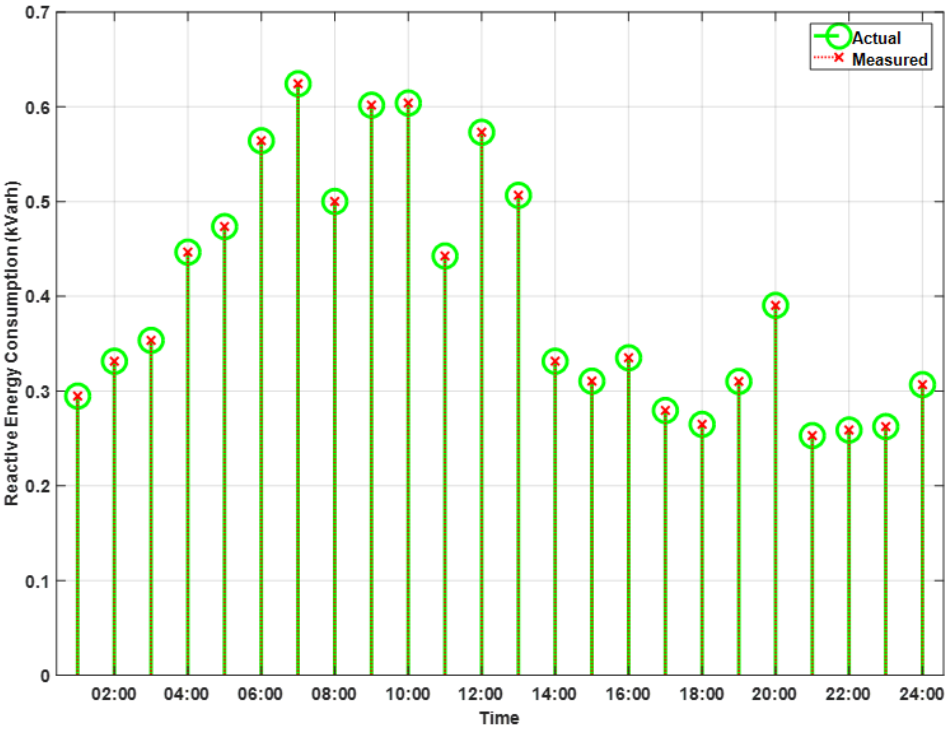

Plots Related to Smart Meter Number 3

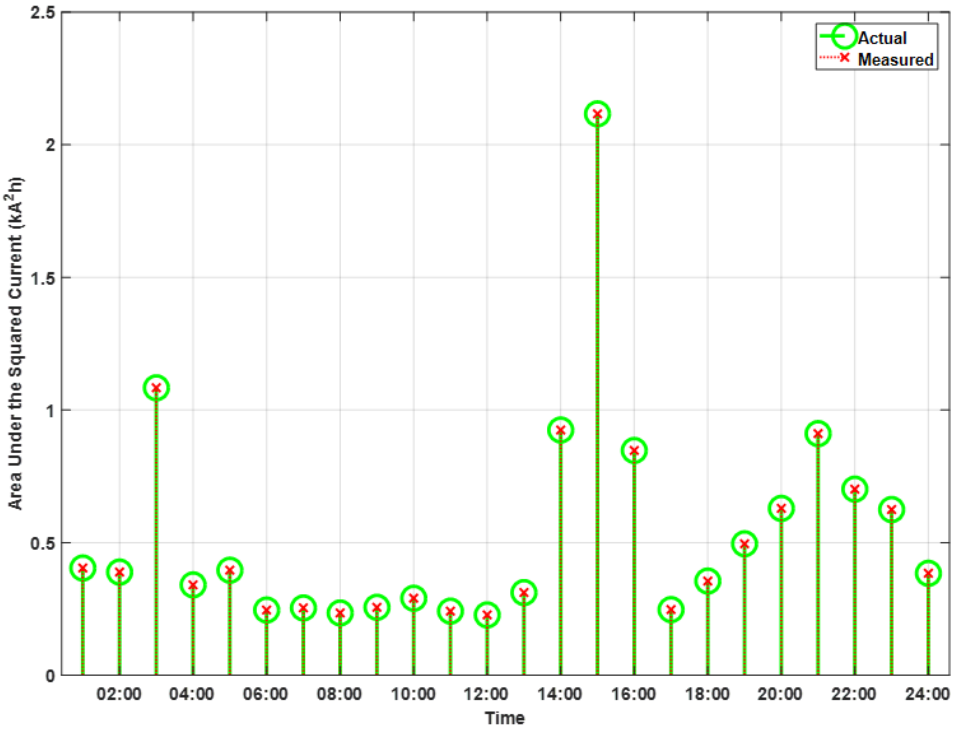

Plots Related to Smart Meter Number 4

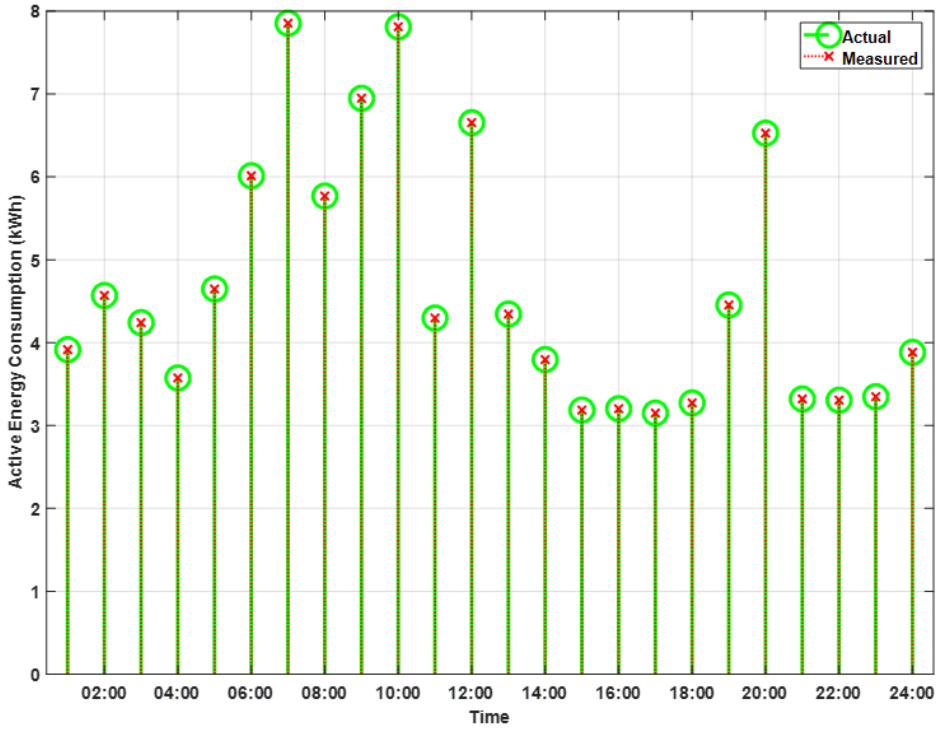

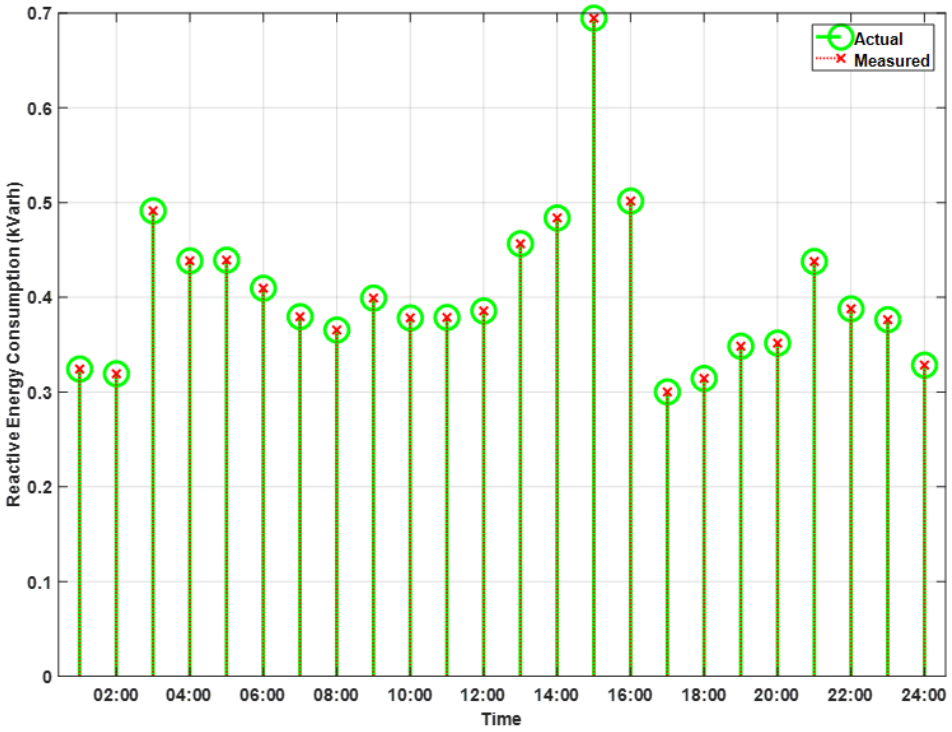

Plots Related to Smart Meter Number 4

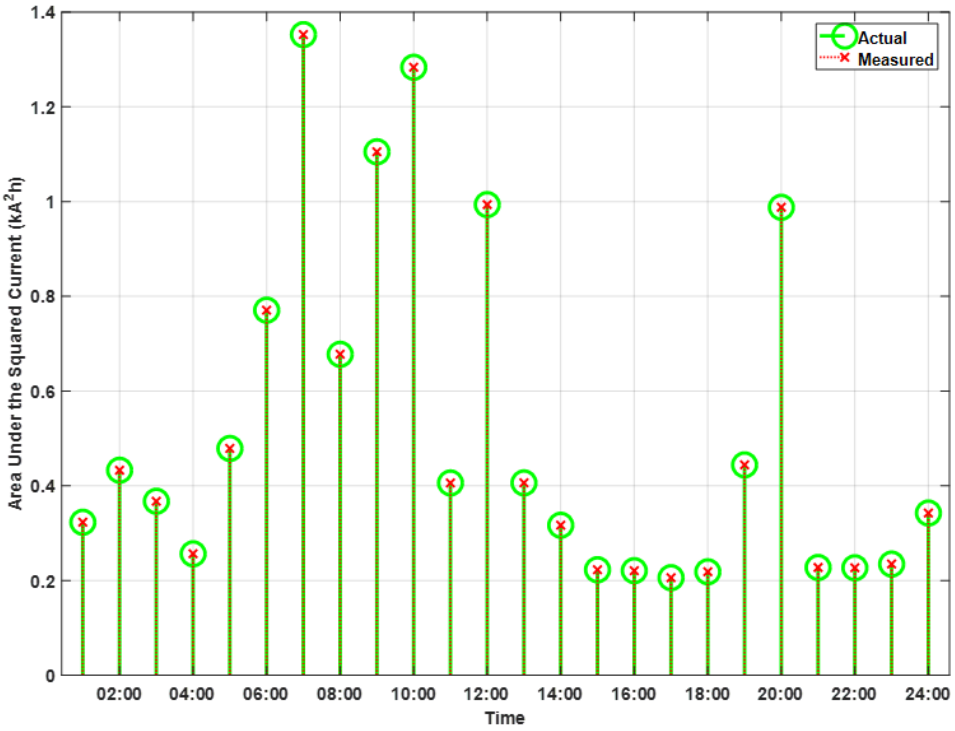

Plots Related to Smart Meter Number 5

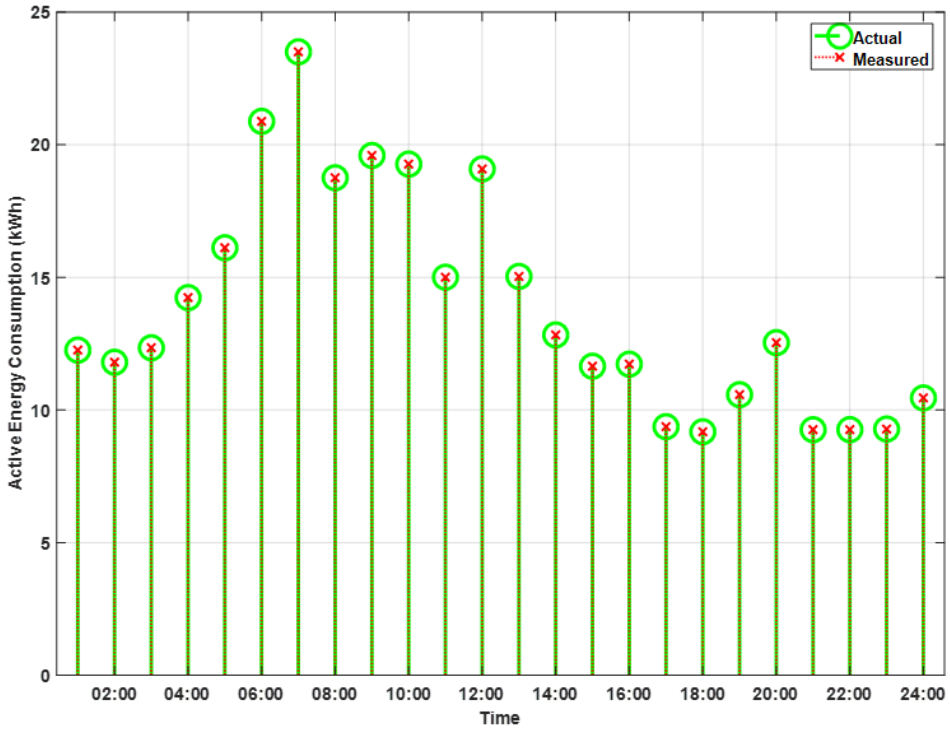

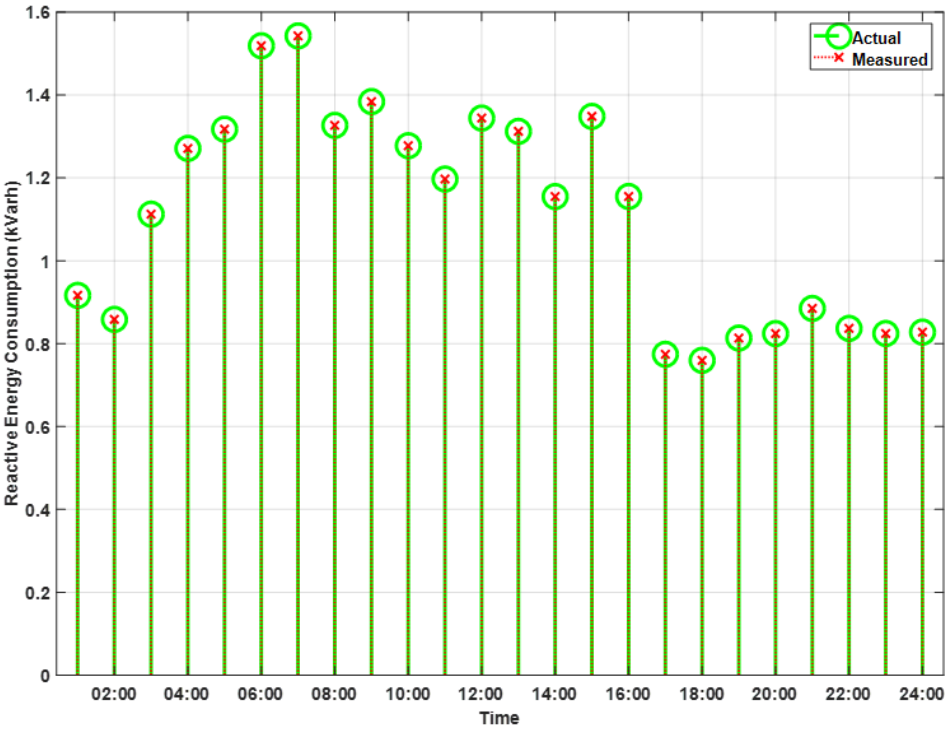

Plots Related to Smart Meter Number 5

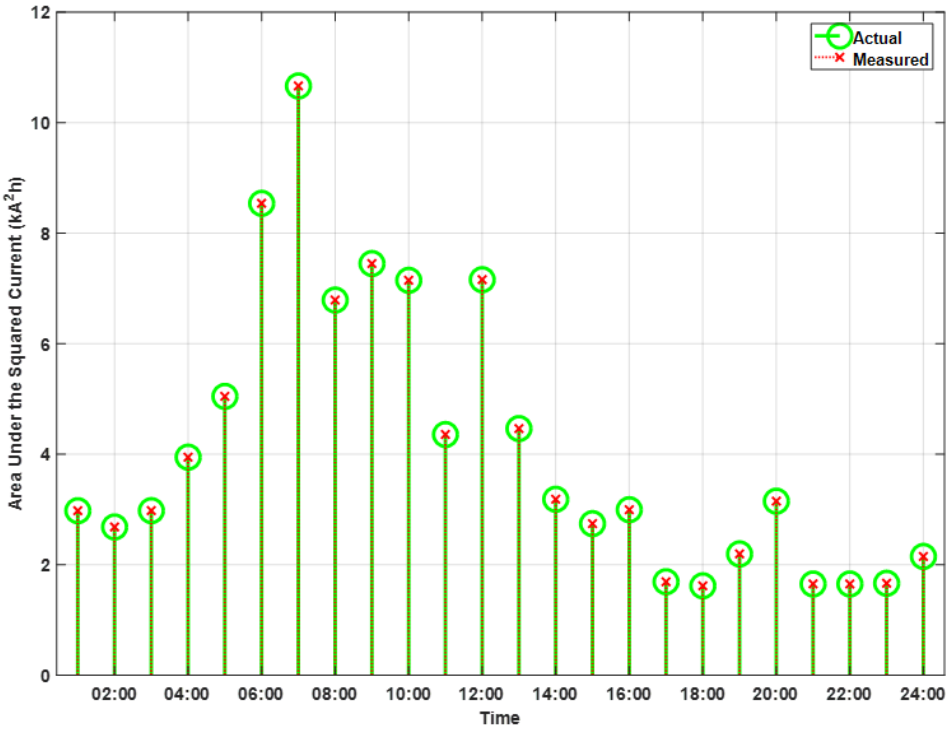

Plots Related to Smart Meter Number 6

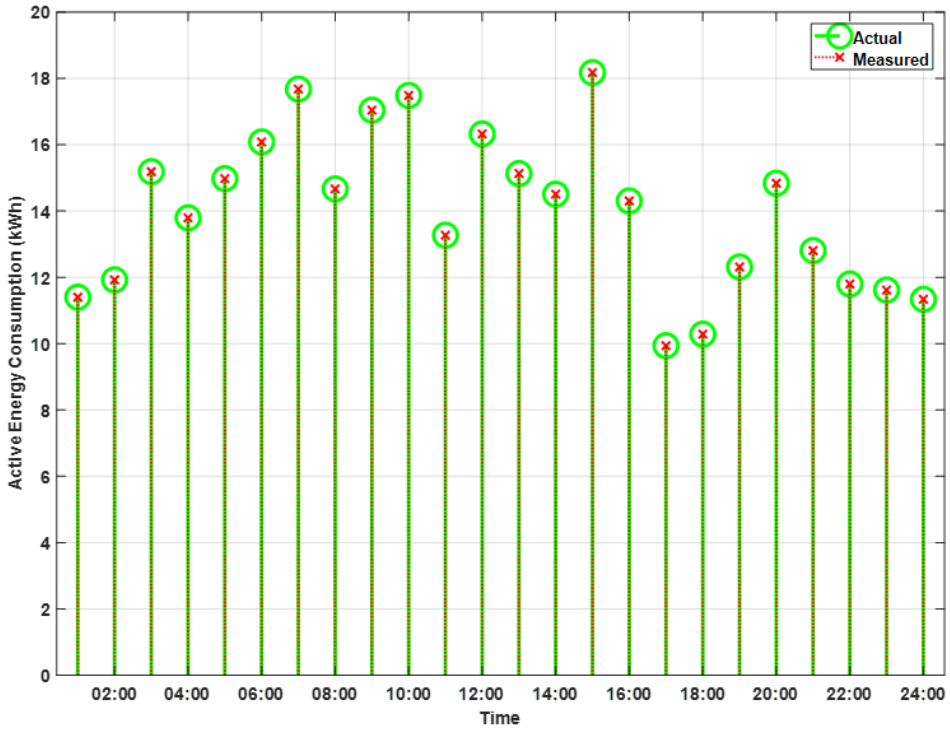

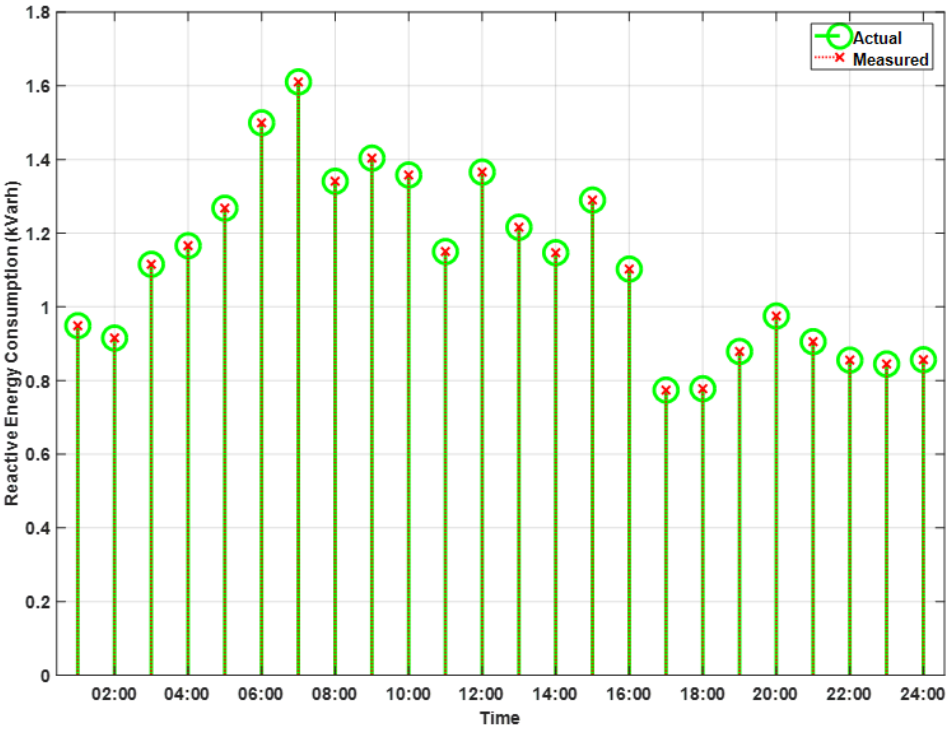

Plots Related to Smart Meter Number 6

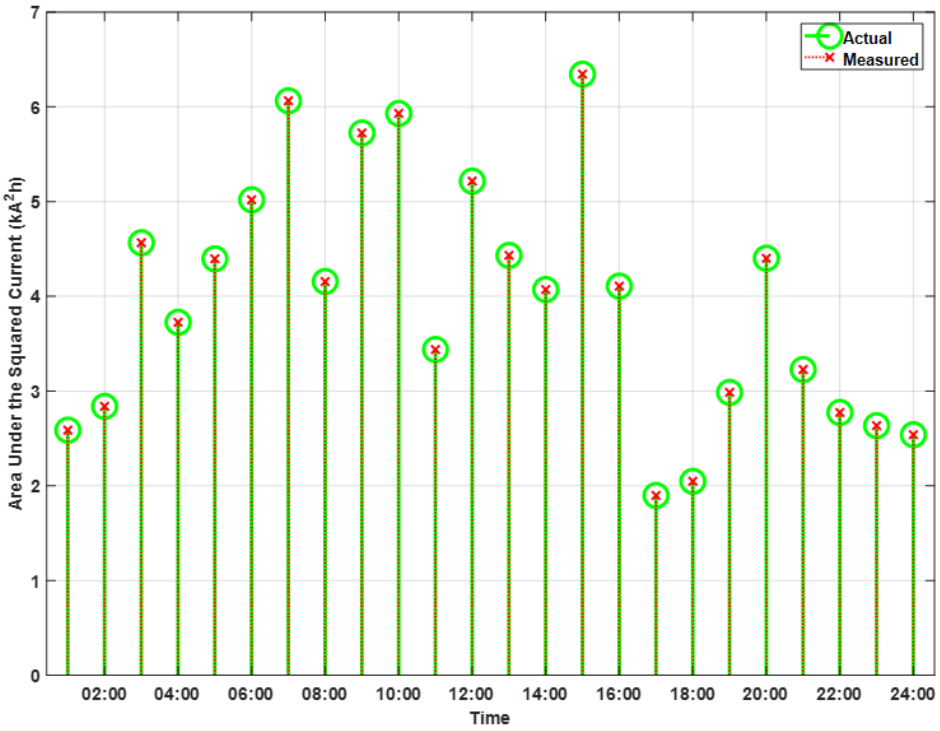

Plots Related to Smart Meter Number 7

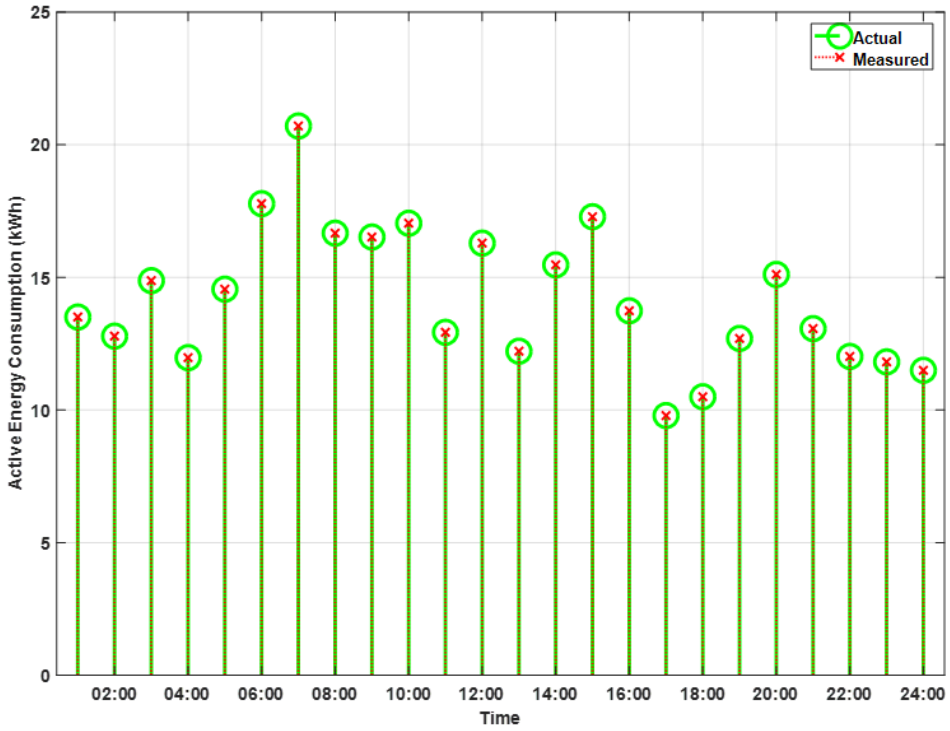

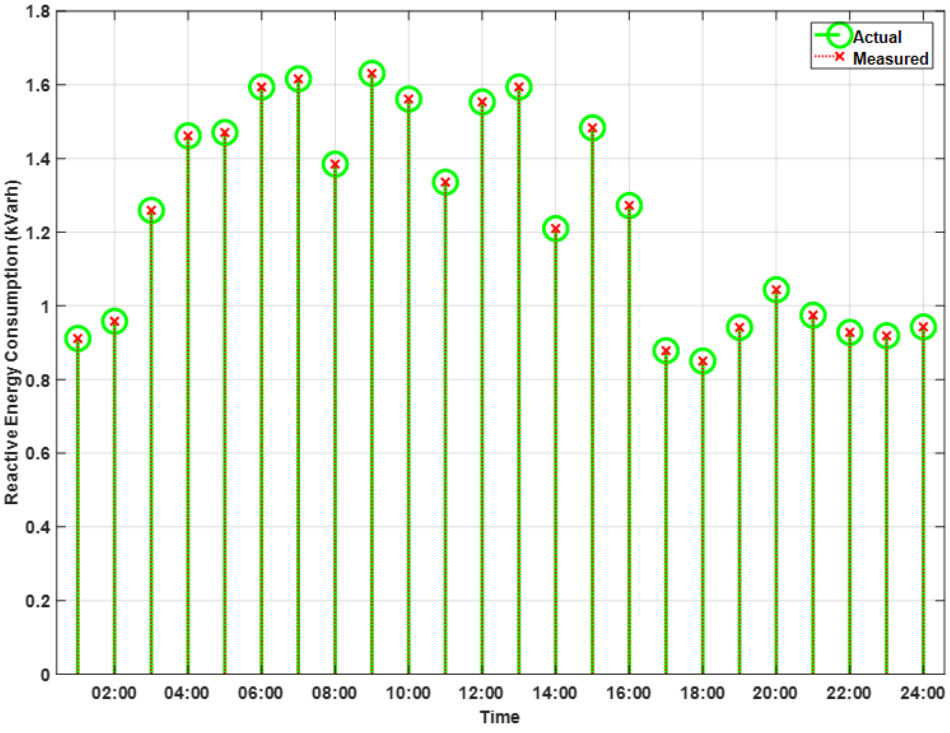

Plots Related to Smart Meter Number 7

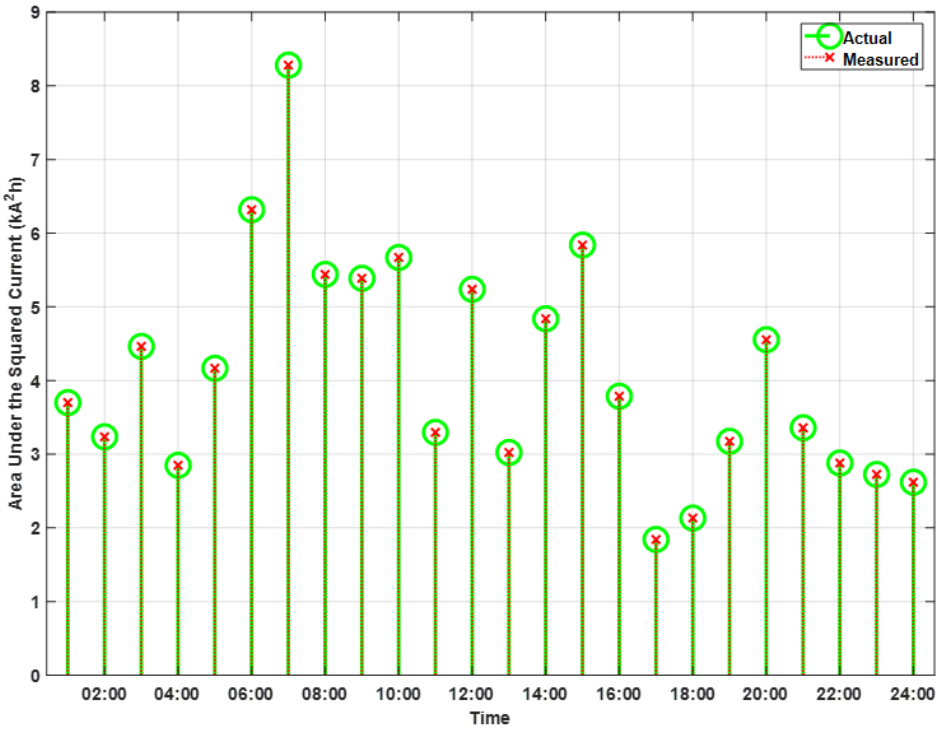

Energy Losses of Cable Number 1

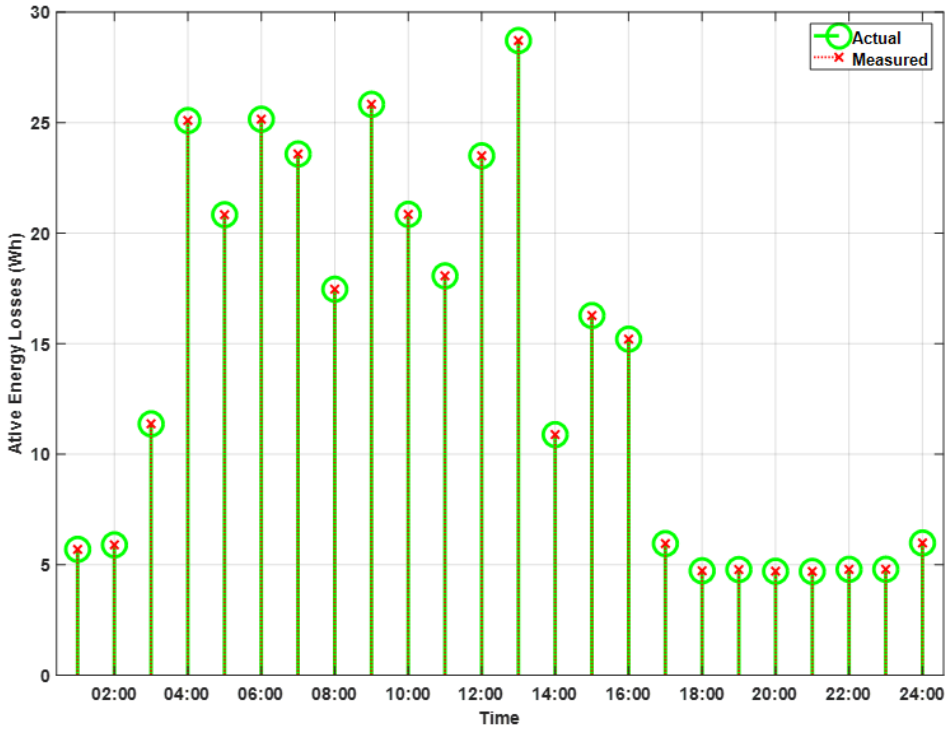

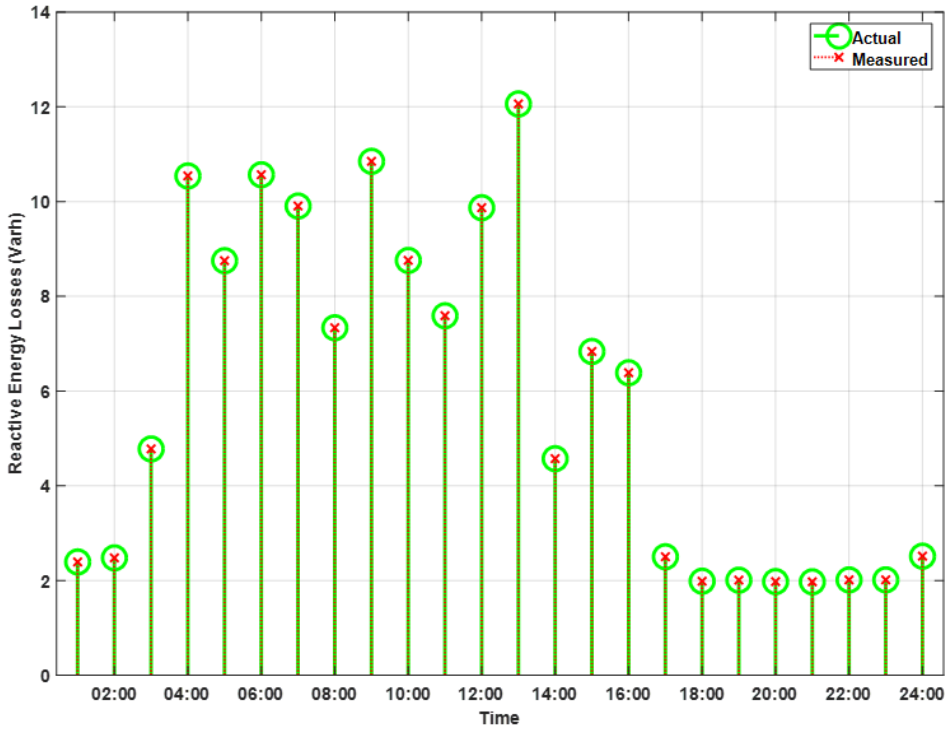

Energy Losses of Cable Number 2

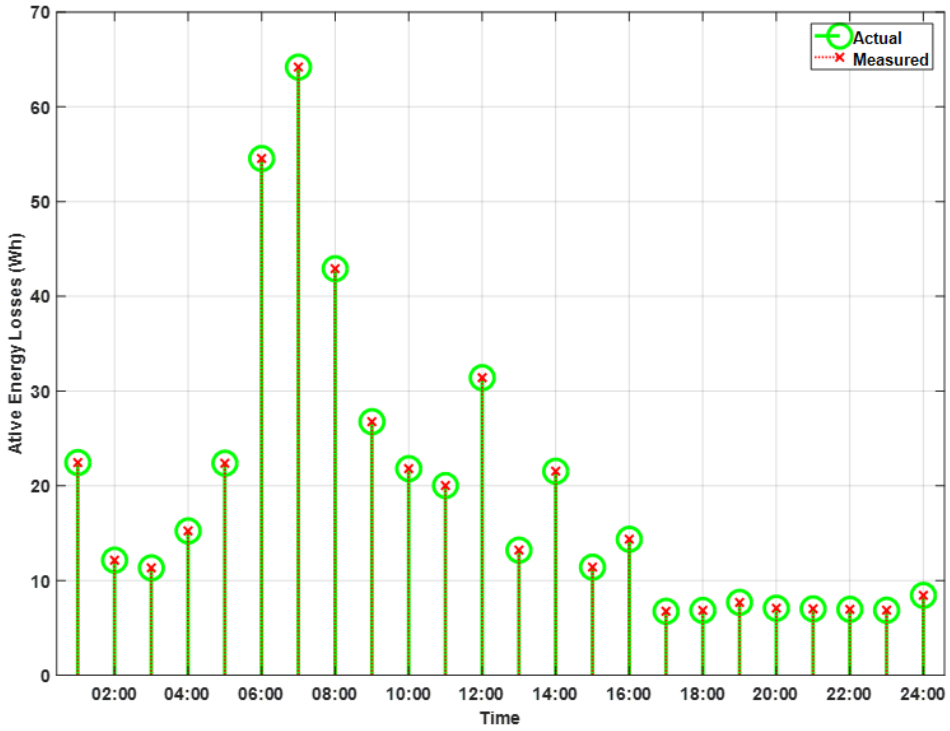

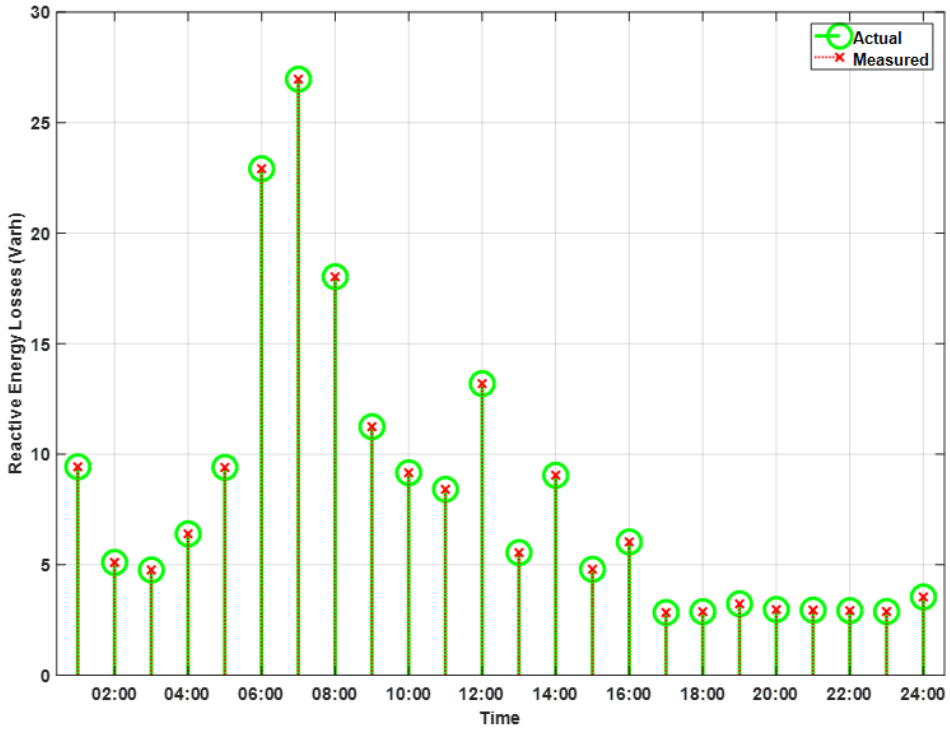

Energy Losses of Cable Number 3

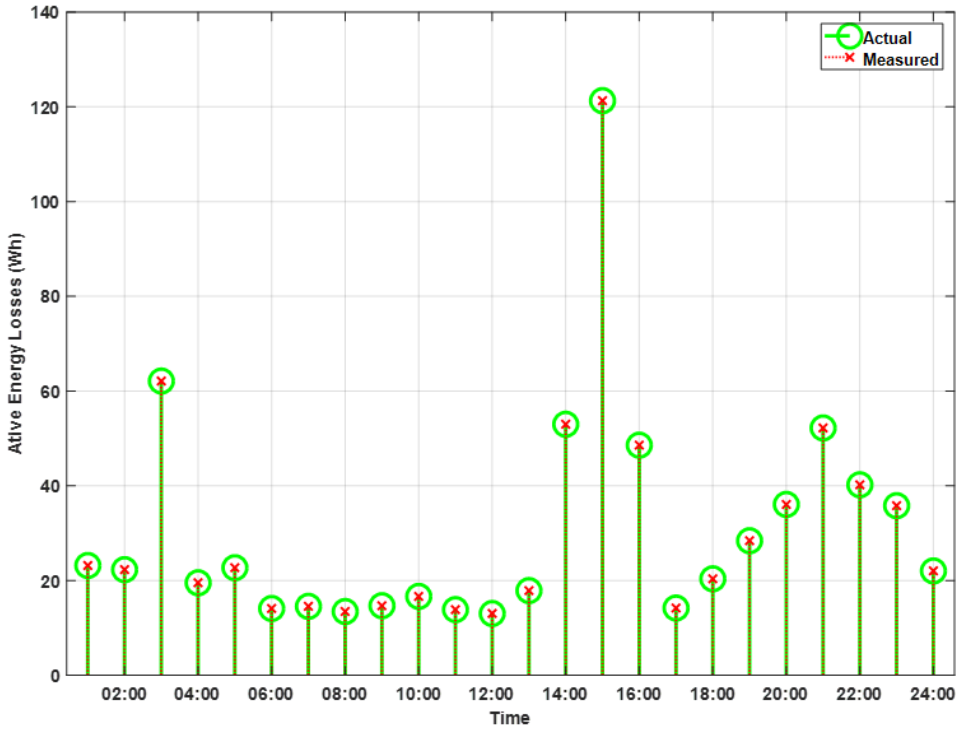

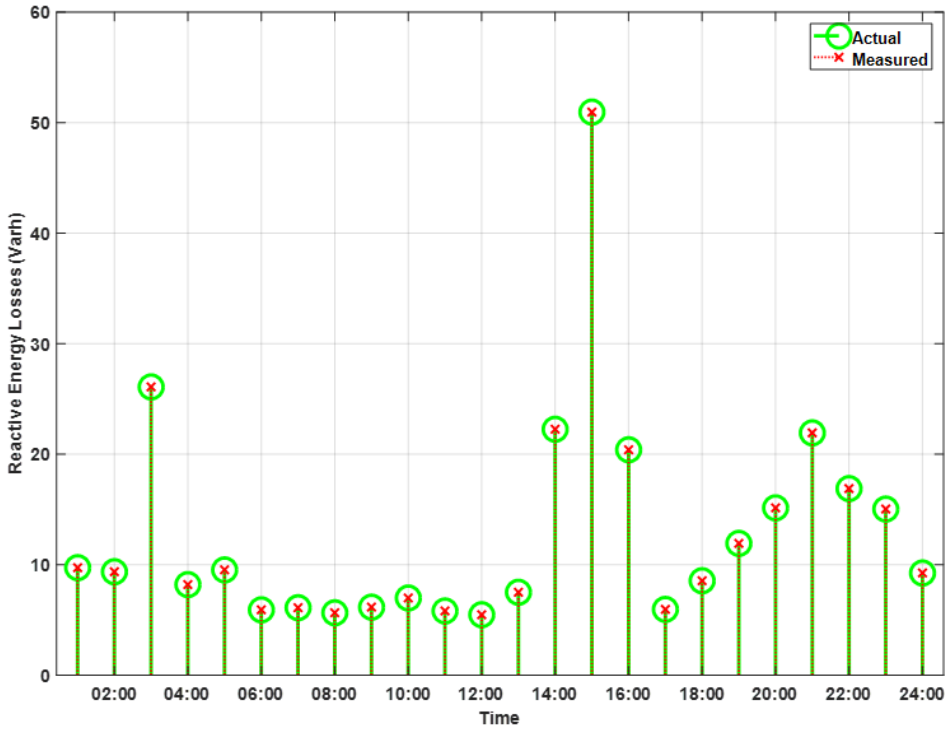

Energy Losses of Cable Number 4

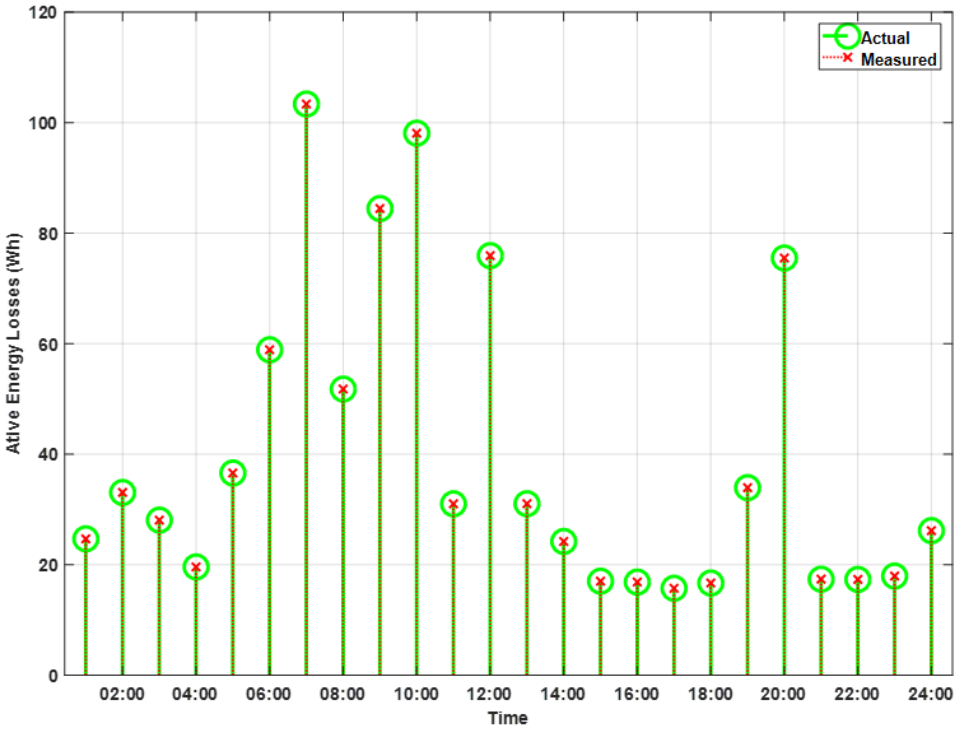

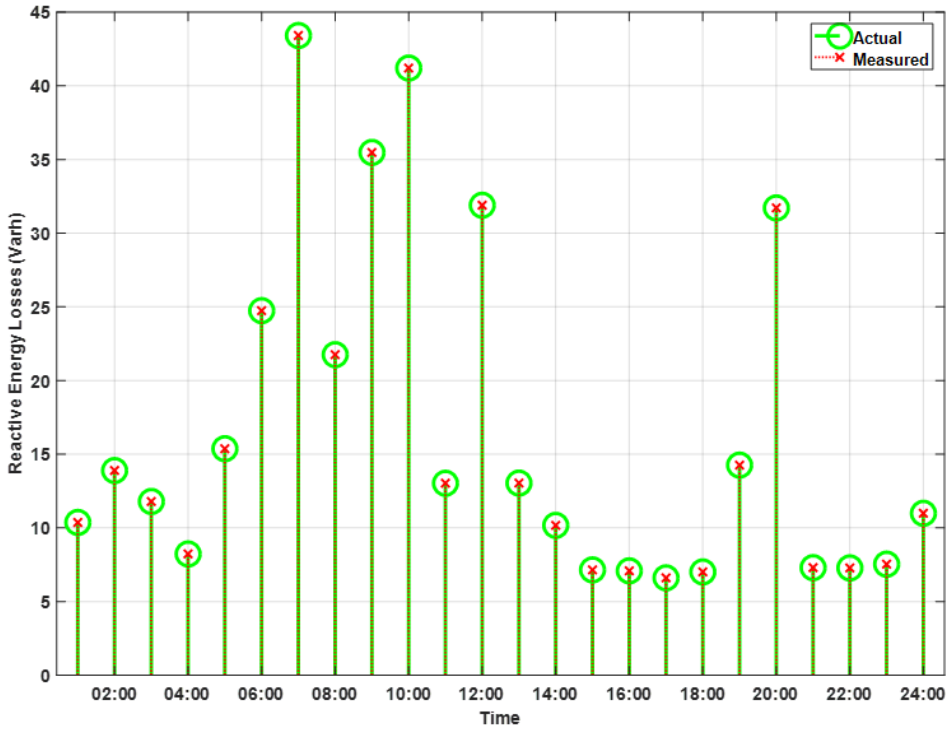

Appendix C

The schematics of the smart meter

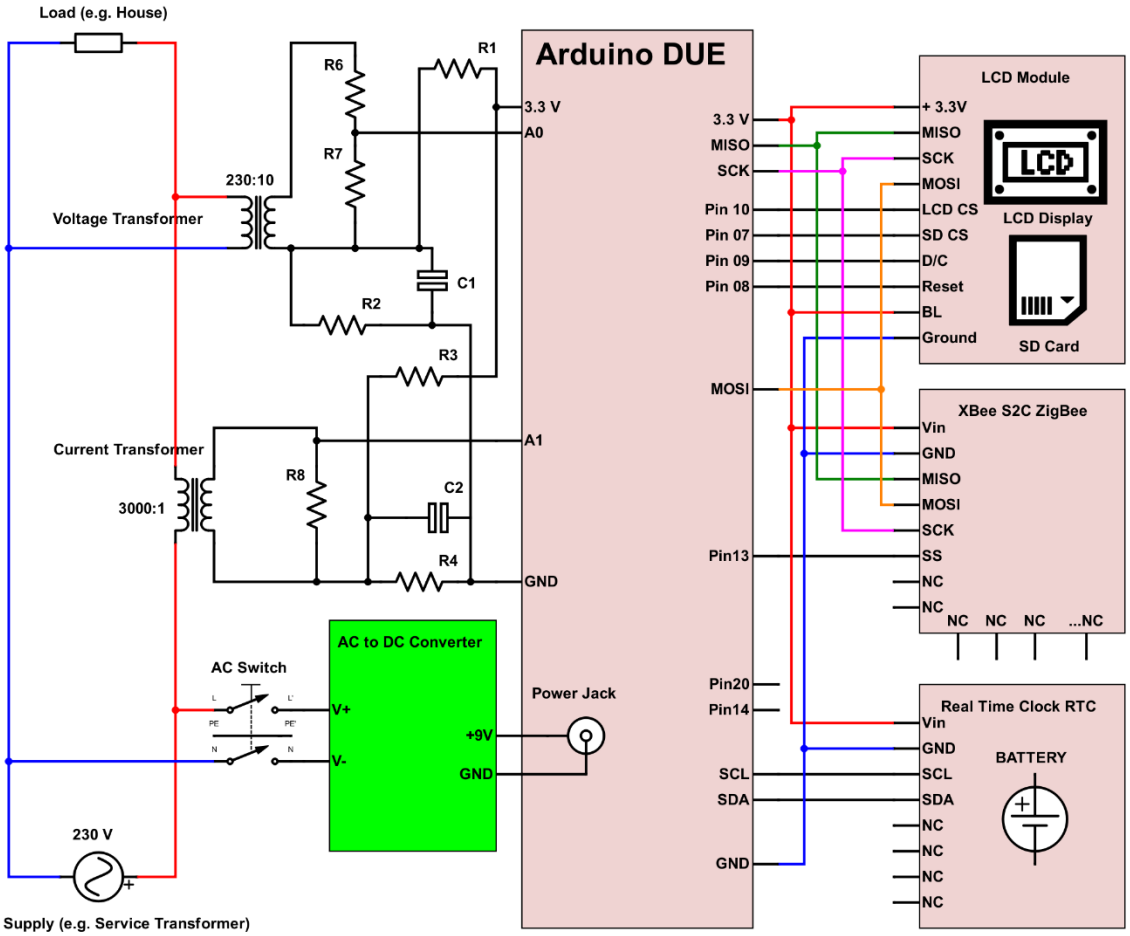

R1	20k Ω
R2	20k Ω
R3	20k Ω
R4	20k Ω
R6	1k Ω
R7	100 Ω
R8	36 Ω for 80A CT 120 Ω for 30A CT
C1	10µ F
C2	10µ F

Vitae

Name :Abdullah Laiq Shah

Nationality :Pakistani

Date of Birth :4/3/1991

Email :abdullahlaiq@hotmail.com

Address :Dhahran 31261, KSA

Academic Background :Abdullah L. Shah received the B.Sc. and MS. degrees in electrical engineering from King Fahd University of Petroleum and Minerals, Dhahran, Saudi Arabia, in 2016 and 2018 respectively. His research interests include smart grid security, renewable energy integration, electricity markets, power system operation and optimization, and power system stability.

Publications : "Financial Benefits by Installing PV Generation and Energy Storage Systems for Households". Accepted in *SASG2017* conference and it will be available soon in *IEEE Xplore Digital Library*.

"Accurate Detection and Correction of Technical and Non-Technical Losses Using Smart Metering". Submitted to *IEEE Transaction on Smart Grids*.

"A Novel Derived Unit of Measurement for Detection and Assessment of Attacks on Smart Metering System". To be submitted to one of *IEEE Journals*.

"Design and Implementation of a Novel Smart Metering System for Tampering Applications". To be submitted to one of *IEEE Journals*.